

# **Università degli Studi di Napoli “Federico II”**



**Dipartimento di Ingegneria Chimica, dei Materiali e della Produzione  
Industriale**

**PhD in Products and Industrial Processes Engineering-XXIX Cycle**

**Development of a System for Electric Energy Production Based on  
Fuel Cells Fueled by Biogas Produced with Anaerobic Digestion of  
Biomass**

**Supervisor**

**Prof. Maria Turco**

**PhD Student**

**Angelo Ausiello**

**Scientific Committee**

**Prof. Maria Turco**

**Prof. Domenico Pirozzi**

**Prof. Giuseppe Toscano**

**Dr. Luca Micoli**

## CONTENTS

<b>Abstract</b>	1
<b>Chapter 1 : Introduction</b>	4
1.1 Energy Demand and Environmental Impact	4
1.2 International legislation for reduction of GHG emissions	9
1.3 Renewable Energy	10
1.4 Biomass	11
1.5 Biomass for Anaerobic Digestion	12
1.5.1 Anaerobic Digestion Steps	13
1.5.2 Substrates for Anaerobic Digestion	17
1.6 Improvement of Biogas Production Techniques	21
1.6.1 Pretreatment of Biomass	21
1.6.1.1 Ultrasound PT	22
1.6.1.2 Chemical PT	22
1.6.1.3 Conventional Heating PT	23
1.6.1.4 Microwave Heating PT	23
1.7 Co-digestion	24
1.8 Reactors	24
1.9 Fuel Cells: generality	26
1.10 History of Fuel Cells	27
1.11 Fuel Cells systems	29
1.11.1 Comparison with Batteries	30
1.11.2 Comparison with Heat Engine	31
1.12 Sectors of Applications	32
1.13 Fuel Cells Fundamentals	33
1.13.1 Fuel Cell Operations	37
1.14 Characteristics and Features	40
1.14.1 High Efficiency	40
1.14.2 Reduced Harmful Emissions	42
1.14.3 Modularity	43
1.14.4 Fuel Flexibility and Applications	43
1.15 Fuel Cells Types	44
1.15.1 Proton Exchange Membrane Fuel Cell (PEMFC)	45
1.15.2 Alkaline Fuel Cell (AFC)	46
1.15.3 Phosphoric Acid Fuel Cells (PAFC)	48
1.15.4 Direct Methanol Fuel Cells (DMFC)	49
1.15.5 Molten Carbonate Fuel Cell (MCFC)	50
1.15.5.1 Components of the Molten Carbonate Fuel Cells	53
1.15.5.2 Cell Configuration	55
1.15.5.3 Steam Reforming	56
1.15.5.4 MCFC Internal Reforming and Steam Reforming	57
Catalyst	
1.15.6 Solid Oxide Fuel Cell (SOFC)	58
1.15.6.1 Components of the Solid Oxide Fuel Cells	60

1.15.6.2 Fuel Reforming	62
1.15.6.3 Solid Oxide Fuel Cell Configurations	63
References	66
<b>Chapter 2: Biohydrogen Production Processes</b>	75
2.1 Introduction	75
2.2 Hydrogen from Renewable Sources	76
2.2.1 Biohydrogen Production by Thermochemical Processes	77
2.2.1.1 Hydrogen from biomass pyrolysis	77
2.2.1.2 Biomass gasification	78
2.2.2 Biohydrogen Production by Biological Processes	79
2.2.2.1 Biophotolysis	79
2.3 Dark Fermentation	81
2.3.1 Dark Fermentation: Operating Conditions	82
2.3.1 pH	82
2.3.2 Temperature	82
2.3.3 Hydrogen Partial Pressure	83
2.3.4 Substrates and Inoculum	83
2.3.5 Kinetics and Kinetic Models of Hydrogen Production	90
2.4 Content of Chapter	92
2.5 Materials	93
2.5.1 Arundo Donax	93
2.5.2 Organic Fraction of Municipal Solid Waste (OFMSW)	94
2.5.3 Litter	95
2.5.4 Manure	96
2.5.5 Synthetic Medium	96
2.6 Methods	96
2.6.1 Biomass Analysis	96
2.6.2 Anaerobic Mixed Culture	97
2.6.3 Preparation of Nutrient Medium	97
2.6.4 Biomass Hydrolysis	98
2.6.5 Fermentation Tests	98
2.6.6 Analytical Techniques	99
2.6.7 Nelson-Somogyi method	99
2.6.8 Microbial biomass measurement	100
2.6.9 Biogas Volume Measurement	101
2.6.10 Selection of H <sub>2</sub> -Producers Bacteria	101
2.7 Results and Discussion	103
2.7.1 Biomethane Production	103
2.7.2 Biohydrogen Production	104
2.7.2.1 Synthetic Medium (SM)	105
2.7.2.2 Arundo Donax not treated (ADH)	109
2.7.2.3 Arundo donax treated with Steam Explosion	111
(ADHexp)	
2.7.2.4 Manure	114
2.7.2.5 Litter	117

2.7.2.6 OFMSW	120
2.8 Conclusions	122
References	125
<b>Chapter 3: The Use of Biogas in Fuel Cells Technology: Adsorption Processes and Adsorbent Materials for Removal of Noxious Compounds</b>	128
3.1 Introduction	128
3.2 Substrates for biogas production and impurities	129
3.3 Biogas to biomethane	131
3.4 Biogas Upgrading	132
3.4.1 Removal of oxygen/air	132
3.4.2 Removal of water	132
3.4.3 Removal of CO <sub>2</sub>	133
3.5 Membrane separation	135
3.6 Cryogenic separation	136
3.7 Biological methane enrichment	136
3.8 Removal of H <sub>2</sub> S	136
3.9 Removal of H <sub>2</sub> S during digestion	138
3.10 Removal of H <sub>2</sub> S after digestion	139
3.11 Separation of H <sub>2</sub> S with Membrane	140
3.12 Biological filter	140
3.13 Adsorption on activated carbon	144
3.14 Ammonia stripping	144
3.15 Materials for Sulphur Removal: Activate carbons and Zeolites	145
3.16 Removal of sulphur compounds in fuels by adsorption processes	151
3.16 The effect of sulphur compounds on MCFC	154
3.16.1 Sulphur poisoning on the MCFC components	154
3.16.2 Effect of SO <sub>2</sub> on cathode and H <sub>2</sub> S on anode	157
3.17 The effect of biogas impurities on SOFC	159
3.18 Effect of halogenated compounds	161
3.19 Effect of sulphur compounds on SOFC	162
3.20 Levels of sulphur containing compounds in biogas	163
3.21 Materials and Methodology	168
3.21.1 Preparation of Activated Carbon	169
3.21.2 Degassing	169
3.21.3. Impregnation	169
3.21.4 Heat treatment	170
3.21.5 Preparation of Zeolites	171
3.21.6 Chemical-physical characterization	173
3.21.6.1 Surface area measurements	173
3.21.6.2 BET model	173
3.21.6.3 Electron Microscopy (SEM) and Elementary Analysis (EDS)	175

3.21.7 Experimental Apparatus for Adsorption tests	176
3.21.7.1 H <sub>2</sub> S adsorption tests	176
3.21.7.2 HCl adsorption tests	178
3.21.7.3 Analytical procedure	179
3.22 Results and Discussion	184
3.22.1 SEM-EDS measurements	184
3.22.2 Surface area measurements	187
3.22.3 Tests of HCl Adsorption capacity	192
3.22.4 Tests of H <sub>2</sub> S Adsorption	198
3.22.5 Mathematic models of experimental data	205
References	211
<b>Chapter 4: Integrated System Anaerobic Digester/Fuel Cell</b>	225
4.1 Introduction	225
4.2 Content of Chapter	228
4.3 Manure to Electricity using Fuel Cells	229
4.3.1 Concept Development and Feasibility Study	230
4.3.2 Plant Design and Development	232
4.3.2 Economic Analysis	240
4.3.2.1 Investment costs	241
4.3.3 Future Scenarios	243
4.4 Evaluation of Biomass for Fueling Biohydrogen	245
References	247
<b>Conclusions</b>	248

## Abstract

The research activity regards the field of innovative technologies for energy production with high efficiency and low environmental impact from renewable sources.

The steady increase in energy demand associated with the reduced availability of fossil fuels and the urgent need to reduce greenhouse gas emissions, are promoted the use of high-efficiency and alternative fuel technologies. The use of biogas is an effective solution to the problems of energy supply with further benefit of recovery and reutilization of the organic waste to energy scope. The biogas, a mixture consisting mainly of methane, carbon dioxide and hydrogen can be produced through thermochemical processes (i.e. pyrolysis and gasification) or biological (i.e. biophotolysis and biofermentation). The last one have the advantage of a significant energy savings and reduced pollutant emissions.

The technology of fuel cells (FCs) is today the most valid alternative to traditional thermal engines for different aspects: the higher efficiency (up to 80-85% in cogeneration systems), the negligible environmental impact, flexibility and modularity that allow to obtain power range from a few W up to MW. Thanks to these advantages the interest of the international scientific community to the FC continues to grow and the technology is beginning to have sufficient maturity to be developed on large scale.

The objective of this PhD thesis is the development of an integrated system for production of electrical energy based on FCs, in particular on high-temperature fuel cells (Solid Oxide Fuel Cells) fueled with biogas and biohydrogen produced by anaerobic digestion of biomass.

The development of integrated systems of this type needs further upgrades to became competitive for industrial applications.

The biomethane production from biomass waste, despite being a well-established process, still needed improvement in relation to the nature of the starting biomass and operating conditions of the digester. The production of biohydrogen for energy applications is still a challenge, and further studies are needed to get hydrogen rich streams and to optimize the digestion process towards  $H_2$  production rather than  $CH_4$ .

The engineering of the integrated system digester/FC deserves particular attention in order to make compatible the characteristics of biogas with the specifics of the FC. This refers in particular to the presence of impurities such as  $H_2S$  and  $HCl$  that are harmful for FCs and require a specific design for clean-up systems and the choice of suitable adsorbent materials.

The PhD thesis is divided in four chapters.

The first chapter, "Introduction", reports the state of the climate change, analyzing their causes and foreseeable future scenarios. It was decided to report the regulations introduced by European and international community that promoted the development of new technologies in the energy field. FCs are then treated as an emerging high-efficiency technology for the production of energy describing the general principles, the main types and applications already present on an industrial scale or foreseeable in a short-medium term. Relevant importance is dedicated to the anaerobic digestion process describing the general characteristics such as the reaction network, the steps involved, the operating conditions (T, pH, retention time) and the nature of the microbial consortia.

The second chapter "Biohydrogen Production Processes" concerned the study and optimization of fermentation processes (Dark Fermentation) aimed to the production of biohydrogen (and biomethane) evaluating the potential for energy exploitation of different biomass.

Different types of biomass have been studied: two lignocellulosic, *Arundo donax* (not treated and pretreated by steam-explosion process) and a litter from animal house for mice; the organic fraction of municipal solid waste and manure from a cattle farm. Sewage sludge, used as inoculum, has been collected from the wastewater treatment plant in Nola (Na). All tests have been conducted under mesophilic conditions at 38 ° C. It has been developed an innovative experimental procedure aimed to the selection of the bacteria hydrogen producers through the use of a salts and nutrients medium specific for these bacteria. Compared with literature data the procedure operates under the same conditions of anaerobic digestion and does not require further additional costs. It was decided to make attractive the development of the process from an industrial point of view.

The results obtained are very interesting due to high biogas production and H<sub>2</sub> concentration (up to 70% vol). This data confirms the efficiency of experimental procedure able to enhance the growth of H<sub>2</sub>-producer bacteria to the detriment of methanogenic ones.

The third chapter "The Use of Biogas in Fuel Cells Technology: Adsorption Processes and Materials Adsorbent for Removal of Noxious Compounds" deals with the purification system of the biogas stream from impurities, which can cause irreversible poisoning phenomena for FCs (particularly H<sub>2</sub>S and HCl). In order to be fed to the FCs, the biogas must have concentration of H<sub>2</sub>S and HCl lower than 1 ppmv. The removal technique used is based on adsorption on microporous materials such as activated carbons and 13X zeolites. Such materials have been properly functionalized in order to increase the adsorbent capacity and selectivity toward H<sub>2</sub>S and HCl. The experimental activity was conducted on two laboratory plants, that appear innovative compared to literature, which allow the continuous monitoring of the H<sub>2</sub>S and HCl concentrations with high accuracy of analysis. From adsorption data breakthrough curves of different materials have been obtained making able to compare the performance of the sorbents and to identify the optimal ones.

The results obtained are encouraging because have been obtained high purity levels with H<sub>2</sub>S and HCl concentrations lower than 1 ppm and longer saturation time compared to literature data.

The fourth and final chapter "Integrated Anaerobic Digester System/Fuel Cell" reports the feasibility study and the development of the integrated plant anaerobic digester/FCs. Part of the research activity has been developed in Switzerland at the Paul Scherrer Institute (Villigen). In the contest of the project Biosweet (Biomass Energy Future for Swiss) has developed the line of research "Manure to Electricity" which includes the development of small plants (2-5 up to 100 kWe) using SOFCs fueled with biogas produced by anaerobic digestion of manure. The project coordinator is Dr. Serge Biollaz. In addition to the participation of Prof. Turco's research group, the project has been developed in collaboration with various research centres (WSL, the Swiss Federal Research Institute) and Swiss Universities (EPFL, University of Applied Sciences in Zurich).

The feasibility study of the integrated system is carried out through the designing of the different sections of the plant: anaerobic digestion (digester, storage tanks), clean-up (upgrading and adsorbent beds), SOFC stack. In particular, a market survey aimed to identify and select the SOFC yet available in the market analyzing several characteristics such as power density, lifetime and resistance to harmful compounds. In addition, an economic analysis with an initial assessment of the costs has been developed.

The integrated plant Digester/SOFCs for the production of small/medium plant size for electrical energy production has characteristics of novelty and may be competitive with other higher power plant engineering realities having lower flexibility for the reuse of the agro-industry waste materials.



## Chapter 1 : Introduction

### 1.1 Energy Demand and Environmental Impact

The global energy demand is growing rapidly, and at present time about 88 % of this demand is met by fossil fuels [1]. Scenarios have shown that the energy demand will increase during this century by a factor of two or three (IEA 2006) [1]. At the same time, concentrations of greenhouse gases (GHGs) in the atmosphere are rising rapidly, with fossil fuel-derived CO<sub>2</sub> emissions being the most important contributor. In order to minimize related global warming and climate change impacts, GHG emissions must be reduced to less than half of global emission levels of 1990 (IPCC 2000). The Kyoto Protocol identifies several key points to curb greenhouse gas emissions (GHG), among which production of renewable fuels from organic waste has a strategic role.

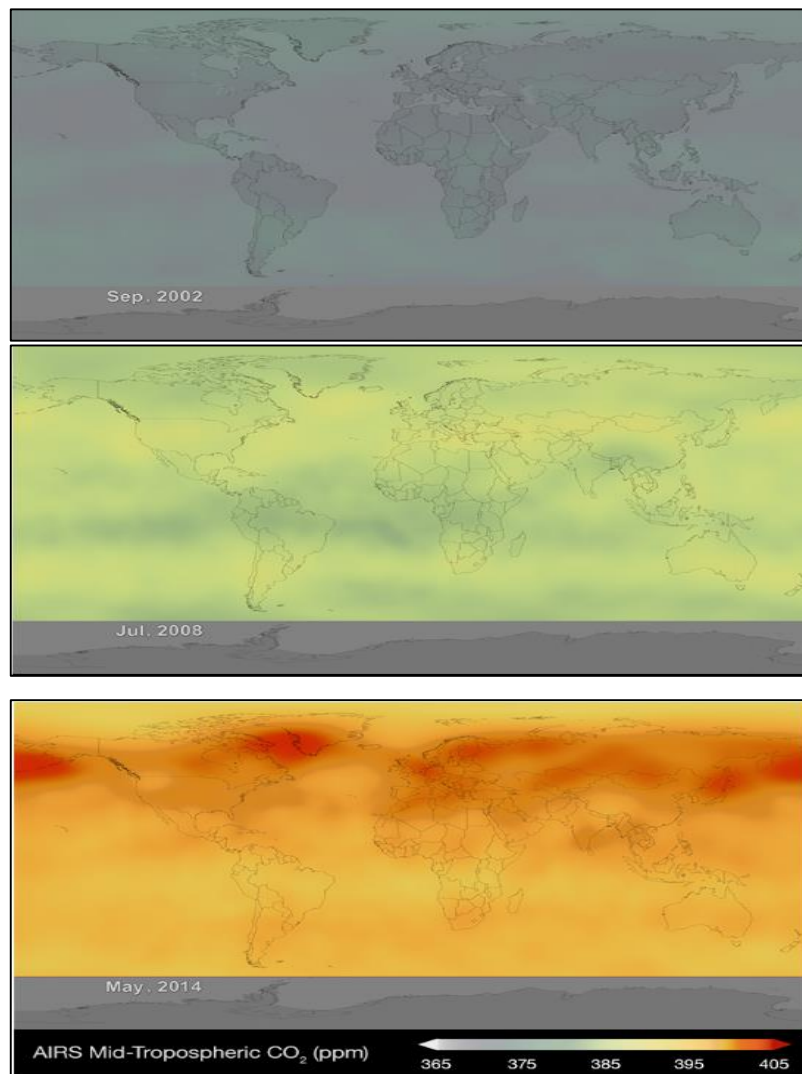


Fig. 1-1 CO<sub>2</sub> concentration change (ppm) in the last 15 years [2]

Figures 1-1 and 1-2 show the concentration change of CO<sub>2</sub> on Earth in the last decade [2]. The change is very significant, since it has increased from a value of about 380 ppm in 2006 to about 405 ppm in the last year.

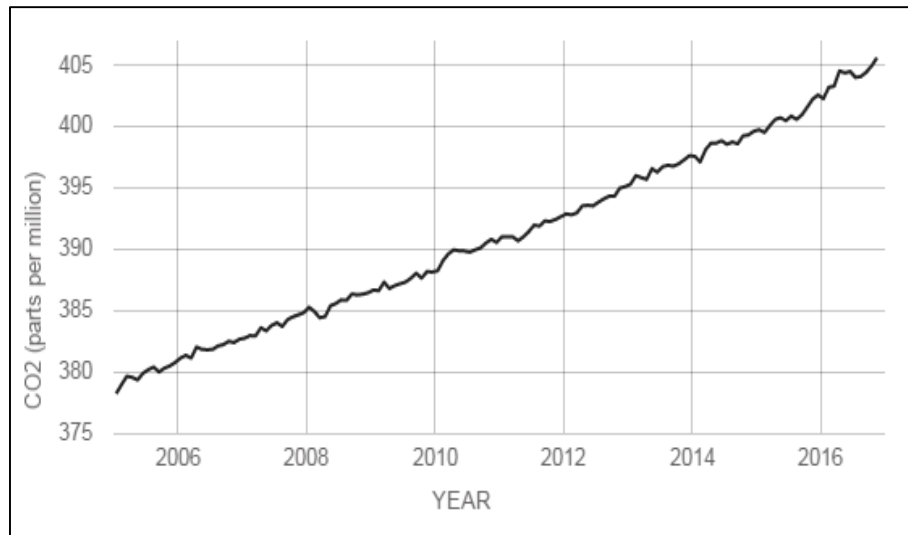


Fig. 1-2 Increase of CO<sub>2</sub> concentration in the last 10 years [2]

CO<sub>2</sub> is not the only gas that causes global warming. Methane is one of the gases present in the atmosphere, and it has a global warming potential 23 times higher compared to carbon dioxide because the methane molecules absorb a fraction of greater thermal infrared photons compared to the carbon dioxide molecules. Currently global warming effect due to methane is equal to one third of that produced by carbon dioxide. It is assumed that the increase in atmospheric levels of methane is the result of human activities, such as increased food production, deforestation and the use of fossil fuels. Biologically methane production occurs through the decomposition of plant material in damp places, such as swamps, ponds and paddy fields. Many-ruminant herbivore animals including cattle, sheep and other wild animals are large producers of methane, which is a by-product of their digestion and is emitted into the air. Another important source of methane is given by the anaerobic decomposition of organic matter present in the waste which they are deposited in landfills [3].

97% of scientists says that the climate is changing and that the main cause is emissions of greenhouse gases and the political will has not been strong enough so far to initiate a change of mass politics away from fossil fuels and towards forms of sustainable energy.

Perhaps the most extreme weather events such as droughts, heat waves, fires and floods will convince the people to make greater pressure on political leaders to take urgent action to reduce carbon emissions and tackle the problem of global warming before it is too late.

Air pollution and climate change are closely related, greenhouse gas emissions in addition to heating the globe are creating, in the major urban centers, smog conditions that endanger people health.

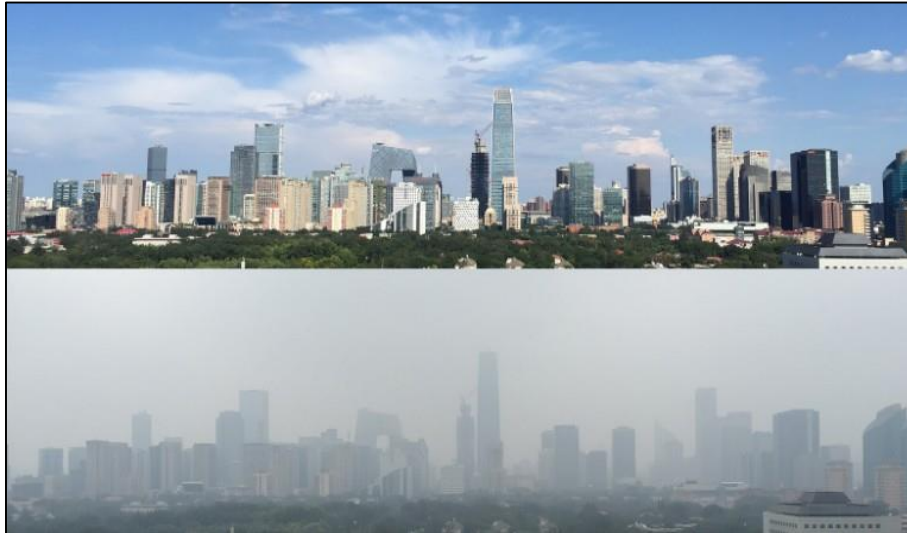


Fig. 1-3 Smog effect in Beijing

The countries that mainly contribute to GHG emission are USA, China, Russia, Brazil and India.

Figure 1-3 shows the effect of smog in Beijing (China), the situation is really alarming because many studies are finding that the smog related to cities such as Beijing and Shanghai is not an environmental phenomenon "isolated" but it is intensifying storms over the Pacific Ocean, and that is promote to make the climatic conditions in the U.S.A. more irregular. Air pollution is a serious problem until now has led to 5.5 million deaths, with only 1.4 and 1.6 million deaths in China and India. However, some European countries are on the same Asian countries plan for the number of deaths due to the air pollution [4].

OECD (Organization for Economic Co-operation and Development) report [4] shows that in China, the registered number of deaths from air pollution is of 957.3 per million inhabitants, while in Hungary is 937.6 per million inhabitants (Fig. 1-4).

Air pollution is the fourth highest factor in the risk of death worldwide, contributing to heart disease, stroke, lung cancer, bronchitis and other [4].

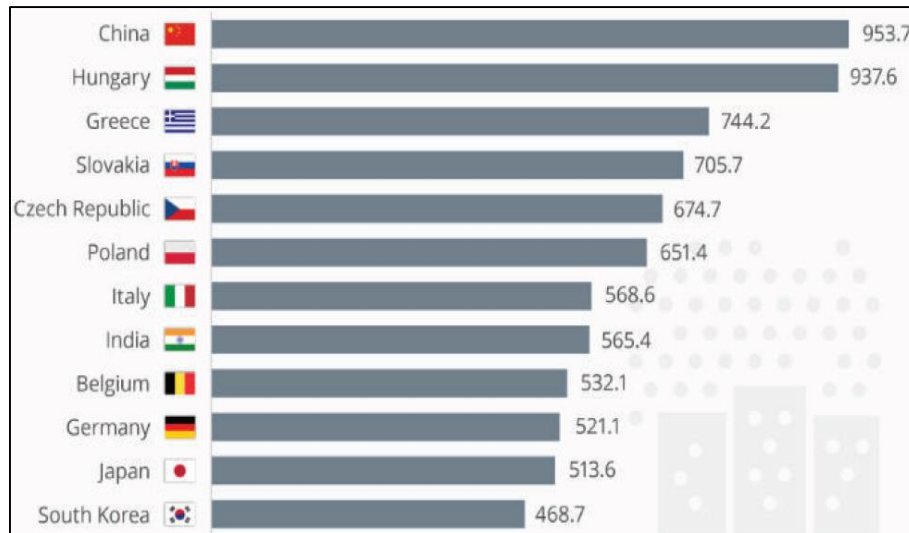


Fig. 1-4 Deaths due to air pollution (per million inhabitants)

According to the latest report of the MIT (Massachusetts Institute of Technology-2014 Energy and Climate Outlook) energy demand in 2050 will double as a result of demographic and economic growth of the world population and it is estimated that greenhouse gas emissions could increase by up to 77 billion tons of CO<sub>2</sub> equivalent in 2050 and reach 92 billion tons in 2100. According to the scientists of the IPCC (International Panel of Climate Change) must try to contain greenhouse gas emissions to limit global warming within the threshold of 2 °C by promoting the use of renewable energy.

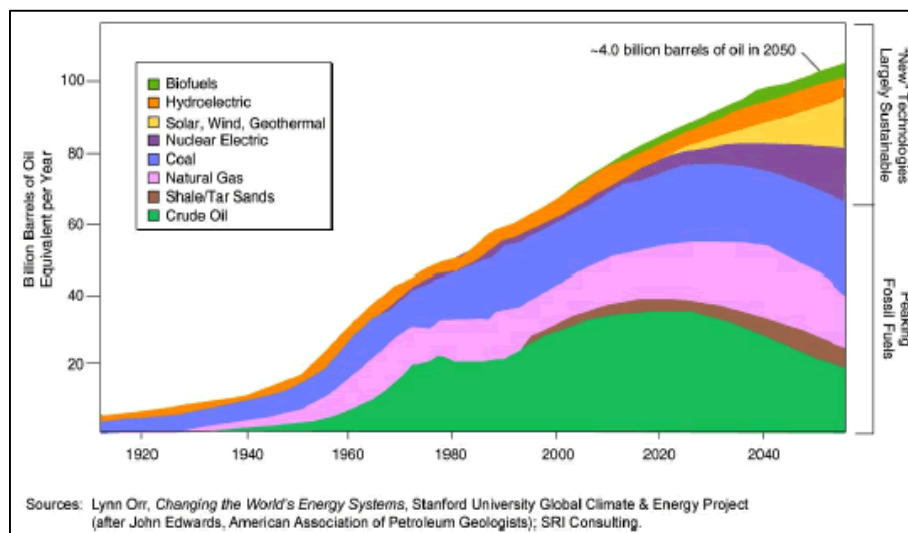


Fig. 1-5 Prospect of energy demand until 2050

The increase in energy demand (Fig. 1-5) as a result of the population growth is the consequence of an increase of the productive activities and increasing production of urban and agro-industrial waste.

A significant part of these residues is biodegradable and therefore susceptible to biochemical transformations which are associable opportunities but also problems.

The production of biodegradable waste in Europe amounts to about 2.5 billion tons per year, of which 60% of agro-industrial origin and the remaining 40% consisting of organic fraction of municipal waste, food industry waste and sewage sludge.

The economist Jeremy Rifkin has been studying for several years the world's energy conditions and hopes the arrival of the "worldwide web energy", a model where every company or home user, on any scale, will have to evolve from a mere consumer of energy in consumer- producer of energy. The production of electricity will be divided into units of small self-dispersed or localized in several points of the area and connected to the electrical distribution grid.

The EPA (Environmental Protection Agency) issued its first standard on methane emission limits for new and modified sources in the oil and gas sector; everything is important to fight global warming but to do so requires strong standards for methane emissions. President Obama has set as a goal the reduction of methane emissions from oil and gas by 40-45% from 2012 to 2020.

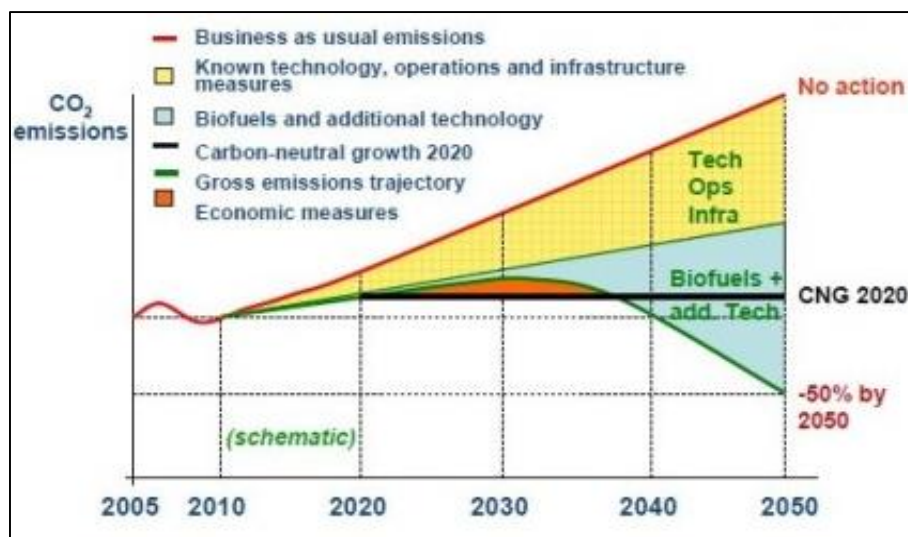


Fig. 1-6 Prospect of CO<sub>2</sub> emission reduction by 2050

In addition to, in the recent conference (COP 21- Paris 2015, COP 22- Marrakesh 2016) have been drawn up several amendments between the countries participating with the aim of reducing pollutant emissions, to limit the temperature increase on our planet and to promote the use of renewable energy through the development of technologies with high efficiency and low

environmental impact. Figure 1-6 shows the prospective of CO<sub>2</sub> emission until 2050. It is possible note that the implementation of biofuels and energy-efficient technologies, spend 50% reduction in carbon dioxide emissions.

## **1.2 International legislation for reduction of GHG emissions**

The first international agreement on the issue of air pollution has been reached in 1979 at Geneva Convention which set the target of limiting emissions of pollutants related to the phenomenon of acid rains. As for gas emissions with global impact, in Montreal in 1987, following the discovery of the ozone hole in Antarctica, it was signed a protocol agreement that restricts the use of ozone-depleting substances: chlorofluorocarbons (CFCs) and hydrochlorofluorocarbons (HCFCs). This act took the name "Montreal Protocol" [5]. In 1992, after the first report of the IPCC (1990), which showed a probable relationship between greenhouse gas emissions from human activities and climate change origin, delegates from 150 countries approved the Framework Convention on Climate Change (United Nations Framework Convention on climate Change, UNFCCC), then entered into force in 1994. It aims to stabilize greenhouse gas concentrations for the protection and balance of the climate system, promotes action at national and international level, but it does not include binding commitments for the reduction of greenhouse gas emissions. An important step in the policy against greenhouse gases has occurred on 11 December 1997 with the approval of the Kyoto Protocol, then entered into force in 2005. This act was ratified by all countries except the United States [6].

The Protocol required that industrialized countries gradually reduce their emission of carbon dioxide, methane, nitrous oxide, hydrofluorocarbons (HFCs), perfluorocarbons (PFCs), sulphur hexafluoride (SF<sub>6</sub>). This protocol envisaged that in the first period, from 2008 to 2012, emissions of greenhouse gases were reduced by 5% worldwide compared to the base year 1990. The reduction levels are different from country to country. As an example, the reduction of emissions from European Union countries had to be 8%, that of the United States by 7%, Japan 6%, and for Russia was not increase the amount of emissions. Any limitation on greenhouse gas emissions was estimated for emerging countries as they have not significantly contributed to the increase of CO<sub>2</sub> concentration in the atmosphere. For this reasons the significant increase in emissions of some developing countries, particularly China and India, that not being required to reduce environmental impacts, have not adopted any significant measures, unlike many industrialized countries have, however, applied policies for the reduction of emissions, in particular the states belonging to the European Union between 2000 and 2011.

On 12 November 2014, the US president, Obama, and the President of the Republic of China, Xi, have decided to take concrete steps to limit greenhouse gas emissions. Obama said that the United States will reduce its emissions by 26-28% by 2050, while Xi said that China emissions will start to decrease by 2030 and that, by that date, 20% of electricity will be produced from renewable sources [7]. These statements are an important achievement, because for the first time the political leaders of the two countries responsible of the largest emissions of greenhouse gases in the world express a specific intent to mitigate those emissions, stating concrete goals and with reference to well-defined deadlines.

### 1.3 Renewable Energy

In recent years, scientific research has been greatly focused on renewable sources. The bioenergy is based on a wide range of potential raw materials and can be used as source of bioenergy to be employed for several purposes in industry for the production of electricity or biofuels.

Bioenergy plays an important role in all three main areas for the use of energy: production of heat, electricity and transport fields. The contribution of bioenergy for heat production far exceeds that related to electricity production and transport (Fig. 1-7) [8].

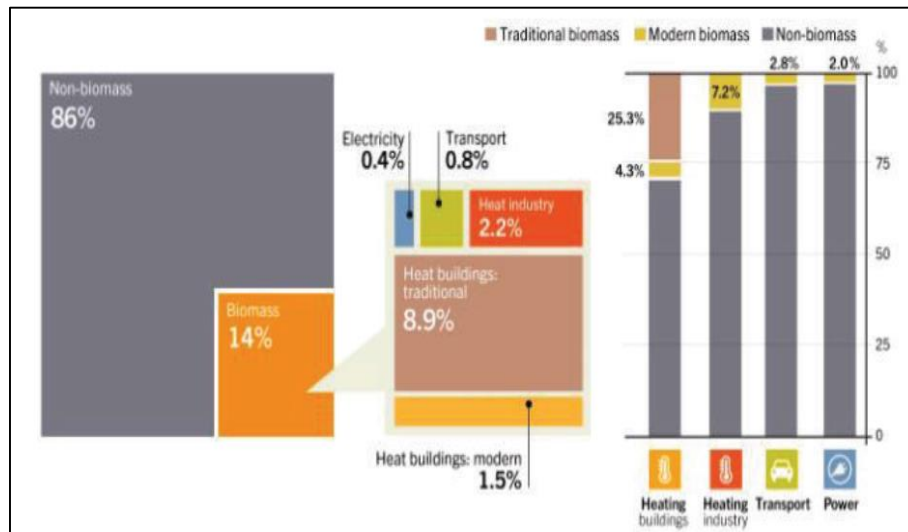


Fig. 1-7 Use of biomass for energy production

Bioenergy can be obtained by different technologies such as the combustion of fuels for the production of heat and energy, anaerobic digestion for the production of methane, heat and energy, the conversion of materials rich in starches or vegetables for the production of biodiesel, the production of liquid fuels from cellulosic materials through thermochemical and biological conversion processes.



The leading country for electricity production is United States, in 2015 the ability of US to produce bioenergy increased by 4% with the 16.7 GW capacity [8].

In China, the production of bio-energy has reached a capacity of 10.3 GW in 2015, an increase of 0.8 GW compared to 2014. It was expected to achieve energy production from 13 GW by 2015 and 30 GW by 2030, but there have been factors that have limited the progress, essentially the high price of raw materials, poor coordination between the various projects and difficulties technical operation.

In Japan was recorded in 2015 an increase in the use of energy power with a power generated of 4.8 GW, especially after the Fukushima nuclear disaster. The market growth is based on imported fuels such as wood pellets (mainly from Canada)[8].

In Brazil, bioenergy production is mainly based on sugar cane, the electric power production increased to 9.7 GW at the end of 2015. Fig. 1-8 shows the amount of worldwide energy production. It is remarkable that the production of green energy has doubled in the last decade (about 200 to 464 terawatt-hours).

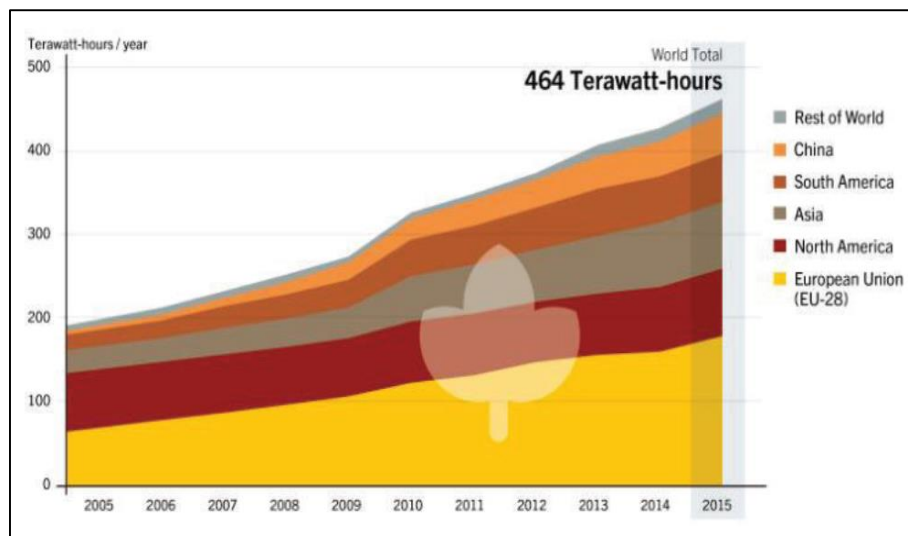


Fig. 1-8 Worldwide bioenergy production

#### 1.4 Biomass

An important renewable source of bioenergy is given by biomass converted to energy by thermal or biological processes.

The production of biomass occurs through the treatment of material of different nature containing organic matrix (to the exclusion of plastic and fossil materials).



The production of these energies by means of combustion processes does not increase the amount of carbon in the atmosphere but it keeps the constant amount. This means that by increasing the production of energy through the use of biomass can contribute decreases not only the total carbon. In the last decade the EU has launched various regulations to promote the use of biomass as energy source. In 2005 has been published the Action Plan for biomass: "Biomass can help in the fight against climate change by reducing greenhouse gas emissions. Used for heating, electricity and fuel for transport, biomass can diversify the energy supply of the EU and create growth and jobs". Green Paper "A European Strategy for Sustainable, Competitive and Secure Energy " in 2006 and "EU Directive on the promotion of energy from renewable sources" in 2008/2009 have further enhanced the use of biomass [8].

In this thesis has been studied the process of anaerobic digestion for biogas and biohydrogen production using different types of biomass.

### **1.5 Biomass for Anaerobic Digestion**

Anaerobic digestion (AD) has been developed mainly to process agricultural wastes in order to provide renewable sources of energy, but other benefits, such as environmental, agronomic, hygienic and social ones, can be obtained by the use of this technology [9].

The agricultural sector deserves great interest: in the European Union (EU), 1500 million tons of biomass could be digested anaerobically each year, and half of this potential is accounted for by energy crops [10].

Anaerobic digester effluents have other agronomic advantages because the pH in manure fed digesters increases from 7.0 to 8.0 during AD. Because of this higher pH, AD effluent is more appropriate to fertilize acid soils [11]. Anaerobic digestion also has the potential to reduce viability of weed seeds in livestock manure [11,12] thereby reducing needs for herbicides and makes the manure suitable for organic farms.

According to the Food and Agriculture Organization of the United Nations (FAO) report entitled "Livestock's Long Shadow" [13], livestock production is achieved at a substantial environmental cost. On a worldwide basis, it contributes 18% of global greenhouse gas (GHG) emissions. GHG emissions from animal production include CH<sub>4</sub> directly emitted from domestic animals or livestock manures, and N<sub>2</sub>O emitted from land applied manures and grazed lands [14].

Methane recovery from animal waste has been extensively investigated and is 0.2–0.4, 0.2–0.3, and 0.35–0.6 L CH<sub>4</sub>/g volatile solids (VS) from swine, cow, and poultry slurries, respectively [15–33].

Reported values for CH<sub>4</sub> recovery from grass, waste grease, and food wastes are 0.55, 1.00, and 0.60 L/g VS, respectively [33]. Farm bioreactor energy output can be substantially increased by improving the C:N ratio via co-digestion of animal manure having low C:N ratio with high C:N

ratio feedstocks: municipal organic wastes, industrial organic wastes [34] or crops such as grasses, grass silages, or crop residues [35–37]. For example, Comino et al. [36] reported a 109% increase of CH<sub>4</sub> yield during co-digestion of cow manure and a crop compared to manure alone. Another important environmental benefit of co-digestion is that it reduces the volume of municipal solid and industrial organic waste going to landfills as these nutrients are recycled onto farmland.

AD can contribute to drastically reduce uncontrolled fugitive CH<sub>4</sub> emissions from stored manure, provided that some conditions occur: (1) bioreactor is properly designed (2) bioreactor retention time is enough to give the almost complete digestion of substrate; (3) the long-term storage tank receiving the biogas should have a gas tight cover to collect and recycle residual CH<sub>4</sub>.

A limited number of studies addressing effects of AD treatment on N<sub>2</sub>O emissions have been reported. Amon et al. [10] indicated that AD is an effective way to reduce GHG emissions from dairy manure slurries, as AD-treated dairy manure emitted 28% less N<sub>2</sub>O than raw manure after field application.

Studies dealing with effects of manure AD on NH<sub>3</sub> emissions from fields have been contradictory with some authors reporting lower NH<sub>3</sub> emissions with digested manure than with raw manure.

One of the main advantages of AD is that it conserves crop nutrients. In addition, the mineralized fraction of N and P is increased [38–42].

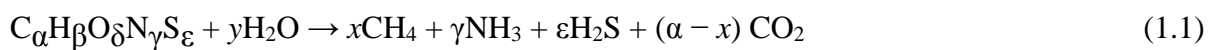
The N/P ratio was increased from 3.9 in raw manure to 5.2 in the bioreactor effluent and to 9.2 in the supernatant fraction of settled effluent. This separation of nutrients increased the agronomic value of manure as it more closely matched crop nutrient requirements. Another advantage of AD manure as fertilizer is reduction in odor, with a high mineralized N content and N:P ratio, increases the window in which it can be applied to land to meet nutrient requirements at various stages of crop growth.

### **1.5.1 Anaerobic Digestion Steps**

Anaerobic digestion is a complex biological process that converts organic materials to methane through three major steps occurring with the help of enzymes acting as catalysts: hydrolysis, acetogenesis, and methanogenesis.

Biogas contains mainly CH<sub>4</sub> 40–75 % vol. and CO<sub>2</sub> 15–60 % vol. Trace amounts of other components such as H<sub>2</sub>O 5–10 % vol., H<sub>2</sub>S 0.005–2 % vol., siloxanes 0–0.02 % vol., halogenated hydrocarbons (VOC) < 0.6 % vol., NH<sub>3</sub> < 1 % vol., O<sub>2</sub> 0–1 % vol., CO < 0.6 % vol., and N<sub>2</sub> 0–2 % vol. can be present and might be inconvenient when not removed [43, 44].

The theoretical or stoichiometric production of methane in anaerobic digestion can be calculated according to [45]:



In which

$$x = (4\alpha + \beta - 2\delta - 3\gamma - 2\epsilon)/8 \quad (1.2)$$

and

$$y = (4\alpha - \beta - 2\delta + 3\gamma + 2\epsilon)/4 \quad (1.3)$$

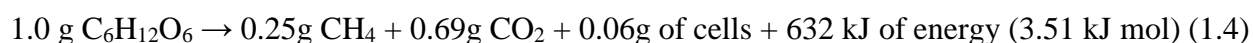
Taking into account the stoichiometry of the above equations, the levels of methane and CO<sub>2</sub> produced from the decomposition of different substrates can be estimated: 50–70 % for CH<sub>4</sub> and 30–50 % for CO<sub>2</sub> [46]. Levels of methane from the decomposition of fat were about 70 %, about 63 % from protein, and about 50 % from cellulose decomposition.

AD process can be divided up into four phases: hydrolysis, acidogenesis, acetogenesis/dehydrogenation, and methanation (Fig. 1.9).

The different phases are carried out by different consortia of microorganisms [47].

A microbial community may contain up to 60 bacterial and Archaeal species growing under anoxic conditions [48, 49]. Their coexistence is based on trophic interactions, growth factor exchange, and the action of physiologically active substances [50, 51].

A microbial community consumes a broad range of organic substrates: poly and monosaccharides, proteins, amino acids, organic acids, alcohols, aromatic compounds, etc. [49, 52, 53]. As reported by Davies [54], the following amounts of final products are produced from one glucose gram:



In other words, 2.8 mol of CH<sub>4</sub> and 2.6 mol of CO<sub>2</sub> can be produced from 1 mol of glucose.

Methane-producing microorganisms (or methanogens) are obligate anaerobes, which represent a dominant group of Archaea. They are included in five orders of the Euryarchaeota phylum: Methanobacteriales, Methanococcales, Methanosarcinales, Methanomicrobiales, and Methanopyrales [55–58]. Methanogens are very diverse in morphology (from simple rods, cocci, or sarcinae to spirals and irregular coccoids), cell wall structure, metabolism, and physiology [59]. Many species can utilize single carbon compounds (methanol, formate, or methylated amines) as carbon sources. For example, methanol is an important methanogenesis substrate. It is formed during the hydrolysis of pectin, which is common in cellulose containing substrates [60, 61]. Recent studies have revealed numerous newly identified methanogen strains and taxa [58].

Methanogens are narrowly focused “specialists.” They consume a limited range of substrates produced by other members of the community.

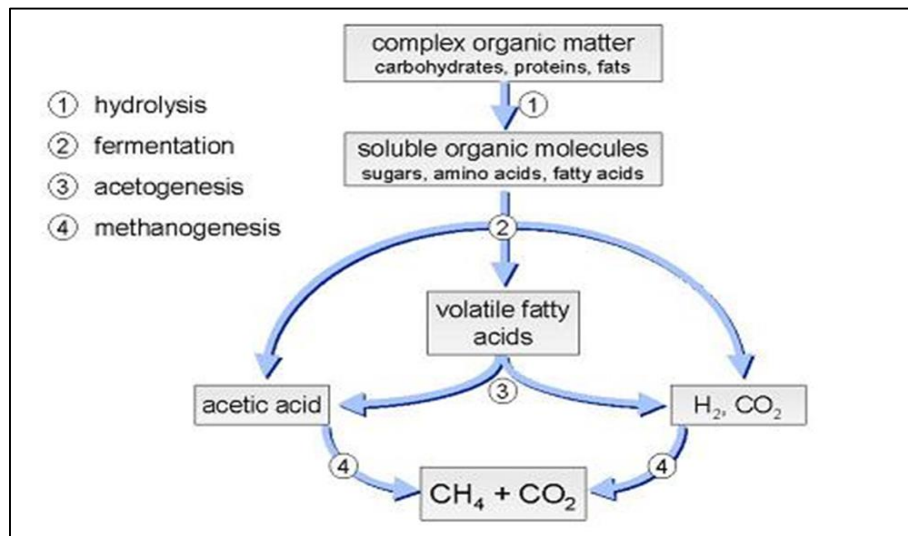
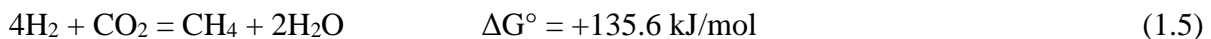


Fig. 1-9 Anaerobic digestion scheme

The main methanogenesis substrates are carbon dioxide and hydrogen (hydrogenotrophic methanogenesis), acetate (acetoclastic methanogenesis), formate, methanol, and methyl amines. The most energetically favorable process is the formation of methane and water [62, 63]:



Hydrolyzing and fermenting microorganisms are responsible for the initial attack on polymers and monomers and produce mainly acetate and hydrogen and some amounts of volatile fatty acids (VFA) such as propionate and butyrate. Hydrolytic microorganisms lead to hydrolytic enzymes, e.g., cellulose, cellobiase, xylanase, amylase, lipase, and protease.

Most of the bacteria are anaerobes such as Bacterioides, Clostridia, and Bifidobacteria, but some facultative anaerobes such as Streptococci and Enterobacteriaceae can take part. The higher VFA are converted into acetate and hydrogen by obligate hydrogen-producing acetogenic bacteria, like as *Acetobacterium woodii* and *Clostridium*. The accumulation of hydrogen can inhibit the metabolism of the acetogenic bacteria. Therefore, an extremely low partial pressure of hydrogen is essential for the acetogenic and hydrogen-producing bacteria. Although many microbial details of metabolic networks in a methanogenic consortium are not clear, present knowledge suggests that hydrogen may be a limiting substrate for methanogens [64]. Since it is recognized that the addition of

hydrogen-producing bacteria to the natural biogas-producing consortium increases the daily biogas production [1].

Acs et al. [65] had found the positive correlation between the enhancement of biogas production and the presence of an added hydrogen-producing new member into the natural consortia such as *Caldicellulosiruptor saccharolyticus* [66].

CO<sub>2</sub> is produced in large amounts from the acetogenesis and methanogenesis while the H<sub>2</sub> produced with very small quantities from acetogenesis process. Approximately 70 % CH<sub>4</sub> in biogas produced from acetate, and 30 % CH<sub>4</sub> produced from CO<sub>2</sub> and H<sub>2</sub> [67].

At the end of the degradation chain, two groups of methanogenic strict anaerobes bacteria produce methane from acetate or hydrogen and carbon dioxide. Only few species are able to degrade acetate into CH<sub>4</sub> and CO<sub>2</sub>, e.g., *Methanosarcina barkeri*, *Metanococcus mazei*, and *Methanotrix soehngenii*, whereas all methanogenic bacteria are able to use hydrogen to form methane. The first and second groups of microbes as well as the third and fourth groups are linked closely with each other [68]. Therefore, the process is completed in two stages that requires equal rates so that anaerobic digestion should be balanced. If the first degradation step is too fast, the acid concentration rises, and the pH drops below 7.0 which inhibits the methanogenic bacteria. On the contrary if the second phase is too fast, methane production is limited by the hydrolytic stage. Thus, the rate-limiting step depends on the nature of the substrate used for AD. For example, compounds like cellulose, proteins, or fats are cracked slowly into monomers within several days, whereas the hydrolysis of soluble carbohydrates occurs within few hours.

It is difficult to describe the whole process by reliable kinetics since hydrolysis of complex insoluble substrate depends on many different parameters such as particle size, production of enzymes, pH, and temperature. A systematic description of the complex kinetics models is given in few works on organic waste digestion [47, 69]. For solid wastes, several kinetic models were developed for mesophilic and thermophilic digestion [70–72]. The kinetic of biogas production from energy crops and manure was studied recently in detail by Anhuradha et al. [73]. Results from quasi-continuous digestion experiments have shown that the degradation can be described by a simple first-order reaction. For the application of this simple model, only the maximum gas yield of the substrate and the specific reaction rate must be known from a continuously digestion test.

### Temperature

The digestion process takes place at psicofilic (5–20 °C), mesophilic (30– 45 °C), or thermophilic (45–60 °C) temperature conditions. It is important to keep a constant temperature during the digestion process, as temperature changes or fluctuations will affect the biogas production negatively.

Thermophilic processes are more sensitive to temperature fluctuations and require longer time to adapt to a new temperature. Mesophilic bacteria tolerate temperature fluctuations of  $\pm 3$  °C without significant reductions in methane production. The growth rate of methanogenic bacteria is higher at thermophilic temperatures making the process faster and more efficient. Therefore, thermophilic digester can operate at higher loadings or at a lower retention times than at mesophilic conditions. But the thermophilic process temperature results in higher instability and a higher risk for ammonia inhibition. Ammonia toxicity increases with increasing temperature, and washout of microbial population can occur [74, 75]. Ammonia is considered to be responsible for process inhibition at high concentrations [76].

#### *Nutrients*

For the growth and survival of the specific groups of microorganisms, several macro- and micronutrients are necessary. Macronutrients are carbon, phosphor, and sulphur. The need of nutrients is very low due to the fact that not much biomass is developed, so that a nutrient ratio of C:N: P:S = 600:15:5:1 is sufficient. Trace elements like iron, nickel, cobalt, selenium, molybdenum, and tungsten are important for the growth rate of microorganisms and must be added if, e.g., energy crops are used for biogas production as the only substrate [77, 78].

The necessary concentration for the micronutrients is very low and in the range between 0.05 and 0.06 mg/L. Only iron is necessary in higher concentration between 1 and 10 mg/L [79].

#### *pH*

Variations in pH may be crucial for the operation of a methanogenic community. Neutral pH values are optimal for methanogen growth, and values below 5.0 suppress it. However, it has been reported by Kim et al. [80] that low pH (4.5) does not inhibit hydrogenotrophic methanogenesis in a methanogenic community grown in a semibatch fermenter process with glucose as a substrate and the hydraulic retention time equal to 9 days. Other authors [81] suppose that a fermenter has niches with neutral pH, where methanogenesis can be initiated. Methane formation takes place within a relatively narrow pH interval, from 6.5 to 8.5 with an optimum interval between 7.0 and 8.0. The process is severely inhibited if the pH decreases below 6.0 or rises above 8.5.

### **1.5.2 Substrates for Anaerobic Digestion**

All types of biomass can be used as substrates for biogas production as long as they contain carbohydrates, proteins, fats, cellulose, and hemicelluloses as main components. The composition of biogas and the methane yield depends on the feedstock type, the digestion system, and the retention time [82]. The theoretical gas yield varies with the content of carbohydrates, proteins, and fats (Table 1.1).

Substrate	Biogas Volume (Nm <sup>3</sup> /t TS)	Concentration (% v/v)	
		CH <sub>4</sub>	CO <sub>2</sub>
Carbohydrates	790-800	50	50
Raw Protein	700	70-71	29-30
Raw fat	1200-1250	67-68	32-33
Lignin	0	0	0

Tab. 1-1 Maxim gas yields and theoretical methane contents [82]

The real methane content in practice is generally higher than the theoretical values shown in Table 1.1 because a part of CO<sub>2</sub> is solubilized in the digestate.

Carbohydrates and proteins show much faster conversion rates but lower gas yields. All substrates should be free of pathogens and other organisms; otherwise, pasteurization at 70 °C or sterilization at 130 °C is necessary prior fermentation.

The contents of nutrients, and the corresponding C/N ratio should be well balanced to avoid process failure by ammonia accumulation. The C/N ratio should be in the range 15–30 [83, 84]. The composition of the fermentation residue should be such that it can be used as fertilizer.

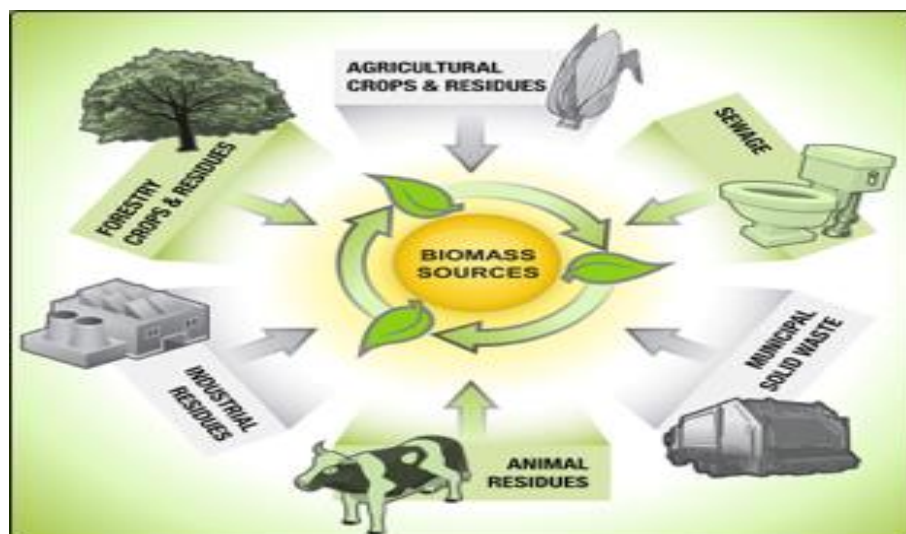


Fig. 1-10 Biomass sources

Forage crops have the advantage of being suitable for harvesting and storing with existing machinery and methods. The specific methane yield is affected by the chemical composition of the crop which changes as the plant matures [85]. Harvesting time and frequency of harvest thus affect the substrate quality and biogas yield. Amon et al. [10] have shown that maize crops were harvested after 97 days of vegetation at milk ripeness produced up to 37 % greater methane yields when

compared with maize at full ripeness. In Table 1.2, the biogas amounts from different substrates are reported [86, 87].

The main materials for biogas production in industrial enterprises are manure and the organic fraction of household and industrial waste in the form of sewage [86, 87]. Studies are being conducted on biogas production from hard to process materials, such as peat coal biochar [88, 89].

<b>Biomass</b>	<b>Biogas Volume (m<sup>3</sup>/t TSV)</b>
Animal residues	200-500
Agricultural residues	350-400
Industrial residues	400-800
Organic waste from slaughter	550-1000
Municipal solid waste	400-600
Energy crops	550-750
Sewage	250-350

Tab. 1-2 Amount of biogas obtainable with different biomass

Numerous basic and biotechnological studies are dedicated to biogas formation from manure, sewage sludge, and various kinds of organic waste [90–93]. Animal manure has a surplus of alkalinity which stabilizes the pH value at VFA accumulation. VFA are a key intermediate in the process and can inhibit methanogenesis in high concentrations. Acetic acid is usually present in higher concentration than other fatty acids, but propionic and butyric acids have more inhibitory effective to methanogens [94, 95].

Anaerobic digestion produces biogas at average rates of 0.30, 0.25, and 0.48 L/g volatile solids from swine, bovine, and poultry slurries, respectively. The biogas produced is of high quality with a CH<sub>4</sub> concentration of 60–80 %.

It is much more profitable from both economic and environmental viewpoints to supplement pure waste with co-substrates, for example, matter obtained from energetic plants. Such plants are purposely grown herbs (sugarcane, maize, millet, sunflower, silver grass, rapeseed, etc.) or underwood [96–98]. Plant waste obtained from wood processing, agriculture, and animal husbandry can also improve the biogas yield significantly. Additional benefit is that their growth, collection,



and processing do not require additional costs [96]. Some authors [49, 99] reported that the yields of biogas with the use of grass, potato tops, maize stems, sunflower husk, and wheat straw were 630, 420, 420, 300, and 340 L CH<sub>4</sub>/kg, respectively, whereas the fermentation of cattle manure alone yields 250 CH<sub>4</sub>/kg. In other studies [97], the yields of biogas from cattle feces, pig feces, and farmyard manure were 25, 30, and 60 L CH<sub>4</sub>/kg of wet biomass, respectively. The fermentation of beet leaves, fodder beet, Sudan grass (*Sorghum vulgare* var. *sudanense*), herb silage, maize silage, and grain residues yielded 60, 90, 130, 160, 230, and 550 L CH<sub>4</sub>/kg of wet biomass, respectively. Maize and herb silages are most commonly used in Germany as co-substrates in fermenters [97].

The most important parameter for choosing energy crops is their net energy yield per hectare. Many conventional forage crops produce large amounts of easily degradable biomass which is necessary for high biogas yields [82].

The methane-rich biogas from lignocellulosic materials comes mostly from hemicelluloses and cellulose [45]. The production of biogas from lignocellulosic materials was dependent on the performance, cost effectiveness, and product generation of pretreatment process. Hence, the methane yield per wastes volume can be further improved.

Few data are reported on cellulose as a substrate for biogas production, although cellulose is the abundant component of municipal solid waste (MSW) [100–102]. Nowadays, the conversion of paper materials to biogas attracts attention again. It is partially related to the separate collection of waste, used in many countries. In addition, paper and cardboard are the largest biodegradable MSW fraction [96, 102, 103] and the sewage formed in anaerobic degradation of cellulose containing materials is nontoxic [103].

The main feature of anaerobic degradation of cellulose is the complex structure of the microbial communities, which form a specific food chain [99]. Due to its complexity, the organic compounds in lignocellulosic material were not fully degraded during the process [111, 112]. Hydrolysis can be the rate-limiting step for anaerobic digestion process in cases that the substrate was in particulate form [113].

Microbial populations converting cellulose to biogas are taxonomically diverse. They are different under psychrophilic, mesophilic, or thermophilic conditions, but they generally act in similar way [104–106]. The composition and stability of a microbial community and, consequently, the efficiency of the whole process depends on the growth conditions (temperature and pH), organic substrate composition and structure, the rate of organic material load in the fermenter, the retention time of the solid matter, and other factors [92, 107–109].

In using the lignocellulosic materials, the biodegradability of the substrate was a key factor in determine the percentage of the theoretical yield [110].

## 1.6 Improvement of Biogas Production Techniques

To enhance biogas production, various techniques can be applied, such as pretreatments (chemical, thermal, enzymatic) and/or biotechnological such as co-digestion of the substrate (manure, sewage sludge) with other wastes that make the anaerobic digestion more profitable [114], the use of serial digester. Co-digestion with other wastes, whether industrial (glycerin), agricultural (fruit and vegetable wastes), or domestic (municipal solid waste) is a profitable option for improving biogas production [114–116]. Serial digester configuration which consists of main digester with long retention time and post-digester with short retention time could improve biogas production and achieve better effluent quality in terms of VFA concentration compared to a single reactor [117].

Maceration of biomass, like as manure, to produce particle sizes below 0.35 mm has increased biogas yield by 15–20 % [118]. Extrusion as pretreatment was reported by Hjorth et al. [111] and it had shown 18–70 % increment of biogas yield after 28 days. Thermal treatment of sewage sludge has been shown to increase the biogas yield by 50 and 80 % after heating to 70 and 170 °C, respectively [119]. Alkaline treatment of sewage sludge had been observed to increase the speed of biogas production and to cause an initial rate increase of 150 % [120]. Pretreatment using *N*-methylmorpholine-*N*-oxide (NMMO or NMO) had been reported by Teghammar et al. [110]. This pretreatment improved the methane yield by 400–1,200 % compared to untreated materials. Ozone oxidation of sewage sludge resulted in an initial biogas yield increase of 200 % [121], while wet oxidation produced 35 % methane yield increase. Ultrasound and microwave treatments of sewage sludge had been shown to increase initial gas production by 20–50 % [122]. Biological pretreatment could also be an effective method for optimizing biodegradability and enhancing the highly efficient biological conversion of lignocellulosic wastes into biogas. Zong et al. [123] used corn straw at ambient temperature (about 20 °C) treated by new complex microbial agents to improve anaerobic biogas production. This treatment resulted in an increase of total biogas yield of 33.07 %, of 75.57 % for methane yield, and 34.6 % shorter technical digestion time compared with the untreated sample.

### 1.6.1 Pretreatment of Biomass

Hydrolysis of organic matter is considered to be the rate limiting step in biomass degradation. If biomass have low biodegradability, high sludge handling/disposal costs, and/or produce a low amount of biogas. Adequate pretreatments (PTs) can be taking into account as sustainable improvements [124]. Such PTs include mechanical, thermal, chemical, biological, and combinations of them [125]. PTs further hydrolyze the so-treated feed, thus improving the AD step,

since organic matter is now more accessible to the anaerobic microorganism consortium [126]. Solubilization of chemical oxygen demand (COD) and reductions of total and volatile solids (TS, VS) are achieved for greater solids reduction rates during mesophilic and thermophilic AD. This typically leads to added pathogen reduction, shorter hydraulic residence times, reduction of residual solids, and smaller reactor volumes.

Such treatments generally favor the access of methanogenic bacteria to the intra-cellular matter, thereby improving biogas production by 30–50 % [127]. It is also important the efficacy of PTs typically increases with the concentration of feed solids, so it could be relevant to evaluate cost and energy demands of concentrating the sludge prior to PT [126]. More research is needed to ascertain the level of benefit that would be gained by applying PTs under full-scale conditions [124, 128].

The PTs described in literature [129] were ultrasound (ULT), chemical (CM), conventional heating (CH), and microwave heating (MWH), based on energy intensiveness, commonality, feasibility, and novelty, respectively.

#### **1.6.1.1 Ultrasound PT**

In recent years have been proposed the use of ultrasound technique as an efficient treatment of biomass in AD processes [124,128]. ULT frequency and specific energy ( $E_s$ ) are the main factors affecting chemical oxygen demand (COD) solubilization and biogas production. Low frequencies (<100 kHz) can promote mechanical and physical degradation while high frequencies promote sonochemical favoring the solubilization of the organic matter. Optimal working ranges (20–42 kHz, 70–300 W, 6,000–18,000 kJ/kg TS) for frequencies and  $E_s$  have been found and do not demonstrate much significant variance regardless of feed characteristics [124, 128].

#### **1.6.1.2 Chemical PT**

Acid and alkaline PTs can be used to degrade complex organic compounds regardless of low temperatures. Acid treatments have been carried out with H<sub>2</sub>SO<sub>4</sub> or HCl solutions (2-10% wt) in range temperature (40-80 °C) [3] Alkaline treatment is performed by increasing the sludge pH to 12 and sustaining it for an optimal duration. Complex organics such as polycyclic aromatic hydrocarbons, lipids, and proteins are hydrolyzed into smaller and more soluble compounds. Desired bacteria can be harmed, however, and chemical addition speeds up equipment corrosion and fouling. Additionally, some of the soluble compounds that are formed are not biodegradable [130, 131] Energy demands in these processes include also mixing and any heating energy. Typical working ranges are: 1–21 kg/m<sup>3</sup> NaOH, 0.25–24 h, pH = 10–12 [129].

### **1.6.1.3 Conventional Heating PT**

Temperatures required for conventional heating PT typically range from 60 to 180 °C. Heating is supplied by heat exchangers or steam injection. Though conventional heating requires a high increase in energy demand, it is balanced by higher sludge biodegradability and by the use of sludge residual heat to maintain the temperature in the digester. Dewaterability and pathogen reduction are increased with thermal pretreatment and result in reduced sludge disposal costs and improved sludge stabilization. Heat transfer is limited by the wastewater's (WW) thermal conductivity, density, viscosity, and specific heat; moreover, heating to the depth of the material is time-consuming [127]. Energy is also lost in the process. Demands in the process of conventional heating include heat and mixing energy. Working ranges are: 50–170 °C, 0.25–1 h.

### **1.6.1.4 Microwave Heating PT**

Microwave irradiation has been studied as an alternative to conventional heating [129, 132, 133]. The irradiation corresponds to  $10^{-3}$ –1 m wavelengths in the electromagnetic spectrum with equivalent frequencies of 300 GHz–300 MHz, respectively. For the heating or drying of thin substances, frequencies of 2,450 MHz with correspondingly short wavelengths (12.24 cm) are adequate. If deep penetration into materials is required, frequencies of 900 MHz with correspondingly long wavelengths (37.24 cm) and energy outputs of up to 100 kW are required. MWH is absorbed selectively by substances containing more moisture, sugars, or fats. The distribution of heat in microwave irradiated WW is thus not uniform because the fluid is two-phase (solid and liquid) and heterogeneous in both phases. Warming or cooling the unit as in conventional heating is not required and energy is conserved because microwaves can be instantly activated or deactivated. Microwave irradiation can be up to 50 % more efficient than conventional heating methods. Microwave units also experience less fouling because their surfaces are not brought to the same high temperatures as the surfaces of conventional heating units [126]. Energy demands in microwave irradiation processes include the necessary conversion efficiencies from “at-the-wall” power to applied heat and mixing energy. Working ranges are: 2,450 MHz, 400–1250 W, 0.03–0.25 h [129].

#### *PTS Economic Analysis*

Bordelau and Droste [129] evaluated the costs of the different pretreatments processes using a model created with Microsoft excel and its Visual Basic Assistant. Net costs per influent flow for ultrasound, chemical, conventional heating, and microwave were 0.0166, 0.0217, 0.0124, 0.0119 \$/m<sup>3</sup> and 0.0264, 0.0357, 0.0187, and 0.0162 \$/m<sup>3</sup> for average and high conditions, respectively.

The average cost increase from results excluding pretreatment use for all processes was 0.003 and 0.0055 \$/m<sup>3</sup> for average and high conditions, respectively.

### **1.7 Co-digestion**

An interesting option for optimizing biogas production yields was using co-digestion technique [134]. This technique can be defined as the combined anaerobic treatment of several substrates with complementary characteristics. The benefits of using co-digestion techniques including dilution of potential toxic compounds, improved balance nutrients, synergistic effect of microorganism, increased load of biodegradable organic matter, and higher biogas yield [135].

According to Mata-Alvarez et al., digestion of more than one substrate in the same digester can establish positive synergism and the added nutrients can support microbial growth [136].

Various co-digestion techniques had been done by mixing the substrate for biogas production with compound such as glycerol, agricultural wastes, and food wastes.

The benefits of using mixing animal manure and glycerol were (1) the elevated content of water in manure acts as solvent for glycerol; (2) the high alkalinity of manure gives a buffering capacity for the temporary accumulation of volatile fatty acids; (3) the wide range of macro- and micronutrients present in the manure were essential for bacterial growth; and (4) glycerol supplies rapidly biodegradable matter [136]. Co-digestion with other wastes, whether industrial (glycerin), agricultural (fruit and vegetable wastes), or domestic (municipal solid waste) was also a suitable option for improving biogas production [115, 116].

### **1.8 Reactors**

Anaerobic digestion for biogas production was commonly carried out in continuously stirred tank reactor (CSTR) [137, 138].

Jeihanipour et al. [139] investigated a two-phase CSTR, modified as stirred batch reactor (SBR) and up-flow anaerobic sludge blanket bed (UASB) process in producing biogas from pretreated and untreated textiles substrates. However, although should enhance digestion performance, the biogas yield by two-phase system was nearly the same as the single CSTR, probably because the two-phase system was sensitive to the substrate with high easily degradable organic load [140]. The main disadvantage of using two-phase system is the separation of acidogenic and methanogenic step can disrupt the syntrophic relationship between bacteria and methanogens, which can cause product inhibition in the acidogenic reactor [140, 141].

An alternative approach to overcome the problems with one-step CSTR and two-phase system is to operate two methanogenic reactors connected in series (serial digestion system) [137]. Some

researches in biogas production using serial digestion have been done. Boe has demonstrated that serial digestion, with percent volume distributions of 90/10 or 80/20 between the two methanogenic reactors, improved biogas production by 11% compared to a traditional one-step CSTR process [142].

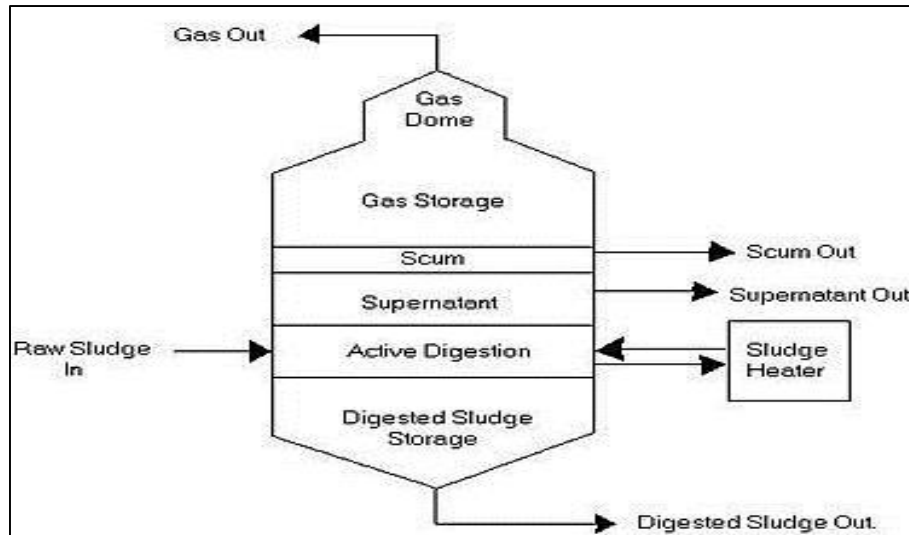


Fig. 1-11 Example of one stage anaerobic digester

Boe and Batstone [143] confirmed that the longer the retention time in the post-digester (second reactor of serial process), the higher the methane recovery of the overall serial digestion. Kaparaju et al. examined the possibility of optimizing biogas production from manure in a bench scale cascade of two methanogenic serial CSTR at termophilic conditions operated at 55 °C with 15 days hydraulic retention time (HRT) [137]. Some works showed that serial digestion improved biogas production from manure, as compared to one-step process, and that the best volume distribution was 70/30 and 50/50%. Ge et al. [144] achieved 44 % volatile solid (VS) reduction in a bench scale system of working volume of 4.6 L, the dual mesophilic digestion of primary sludge with HRTs 2 and 14 days for first and second stage, respectively. Thus, serial digestion can be considered a method to improve conversion efficiency. However, the extra installation costs and process complexity in executing serial digestion concept should be evaluated with the economic gain achieved due to extra biogas produced.

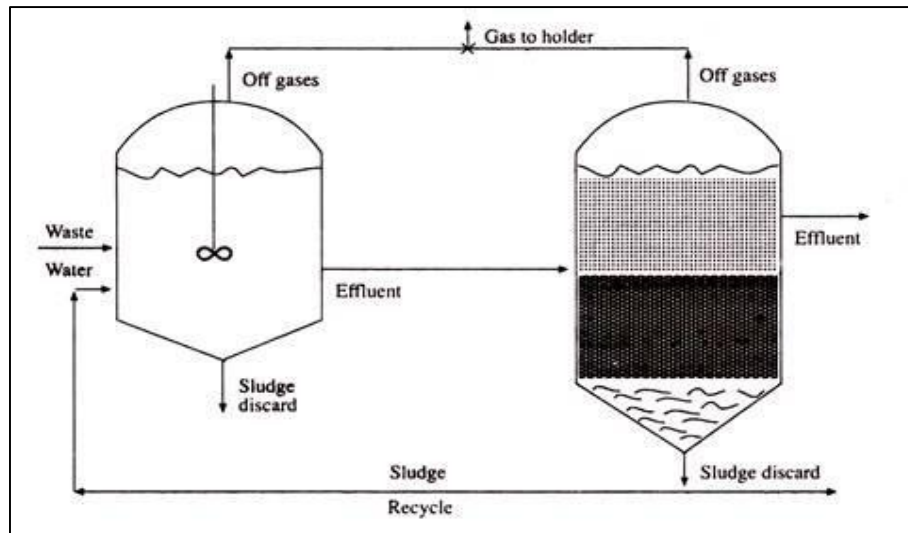


Fig. 1-12 Example of two stage anaerobic digester

### 1.9 Fuel Cells: generality

The current movement towards environmentally friendlier and more efficient power production has caused an increased interest in alternative fuels and power sources [3,145]. Fuel cells are one of the older energy conversion technologies, but only within the last decade they have been extensively studied for commercial use. The scenarios of environmental criticality, climate changes and energy supply required power sources with low pollutants emissions, high efficiency and unlimited supply fuel for a growing world population.

Many other alternative energy technologies have been researched and developed [146]. These include solar, wind, hydroelectric power, bio-energy, geothermal energy, and many others. Each of these alternative energy sources have their advantages and disadvantages, and are in varying stages of development. In addition, most of these energy technologies cannot be used for transportation or portable electronics. Other portable power technologies, such as batteries and supercapacitors also are not suitable for transportation technologies, military applications, and the long-term needs of future electronics. The ideal option for a wide variety of applications is using a hydrogen fuel cell combined with solar or hydroelectric power. Compared to other fuels, hydrogen does not produce any carbon monoxide or other pollutants. When it is fed into a fuel cell, the only by-products are oxygen and heat. The oxygen is recombined with hydrogen to form water when power is needed [147,148].

Fuel cells can utilize a variety of fuels to generate power from hydrogen, methane, methanol and fossil fuels to biomass-derived materials. Using fossil fuels to generate hydrogen is regarded as an intermediate method of producing hydrogen, methane, methanol, or ethanol for utilization in a fuel cell before the hydrogen infrastructure has been set up. Fuels can also be derived from many

sources of biomass, including methane from municipal wastes, sewage sludge, forestry residues, landfill sites, and agricultural and animal waste [149-151].

Fuel cells can also help provide electricity by working with large power plants to become more decentralized and increase efficiency [150]. Most electricity produced by large fossil-fuel burning power plants is distributed through high voltage transmission wires over long distances. These power plants seem to be highly efficient because of their large size; however, a 7 to 8% electric energy loss in Europe, and a 10% energy loss in the United States occurs during long distance transmission [152]. One of the main issues with these transmission lines is that they do not function properly all the time. It would be safer for the population if electricity generation did not occur in several large plants, but is generated where the energy is needed. Fuel cells can be used wherever energy is required without the use of large transmission lines.

Fossil fuels are limited in supply, and are located in select regions throughout the world. This leads to regional conflicts and wars which threaten peace. The limited supply and large demand drives up the cost of fossil fuels tremendously.

### **1.10 History of Fuel Cells**

Fuel cells have been known to science for about 150 years. They were minimally explored in the 1800s and extensively researched in the second half of the twentieth century. Initial design concepts for fuel cells were explored in 1800, and William Grove is credited with inventing the first fuel cell in 1839 [3,153]. Various fuel cell theories were contemplated throughout the nineteenth century, and these concepts were studied for their practical uses during the twentieth century. Extensive fuel cell research was started by NASA in the 1960s, and much has been done since then [154]. During the last decade, fuel cells were extensively researched, and are finally nearing commercialization. A summary of fuel cell history is shown in Figure 1-13.

In 1800, William Nicholson and Anthony Carlisle described the process of using electricity to break water into hydrogen and oxygen. William Grove is credited with the first known demonstration of the fuel cell in 1839. Grove saw notes from Nicholson and Carlisle and thought he might “recompose water” by combining electrodes in a series circuit, and soon accomplished this with a device called a “gas battery”. It operated with separate platinum electrodes in oxygen and hydrogen submerged in a dilute sulphuric acid electrolyte solution. The sealed containers contained water and gases, and it was observed that the water level rose in both tubes as the current flowed. The Grove cell, as it came to be called, used a platinum electrode immersed in nitric acid and a zinc electrode in zinc sulphate to generate about 12 amps of current at about 1.8 volts.



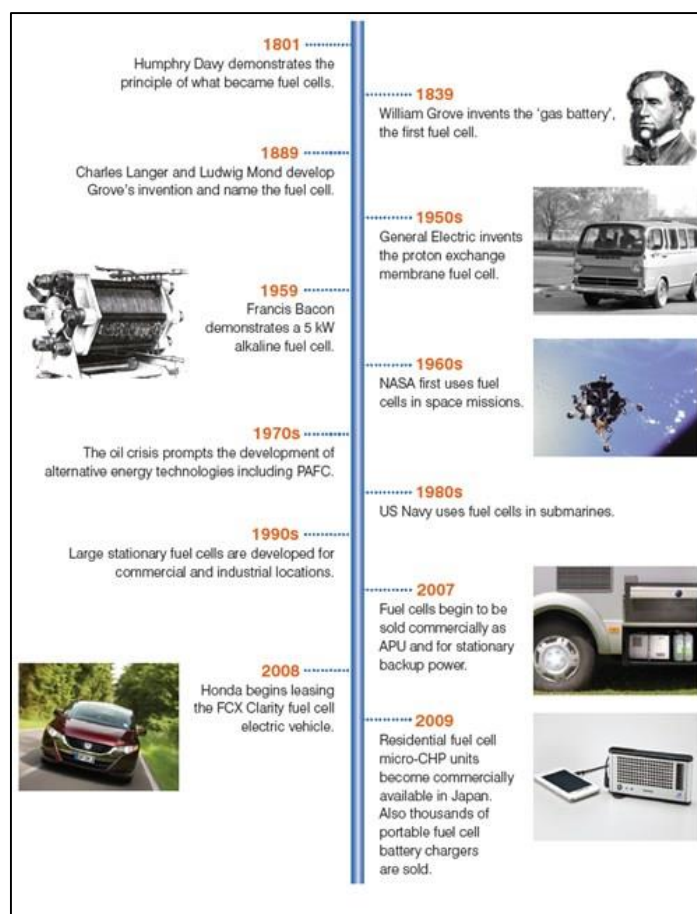


Fig. 1-13 Main milestones in the history of fuel cells.

Friedrich Wilhelm Ostwald (1853–1932), one of the founders of physical chemistry, provided a large portion of the theoretical understanding of how fuel cells operate. In 1893, Ostwald experimentally determined the roles of many fuel cell components.

Ludwig Mond (1839–1909) was a chemist that spent most of his career developing soda manufacturing and nickel refining. In 1889, Mond and his assistant Carl Langer performed numerous experiments using a coal-derived gas. They used electrodes made of thin, perforated platinum, and had many difficulties with liquid electrolytes. They achieved 6 amps per square foot (the area of the electrode) at 0.73 volts.

Charles R. Alder Wright (1844–1894) and C. Thompson developed a similar fuel cell around the same time. They had difficulties in preventing gases from leaking from one chamber to another. This and other causes prevented the battery from reaching voltages as high as 1 volt. They felt that if they had more funding, they could create a better, robust cell that could provide adequate electricity for many applications.

The French team of Louis Paul Cailletet (1832–1913) and Louis Joseph Colardeau came to a similar conclusion, but thought the process was not practical due to needing precious metals. In

addition, many papers were published during this time saying that coal was so inexpensive that a new system with a higher efficiency would not decrease the prices of electricity drastically.

William W. Jacques (1855–1932), an electrical engineer and chemist, did not pay attention to these critiques, and startled the scientific world by constructing a carbon battery in 1896. Air was injected into an alkali electrolyte to react with a carbon electrode. He thought he was achieving an efficiency of 82%, but actually obtained only an 8% efficiency.

Emil Baur (1873–1944) of Switzerland and several of his students conducted many experiments on different types of fuel cells during the early 1900s. His work included high-temperature devices, and a unit that used a solid electrolyte of clay and metal oxides.

O. K. Davtayan of the Soviet Union did many experiments to increase the conductivity and mechanical strength of the electrolyte in the 1940s. Many of the designs did not yield the desired results, but Davtayan's and Baur's work contributed to the necessary preliminary research for current molten carbonate and solid oxide fuel cell devices [3,154].

### **1.11 Fuel Cells systems**

Fuel cells are energy conversion devices that continuously transform the chemical energy of a fuel and an oxidant into electrical energy. The fuel and oxidant gases lick the anode and cathode and are continuously fed promoting the oxidation reaction of fuel and oxidant gas reduction. Fuel cells will continue to generate electricity as long as both fuel and oxidant are available [3,145-154].

There are different types of fuel cells, showing a flexibility that could replace most of the devices for the production of electricity covering outputs ranging from a few W to several MW [149,153,154].

A first classification distinguishes cells in high temperature (HT) up to 1100 °C, used in stationary systems for cogeneration processes, aerospace and marine applications, and low temperature (LT), from 60 to 120 °C, for low-cost portable devices and automotive.

Power can be provided by fossil fuels, coal, biogas, and biomass (for PAFC, PEMFC, MCFC, SOFC), alcohol (DMFC), and hydrogen (PEMFC and AF).

A further classification of FCs is based on the electrolyte. In PEMFC and DMFC the electrolyte is a polymeric material with cation exchange capacity; Alkaline FCs (AFCs) have a KOH solution as electrolyte; MCFCs have electrolyte based on molten carbonate of lithium and potassium; SOFC is based on phosphoric acid.

FCs technology presents several advantages: low emissions, but depend on the fuel used, especially as regards the release of NO<sub>x</sub>, CO, and particulate; high energy efficiency, especially when compared to those of thermal machines; weak noise; different operating temperatures; modular

construction, so by putting in series or in parallel several elementary units you are covering the power range required; more simple construction, and thus greater reliability and easier maintenance [3,153,154].

These advantages justify the strong interest, particularly from many automotive companies, to develop the technology based on fuel cells for automotive [155,156].

Nevertheless, there are some problems to be solved in order that fuel cells can be competitive and penetrate the market: the cost, due to the high value components; the weight and volume, especially in the automotive; the length of life, still very low (a few thousand hours for cars, about 40,000 for stationary systems); thermal management, for the large amount of heat exchange with an operative cooling system [153-156].

### 1.11.1 Comparison with Batteries

A fuel cell has many similar characteristics with batteries, but also differs in many respects. Both are electrochemical devices that produce energy directly from an electrochemical reaction between the fuel and the oxidant. The battery is an energy storage device with the maximum energy available determined by the amount of chemical reactant stored in the battery itself. A battery has the fuel and oxidant reactants built into itself (onboard storage), in addition to being an energy conversion device. In a secondary battery, recharging regenerates the reactants. This involves putting energy into the battery from an external source.

The fuel cell is an energy conversion device that theoretically has the capability of producing electrical energy for as long as the fuel and oxidant are supplied to the electrodes [153,154]. Figure 1-13 shows a comparison of a fuel cell and battery.

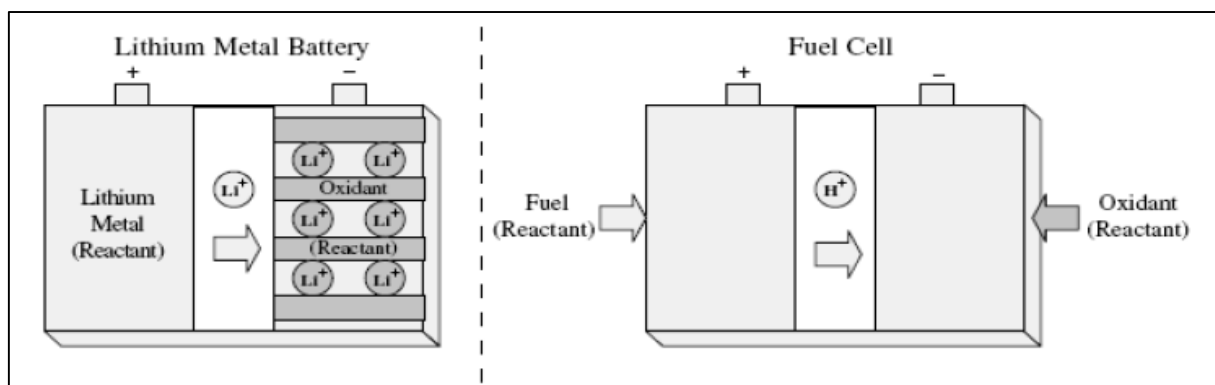


Fig. 1-14 Comparison of a fuel cell and a battery

The lifetime of a primary battery is limited because when the amount of chemical reactants stored in a battery runs out, the battery stops producing electricity. In addition, when a battery is not being

used, a very slow electrochemical reaction takes place that limits the lifetime of the battery. The electrode of a battery is also used in the process; therefore, the lifetime of the battery is dependent on the lifetime of the electrode. In comparison, a fuel cell is an energy conversion device where the reactants are supplied. The fuels are stored outside the fuel cell. A fuel cell can supply electrical energy as long as fuel and oxidant are supplied. The amount of energy that can be produced is theoretically unlimited as long as the fuel and oxidant are supplied. Also, no leakage occurs in a fuel cell, and no corrosion of cell components occurs when the system is not in use [3,150-156]

### 1.11.2 Comparison with Heat Engine

A heat engine converts chemical energy into electric energy like fuel cells, but through intermediate steps. The chemical energy is first converted into thermal energy through combustion, then thermal energy is converted into mechanical energy by the heat engine, and finally the mechanical energy is converted into electric energy by an electric generator.

This multistep energy process requires several devices in order to obtain electricity. The maximum efficiency is limited by Carnot's law because the conversion process is based upon a heat engine, which operates between a low and high temperature [3,150-156]. The process also involves moving parts, which implies that they wear over time. Regular maintenance of moving components is required for proper operation of the mechanical components. Figure 1-14 shows a comparison between a fuel cell and a heat engine/electrical generator.

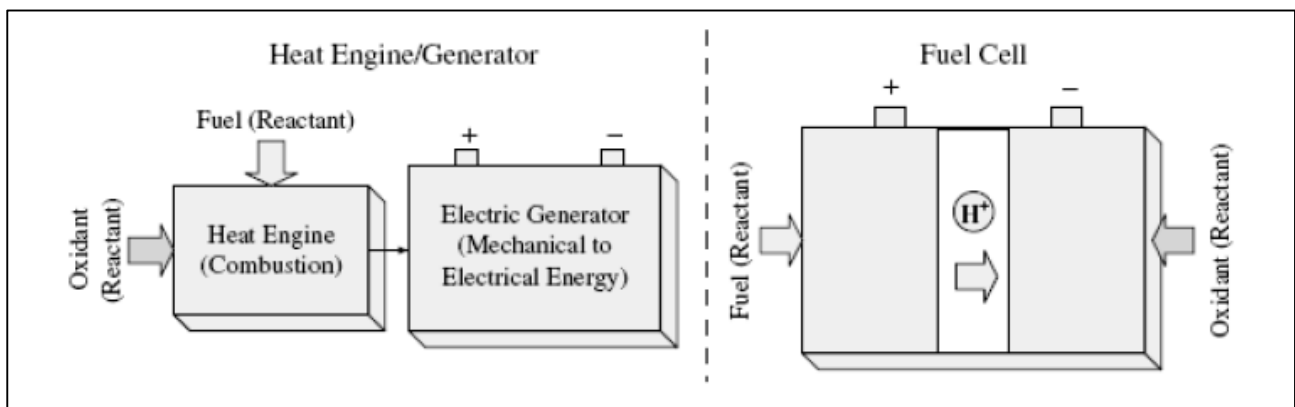


Fig. 1-15 Comparison of a fuel cell with a heat generator

Since fuel cells are free of moving parts during operation, they can work reliably and with less noise. This results in lower maintenance costs, which make them especially advantageous for space and underwater missions. Electrochemical processes in fuel cells are not governed by Carnot's law, therefore high operating temperatures are not necessary for achieving high efficiency. In addition, the efficiency of fuel cells is not strongly dependent on operating power. It is their inherent high

efficiency that makes fuel cells an attractive option for a wide range of applications, including road vehicle power sources, distributed electricity and heat production, and portable systems [3,145-156].

### **1.12 Sectors of Applications**

Fuel cells provide electric power in applications that are currently energy limited as described in the following.

#### *Portable sector*

In coming years, portable devices, such as laptops, cell phones, video recorders, and others, will need greater amounts of power for longer periods of time. Fuel cells are very scalable and have easy recharging capabilities compared to batteries. Cell phone technology is advancing rapidly, but the limiting factor for the new technology is the power. More power is required to provide consumers with all of the functions in devices they require and want. The military also has a need for long-term portable power for new soldier's equipment. In addition, fuel cells operate silently, and have low heat signatures, which are clear advantages for the military [157-161].

#### *Stationary sector*

Stationary fuel cells can produce enough electricity and heat to power an entire house or business, which can result in significant savings. These fuel cells may even make enough power to sell some of it back to the grid. Fuel cells can also power residences and businesses where no electricity is available. Sometimes it can be extremely expensive for a house not on the grid to have the grid connected to it. Fuel cells are also more reliable than other commercial generators used to power houses and businesses. This can benefit many companies; given how much money they can lose if the power goes down for even a short time [162-166].

#### *Transportation sector*

Many factors are contributing to the fuel cell push in the automotive market. The availability of fossil fuels is limited, and due to this, an inevitable price increase will occur. In addition, legislation is becoming stricter about controlling environmental emissions in many countries all over the world. One of the new pieces of legislation that will help introduce the fuel cell automobile market in the United States is the Californian zero emission vehicle (ZEV) mandate, which requires that a certain number of vehicles be sold annually in California. Fuel cell vehicles also have the ability to be more fuel efficient than vehicles powered by other fuels. This power technology allows a new range of power use in small two-wheeled and four-wheeled vehicles, boats, scooters, unmanned vehicles, and other utility vehicles [167-171].

### 1.13 Fuel Cells Fundamentals

To understand and quantify fuel cell performance, one must begin with the thermodynamic description of the fuel cell [3,154,157-171]. A fuel cell continuously produces electrical work and waste heat. The fuel cell can generate electricity continuously since it is an open system. The fuel cell is operated continuously for a given time period,  $\Delta t$ , during which reactants (fuel and oxidant) are added and products removed to maintain an electrical potential. If current is allowed to flow, a difference in electrical potential (also known as electrochemical overpotential) is maintained at the electrode interface through which charge transfer can occur. Charge carriers migrate across the cell when there is not equilibrium between the electrical and chemical potentials across the cell. The movement occurs from a higher to lower potential energy. Thus, the chemical affinity or change in Gibbs free energy of reaction drives an electric current. The change in Gibbs free energy of reaction is available at any instant to perform electrical work.

The Gibbs free energy,  $G$ , is defined to be [3,154]

$$G = E + PV - TS \quad (1.6)$$

where  $P$  = pressure,  $V$  = volume,  $T$  = temperature,  $E$  = energy, and  $S$  = entropy.

At constant pressure and temperature (usual conditions of an electrochemical reaction), the change in the Gibbs free energy for a reaction,  $\Delta G$  (J/mole) is

$$G = E + P V - T \Delta S \quad (1.7)$$

From the first law of thermodynamics, assuming the fuel cell is operated reversibly,

$$\Delta E = q + w = q + w_{\text{electrical}} + P \Delta V \quad (1.8)$$

where  $q$  = heat and  $w$  = work (J/mole). Thus, equating terms and simplifying,

$$\Delta G = q + w_{\text{electrical}} - T \Delta S \quad (1.9)$$

Again, assuming reversible operation of the fuel cell,

$$q = q_{\text{reversible}} = T \Delta S \quad (1.10)$$

Thus,

$$G = W_{\text{electrical}} \quad (1.11)$$

The change in Gibbs free energy of reaction (J/mole) is referenced to the amount of fuel. The electrical work (J) in an open system operated continuously over a given time period,  $\Delta t$ , where reactants (mole/s) are added and products removed to maintain the electrical potential are given for hydrogen–oxygen reaction by

$$m_{\text{H}_2} \Delta G \Delta t = m_{\text{H}_2} W_{\text{electrical}} \Delta t = W_{\text{electrical}} \quad (1.12)$$

where  $m_{\text{H}_2}$  = flow rate of hydrogen for the  $\text{H}_2/\text{O}_2$  reaction (mole/s) and  $\Delta t$  = operation time (s).

The average rate of work generation during the time interval,  $\Delta t$ , is the power (J/s).

One can mathematically demonstrate that for any direct anodic oxidation reaction for any fuel cell or hybrid system containing any fuel cell at any operating temperature and any pressure, the reversible work,  $W_{\text{electrical}}$ , (J/mole) is equal to the change in Gibbs free energy of reaction at the standard state (STP),  $\Delta G^0$  [172,173].

This reversible work is regarded as the maximum work. For the case of direct oxidation of hydrogen, one has

$$W_{\text{rev}} = m_{\text{H}_2\text{inlet}} W_{\text{rev}} = m_{\text{H}_2\text{inlet}} \Delta G^0 \Delta t \quad (1.13)$$

where  $m_{\text{H}_2\text{inlet}}$  = flow rate of hydrogen fuel into system.

Inerts and/or water are added to or are present in a reformat with the hydrogen entering the system. Exergy is a measure of heat quality or capability to do work. Exergetic efficiency,  $\zeta$ , is the ratio of actual electrical work and the reversible work:

$$\zeta = W_{\text{electrical}} / W_{\text{rev}} \quad (1.14)$$

Using Eq. (1.13), the actual or observed electrical work for direct oxidation of hydrogen, a fuel cell is given by

$$m_{\text{H}_2\text{utilized}} \Delta G_{\text{act}} \Delta t = W_{\text{electrical}} \quad (1.15)$$

where  $\Delta G_{\text{act}}$  = actual change in Gibbs free energy of reaction associated with the electrical work, J/mole,  $m_{\text{H}_2\text{utilized}}$  = flow rate of hydrogen utilized by fuel cell (moles/s) ( $m_{\text{H}_2\text{utilized}}$  equals the

amount in the fuel cell anode inlet;  $m_{H2anode}$  inlet; minus the amount in the anode outlet;  $m_{H2anode}$  outlet).

For reforming done prior to the system,  $m_{H2inlet} = m_{H2anode}$  inlet. Thus, from Eqs. (1.13), (1.14), and (1.15)

$$\zeta = (m_{H2utilized} \Delta G_{act} \Delta t) / m_{H2inlet} \Delta G^0 \Delta t = \mu_F \Delta G_{act} / \Delta G^0 \quad (1.16)$$

where fuel utilization ( $\mu_F$ ) is

$$\mu_F = m_{H2utilized} / m_{H2inlet} \quad (1.17)$$

Using Eq. (1.13) for the reversible work, one can calculate the maximum thermal efficiency (maximum work for given energy input) of a fuel cell or fuel cell hybrid (fuel cell and heat engine) system for the  $H_2$  oxidation reaction, where  $\Delta H^0$  is the reaction enthalpy for hydrogen direct oxidation (J/mole) at STP and where the inlet hydrogen is completely utilized in the fuel cell:

$$\eta_{th \max} = \Delta G^0 / \Delta H^0 \quad (1.18)$$

For the  $H_2$  oxidation reaction,  $\eta_{th \max}$  equals 0.83 (HHV) and 0.945 (LHV). One can also define a fuel cell intrinsic thermal efficiency at any temperature  $\eta_{int}(T)$  by  $\Delta G_{th}(T)/\Delta H^0$ . One can also define for the fuel cell an intrinsic exergetic efficiency at any temperature [172,173]:

$$\zeta_{int}(T) = \Delta G_{th}(T) / \Delta G^0 \quad (1.19)$$

$\Delta G_{th}(T)$  is defined as the free energy of the reaction, here the  $H_2$  oxidation reaction, at temperature,  $T$ , for unit concentrations of products and reactants.  $\Delta G_{th}(T)$  is associated with  $E^0(T)$ .  $\Delta G^0$  at STP with unit species concentrations is associated with  $E^0$ .

The actual thermal efficiency of the fuel cell is defined as the ratio of the work output to energy input, so we have

$$\eta = m_{H2utilized} \Delta G_{act} \Delta t / (m_{H2inlet} \Delta H^0 \Delta t) = \mu_F \Delta G_{act} / \Delta H^0 \quad (1.20)$$

It can be shown from Eqs. (1.16), (1.18), (1.19), and (1.20) that



$$\eta = \mu_F \Delta G_{act} / \Delta H^0 = \eta_{int}(T) \zeta / \zeta_{int}(T) = \zeta \eta_{th \max} \quad (1.21)$$

If one knows the reversible work which is a function of fuel, system components, and system structure, one can separate thermal efficiency into an exergetic component and a fuel component. Exergetic performance is determined by fuel cell performance which ultimately means fuel cell voltage. The link between the macroscopic thermodynamic parameters and fuel cell voltage can be developed as follows:  $W_{electrical}$  is also defined electrically as

$$W_{electrical} = -nFE \quad (1.22)$$

where  $n$  = mole,  $F$  = Faraday's constant (J/mole/volt),  $E$  = fuel cell voltage (volt).

In general, from Eqs. (1.12), (1.15), and (1.22)

$$m_{H_2} \Delta G \Delta t = W_{electrical} = -nFE \quad (1.23)$$

Since for the  $H_2$  direct oxidation reaction,

$$2 m_{H_2} \Delta t = n \quad (1.24)$$

then, in general

$$\Delta G = -2FE \quad (1.25)$$

Specifically, using Eq. (1.25),

$$\Delta G_{act} = -2FE, \quad (1.26)$$

And

$$\Delta G^0 = -2FE^0 \quad (1.27)$$

So

$$\zeta = m_{H_2 \text{ utilized}} \Delta G_{act} \Delta t / (m_{H_2 \text{ inlet}} \Delta G^0 \Delta t) = \mu_F (-2FE \Delta t) / (-2FE^0 \Delta t) = \mu_F E / E^0 \quad (1.28)$$

One of the central, steady-state fuel cell performance equations is thus given by

$$\zeta = \mu_F E / E^0 \quad (1.29)$$

and combining with Eq. (1.21), one has

$$\eta = \zeta \eta_{th \max} = \eta_{th \max} \mu_F E / E^0 \quad (1.30)$$

Exergetic efficiency and thermal efficiency are actually time-dependent functions describing the performance of the fuel cell at any time  $t$ .

These can be written as

$$\zeta(t) = \mu_F(t) E(t) / E^0 \quad (1.31)$$

and

$$\eta(t) = \zeta(t) \eta_{th \max} = \eta_{th \max} \mu_F(t) E(t) / E^0 \quad (1.32)$$

$DR_\zeta(t)$ , the exergetic efficiency rate of change, is a natural and instantaneous measure of the change in fuel cell performance occurring at any time  $t$ :

$$\partial (\zeta(t)) / \partial t = DR_\zeta(t) \quad (1.33)$$

It can be seen from Eqs. (1.31) and (1.32) that the rate of change in exergetic efficiency and rate of change of thermal efficiency are directly proportional.

Equation (1.33) is the second central equation for fuel cell performance since it is an equation that can be used in the assessment of degradation, generally defined as the change of area-specific resistance (ASR) with time [174].

### 1.13.1 Fuel Cell Operations

Fuel cells can be operated in a variety of modes, including constant fuel utilization, constant fuel flow rate, constant voltage, constant current, etc. For the case of constant  $m_F$  and constant  $E$ , from

Eq. (1.33),  $DR_z(t) = 0$ , in which case the fuel cell is operating at constant exergetic efficiency. This mode of operation is achieved by lowering the current by lowering the hydrogen flow rate as the fuel cell degrades. As can be seen from Eqs. (1.31) and (1.32), to operate at constant exergetic efficiency is to operate at constant thermal efficiency [3,160-174].

However, efficiency is not the only important performance measure. As the current is lowered at constant voltage operation, the fuel cell power density is decreasing. Below a certain level of power or power density, given by

$$P(t) = E(t) J(t) \quad (1.34)$$

It is no longer economical to operate a fuel cell or fuel cell system. Power is the third central equation for fuel cell performance. General expressions can be derived for fuel cell performance involving the variables  $E$ ,  $J$ ,  $mF$ , pressure, and fuel flow rate to explore the full envelope of fuel cell operation.

The actual fuel cell potential is decreased from its full potential, the Nernst potential, because of irreversible losses. Multiple phenomena contribute to irreversible losses in an actual fuel cell. For the hydrogen oxidation reaction, the functionality of fuel cell voltage,  $E$ , is typically given by [175-177]

$$E(T) = E_N(T) - LJ/A\sigma - R_{ohmic}J - \eta_{act}^a - \eta_{act}^c - \eta_{conc}^a - \eta_{conc}^c \quad (1.35)$$

$$E_N(T) = E_{H_2/O_2rxn}^0(T) + RT/2F \ln (P_{H_2(a)}P_{O_2(c)}^{1/2}/P_{H_2O(a)}) = \text{Nernst voltage} \quad (1.36)$$

where:  $F$  = Faraday's constant,  $J$  = appropriate current ( $A/cm^2$ ),  $s$  = electrolyte charge carrier conductivity ( $S/cm$ ),  $L$  = electrolyte thickness ( $cm$ ),  $A$  = fuel cell active area ( $cm^2$ ),  $\eta_{act}^a$  = activation polarisation for the anode,  $\eta_{act}^c$  = activation polarisation for the cathode,  $\eta_{conc}^a$  = concentration polarisation for the anode,  $\eta_{conc}^c$  = concentration polarisation for the cathode,  $R_{ohmic}$  = series ohmic resistance of all non-electrolyte fuel cell components,  $E_{H_2/O_2rxn}^0(T)$  = voltage at unit concentrations for  $H_2/O_2$  reaction at temperature  $T$ .

The six negative terms on the RHS of Eq. (1.35) are the usual definition of ASR. The comprehensive functionality of  $E$  and the more general definition of ASR have recently been developed for solid-state fuel cells with dense, mixed, ionic-electronic conducting electrolytes using the Wagner mass transfer model (MTM) [3,170-177]:

$$E = E_{\text{MTM}} (1 - (J_0^- - J_{\text{ext}})/J_0^-) - L J_0^- / A \sigma_0^- - R_{\text{ohmic}} J - \eta_{\text{act}}^a - \eta_{\text{act}}^c - \eta_{\text{conc}}^a - \eta_{\text{leakage}} \quad (1.37)$$

where  $R_{\text{ohmic}}$  = series ohmic resistance of all non-electrolyte fuel cell components, including interconnect, interlayers, and contact layers, which is multiplied by the appropriate current,  $J$ , for each type,  $J_0 = J_e$  and  $J_{\text{ext}}$  are the current terms from the Wagner MTM,  $(J_0^- - J_{\text{ext}})/J_0^-$  = the shorting ratio,  $\eta_{\text{leakage}}$  = fuel leakage polarisation,  $E_{\text{MTM}}$  (anode–electrolyte interface to cathode–electrolyte interface) is the reversible voltage in the Wagner MTM model.

The comprehensive model for solid-state fuel cells incorporates not only the typical definition of ASR, but also electronic shorting, leakage, and other current loss mechanisms. The first term on the RHS of Eq. (1.37) is not an ASR term. A general ASR definition for solid-state fuel cells can be defined as follows:

$$\text{ASR} = R_{\text{ionic}} + R_{\text{ohmic}} + (\eta_{\text{act}}^a + \eta_{\text{act}}^c + \eta_{\text{conc}}^a + \eta_{\text{conc}}^c)/J_0^- + R_{\text{leakage}} \quad (1.38)$$

where  $R_{\text{ionic}} = L/A\sigma_0$  = ionic resistance of electrolyte and  $R_{\text{leakage}} = \eta_{\text{leakage}}/J_{\text{leakage}}$  = resistance attributed to fuel leakage.

This definition of ASR is very general. However, when generalized, ASR and rate of change of ASR are not broad enough concepts to describe all the phenomena affecting fuel cell performance, such as electronic shorting.

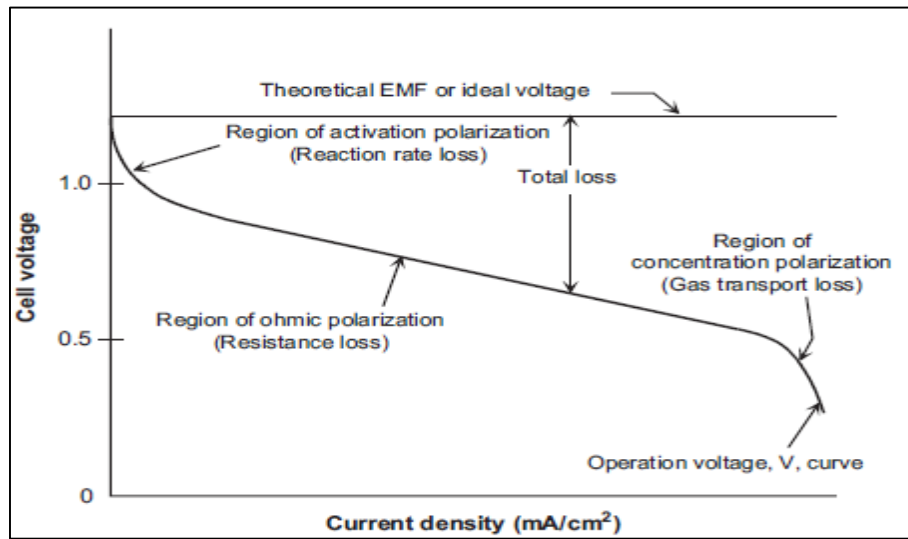


Fig. 1-16 Typical current voltage performance

The goal of a fuel cell should be to maximize exergetic or thermal efficiency and to minimize degradation while producing as much power as possible. These three goals can be achieved by improving the fuel cell design (more conductive electrolyte, better electrocatalysts, improvement in electrode structures, thinner cell components, etc.) [3,153] and/or by adjusting the operating conditions (e.g., higher temperature, higher gas pressure, and change in gas composition to lower the contaminant concentration).

As shown in Figure 1-16, the activation polarisation (reaction rate loss) is significant at lower current densities [3,153,158]. At this point, electronic barriers must be overcome prior to ion and current flow.

Ohmic polarisation (resistance loss) changes directly with current, increasing over the entire range of current because cell resistance remains essentially constant. Concentration polarization (gas transport loss) occurs over the entire range of current density, but they become significant at high limiting currents where it becomes difficult to provide enough reactant flow to the cell reaction sites.

Changing the cell operating parameters (pressure and temperature) can have an advantageous or a disadvantageous impact on fuel cell performance and compromises in the operating parameters are essential to meet the application requirements of lower system cost and acceptable cell life [3,158,170-177].

## **1.14 Characteristics and Features**

Fuel cells have many inherent advantages over conventional combustion-based systems, making them one of the strongest candidates to be the energy conversion device of the future (Fig. 1-17). They also have some inherent disadvantages that require further research and development to overcome them.

### **1.14.1 High Efficiency**

The amount of heat that could be converted to useful work in a heat engine is limited by the ideal reversible Carnot efficiency, given by the following equation:

$$\eta_{\text{Carnot}} = (T_i - T_e) / T_i \quad (1.39)$$

where  $T_i$  is the absolute temperature at the engine inlet and  $T_e$  is the absolute temperature at the engine exit.

However, a fuel cell is not limited by the Carnot efficiency since a fuel cell is an electrochemical device that undergoes isothermal oxidation instead of combustion oxidation. The maximum

conversion efficiency of a fuel cell is bounded by the chemical energy content of the fuel and is found by

$$\eta_{\text{rev}} = \Delta G_f / \Delta H_f \quad (1.40)$$

where  $\Delta G_f$  is the change in Gibbs free energy of formation during the reactions and  $\Delta H_f$  is the change in the enthalpy of formation (using lower heating value (LHV) or higher heating value (HHV)) [3,153,158-170].

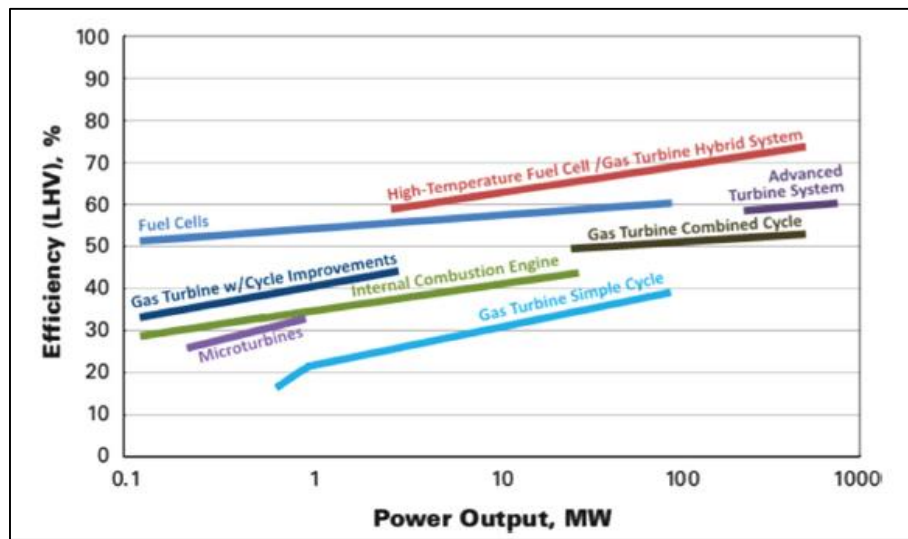


Fig.1-17 Efficiency comparison between fuel cells and other energy conversion devices with respect to system size

Figure 1-18 illustrates the thermodynamic efficiency for fuel cells and Carnot efficiency for heat engines [3]. In light vehicles, for instance, the efficiency of a fuel cell-powered car is nearly twice the efficiency of an internal combustion engine-powered car. The fact that the number of energy transformations that occur within a fuel cell stack is less than that of any combustion-based device, when the required output is electricity, plays a significant role. This is because losses are associated with each energy transformation process; thus, the overall efficiency of a system generally decreases as the number of energy transformations increases.

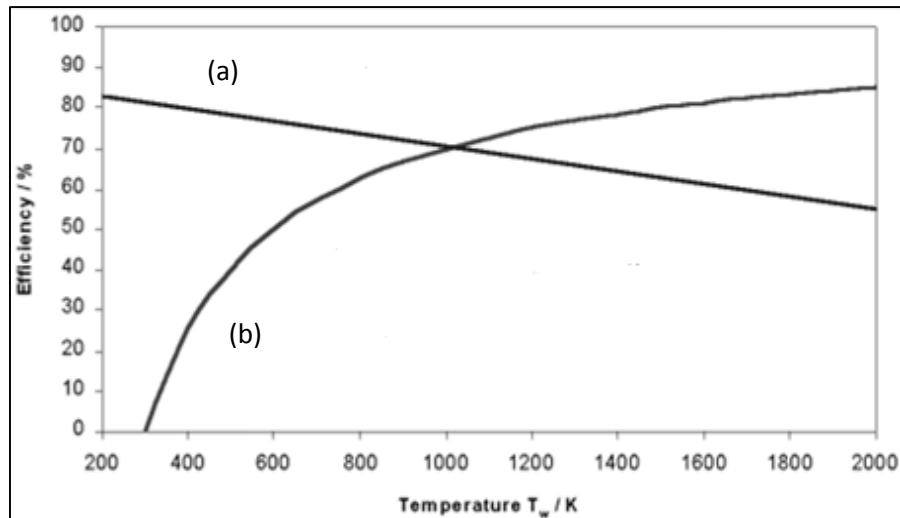


Fig.1-18 Thermodynamic efficiency for  $H_2/O_2$  fuel cells (a) and Carnot for heat engines (b)

### 1.14.2 Reduced Harmful Emissions

The only products from a fuel cell stack fuelled by hydrogen are water, heat, and DC electricity. And with the exception of controllable  $NO_x$  emissions from high-temperature fuel cells, a hydrogen fuel cell stack is emission-free. However, the clean nature of a fuel cell depends on the production path of its fuel.

For instance, the products of a complete fuel cell system that includes a fuel reformation stage include greenhouse emissions (e.g., CO and  $CO_2$ ). When the hydrogen supplied to the fuel cell is pure (i.e., not reformation-based hydrogen which is always contaminated with  $CO_x$ ), the durability and reliability of the fuel cell significantly improve in comparison to when we run the fuel cell on reformation-based hydrogen. This is one of the most important advantages of fuel cells in comparison to heat engines, i.e., fuel cells are inherently clean energy converters that ideally run on pure hydrogen. This fact is actually pressingly driving researchers and the industry to develop efficient and renewable-based hydrogen generation technologies based on clean water electrolysis to replace the conventional reformation-based ones. Systems that integrate renewable-based hydrogen generation with fuel cells are genuinely clean energy generation and conversion systems that resemble what the energy industry is striving to achieve. It is worth mentioning that when we take into consideration the emissions from the fossil fuel reformation process, some heat engine systems appear to be less polluting than fuel cell systems [178,179]. For non-renewable energy-based water electrolysis, the emissions and energy used for the electrolysis process make it more harmful to the environment than conventional combustion heat engines. Moreover, it is economically unfeasible since any fossil energy used for hydrogen production is going to be always more than the energy content of hydrogen. According to the studies by Argonne National Laboratory [180], 3,000,000–3,500,000 BTUs of fossil energy are used for the production of

1,000,000 BTUs of hydrogen through fossil energy-based water electrolysis. This only stresses the significance of the aforementioned conclusions regarding using renewable-based water electrolysis for hydrogen production [181].

### **1.14.3 Modularity**

Fuel cells have excellent modularity. In principle, changing the number of cells-per-stack and/or stacks-per-system allows us to control the power output of any fuel cell system. Unlike combustion-based devices, a fuel cell's efficiency does not vary much with system size or load factor. In fact, as opposed to conventional power plants, fuel cells have higher efficiencies at part loads compared to full loads. This would prove advantageous in large-scale fuel cell systems that would normally run on part load instead of full load. Additionally, the high modularity of fuel cells means that smaller fuel cell systems have similar efficiencies to larger systems. This feature greatly facilitates the future integration of fuel cells (and hydrogen systems in general) in small-scale distributed generation systems, which hold a great potential in the power generation industry. It is worth noting, however, that reformation processors are not as modular as fuel cell stacks. This presents another reason to shift to renewable-based hydrogen production technology.

### **1.14.4 Fuel Flexibility and Applications**

Fuel cells have diverse applications ranging from micro-fuel cells with less than 1 W power outputs to multi-MW prime power generation plants. This is attributed to their modularity, static nature, and variety of fuel cell types. This qualifies fuel cells to replace batteries used in consumer electronics and auxiliary vehicular power. These same properties also qualify a fuel cell to replace heat engines used in transportation and power generation. Fuel cells are also highly integrable to most renewable power generation technologies. Fuel cells that operate on low-temperature ranges require short warm-up times, which is important for portable and emergency power applications.

While for fuel cells that operate on medium-to-high temperature ranges, utilization of waste heat both increases the overall efficiency of the system and provides an additional form of power output useful for domestic hot water and space heating residential applications or CHP industrial-level applications. Fuels for a reformation-based fuel cell system include methanol, methane, and hydrocarbons such as natural gas and propane. These fuels are converted into hydrogen through a fuel reformation process. Alternatively, direct alcohol fuel cells (e.g., direct methanol fuel cells) can run directly on an alcohol. And even though fuel cells run best on hydrogen generated from water electrolysis, a fuel cell system with natural gas reformation also possesses favorable features to conventional technologies [3,153,156].



Fuel cells have been rapidly developing during the past 20 years due to the revived interest in them that started during the 1990s. However, they are still not at the widespread-commercialization stage due to many technical and sociopolitical factors, with cost and durability being the main hurdles that prevent fuel cells from becoming economically competitive in the energy market.

### 1.15 Fuel Cells Types

Fuel cells can be designed in various ways including many geometries, planar, tubular, radial, etc., and using many fuels and electrolyte charge carriers. Distinction of fuel cell types begins with the type of electrolyte used in the cells, the charge carrier, and the operating temperature. Low-temperature fuel cells (Proton Exchange Membrane FC, Alkaline FC, and Phosphoric Acid FC) require noble metal electrocatalysts to achieve practical reaction rates at the anode and cathode, and H<sub>2</sub> is the only acceptable fuel for the PEMFC. With high-temperature fuel cells (Molten Carbonate FC and Solid Oxide FC), the requirements for catalysis are relaxed, and the number of potential fuels expands. Other types of fuel cells are not addressed here, such as biological and enzymatic fuel cells. For example, carbon monoxide “poisons” a noble metal anode catalyst such as platinum in low-temperature fuel cells, but it competes with H<sub>2</sub> as a reactant in high-temperature fuel cells where non-noble metal catalysts such as nickel can be used.

The operating temperature and required useful life of a fuel cell dictate the physicochemical and thermomechanical properties of materials used in the cell components (e.g., electrolyte, electrodes, and interconnect) [3,153].

Fuel cell	Cell voltage	Start up time	Power density (W/m <sup>2</sup> )	Temperature (°C)
PEMFC	0.7-0.8	Seconds	3.8-6.5	60-100
AFC	1.0	Seconds	1.0	100-250
PAFC	1.0	Few minutes	0.8-1.9	150-250
MCFC	0.7-1.0	Few minutes	1.5-2.6	500-700
SOFC	0.8-1.0	Few minutes	0-0.15	700-1000
DMFC	0.2-0.4	Few seconds	1.0-2.0	60-200

Table 1-3 Comparison of FCs with their performance parameters

Aqueous electrolytes are limited to temperatures of >200 °C because of their high water vapour pressure and/or rapid degradation at higher temperatures. The operating temperature also determines the type of fuel that can be used in a fuel cell. The low-temperature fuel cells with aqueous electrolytes are, in most practical applications, restricted to H<sub>2</sub> as a fuel. In high

temperature fuel cells, CO and even CH<sub>4</sub> can be used because of the inherently rapid electrode kinetics and the lesser need for high catalytic activity at high temperature.

Table 1-3 summarizes the main differences between the most common fuel cell types [3]

### 1.15.1 Proton Exchange Membrane Fuel Cell (PEMFC)

Proton exchange membrane fuel cells (PEMFC) are believed to be the best type of fuel cell as the vehicular power source to eventually replace the gasoline and diesel internal combustion engines. PEMFCs are currently being developed and demonstrated for systems ranging from 1 W to 2 kW.

PEM fuel cells use a solid polymer membrane (a thin plastic film) as the electrolyte. The standard electrolyte material currently used in PEM fuel cells is a fully fluorinated Teflon-based material produced by DuPont for space applications in the 1960s. The DuPont electrolytes have the generic brand name Nafion, and the types used most frequently are 113, 115, and 117 [182-189]. The Nafion membranes are fully fluorinated polymers that have very high chemical and thermal stability. This polymer is permeable to protons when it is saturated with water, but it does not conduct electrons.

The fuel for the PEMFC is hydrogen and the charge carrier is the hydrogen ion (proton).

The best catalyst for both the anode and cathode is platinum. This catalyst was used at a content of 28 mg/cm<sup>2</sup> of Pt. Due to the high cost of Pt in recent years the usage has been reduced to around 0.2 mg/cm<sup>2</sup>, yet with power increasing [3,182]. Platinum is dispersed on porous and conductive material, such as carbon cloth or carbon paper. PTEF will often be added also, because it is hydrophobic and so will expel the product water to the surface from where it can evaporate [153, 182-189].

At the anode, the hydrogen molecule is split into hydrogen ions (protons) and electrons. The hydrogen ions permeate across the electrolyte to the cathode while the electrons flow through an external circuit and produce electric power. Oxygen, usually in the form of air, is supplied to the cathode and combines with the electrons and the hydrogen ions to produce water. The reactions at the electrodes are as follows:



Compared to other types of fuel cells, PEMFCs generate more power for a given volume or weight of fuel cell [183-188]. This high-power density characteristic makes them compact and lightweight. In addition, the operating temperature is less than 100 °C, which allows rapid start-up. These traits and the ability to rapidly change power output are some of the characteristics that make the PEMFC the top candidate for automotive power applications [183-188].



Fig.1-19 Toyota Mirai equipped with PEMFC stack

Other advantages result from the electrolyte being a solid material, compared to a liquid. The sealing of the anode and cathode gases is simpler with a solid electrolyte, and therefore, less expensive to manufacture. The solid electrolyte is also more immune to difficulties with orientation and has less problems with corrosion, compared to many of the other electrolytes, thus leading to a longer cell and stack life.

One of the disadvantages of the PEMFC for some applications is that the operating temperature is low. Temperatures near 100 °C are not high enough to perform useful cogeneration. Also, since the electrolyte is required to be saturated with water to operate optimally, careful control of the moisture of the anode and cathode streams is important.

### 1.15.2 Alkaline Fuel Cell (AFC)

Alkaline fuel cells (AFCs) have been used by NASA on space missions and can achieve power-generating efficiencies of up to 70 % [3,182,190-192]. The operating temperature of these cells range between room temperature to 250 °C. The electrolyte is aqueous solution of alkaline potassium hydroxide (30–75 wt %) soaked in a matrix [182]. (This is advantageous because the cathode reaction is faster in the alkaline electrolyte, which means higher performance).

Several companies are examining ways to reduce costs and improve operating flexibility. AFCs typically have a cell output from 300 W to 5 kW [191]. The chemical reactions that occur in this cell are as follows:



Another advantage of AFCs are the materials such as the electrolyte and catalyst used are low cost [190,191]. The catalyst layer can use either platinum or non-precious metal catalysts such as nickel [193-195]. Successful achieving of very active and porous form of a metal which has been used for alkaline fuel cells from the 1960s to the present, is the use of Raney metals.

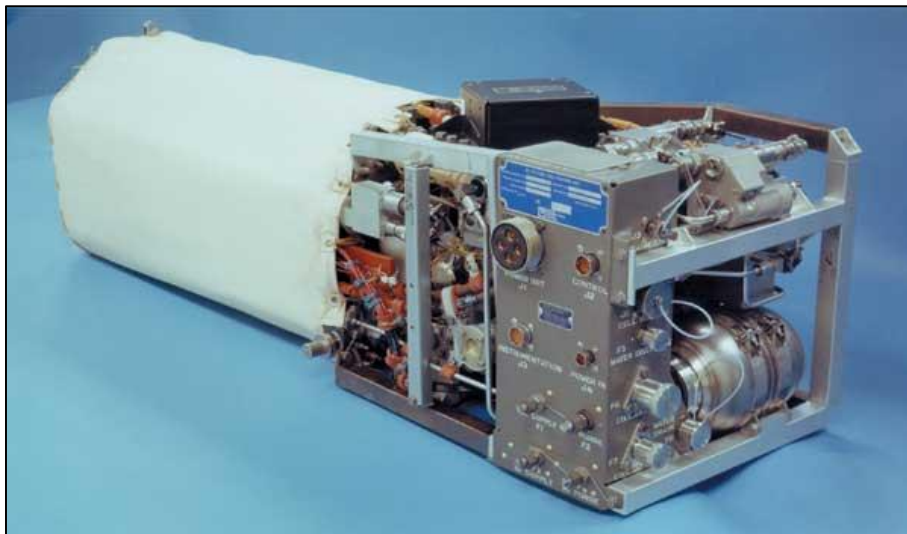


Fig.1-20 Alkaline cell used by NASA in the Apollo mission

These are prepared by mixing the active metal (Ni) with an inactive metal, usually aluminum. The mixture is then treated with a strong alkali that dissolves out the aluminum. This leads a porous material, with very high surface area [3,182]. A disadvantage of AFCs is that pure hydrogen and oxygen have to be fed into the fuel cell because it cannot tolerate the small amount of carbon dioxide from the atmosphere.

Over time, carbon dioxide degrades the KOH electrolyte which can lead to significant issues. Two commonly used solutions are refreshing the KOH electrolyte or carbon dioxide scrubbers. Due to these limitations, AFCs are not used for many power applications.

### 1.15.3 Phosphoric Acid Fuel Cells (PAFC)

PAFCs are very efficient fuel cells, generating electricity at more than 50 % efficiency [182]. About 85 % of the steam produced by the PAFC is used for cogeneration. This efficiency may be compared to about 35 % for the utility power grid in the United States. As with the PEMFC Pt or Pt alloys are used as catalysts at both electrodes [196]. The electrolyte is inorganic acid, concentrated phosphoric acid (100 %) which will conduct protons [197-199]. Operating temperatures are in the range of 150–220 °C. At lower temperatures, PAFC is a poor ionic conductor, and carbon monoxide (CO) poisoning of the platinum catalyst in the anode can become severe [76, 80, 81]. Two main advantages of the phosphoric acid fuel cell include a cogeneration efficiency of nearly 85 % and its ability to use impure hydrogen as fuel. PAFCs can tolerate a carbon monoxide concentration of about 1.5 % which increases the number of fuel types that can be used.

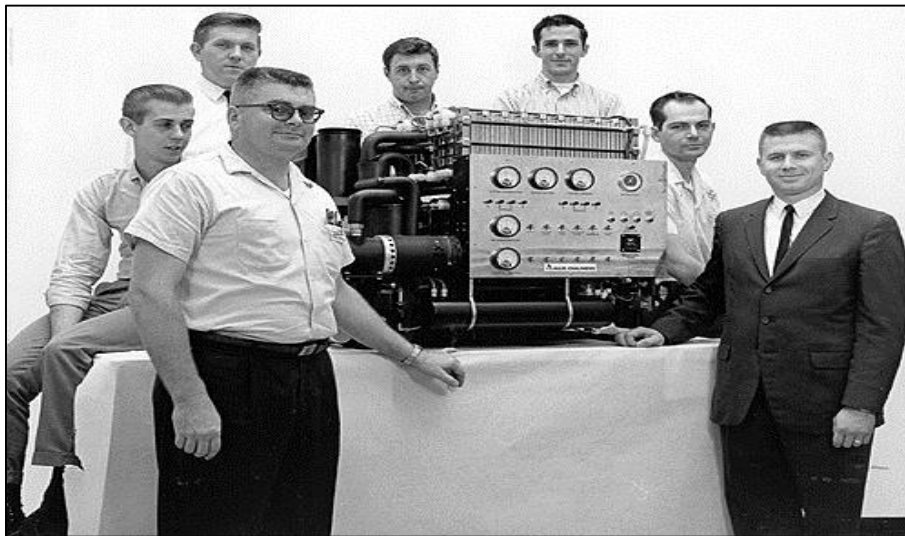


Fig.1-21 PAFC stack developed in 1965 by U.S.A. army scientists

Disadvantages of PAFCs include their use of platinum as a catalyst (like most other fuel cells) and their large size and weight. PAFCs also generate low current and power comparable to other types of fuel cells [3,182].

Phosphoric acid fuel cells are the most mature fuel cell technology. The commercialization of these cells was brought about through the Department of Energy (DOE) and ONSI (which is now United

Technologies Company (UTC) Fuel Cells) and organizational linkages with Gas Research Institute (GRI), electronic utilities, energy service companies, and user groups.

The chemical reactions for PAFCs are as follows:

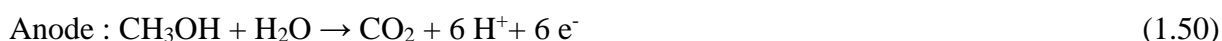


#### 1.15.4 Direct Methanol Fuel Cells (DMFC)

A Direct Methanol Fuel Cell (DMFC) works creating an electric potential by the reaction between methanol and oxygen, specifically it produces electricity through an electrochemical process without combustion and without the need for a reformer system for the fuel [200].

The electric potential is created using a polymeric membrane that is selective to certain chemical molecules, in this case the membrane allows the passage of  $\text{H}^+$  ions (proton conductivity). On one side of the membrane, an aqueous solution of methanol with  $\text{CH}_3\text{OH}$  concentration of around 1 M (3 wt%) is feed to the anode catalyst where the catalytic decomposition of methanol molecules producing  $\text{CO}_2$  and  $\text{H}_2$  is oxidized to  $\text{H}^+$  ions at the anode [182]. The protons produced can migrate to the cathode of the cell through the membrane where the electrons produced to the anode, passing through an external circuit, reduce the oxygen that is plugged in, allowing the formation of water.

The reactions occurring in the DMFC are as follows:



Because none of the methanol oxidation reaction proceeds as readily as the oxidation of hydrogen, there are considerable activation overvoltages at the fuel anode, as well as at the cathode in the DMFC. This is the main cause for the lower performance. Much work has been done to develop suitable catalysts for the anode of the DMFC. It is usually used as mixture of Pt and Ru in equal proportions. Other bimetal catalysts have been tried but this 50:50 Pt/Ru combination seems to

guarantee the best performances [182, 200-202]. The cathode reaction in the DMFC is the same as that for the hydrogen fuel cells with acid electrolyte, so the same catalyst is used. There is no advantage in using the more expensive Pt/Ru bimetal catalyst used on the anode [182, 200-202].



Fig.1-22 DMFC for smartphone recharge supplied by Toshiba (2009)

The research and development of novel proton exchange membranes (PEMs) is known to be one of the most challenging issues regarding the direct methanol fuel cell technology [203-205]. The PEM is usually designated as the heart of the DMFC, and should ideally combine high proton conductivity (electrolyte properties) with low permeability toward DMFC species. Additionally, it should have a very high chemical and thermal stability in order to enable the DMFC operation at up to 150 °C. For this reason, a variety of PEMs have been developed by various researchers using different preparation methods [203-206].

The different companies producing polymer electrolyte membranes have their specific patents. However, a common theme is the use of a sulphonated fluoropolymers, usually fluoroethylene. The most well known and well established of these is Nafion (®Dupont), which has been developed through several variants since 1960s.

#### **1.15.5 Molten Carbonate Fuel Cell (MCFC)**

The electrolyte in the molten carbonate fuel cell uses a liquid solution of lithium, sodium, and/or potassium carbonates, soaked in a matrix. MCFCs have high fuel-to-electricity efficiencies ranging from 60 to 85 % with cogeneration, and operate at about 620–660 °C [207-209]. The high operating temperature is an advantage because it enables a higher efficiency and the flexibility to use more



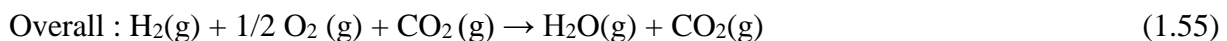
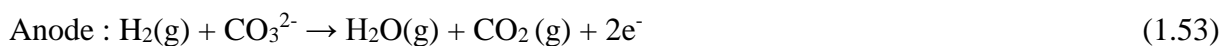
types of fuels and inexpensive catalysts. This high operating temperature is needed to achieve sufficient conductivity of the electrolyte [182,207,208].

Molten carbonate fuel cells can use hydrogen, carbon monoxide, natural gas, propane, landfill gas, marine diesel, and coal gasification products as the fuel. MCFCs producing 10 kW to 2 MW MCFCs have been tested with a variety of fuels and are primarily targeted to electric utility applications. MCFCs for stationary applications have been successfully demonstrated in several locations through-out the world.



Fig.1-23 MCFC stack DFC 300 for stationary energy production (Supplier: Fuel Cell Energy)

The reactions at the anode, cathode, and the overall reaction for the MCFC are



The high operative temperatures and the electrolyte chemistry can be responsible of some issues. The high temperature requires significant time to reach operating conditions and responds slowly to changing power demands. These characteristics make MCFCs more suitable for constant power applications. The carbonate electrolyte can also cause electrode corrosion problems [210,211]. Furthermore, since  $\text{CO}_2$  is consumed at the anode and transferred to the cathode, introduction of



CO<sub>2</sub> and its control in air stream becomes an issue for achieving optimum performance that is not present in any other fuel cell [182].

The history of Molten Carbonate Fuel Cell (MCFC) can be traced back to the late nineteenth century when W.W. Jacques had produced his carbon–air fuel cell, a device for producing “electricity from coal.” This device used an electrolyte of molten potassium hydroxide at 400–500 °C in an iron pot [212]. Jacques suggested to replace molten alkali electrolytes with molten salts such as carbonates, silicates, and borates.

By the 1930s Davtyan proposed a baked mixture of 43 % calcined Na<sub>2</sub>CO<sub>3</sub>, 27 % monazite sand (a mixture of rare earth oxides), 20 % WO<sub>3</sub>, and 10 % soda glass [213]. By treatment at 850 °C a mixture containing Na<sub>3</sub>PO<sub>4</sub>, Na<sub>2</sub>CO<sub>3</sub>, Na<sub>2</sub>WO<sub>4</sub>, Na<sub>2</sub>SiO<sub>3</sub>, and oxides of CeO<sub>2</sub>, La<sub>2</sub>O<sub>3</sub>, and ThO<sub>2</sub> was obtained [213]. The mixture was constituted by a porous framework of high-melting rare earth oxides in which was constrained a eutectic mixture of molten carbonates, phosphates, tungstates, and silicates. The eutectic mixture provided the means of ionic conduction.

The works of Broers and Ketelaar [213] established that molten carbonates as the preferred electrolyte for carbon containing fuels, since other molten salts tested were decomposed by steam produced at the anode of the fuel cell. Broers and Ketelaar [213] proposed a mixture of lithium, sodium, and/or potassium carbonates impregnated into a porous disk of magnesium oxide. Using carbonates there was no problem in replacing CO<sub>2</sub> at the cathode, which was effectively transferred through the molten electrolyte to the anode.

There was a general decline in interest in MCFCs during the 1970s but by the mid-1980s R&D the interest for MCFC has growth mainly in Japan and Europe [182, 213].

In recent years, MCFC development has been focused mainly on large-scale stationary and marine applications, where the relatively large size and weight of the MCFC and slow start-up time are not a problem. Molten carbonate fuel cells are under development for use with a wide range of conventional and renewable fuels.

The modern MCFC system has a high efficiency typically above 50 % and very low emissions. Since it operates at high temperature (about 650 °C) it can be used for cogeneration, combined heat and power, and distributed electricity generation. Most applications have so far been for stationary plants in hospitals, hotels, and resorts where the fuel is natural gas. The MCFC has been demonstrated to run on propane, coal gas, and anaerobic digester gas [3,182]. Plants have been published for integrated coal gasifier/MCFC systems.

### 1.15.5.1 Components of the Molten Carbonate Fuel Cells

#### *Materials*

The heart of the molten carbonate fuel cell (MCFC) is the electrolyte, which is an ion-conducting molten salt [3,182,200-213]. This is typically a mixture of two or three alkali metal lithium, potassium, or sodium carbonates. The mixture is solid at room temperature but about 400 °C and above it becomes molten and is able to conduct carbonate ( $\text{CO}_3^{2-}$ ) ions. The molten carbonate in an MCFC is constrained within a porous solid material named electrolyte matrix. An important feature of the electrolyte matrix is the chemical stability toward the molten salt that penetrates in the matrix framework and many efforts have been done in the last 20–30 years for the development of new materials [207,212]. Alumina can be used as an MCFC matrix since it can be obtained by simple coprecipitation from an aqueous solution of aluminum nitrate, and can be made into a thin sheet. The so obtained  $\gamma$ -alumina, changes phase to more stable  $\alpha$ -form at high temperatures (1200 °C). For this reason, the long-term stability of the matrix could be an issue and has been investigated [101–105]. In particular lithium from the electrolyte will react over time with the alumina to form lithium aluminate ( $\text{LiAlO}_2$ ), which also exists in two interchangeable  $\alpha$  and  $\gamma$  phases: above 700 °C,  $\gamma$ - $\text{LiAlO}_2$  appears to be the more stable form, at 600–650 °C, the  $\alpha$  form is more stable. The industry is directed to the use of  $\alpha$ - $\text{LiAlO}_2$  for long-term stability [182].

The powdered matrix material is mixed with a binder to obtain sheets of 100–300 mm thickness. The carbonate electrolyte is also manufactured as similar thin sheets: cells are usually made by a sandwich of electrolyte and matrix sheets. The stacks are assembled by building up layers of cells inserting current collectors and separator plates between one cell and the next. Once the cell or stack is assembled and mechanically clamped together, it is slowly heated up to above the melting temperature of the electrolyte. Once the electrolyte melts, it penetrates into the pores of the matrix. Materials of anode and cathode of the MCFC are typically porous nickel and nickel oxide, respectively, in form of thin sheets [213].

#### *Electrolyte*

State-of-the-art MCFC electrolytes contain typically 60 wt % carbonate constrained in a matrix of 40 wt %  $\text{Li-AlO}_2$ . The  $\alpha$  form of  $\text{Li-AlO}_2$  is the most stable in the MCFC electrolyte at low temperatures and is used in the form of fibres of 0.1 mm diameter. Other materials (e.g., larger size particles of  $\text{Li-AlO}_2$ ) may be added and many details are proprietary [3,182].

The ohmic resistance of the MCFC electrolyte has an important and large effect on the operating voltage compared with most other fuel cells. Under typical MCFC operating conditions, it has been established that the electrolyte matrix contributes some 70 % of the ohmic losses. There is a direct relationship between the thickness of the electrolyte layer and the ionic conductivity. The thinner

the electrolyte, the lower the ohmic resistance, and electrolyte matrices 0.2–0.5 mm in thickness can give better performances. However thicker materials are more stable, so low resistance and long-term stability must be optimized. For the MCFCs the typical power density at 650 °C is 0.16 Wcm<sup>2</sup>[3,182].

It has been found that for the carbonates, a eutectic mixture of lithium and potassium carbonates Li<sub>2</sub>CO<sub>3</sub>-K<sub>2</sub>CO<sub>3</sub> (62:38 mol %) is good for atmospheric pressure operation, whereas the lithium and sodium carbonate mixture Li<sub>2</sub>CO<sub>3</sub>-Na<sub>2</sub>CO<sub>3</sub> (60:40 mol %) is better for improved cathode stability when the cell is operated at elevated pressure [3,182,214-216].

An important difference between MCFC and other fuel cells is the conditioning of the electrolyte that is carried out once the stack is assembled. Layers of electrodes, electrolyte and matrix, and the various nonporous components are assembled together, and the stack is heated slowly. As the carbonate reaches its melt temperature (over 450 °C), it is absorbed into the ceramic matrix. This process can lead to some shrinkage of the components, and it is needed to pay attention to the mechanical design of the stack. An MCFC stack typically takes 14 h or more to reach the operating temperature. Another important aspect is that every time the MCFC stack is heated and cooled through the electrolyte melt temperature, stresses are set up, which can lead to cracking of the electrolyte matrix and permanent cell damage caused by fuel crossover. Thermal cycling of MCFC stacks is therefore best avoided and MCFC systems are ideally suited to applications that need a continuous power supply.

#### *Anode*

Because the anode reaction is relatively fast at MCFC temperatures, a high surface area anode catalyst is not required [3,182, 217-220]. State-of-the-art anodes are made of a sintered Ni–Cr/Ni–Al alloy with a thickness of 0.4–0.8 mm and porosity of 55–75 %. Fabrication is carried out usually by tape casting a slurry of the powdered material, which is subsequently sintered. Chromium is added to the basic nickel component to reduce the nickel sintering that could give rise to a decay in the MCFC, performances. However, chromium can react with lithium of the electrolyte causing some loss of electrolyte. Addition of aluminum can improve both creep resistance in the anode and electrolyte loss due to the formation of LiAlO<sub>2</sub> within the nickel particles. Ni–Cr/Ni–Al alloy are well established materials for the anodes, however nowadays the research is addressed to obtain new and less expensive materials. Moreover, many efforts are addressed toward sulphur resistance materials such as LiFeO<sub>2</sub>.

#### *Cathode*

One of the major problems with the MCFC is that the state-of-the-art nickel oxide cathode material shows a weak, but significant, solubility in molten carbonates [3,182]. Through dissolution, some

$\text{Ni}^{2+}$  ions are formed in the electrolyte and diffuse toward the anode, leading to precipitation of metallic nickel dendrites. This precipitation can cause internal short circuits with subsequent loss of power. It has been reported [3,182] that solubility is reduced if the more basic, carbonates are used in the electrolyte. The addition of some alkaline earth oxides (CaO, SrO, and BaO) to the electrolyte has also been found to be beneficial [182].

With state-of-the-art nickel oxide cathodes, nickel dissolution can be minimized by (1) using a basic carbonate, (2) operating at atmospheric pressure and keeping the  $\text{CO}_2$  partial pressure in the cathode compartment low, and (3) using a relatively thick electrolyte matrix to increase the  $\text{Ni}^{2+}$  diffusion path. By these means, cell lifetimes of 40,000 h have been demonstrated under atmospheric pressure conditions. For operation at higher pressure, alternative cathode materials such as  $\text{LiCoO}_2$  have been investigated. This has a dissolution rate in molten carbonate an order of magnitude lower than that of NiO at atmospheric pressure. Dissolution of  $\text{LiCoO}_2$  also shows a lower dependency on the partial pressure of  $\text{CO}_2$  than NiO.

#### 1.15.5.2 Cell Configuration

MCFC can have different configurations depending on the flows of fuel and oxidant streams. Fuel and oxidant that flow on opposite sides of each cell can be flowing in the same direction from inlet to outlet (coflow), in opposite directions (counterflow), or at  $90^\circ$  to each other (crossflow) [3,182,221-225].

If the gases supplied to the cells are connected manifold externally to the stack, then the crossflow configuration is the only option and gas inlets and outlets for the fuel and oxidant can be located on the four sides of the stack. Figure 1.24 shows the cross-flow configuration adopted by CFC Solutions.

Cross-flow has many advantages: it allows a homogeneous reactant distribution to the cell, a uniform fuel utilization over the cell, a low pressure drops through the gas channels. Moreover, simple and less expensive separator plates than other configurations can be employed.

However, the significant disadvantages of large temperature profiles across the face of the electrodes and gas leakage and migration (ion pumping) of the electrolyte must be taken into account [224,225].

If internal manifolding is applied, then co-flow or counterflow can be configured [182,224,225]. With co-flow, the concentrations of reactants on both sides of the cells are highest at the inlet and decrease toward the outlet. Concentrations of products increase toward each outlet. Co-flow produces a larger temperature gradient across the cell than counterflow, especially when internal

reforming is applied. With internal reforming, counterflow is normally the best option and results in the best distribution of current density and temperature throughout the cell.

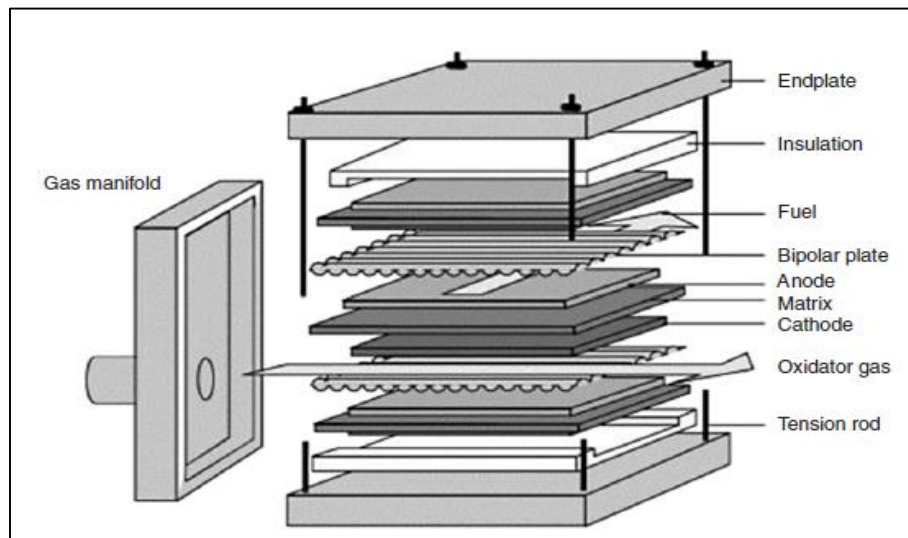
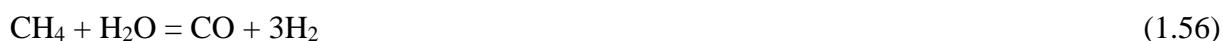


Fig. 1-25 Configuration of MCFC [13]

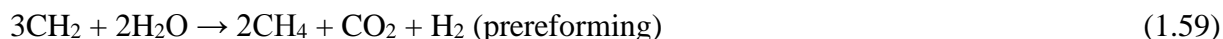
The operating temperature of the MCFC of around 650 °C provides ideal opportunities from a system design perspective. At these temperatures with a suitable catalyst, internal reforming can be carried out. Most available fuels, such as natural gas, liquefied petroleum gas, and biogas, need to be reformed to a hydrogen-rich gas for the fuel cell. This can be done external to the cell or stack but by carrying out the endothermic reforming reactions inside the MCFC (internal reforming), advantage is taken of the reaction to provide cell or stack cooling [3,182].

### 1.15.5.3 Steam Reforming

Methane reforming Eq. (1.56) is the simplest example of steam reforming (SR). This reaction is endothermic at MCFC temperatures and over an active solid catalyst the product of the reaction in a conventional reforming reactor is dictated by the equilibrium of Eq. (1.56) and the water gas shift (WGS) reaction Eq. (1.57). This means that the product gas from a reformer depends only by the inlet steam/methane ratio (or more generally steam/carbon ratio) and the reaction temperature and pressure. Similar reaction can be written for other hydrocarbons such as natural gas, naphtha, purified gasoline, and diesel. In the case of reforming oxygenates such as ethanol [226,227], the situation is in some way more complex, as other side reactions can occur. With simple hydrocarbons, like as methane, the formation of carbon by pyrolysis of the hydrocarbon or decomposition of carbon monoxide via the Boudouard reaction Eq. (1.58) is the only unwanted product.



In the MCFC carbon formation can be avoided by carrying out some degree of pre-reforming externally to the fuel cell stack. Pre-reforming consists of vaporizing the fuel and passing this with steam over a suitable catalyst. It converts high-molecular-weight hydrocarbons to methane, thereby reducing the risk that they pyrolyze or decompose to carbon in the MCFC stack [3,182]. Moreover, in this way some hydrogen is present at the inlet of the fuel cell. If excess steam is used carbon monoxide decomposition is avoided due the Boudouard equilibrium. A hydrocarbon fuel such as diesel may be represented by the empirical formula  $\text{CH}_2$  and pre-reforming of this fuel may be represented as



Pre-reforming is usually carried out at modest temperatures (i.e., 320 °C) over a supported nickel catalyst in an adiabatic reactor [182].

Any fuel, including gases produced by the gasification of coal, wood waste, or other organic waste or biogas from digesters, that is fed to either the anode compartment directly or to an external reformer or pre-reformer must contain low sulphur to avoid poisoning of the reforming or pre-reforming catalyst [3,182].

#### **1.15.5.4 MCFC Internal Reforming and Steam Reforming Catalyst**

One of the advantages of the MCFC over low-temperature fuel cells is the ability to internally convert fuels such as methane or natural gas directly into hydrogen via internal steam reforming [3,182]. The reforming reaction is endothermic, therefore by cooling the stack can reduce the heat that is removed out of the stack in the cathode exhaust stream. So the flow of air to the cathode (which normally provides the cooling for the stack) can be reduced. In this way the  $\text{CO}_2$  partial pressure through the cathode compartment is raised, leading to a higher cell voltage, moreover it reduces the parasitic electrical load on the system related the cathode air compressor. For these

reasons an internal reforming MCFC system has a higher efficiency than an external reforming system.

There are two approaches to internal reforming. Indirect internal reforming (IIR): the reforming reaction takes place in channels or compartments within the stack that are adjacent to the anode compartments, the heat generated in the cell is transferred to the reforming channels, and the product from the reforming is fed to the anode channels.

In direct internal reforming (DIR) the reforming reaction is carried out on the fuel cell anode itself (or as close to it as possible); in this way hydrogen produced by reforming is immediately consumed by the electrochemical cell reaction allowing to shift the equilibrium of the reforming and WGS reactions to the right as product is consumed by the electrochemical reaction [3,182]. The DIR approach is best carried out at low pressures with catalyst inside the anode compartment close to the anode of the cell.

In the IIR configuration, commercial reforming catalyst (e.g., nickel/alumina) exhibits little deactivation because the cell temperature is generally much lower than in a conventional reforming plant (usually above 800 °C) [3,182]. The stability of a DIR catalyst, however, is strongly affected by the anode environment. Conventional catalysts decay usually via two mechanisms-sintering of the metal particles or support leading to a loss of catalytic surface area, or poisoning of catalyst active sites by sulphur [3,182].

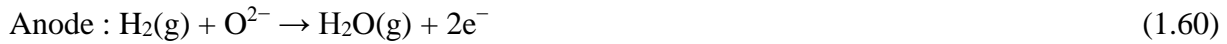
Carbonate retention has been the biggest issue for MCFC developers. There are two mechanisms for loss of carbonate from the cells, namely, creepage and loss by vapor phase transport [3,182].

Steam reforming of ethanol has been demonstrated in the MCFC and proceeds rather differently to the reforming of hydrocarbons [3,182]. Rinaldi et al. [222] studied ethanol reforming over supported metal catalyst (nickel on doped magnesium oxide). They concluded that acetaldehyde is the main unwanted product. Further catalyst optimization may improve the selectivity in the MCFC. Some tests have been carried out recently with catalysts of titanium dioxide promoted with lanthanum or samarium oxides [182].

#### **1.15.6 Solid Oxide Fuel Cell (SOFC)**

The SOFC is a complete solid-state device that uses an oxide ion-conducting ceramic material as the electrolyte. The electrolyte is a nonporous solid, such as Y<sub>2</sub>O<sub>3</sub> stabilized ZrO<sub>2</sub> with conductivity-based oxygen ions [3,182,223,224]. Yttria-stabilized zirconia (YSZ) is the most commonly used material for the electrolyte. It was first used as a fuel cell electrolyte by Baur and Preis in 1937 [145]. The anode is usually made of a Co-ZrO<sub>2</sub> or Ni-ZrO<sub>2</sub> cement [3,182], while the cathode is made of Sr-doped LaMnO<sub>3</sub> (LSM) [228-230].

The anode, cathode, and overall cell reactions are



SOFCs efficiency is lower than MCMF although the operating temperature (850-1000 °C) is higher. The high operating temperatures imply that precious metal electro catalysts are not needed, hence reducing the cost of cell components; it is also possible to use carbon-based fuels directly, removing the need for external reformers, further reducing the cost [3,182]. The high operating temperature of SOFC enables relatively inexpensive electrode materials to be used. Moreover, SOFC has high tolerance to impurities due to the catalytic properties of the nickel anode catalyst unlike PEMFC. The conductivity of the fuel cell materials increases with temperature [231,232]. The dominant losses in SOFCs is mainly due to the ohmic resistance losses, thus increasing the temperature enhances the SOFC efficiency. Noticeable interest to develop electrolytes that are able to operate at lower temperatures is ongoing for several reasons: lowering the operating temperature would reduce the costs and improve cell lifetime [232].

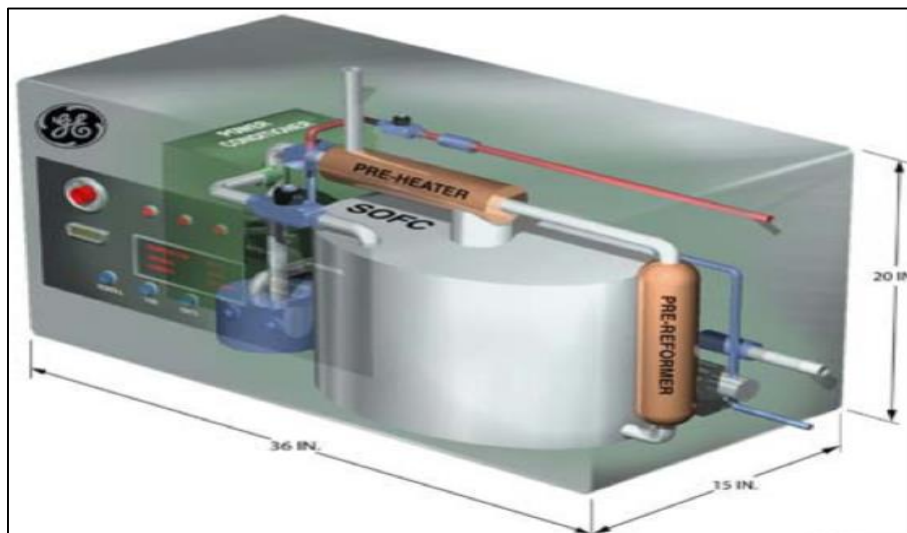


Fig. 1-26 SOFC stack developed by General Electric

The main configurations of SOFC are tubular, bipolar, and a planar, this last being developed more recently [3,182]. SOFCs can operate at a high enough temperature to incorporate an internal fuel



reformer that uses heat from the fuel cell. The recycled steam and a catalyst can convert the natural gas directly into a hydrogen-rich fuel. The waste heat allows the development of cogenerative processes enhancing energy efficiency to very attractive levels.

Power-generating efficiencies could reach 60 to 85 % with cogeneration [3,182]. Tubular SOFC technology has produced as much as 220 kW [233,234]. Japan has two 25-kW units online, and a 100 kW plant is being tested in Europe [3,149,182]. SOFCs coupled with small gas turbines are high-efficiency systems that have a combined rating in the range of 250 kW to 25 MW, and are expected to fit into grid support or industrial onsite generation markets [3,149,182].

#### **1.15.6.1 Components of the Solid Oxide Fuel Cells**

##### *Electrolyte*

In an SOFC the electrolyte is exposed to both oxidizing (air side) and reducing species (fuel side) at high temperatures. Several properties of the SOFC electrolyte are required: (1) Sufficient ionic conductivity (the electronic conductivity of the electrolyte must be sufficiently low in order to provide a high energy conversion efficiency); also the oxide ion conductivity must be high to minimize the ohmic loss. (2) Dense structure, in order to produce maximum electrochemical performance. (3) Stability since the electrolyte is exposed to the air and the fuel at elevated temperatures. This requires that the thermal expansion coefficients must match at the interfaces.

Typical electrolyte materials for SOFCs are oxides with low valence element substitutions, sometimes named acceptor dopants [3,182] which create oxygen vacancies through charge compensation. For SOFC applications, there are various materials that have been explored as electrolyte, yttria-doped zirconia (YSZ) and gadolinium-doped ceria (GDC) are the most common materials used for the oxide-conducting electrolyte. Above 800 °C, YSZ becomes a conductor of oxygen ions ( $O^{2-}$ ); zirconia-based SOFC operates between 800 and 1100 °C. The ionic conductivity of YSZ is  $0.02 \text{ S m}^{-1}$  at 800 °C and  $0.1 \text{ S cm}^{-1}$  at 1000 °C. A thin electrolyte (25–50  $\mu\text{m}$ ) ensures that the contribution of electrolyte to the ohmic loss in the SOFC is kept to a minimum.

##### *Zirconium oxide-based electrolyte (YSZ)*

Yttria-doped zirconia (YSZ) is stable under reducing and oxidizing conditions. It is a pure ionic conductor, completely nonreactive with anode and cathode at operating and production temperatures. Above 800 °C, YSZ becomes a conductor of oxygen ions ( $O^{2-}$ ) and typically operates at 800–1100 °C. The ionic conductivity of YSZ is  $0.02 \text{ S m}^{-1}$  at 800 °C and  $0.1 \text{ S cm}^{-1}$  at 1000 °C. A thin electrolyte (25–50  $\mu\text{m}$ ) ensures that the contribution of electrolyte to the ohmic loss in the SOFC is kept to a minimum. Its thermal expansion has to be close to other fuel cell components and

it must be gas tight to prevent direct combination of fuel and oxidant. Pure zirconia is not used, as its ionic conductivity is too low for fuel cell use [235].

#### *Cerium oxide-based electrolyte*

Doped cerium dioxide materials are candidates for the electrolyte for cell operation at  $T \leq 600\text{ }^{\circ}\text{C}$ , because of their higher oxide ion conductivity ( $\text{Ce}_{0.9}\text{Gd}_{0.1}\text{O}_{1.95}$ :  $0.025\text{ }\Omega^{-1}\text{ cm}^{-1}$  at  $600\text{ }^{\circ}\text{C}$ ) compared to YSZ ( $<0.005\text{ }\Omega^{-1}\text{ cm}^{-1}$ ). Gadolinium- or samarium-doped cerium dioxide provides the highest ionic conductivity in cerium dioxide-based materials owing to similar ionic radii of  $\text{Gd}^{3+}$ / $\text{Sm}^{3+}$  and  $\text{Ce}^{4+}$ . The main issue of doped cerium dioxide is the onset of electronic conduction in reducing conditions at  $T \geq 650\text{ }^{\circ}\text{C}$  owing to the reduction of  $\text{Ce}^{4+}$  to  $\text{Ce}^{3+}$  to compensate the formation of oxygen vacancies [3,182].

#### *Perovskite electrolytes*

The perovskite structure ( $\text{ABO}_3$ ) offers an opportunity for a material scientist to selectively substitute either the A or the B ion by introducing isovalent or aliovalent cations. The compound  $(\text{La}, \text{Sr})(\text{Mg}, \text{Ga})\text{O}_3$  (LSMG) has been developed as an oxide ion conductor. The use of LSMG is attractive because it has reasonable oxide ion conductivity and is compatible with a variety of cathodes, in particular the highly active ones. Other interesting materials, such as  $\text{Bi}_4\text{V}_2\text{O}_{11}$  (BIMEVOX (bismuth metal vanadium oxide)), have also been mentioned in the literature.

#### *Cathode*

The cathode electrode operates in an oxidizing environment of air at  $1000\text{ }^{\circ}\text{C}$ . The cathode electrode is a porous structure that allows mass transport of reactants and products.

Materials suitable for an SOFC cathode have to satisfy the following requirements: high electronic conductivity; stability in oxidizing atmospheres at high temperature; thermal expansion match with other cell components; compatibility and minimum reactivity with different cell components; sufficient porosity to allow transport of the fuel gas to the electrolyte/electrode interface [3,182].

LSM,  $(\text{La}_{0.84}\text{Sr}_{0.16})\text{MnO}_3$ , a p-type semiconductor, is most commonly used for the cathode material. Although adequate for most SOFCs, other materials may be used, particularly attractive being p-type conducting perovskite structures that exhibit mixed ionic and electronic conductivity [182]. The advantages of using mixed conducting oxides become apparent in cells operating at around  $650\text{ }^{\circ}\text{C}$ . As well as the perovskites, lanthanum strontium ferrite, lanthanum strontium cobalite, are proposed in literature [3,182].

$\text{LaMnO}_3$  can react with the YSZ electrolyte at high temperature producing insulating phases of lanthanum zirconate [182].

### *Anode*

The key requirements for the anode are high conductivity, stability in reducing atmospheres, and sufficient porosity to allow good mass transport. The most common anode for SOFCs is the Ni/YSZ cermet. Ni is chosen among other components because of its high electronic conductivity and stability under reducing conditions. Moreover, Ni activates both direct oxidation and steam reforming. The use of YSZ has multiple purposes: to inhibit sintering of the nickel [3,182,235], to guarantee thermal expansion coefficient (TEC) comparable with other fuel cell components (mainly the electrolyte), and to increase the triple phase boundary (TPB) [236,237]. The anode porosity (20–40 %) ensures good mass transport and improves the triple boundary by allowing  $O^{2-}$  ion movement within the anode electrode [13, 160]. A small amount of ceria is added to the anode cermet to improve ohmic polarization loss at the interface between the anode and the electrolyte. This also improves the tolerance of the anodes to temperature cycling and redox changes within the anode gas [182,235].

The TPB is a key area and it is important to increase this surface area since in this point the oxygen ions and the hydrogen gas are brought together to react at the surface of the nickel site [3,182,235-237].

#### **1.15.6.2 Fuel Reforming**

The high operational temperature of SOFCs has two benefits: high efficiency and fuel flexibility. The high operating temperature allows the production of high-quality off-gases, which can be used for cogeneration processes [3,182], or to heat the reformer for endothermic steam reforming reactions, or even to fire a secondary gas turbine. Therefore, SOFCs have a high electrical efficiency, higher than other fuel cells [182]. Moreover, a variety of fuels can be reformed within the cell stack (internal reforming) or through a separate fuel reformer (external reforming). This flexibility allows use of fuels such as biogas [3], liquid hydrocarbon fuels, and landfill gas. These fuels can be reformed to a mixture of hydrogen and carbon monoxide.

In the internal reforming arrangement, two configurations are employed: the direct internal reforming (DIR), and indirect internal reforming (IIR).

In the DIR the fuel reforming occurs directly on the fuel cell anode where the fuel is converted into a hydrogen-rich mixture directly inside the anode compartment: electrochemical reaction and fuel reforming reactions simultaneously take place at the anode. This is a simple and very efficient design and involves low capital costs. However, some issue must be taken into account: the anode compartment must be equipped with a proper catalyst for the steam reforming; carbon deposition is

avored due to the larger content of fuel at the anode side; temperature distribution should not be homogeneous due to cooling caused by the endothermic reaction [3,182].

The problems of DIR can be in some way overcome by the indirect internal reforming (IIR) configuration. IIR uses a separate fuel reforming catalyst that is integrated within the SOFC stack upstream of the anode side, and typically utilizes heat and water from the SOFC stack. Therefore, in this case only a thermal coupling between the reformer and the SOFC stack exists. Obviously, the IIR configuration results in a higher system complexity and in higher capital costs [3,182].

IIR should not be as efficient as DIR, however it allows a more stable cell performance. Since the external reformer is physically separated from the fuel cell stack it can be operated at different pressures and temperatures if necessary. This is of particular importance because in this way it is possible to eliminate the problem of carbon deposition via fuel decomposition that deactivates the anode [3,182].

#### 1.15.6.3 Solid Oxide Fuel Cell Configurations

The most common SOFC designs are planar and tubular, and their many variants. In the planar SOFC, cell components are thin and flat plates electrically connected in series. A generic schematic of a planar SOFC design is shown in Figure 1.27 [238]. The planar cells can be electrolyte supported, electrode supported, or metal supported. For instance, the cell may be in the form of a circular disk fed with fuel from the central axis, or it may be in the form of a square plate fed from the edges. Planar designs offer several potential advantages, including simpler and less expensive manufacturing processes and higher power densities, than tubular cells.

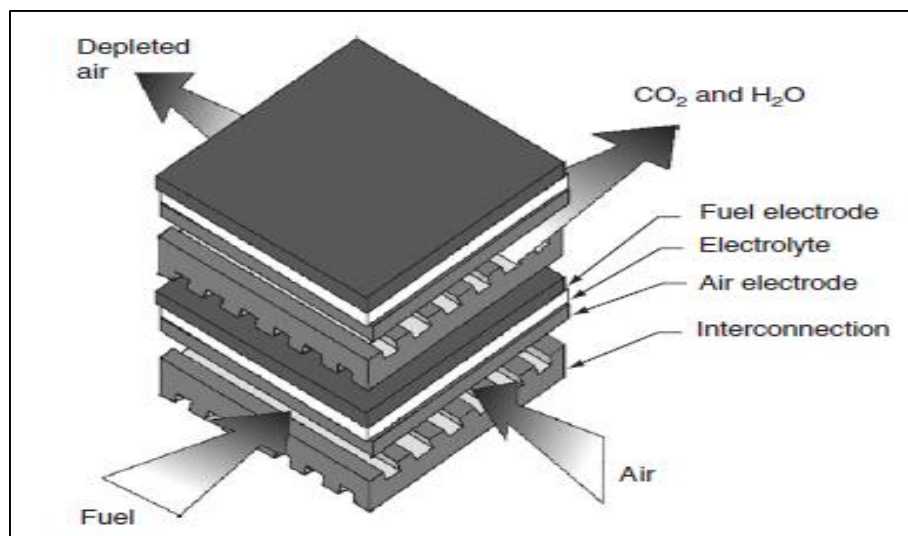


Fig. 1-27 Planar SOFC design

However, planar designs need high-temperature gas-tight seals between the components in the SOFC stack; but these still remain a challenging area for the successful commercialization of planar SOFCs [239,240]. The electrochemical performance is highly dependent on cell materials, electrode microstructures, and cell geometric parameters. The cell was optimized with an anode of thickness 0.5 mm and porosity ~57 %. The anode interlayer was ~20 mm. The electrolyte was ~8 mm and cathode interlayer ~20 mm.

The flow rates of humidified hydrogen and air were 300 and 550 mL min<sup>-1</sup>, respectively. The maximum power density obtained is about 1.8 Wcm<sup>2</sup> at 800 °C [3,182]. In the tubular SOFC design, components are flat tubes and joined together to give higher power density and easily printable surfaces for depositing the electrode layers. It may be of a large diameter (>15 mm), or a microtubular cells with a smaller diameter (<5 mm) [3,182]. Figure 1.28 illustrates a tubular SOFC in which the oxidant (air or oxygen) is introduced through an alumina injector tube positioned inside the cell. The oxidant is discharged near the closed end of the cell and flows through the annular space formed by the cell and the coaxial injector tube. The fuel flows on the outside of the cell from the closed end and is electrochemically oxidized while flowing to the open end of the cell generating electricity. Part of the fuel is recirculated in the fuel stream and the rest combusted to preheat the incoming air and/or fuel. The exhaust gas from the fuel cell is at 600–900 °C depending on the operating conditions. The single biggest advantage of tubular cells over planar cells is that they do not require any high-temperature seals to isolate the oxidant from the fuel, and this leads to very stable performance of tubular cell stacks over long periods of time (several years). However, their areal power density is much lower (about 0.2 Wcm<sup>-2</sup>) compared to planar cells, and manufacturing costs are high [241-243].

A single planar or tubular SOFC generally produces a low voltage and power and the connection into a stack is needed in order to give higher power. Electrochemical performance, structural and mechanical integrity gas manifold and ease of fabrication are important targets for the improvements of cell performances [3,182].

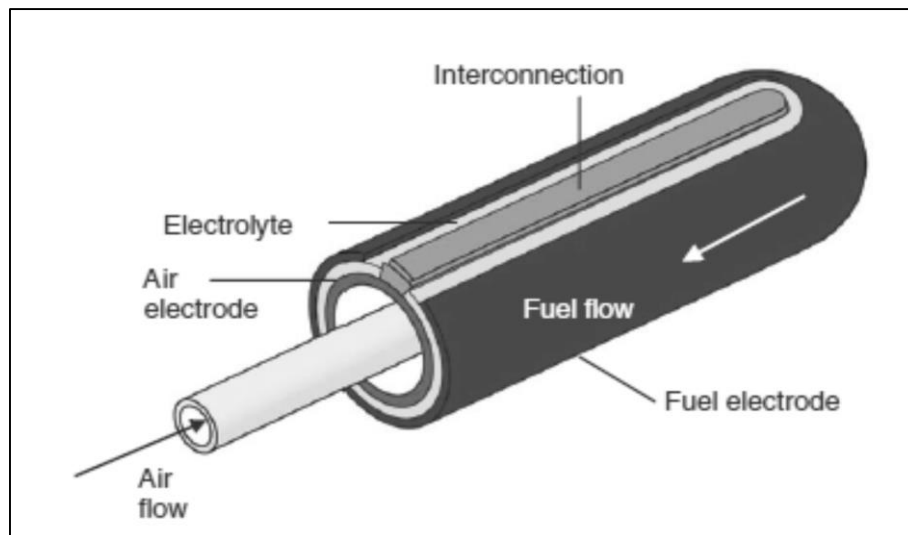


Fig.1-28 Tubular SOFC design

## References

1. Weiland P (2010) Biogas production: current state and perspectives. *Appl Microbiol Biotechnol* 85:849–860
2. <http://climate.nasa.gov/vital-signs/carbon-dioxide/> access 10 Feb 2017
3. Turco M, Ausiello A, Micoli L (2016) Treatment of Biogas for Feeding High Temperature Fuel Cells, Springer International Publishing Switzerland, Green Energy and Technology, DOI 10.1007/978-3-319-03215-3\_1
4. <https://www.statista.com/chart/4801/europe-matches-asian-giants-in-air-pollution-deaths/> access 10 Feb 2017
5. [unfccc.int/resource/docs/convkp/kpeng.pdf](http://unfccc.int/resource/docs/convkp/kpeng.pdf); access 10 Feb 2017
6. <http://www.lastampa.it/2014/11/12/esteri/stati-uniti-cina-raggiunto-laccordo-sullemissione-di-gas-serraCh4Jqw3HLpeoNBCUV9777O/pagina.html>; access 10 Feb 2017
7. [www.ilsoleovunque.it](http://www.ilsoleovunque.it); access 10 Feb 2017
8. <http://www.ren21.net/status-of-renewables/global-status-report/> access 10 Feb 2017
9. Yiridoe EK, Gordon R, Brown BB (2009) Nonmarket cobenefits and economic feasibility of on-farm biogas energy production. *Energy Policy* 37:1170–1179
10. Amon T, Amon B, Kryvoruchko V, Machmüller A, Hopfner-Sixt K, Boriroza V, Hrbek R, Friedel J, Pötsch E, Wagentristel H, Schreiner M, Zollitsch W (2007) Methane production through anaerobic digestion of various energy crop grown in sustainable crop rotations. *Bioresour Technol* 98:3204–3212
11. Kvasauskas M, Baltrenas P (2009) Research on anaerobically treated organic waste suitability for soil fertilisation. *J Environ Eng Landsc Manage* 17:205–211
12. Kramer JM, Kuzel FJ (2003) Farm-scale anaerobic digesters in the great lakes states. *BioCycle* 44:58–61
13. Steinfeld H, Gerber P, Wassenaar T, Castel V, Rosales M, de Haan C (2006) FAO: live-stock's long shadow environmental issues and options". FAO, Rome, Italy, 416 pp
14. Kebread E, Clark K, Wagner-Riddle C, France J (2006) Methane and nitrous oxide emissions from Canadian Animal agriculture: a review. *Can J Anim Sci* 86:135–158 (2006)
15. Fischer JR, Iannotti EL, Sievers DM (1981) Anaerobic digestion of manure from swine fed on various diets. *Agric Wastes* 3:201–214
16. Stevens MA, Schulte DD (1977) Low temperature anaerobic digestion of swine manure. ASAE paper No. 77-1013. St. Joseph, MI, USA, p 19
17. Ke-Xin I, Nian-Guo L (1980) Fermentation technology for rural digesters in China. *Proc. Bioenergy* 80:440–442
18. Hashimoto AG (1983) Thermophilic and mesophilic anaerobic fermentation of swine manure. *Agric Wastes* 6:175–191
19. Wellinger A, Kaufmann R (1982) Psychrophilic methane production from pig manure. *Process Biochem* 17:26–30
20. Henze M, Harremoes P (1983) Anaerobic treatment of wastewater in fixed film reactors: a literature review. *Water Sci Technol* 15:1–101
21. Chandler JA, Hermes SK, Smith KD (1983) A low cost 75 kW covered lagoon biogas system. In: Proceedings of the Symposium on Energy from Biomass and Waste VII, Lake Buena Vista, FL, USA, pp 627–646
22. Wellinger A (1984) Anaerobic digestion: a review comparison with two types of aeration systems for manure treatment and energy production on the small scale farm. *Agric Wastes* 10:117–133
23. Cullimore RR, Maule A, Mansui N (1985) Ambient temperature methanogenesis from pig manure waste lagoons: thermal gradient incubator studies. *Agric Wastes* 12:147–157
24. Sutter K, Wellinger A (1987) ACF-system: a new low temperature biogas digester. In: Szabolcs I, Welte E (eds) Agricultural waste management and environmental protection. 4th International CIEC symposium. Braunschweig, Germany, p 554
25. Balsari P, Bozza E (1988) Fertilizers and biogas recovery installation in a slurry lagoon. In: Szabolcs I, Welte E (eds) Agricultural waste management and environmental protection, 4th International CIEC symposium. Braunschweig, Germany, pp 71–80
26. Chen TH, Shyu WH (1998) Chemical characterization of anaerobic digestion treatment of poultry mortalities. *Bioresour Technol* 63:37–48
27. Safley LM, Westerman PW (1992) Performance of a dairy manure anaerobic lagoon. *Bioresour Technol* 42:43–52
28. Safley LM, Westerman PW (1994) Low temperature digestion of dairy and swine manure. *Bioresour Technol*

29. Massé DI, Patni NK, Droste RL, Kennedy KJ (1996) Operation strategies for psychrophilic anaerobic digestion of swine manure slurry in sequencing batch reactors. *Can J Civ Eng* 23:1285–1294
30. Massé DI, Droste RL, Kennedy KJ, Patni NK, Munroe JA (1997) Potential for the psychrophilic anaerobic treatment of swine manure using a sequencing batch reactor. *Can Agric Eng* 392:5–33
31. Hansen KH, Angelidaki I, Ahring BK (1998) Anaerobic digestion of swine manure: inhibition by ammonia. *Water Res* 32:5–12
32. Lusk PD (1998) Methane recovery from animal manures: the current opportunities. Casebook. National Renewable Energy Laboratory US Department of Energy, Washington, DC, USA, 150 pp
33. Steffen R, Szolar O, Braun R (2000) Feedstocks for anaerobic digestion. In: Ørtenblad H (ed) *Anaerobic digestion: making energy and solving modern wastes problems*. AD-NETT. The European Anaerobic Digestion Network, pp 34–52
34. Hartmann H, Ahring BK (2005) Anaerobic digestion of the organic fraction of municipal waste: influence of co-digestion with manure. *Water Res* 39:1543–1552
35. El-Mashad HM, Zhang R (2010) Biogas production from co-digestion of dairy manure and food waste. *Bioresour Technol* 101:4021–4028
36. Comino E, Rosso M, Riggio V (2010) Investigation of increasing organic loading rate in the co-digestion of energy crops and cow manure mix. *Bioresour Technol* 101:3013–3019
37. Wu X, Yao W, Zhu J, Miller C (2010) Biogas and CH<sub>4</sub> productivity by co-digesting swine manure with three crop residues as an external carbon source. *Bioresour Technol* 101:4042–4047
38. Field JA, Caldwell JS, Jeyanayagam S, Reneau RB Jr, Kroontje W, Collins ER Jr (1984) Fertilizer recovery from anaerobic digesters. *Trans ASAE* 27:1871–1876
39. Larsen KE (1986) Fertilizer value of anaerobic treated cattle and pig slurry to barley and beet. In: Kofoed AD, Williams JH, L'Hermite P (eds) *Efficient land use of sludge and manure*. Elsevier Applied Science Publishers, London, UK, pp 56–60
40. Messner H, Amberger A (1987) Composition, nitrification and fertilizing effect of anaerobically fermented slurry. In: Szabolcs I, Welte E (eds) *Agricultural waste management and environmental protection*. 4th International CIEC symposium. Braunschweig, Germany, pp 125–130
41. Plaixats J, Barcelo J, Garcia-Moreno J (1988) Characterization of the effluent residue from anaerobic digestion of pig excreta for its utilization as fertilizer. *Agrochimica* 32:236–239
42. Massé DI, Croteau F, Masse L (2007) The fate of crop nutrients during the low temperature anaerobic digestion of swine manure slurries in sequencing batch reactors. *Bioresour Technol* 98:2819–2823
43. Ryckebosch E, Drouillon M, Vervaeren H (2011) Techniques for transformation of biogas to biomethane. *Biomass Bioenergy* 35:1633–1645
44. Wellinger A, Lindberg A (2002) Biogas upgrading and utilisation. IEA Bioenergy, Task 24—Energy from biological conversion of organic waste, pp 1–20
45. Wellinger A, Lindberg A (2002) Biogas upgrading and utilisation. IEA Bioenergy, Task 24—Energy from biological conversion of organic waste, pp 1–20
46. Tortora GJ, Funke BR, Case CL (2010) *Microbiology, an introduction*, 10th edn. Benjamin Cummings, Redwood City
47. Angelidaki I, Ellegard L, Ahring BK (1999) A comprehensive model of anaerobic bioconversion of complex substrates to biogas. *Biotechnol Bioeng* 63:363–372
48. Palatsi J, Viñas M, Guivernau M, Fernandez B, Flotats X (2011) Anaerobic digestion of slaughterhouse waste: main process limitations and microbial community interactions. *Bioresour Technol* 102:2219–2227
49. Tsavkelova EA, Netrusov AI (2012) Biogas production from cellulose containing substrates: a review. *Appl Biochem Microbiol* 48:421–433
50. Shin SG, Lee S, Lee C, Hwang K, Hwang S (2010) Qualitative and quantitative assessment of microbial community in batch anaerobic digestion of secondary sludge. *Bioresour Technol* 101:9461–9470
51. Stams AJM (1994) Metabolic interactions between anaerobic bacteria in methanogenic environments. *Antonie Van Leeuwenhoek* 66:271–294
52. Pöschl M, Ward S, Owende P (2010) Evaluation of energy efficiency of various biogas production and utilization pathways. *Appl Energy* 87:3305–3321
53. Zinder SH (1993) Physiological ecology of methanogens, In: Ferry JG (ed) *Methanogenesis: ecology, physiology, biochemistry and genetics*. Chapman Hall, New York, pp 128–206



54. Davies ZS, Mason D, Brooks AE, Griffith GW, Merry RJ, Theodorou MK (2000) An automated system for measuring gas production from forages inoculated with rumen fluid and its use in determining the effect of enzymes on grass silage. *Anim Feed Sci Technol* 83:205–221
55. Boone DR, Whitman WB, Rouviere P (1993) Diversity and taxonomy of methanogens. In: Ferry JG (ed) *Methanogenesis: ecology, physiology, biochemistry and genetics*. Chapman Hall, New York, pp 35–80
56. Garrity G (ed) (2001) *Bergey's Manual of Systematic Bacteriology*, 2nd edn. Springer, New York
57. Ferry G (2010) How to make a living by exhaling methane. *Annu Rev Microbiol* 64:453–473
58. Liu Y (2010) Taxonomy of methanogens. In: Timmis KN (ed) *Handbook of hydrocarbon and lipid microbiology*. Springer, Berlin, pp 549–558
59. Ferry JG (1993) *Methanogenesis: ecology, physiology, biochemistry and genetics*. Chapman Hall, New York
60. Schink B, Zeikus JG (1982) Microbial ecology of pectin decomposition in anoxic lake sediments. *J General Microbiol* 128:393–404
61. Pol A, Demeyer DI (1988) Fermentation of methanol in the sheep rumen. *Appl Environ Microbiol* 54:832–834
62. Whitman WB, Bowen TL, Boone DR (1992) The methanogenic bacteria. In: Balows A, Truper HG, Dworkin M, Harder W, Schleifer K (eds) *The Prokaryotes*, 2nd edn. Springer, New York, pp 719–760
63. Stams AJM, Oude Elferink SJWH, Westermann P (2003) Metabolic interactions between methanogenic consortia and anaerobic respiring bacteria. *Adv Biochem Eng Biotechnol* 81:31–56
64. Bagi Z, Acs N, Balint B, Hovrath L, Dobo K, Perei KR, Rakhely G, Kovacs KL (2007) Biotechnological intensification of biogas production. *Appl Microbiol Biotechnol* 76:473–482
65. Ács N, Bagi Z, Rakhely G, Kovács E, Wirth R, Kovács KL (2011) Improvement of biogas production by biotechnological manipulation of the microbial population. In: 3rd IEEE International Symposium on Exploitation of Renewable Energy Sources. Subotica, Serbia
66. Ács N (2010) Monitoring the biogas producing microbes. *Act Biologica Szegediensis* 54(1):59–73
67. Ritchie DA, Edwards C, McDonald IR, Murrell JC (1997) Detection of methanogen and methanotrophs in natural environment. *Glob Change Biol* 3:339–350
68. Schink B (1997) Energetics of syntrophic cooperation in methanogenic degradation. *Microbiol Mol Biol Rev* 61:262–280
69. Gavala HN, Angelidaki I, Ahring BK (2003) Kinetics and modelling of anaerobic digestion processes. In: Scheper T, Ahring BK (eds) *Biomethanation I*. Springer, Berlin
70. Andara AR, Esteban JMB (1999) Kinetic study of the anaerobic digestion of the solid fraction of piggy slurries. *Biomass Bioenergy* 17:435–443
71. Linke B (2006) Kinetic study of thermophilic anaerobic digestion of solid wastes from potato processing. *Biomass Bioenergy* 30:892–896
72. Biswas L, Chowdhury R, Battacharya P (2007) Mathematical modeling for the prediction of biogas generation characteristics of an anaerobic digester based on food/vegetable residues. *Biomass Bioenergy* 31:80–86
73. Anhuradha S, Bakiya P, Mullai P (2013) The kinetics of biogas production in an anaerobic hybrid reactor. *Int J Environ Bioenergy* 7:168–177
74. Angelidaki I, Ellegaard L, Ahring B (2003) Application of the anaerobic digestion process. In: *Biomethanation II. Advances in Biochemical Engineering/Biotechnology*. Springer, pp 2–33
75. Nielsen HB, Agelidaki I (2008) Strategies for optimizing recovery of the biogas process following ammonia inhibition. *Bioresour Technol* 99:7995–8001
76. Wiegant WM, Zeeman G (1986) The mechanism of ammonia inhibition in the thermophilic digestion of livestock wastes. *Agric Wastes* 16:243–253
77. Abdoun E, Weiland P (2009) Optimization of monofermentation from renewable raw materials by the addition of trace elements. *Bornimer Agrartechnische Berichte* 68:69–78
78. Jarvis A, Nordberg A, Jarlsvik T, Mathisen B, Svensson BH (1997) Improvement of a grass-clover silage-fed biogas process by the addition of cobalt. *Biomass Bioenergy* 12:453–460
79. Bischoff M (2009) Erkenntnisse beim Einsatz von Zusatz- und Hilfsstoffen sowie von Spurenelementen in Biogasanlagen. *VDI-Ber* 2057:111–123
80. Kim IS, Hwang MH, Jang NJ, Hyun SH, Lee ST (2004) Effect of low pH on the activity of hydrogen utilizing methanogen in bio-hydrogen process. *Int J Hydr Energy* 29:1133–1140
81. Staley BF, Reyes III FL, Barlaz MA (2011) Effect of spatial differences in microbial activity, pH, and substrate levels on methanogenesis initiation in refuse. *Appl Environ Microbiol* 77, 2381–2391
82. Braun R (2007) *Anaerobic digestion: a multi-faceted process for energy, environmental management and*

- rural development. In: Ranalli P (ed) *Improvement of crop plants for industrial end uses*. Springer, Dordrecht, pp 335–415
83. Braun R (1982) *Biogas-Methangärung organischer*. Springer Wien, Abfallstoffe
  84. Zubr J (1986) Methanogenic fermentation of fresh and ensiled plant materials. *Biomass* 11:159–171
  85. Döhler H, Eckel H, Frisch J (2006) *Energiepflanzen*. KTBL, Darmstadt
  86. Angelidaki I, Karakashev D, Batstone DJ, Plugge CM, Stams AJ (2011) Biomethanation and its potential. In: Rosenzweig, C, Ragsdale W (eds) *Methanogenesis (Methods in Enzymology)*, vol 494. Academic Press, pp 327–351
  87. Hecht C, Griehl C (2009) Investigation of the accumulation of aromatic compounds during biogas production from kitchen waste. *Bioresour Technol* 100:654–658
  88. Ferry JG (2011) Fundamentals of methanogenic pathways that are key to the biomethanation of complex biomass. *Curr Opin Biotechnol* 22:351–357
  89. Jones EJ, Voytek MA, Corum MD, Orem WH (2010) Stimulation of methane generation from nonproductive coal by addition of nutrients or a microbial consortium. *Appl Environ Microbiol* 76:7013–7022
  90. Björnsson P, Mattiasson B (2008) Biogas as a resource-efficient vehicle fuel. *Trends Biotechnol* 26:7–13
  91. Di Stefano TD, Ambulkar A (2006) Methane production and solids destruction in an anaerobic solid waste reactor due to post-reactor caustic and heat treatment. *Water Sci Technol* 53:43–51
  92. Ferrer I, Vazquez F, Font X (2010) Long term operation of a thermophilic anaerobic reactor: Process stability and efficiency at decreasing sludge retention time. *Bioresour Technol* 101:2972–2980
  93. Diaz EE, Stams AJM, Amils R, Sanz JL (2006) Phenotypic properties and microbial diversity of methanogenic granules from a full-scale upflow anaerobic sludge bed reactor treating brewery wastewater. *Appl Environ Microbiol* 72:4942–4949
  94. Wang QH, Kuninobu M, Ogawa H, Kato Y (1999) Degradation of volatile fatty in highly efficient anaerobic digestion. *Biomass Bioenergy* 16:407–416
  95. Mösche M, Jördening HJ (1999) Comparison of different models of substrate and product inhibition in anaerobic digestion. *Water Res* 33:2545–2554
  96. Antizar-Ladislao B, Turrión-Gómez JL (2008) *Biofuels Bioprod Bioref* 2:455–469
  97. Weiland P (2006) Biomass digestion in agriculture: a successful pathway for the energy production and waste treatment in Germany. *Eng Life Sci* 6:302–309
  98. Yadavika S, Sreekrishnan TR, Kohli S (2004) Enhancement of biogas production from solid substrates using different techniques: a review. *Biores Technol* 95:1–10
  99. Gladchenko MA, Gaydamaka SN, Murtygina VP, Varfolomeev SD (2013) The optimization of the conversion of agricultural waste into volatile fatty acids under anaerobic conditions. *Biocatalysis* 69:187–193
  100. Song H, Clarke P (2009) Cellulose hydrolysis by a methanogenic culture enriched from landfill waste in a semi-continuous reactor. *Biores Technol* 100:1268–1273
  101. Pommier S, Manas LA, Lefebvre X (2010) Analysis of the outcome of shredding pretreatment on the anaerobic biodegradability of paper and cardboard materials. *Biores Technol* 101:463–468
  102. Eleazer WE, Odle WS, Wang YS, Barlaz MA (1997) Biodegradability of municipal solid waste components in laboratory-scale landfills. *Environ Sci Technol* 31:911–917
  103. Wolfe RS (1996) *ASM News* 62(10):529–534
  104. Smiti N, Ollivier B, Garcia JL (1986) *FEMS Microbiol Letts* 35(1):93–97
  105. Nozhevnikova AN, Zepp K, Vazquez F, Zehnder AJB, Holliger C (2003) Evidence for the existence of psychrophilic methanogenic communities in anoxic sediments of deep lakes. *Appl Environ Microbiol* 69:1832–1835
  106. Li T, Mazeas Sghir A, Leblon G, Bouchez T (2009) Insights into networks of functional microbes catalysing methanization of cellulose under mesophilic conditions. *Environ Microbiol* 11:889–904
  107. Leven L, Eriksson ARB, Schnurer A (2007) Effect of process temperature on bacterial and archaeal communities in two methanogenic bioreactors treating organic household waste. *FEMS Microbiol Ecol* 59:683–693
  108. Gao WJ, Leung KT, Qin WS, Liao BQ (2011) Effects of temperature and temperature shock on the performance and microbial community structure of a submerged anaerobic membrane bioreactor. *Bioresour Technol* 102:8733–8740
  109. Wijekoon KC, Visvanathan C, Abeynayaka A (2011) Effect of organic loading rate on VFA production, organic matter removal and microbial activity of a two-stage thermophilic anaerobic membrane bioreactor.

110. Teghammar A, Yngvesson J, Lundin M, Taherzadeh MJ, Sarvari HI (2010) Pretreatment of paper tube residuals for improved biogas production. *Bioresour Technol* 101:1206
111. Hjorth M, Christensen KV, Christensen ML, Sommer SG (2010) Solid–liquid separation of animal slurry in theory and practice: a review. *Agron Sustain Dev* 3:153–180
112. Mosier N, Wyman C, Dale B, Elander R, Lee YY, Holtzapple M, Ladisch M (2005) Features of promising technologies for pretreatment of lignocellulosic biomass. *Bioresour Technol* 96:673–686
113. Vavilin VA, Fernandez B, Palatsi J, Flotats X (2008) Hydrolysis kinetics in anaerobic degradation of particulate organic material: An overview. *Waste Manage* 28:939–951
114. Marañón E, Castrillón L, Quiroga G, Fernández-Nava Y, Gómez L, García MM (2012) Codigestion of cattle manure with food waste and sludge to increase biogas production. *Waste Manage* 32:1821–1825
115. Amon T, Amon B, Kryvoruchko V, Bodiroza V, Pötsch E, Zollitsch W (2006) Optimising methane yield from anaerobic digestion of manure: effects of dairy systems and of glycerin supplementation. *Int Congr Ser* 1293:217–220
116. Macias-Corral M, Samani Z, Hanson A, Smith G, Funk P, Yu H, Longworth J (2008) Anaerobic digestion of municipal solid waste and agricultural waste and the effect of co-digestion with dairy cow manure. *Biores Technol* 99:8288–8293
117. Boe K, Karakashev D, Trably E, Angelidaki I (2009) Effect of post-digestion temperature on serial CSTR biogas reactor performance. *Water Res* 43:669–676
118. Angelidaki I, Ahring BK (2000) Methods for increasing the biogas potential from the recalcitrant organic matter contained in manure. *Water Sci Technol* 41:189–194
119. Bougrier C, Delgenès JP, Carrere H (2006) Combination of thermal treatments and anaerobic digestion to reduce sewage sludge quantity and improve biogas yield. *Process Saf Environ Prot* 84:280–284
120. Lin JG, Chang CN, Chang SC (1997) Enhancement of anaerobic digestion of waste activated sludge by alkaline solubilisation. *Biores Technol* 62:85–90
121. Bougrier C, Battimelli A, Delgenès JP, Carrere H (2007) Combined ozone pretreatment and anaerobic digestion for the reduction of biological sludge production in wastewater treatment. *Ozone Sci Eng* 29:201–206
122. Xie R, Xing Y, Ghani YA, Ooi KE, Ng SW (2007) Full-scale demonstration of an ultrasonic disintegration technology in enhancing anaerobic digestion of mixed primary and thickened secondary sewage sludge. *J Environ Eng Sci* 6:533–541
123. Zeng X, Ma Y, Ma L (2007) Utilization of straw in biomass energy in China. *Renew Sustain Energy Rev* 11:976–987
124. Benabdallah El-Hadj T, Dosta J, Marquez-Serrano R, Mata-Alvarez J (2007) Effect of ultrasound pretreatment in mesophilic and thermophilic anaerobic digestion with emphasis on naphthalene and pyrene removal. *Water Res* 41:87–94
125. Toreci I, Eskicioglu C, Terzian N, Droste RL, Kennedy KJ (2007) Mesophilic anaerobic digestion with high temperature microwave pretreatment. *Water Res* 43:1273–1284
126. Eskicioglu C, Terzian N, Kennedy KJ, Droste RL, Hamoda M (2007) A thermal microwave effects for enhancing digestibility of waste activated sludge. *Water Res* 41:2457–2466
127. Phothilangka P, Schoen MA, Huber M, Luchetta P, Winkler T, Wett B (2006) Prediction of thermal hydrolysis pretreatment on anaerobic digestion of waste activated sludge. *Water Sci Technol* 58:1467–1473
128. Bougrier C, Carrere H, Delgenes JP (2005) Solubilisation of waste activated sludge by ultrasonic treatment. *Chem Eng J* 106:163–169
129. Bordeleau EL, Droste RL (2011) Comprehensive review and compilation of pretreatments for mesophilic and thermophilic anaerobic digestion. *Water Sci Technol* 63:291–296
130. Mendez JM, Jimenez BE, Barrios JA (2002) Improved alkaline stabilization of municipal wastewater sludge. *Water Sci Technol* 46:139–146
131. Neyens E, Baeyens J, Creemers C (2003) Alkaline thermal sludge hydrolysis. *J Hazard Mater* 97:295–314
132. Passos F, Carretero J, Ferrer I (2015) Comparing pretreatment methods for improving microalgae anaerobic digestion: thermal, hydrothermal, microwave and ultrasound. *Chem Eng J* 279:667–672
133. Ara E, Sartaj M, Kennedy K (2014) Effect of microwave pre-treatment of thickened waste activated sludge on biogas production from co-digestion of organic fraction of municipal solid waste, thickened waste activated sludge and municipal sludge. *Waste Manage Res* 32:1200–1209

134. Callaghan FJ, Wase DAJ, Thayanithy K, Foster CF (1999) Co-digestion of waste organic solids: batch studies. *Biores Technol* 67:117–122
135. Agdag ON, Sponza DT (2007) Co-digestion of mixed industrial sludge with municipal solid wastes in anaerobic simulated landfilling bioreactors. *J Hazard Mater* 140:75–85
136. Mata-Alvarez J, Macé S, Llabrés P (2000) Anaerobic digestion of organic solid wastes: an overview of research achievements and perspectives. *Biores Technol* 74:3–16
137. Kaparaju P, Ellegaard L, Angelidaki I (2009) Optimization of biogas production from manure through serial digestion: lab-scale and pilot-scale studies. *Biores Technol* 100:701–709
138. Wilkie AC, Castro HF, Cubisnki KR, Owens JM, Yan SC (2004) Fixed-film anaerobic digestion of flushed dairy manure after primary treatment: wastewater production and characterization. *Biosyst Eng* 89:457–471
139. Jeihanipour A, Aslanzadeh S, Rajendran K, Balasubramanian G, Taherzadeh MJ (2013) High-rate biogas production from waste textiles using two-stage process. *Renew Energy* 52:128–135
140. Boe K, Angelidaki I (2009) Serial CSTR digester configuration for improving biogas production from manure. *Water Res* 43:166–172
141. Smith DP, McCarty PL (1989) Reduced product formation following perturbation of ethanol- and propionate-fed methanogenic CSTRs. *Biotechnol Bioeng* 34:885–895
142. Boe K (2006) Online monitoring and control of the biogas process. Ph.D. thesis, Technical University of Denmark
143. Boe K, Batstone DJ (2005) Optimisation of serial CSTR biogas reactors using modeling by ADM1. In: *Proceedings of the first international workshop on the IWA Anaerobic Digestion Model No. 1 (ADM1)*, 2–4 Sept 2005, Lyngby, Denmark, pp 219–221
144. Ge HQ, Jensen PD, Batstone DJ (2011) Increased temperature in the thermophilic stage in temperature phased anaerobic digestion (TPAD) improves degradability of waste activated sludge. *J Hazard Mater* 187:355–361
145. Dincer I, Zamfirescu C (2014) Advanced power generation systems. In: *Chapter 3—Fossil fuels and alternatives*, 95–141
146. Abas N, Kalair A, Khan N (2015) Review of fossil fuels and future energy technologies. *Futures* 69:31–49
147. Ball M, Weeda M (2015) The hydrogen economy—Vision or reality? *Int J Hydrogen Energy* 40:7903–7919
148. Andrews J, Shabani B (2012) Where does hydrogen fit in a sustainable energy economy? *Procedia Eng* 49:15–25
149. Sharaf OZ, Orhan MF (2014) An overview of fuel cell technology: fundamentals and applications. *Renew Sustain Energy Rev* 32:810–853
150. Elmer T, Worall M, Wu S, Riffat SB (2015) Fuel cell technology for domestic built environment applications: state-of-the-art review. *Renew Sustain Energy Rev* 42:913–931
151. Alves HJ, Bley C, Niklevicz RR, Pires Frigo E, Sato Frigo M, Coimbra-Araújo CH (2013) Overview of hydrogen production technologies from biogas and the applications in fuel cells. *Int J Hydrogen Energy* 38:5215–5225
152. The Department of Energy hydrogen and fuel cells program plan: an integrated strategic plan for the research, development, and demonstration of hydrogen and fuel cell technologies US Department of Energy (2011)
153. National Energy Technology Laboratory, U.S. Department of Energy Fuel Cell Handbook 7th ed. Morgantown, 1–35 (2005)
154. Shekhawat D, Spivey JJ, Berry DA (2011) Fuel cells: technologies for fuel processing, Elsevier (2011)
155. Park SY, Kim JW, Lee DH (2011) Development of a market penetration forecasting model for hydrogen fuel cell vehicles considering infrastructure and cost reduction effects. *Energy Policy* 39:3307–3315
156. Simons A, Bauer C (2015) A life-cycle perspective on automotive fuel cells. *Appl Energy* 157:884–896
157. Cowey K, Green KJ, Mepsted GO, Reeve R (2004) Portable and military fuel cells. *Curr Opin Solid State Mater Sci* 8:367–371
158. Patil AS, Dubois TG, Sifer N, Bostic E, Gardner K, Quah M (2004) Portable fuel cell systems for America's army: technology transition to the field. *J Power Sources* 136:220–225
159. Wang Y, Chen KS, Mishler J, Cho SC, Adroher XC (2011) A review of polymer electrolyte membrane fuel cells: technology, applications, and needs on fundamental research. *Appl Energy* 88:981–1007
160. Breakthrough Technologies Institute Fuel cell technologies market report US Department of Energy (2011)
161. Abdullah MO, Yung VC, Anyi M, Othman AK, Hamid KBAb, Tarawe J (2010) Review and comparison study of hybrid diesel/solar/hydro/fuel cell energy schemes for a rural ICT Telecenter. *Energy* 35:639–646

162. Bauen A, Hart D, Chase A (2003) Fuel cells for distributed generation in developing countries: an analysis. *Int J Hydrog Energy* 28:695–701
163. Munuswamy S, Nakamura K, Katta A (2011) Comparing the cost of electricity sourced from a fuel cell-based renewable energy system and the national grid to electrify a rural health centre in India: a case study. *Renew Energy* 36:2978–2983
164. Santarelli M (2004) Design and analysis of stand-alone hydrogen energy systems with different renewable sources. *Int J Hydrog Energy* 29:1571–1586
165. Kazempoor P, Dorer V, Weber A (2011) Modelling and evaluation of building integrated SOFC systems. *Int J. Hydrog Energy* 36:13241–13249
166. Alcaide F, Cabot PL, Brillas E (2006) Fuel cells for chemicals and energy cogeneration. *J Power Sources* 153:47–60
167. Agnolucci P (2007) Prospects of fuel cell auxiliary power units in the civil markets. *Int J Hydrog Energy* 32:4306–4318
168. Lutsey N, Brodrick CJ, Sperling D, Dwyer HA (2002) Markets for fuel cell auxiliary power units in vehicles: a preliminary assessment. Institute of Transportation Studies. UCD-ITS-RP-02-44
169. Hochgraf C (2009) Application: transportation: electric vehicles: fuel cells. In: Garche J (ed) *Encyclopedia of electrochemical power sources*. Elsevier, Amsterdam
170. Bradley TH, Moffitt BA, Mavris D, Parekh DE (2009) Applications: transportation: aviation: fuelcells. In: Garche J (ed) *Encyclopedia of Electrochemical Power Sources*, Elsevier Amsterdam
171. Saxe M, Folkesson A, Alvfors P (2008) Energy system analysis of the fuel cell buses operated in the project: clean urban transport for Europe. *Energy* 33:689–711
172. Williams MC, Yamaji K, Yokokawa H, Fundamental thermodynamic studies of fuel cells using MALT2. *J Fuel Cell Sci Technol* 6:97–102 and 113–116 (2009)
173. Winkler W (2003) High temperature solid oxide fuel cells: fundamentals, design, and applications Thermodynamics. In: Singhal SC, Kendall K (eds) Oxford. Elsevier, UK, pp 53–82
174. Williams M, Yamaji K, Horita T, Sakai N, Yokokawa H (2009) Exergetic studies of intermediate temperature, solid oxide fuel cell electrolytes. *J Electrochem Soc* 156:546–551
175. Virkar A, Williams MC, Singhal SC (2007) Concepts for ultrahigh power density solid oxide fuel cells In: Williams M, Krist K (eds) *ECS Transactions*, vol 5. pp 401–422
176. Virkar AV (2005) Theoretical analysis of the role of interfaces in transport through oxygen ion and electron conducting membranes. *J Power Sources* 147:8–31
177. Zhao, Virkar AV (2005) Dependence of polarization in anode-supported solid oxide fuel cells on various cell parameters. *J Power Sources* 141:79–95
178. Space applications of hydrogen and fuel cells (2015) National Aeronautics and Space Administration. [http://www.nasa.gov/topics/technology/hydrogen/hydrogen\\_2009.html](http://www.nasa.gov/topics/technology/hydrogen/hydrogen_2009.html). Accessed 30 Oct 2015
179. Sheffield JW (2007) Assessment of hydrogen energy for sustainable development. In: Sheffield C (ed) Springer, Netherlands (2007)
180. Gaines LL, Elgowainy A, Wang MQ (2008) Full fuel-cycle comparison of forklift propulsion systems. In: Argonne National Laboratory. ANL/ESD/08-3
181. Wang M, Elgowainy A, Han J (2010) Life-cycle analysis of criteria pollutant emissions from stationary fuel cell systems. US Department of Energy Hydrogen and Fuel Cells Program AN012
182. Larminie J, Dicks A (2003) In: *Fuel Cell Systems Explained*, 2nd edn, Wiley
183. Zhang Y, Li J, Ma L, Cai W, Cheng H (2015) Recent developments on alternative proton exchange membranes: strategies for systematic performance improvement. *Energy Technol* 3:675–691
184. Dubau L, Castanheira L, Maillard F, Chatenet M, Lottin O, Maranzana G, Dillet J, Lamibrac A, Perrin JC, Moukheiber E et al (2014) A review of PEM fuel cell durability. *Wiley Interdisc Rev Energy Environ* 3:540–560
185. Banham D, Feng F, Furstenhaupt T, Pei K, Ye S, Birss V (2015) Novel mesoporous carbon supports for PEMFC catalysts. *Catalysts* 5:1046–1067
186. Anstrom JR (2014) Hydrogen as a fuel in transportation. *Energy* 63:499–524
187. Chirachanchar S, Pagon A, Jarumaneeroj C (2013) High temperature performance polymer electrolyte membranes. *Membr Process. Sustain. Growth* 247–287
188. Sim V, Han W, Poon HY, Lai YT, Yeung KL (2014) Confinement as a new architecture for self-humidifying proton-exchange membrane for PEMFC Abstracts of Papers. In: 248th ACS National Meeting & Exposition,

San Francisco, CA, United States, 10–14 Aug 2014

189. Boyaci SFC, Isik-Gulsac I, Osman OO (2013) Analysis of the polymer composite bipolar plate properties on the performance of PEMFC (polymer electrolyte membrane fuel cells) by RSM (response surface methodology). *Energy* 55:1067–1075
190. Lin BYS, Kirk DW, Thorpe SJ (2006) Performance of alkaline fuel cells: a possible future energy system. *J Power Sources* 161:474–483
191. Fuel Cell Basics (2000). Fuel Cells. <http://www.fuelcells.org/basics/how.html>. Accessed 10 Feb 2017
192. Marino MG, Kreuer KD (2015) Alkaline stability of quaternary ammonium cations for alkaline fuel cell membranes and ionic liquids. *ChemSusChem* 8:513–523
193. Ishimoto T, Hamatake Y, Kazuno H, Kishida T, Koyama M (2015) Theoretical study of support effect of Au catalyst for glucose oxidation of alkaline fuel cell anode. *Appl Surf Sci* 324:76–81
194. Geng F, Zeng WM, Ma YL (2013) Preparation and characterization of foam-Ni deposit Pt and Pd catalysts for alkaline fuel cell. *Dianyu Jishu* 37:387–389
195. Aziznia, Oloman CW, Gyenge EL (2013) Platinum- and membrane-free swiss-roll mixed-reactant Alkaline Fuel cell. *ChemSusChem* 6:847–855
196. Fuller TF, Perry M, Reiser C (2006) Applying the lessons learned from PAFC to PEM fuel cells. *ECS Trans* 1:337–344
197. Fuller TF, Gallagher KG (2008) Phosphoric acid fuel cells. *Mater Fuel Cells* 209–247
198. Sammes N, Bove R, Stahl K (2004) Phosphoric acid fuel cells: fundamentals and applications. *Curr Opin Solid State Mater Sci* 8:372–378
199. Steele BCH (2001) Material science and engineering: the enabling technology for the commercialisation of fuel cell systems. *J. Mater Sci* 36:1053–1068
200. Hogarth M, Hards G (1996) Direct methanol fuel cells: technological advances and further requirements. *Plat Met Rev* 40:150–159
201. Hamnett A, Kennedy BJ (1988) Bimetallic carbon supported anode for the direct methanol-air fuel cell. *Electrochim Acta* 33:1613–1618
202. Hamnett A (1997) Mechanism and electrocatalysis in the direct methanol fuel cell. *Catal Today* 38:445–457
203. Libby B, Smyrl WH, Cussler EL (2003) Polymer-Zeolite composite membranes for direct methanol fuel cells. *AIChE J* 49:991–1001
204. R. F. Service (2002) Fuel cells. Shrinking fuel cells promise power in your pocket. *Science* 296:1222–1224
205. Lu GQ, Wang CY, Yen TJ, Zang X (2004) Development and characterization of a silicon-based micro direct methanol fuel cell. *Electrochim Acta* 49:821
206. Li X, Roberts EPL, Holmes SM (2006) Evaluation of composite membranes for direct methanol fuel cells. *J Power Sources* 154:115–123
207. Tomczyk P (2006) MCFC versus other fuel cells—characteristics, technologies and prospects. *J Power Sources* 160(2006):858–862
208. Zhu XJ, Huang B (2012) Molten carbonate fuel cells. *Electrochim Technol Energy Storage Convers* 2:729–775
209. Rossi et al C (1999) In: *Proceedings of Micro Nanotechnology for Space Applications*, vol 1, Apr (1999)
210. Blomen L, Leo JMJ, Mugerwa M (1993) Fuel cell systems. Plenum Publishing, New York
211. Kunz HR (1987) Transport of electrolyte in molten carbonate fuel cells. *J Electrochem Soc* 134:195–113
212. Perry ML, Fuller TF (2002) A historical perspective of fuel cell technology in the 20th century. *J Electrochem Soc* 149:S59–S67
213. Fuel Cell Technology Handbook (2002) In: Hoogers G (ed), CRC Press
214. Kaun TD, Schoeler A, Centeno CJ, Krumpelt M (1999) Improved MCFC performance with Li/Na/Ba/Ca carbonate electrolyte. *Proc Electrochem Soc* 99:219–227
215. Makkus RC, Sitters EF, Nammensma P, Huijsmans JPP (1997) MCFC electrolyte behavior; Li/K versus Li/Na carbonate. *Proc Electrochem Soc* 97:344–352
216. Ketelaar JAA (1987) Molten carbonate fuel cells. *From Fuel Cells Trends Res Appl [Proc. Workshop]* 161–72
217. Cigolotti V, McPhail S, Moreno A, Yoon SP, Han JH, Nam SW, Lim TH (2011) MCFC fed with biogas: Experimental investigation of sulphur poisoning using impedance spectroscopy. *Int J Hydrogen Energy* 36:10311–10318
218. Lee D, Kim J, Jo K (2011) A Study on In-Situ Sintering of Ni-10 wt % Cr Anode for MCFC. *J Electrochem Soc* 158:B500–B504

- 219.Devianto H, Yoon SP, Nam SW, Han J, Lim TH (2006) Study on ceria coating effect of H<sub>2</sub>S tolerance in the anode of molten carbonate fuel cell. *Stud Surf Sci Catal* 159:601–604
- 220.Hirschenhofer JH, Stauffer DB, Hengelman RR (1998) Fuel cell handbook 4th edn. Passons Co. for US Department of Energy
- 221.Sciavovelli A, Verda V, Amelio C, Repetto C, Diaz G (2012) Performance improvement of a circular MCFC through optimal design of the fluid distribution system. *J Fuel Cell Sci Technol* 9:041011/1–041011/8
- 222.Rinaldi G, McLarty D, Brouwer J, Lanzini A, Santarelli M (2015) Study of CO<sub>2</sub> recovery in a carbonate fuel cell tri-generation plant. *J Power Sources* 284:16–26
- 223.Minutillo M, Perna A, Jannelli E (2014) SOFC and MCFC system level modeling for hybrid plants performance prediction. *Int J Hydrogen Energy* 39:21688–21699
- 224.Kim YJ, Chang IG, Lee TW, Chung MK (2010) Effects of relative gas flow direction in the anode and cathode on the performance characteristics of a Molten Carbonate Fuel Cell. *Fuel* 89:1019–1028
- 225.Law MC, Lee VC-C, Tay CL (2015) Dynamic behaviors of a molten carbonate fuel cell under a sudden shut-down scenario: the effects on temperature gradients. *Appl Therm Eng* 82:98–109
- 226.Zanchet D, Santos JBO, Damyanova S, Gallo JMR, Bueno JMC (2015) Toward Understanding Metal-Catalyzed Ethanol Reforming *ACS Catalysis* 5:3841–3863
- 227.Guerrero L, Castilla S, Cobo M (2014) Martha Advances in ethanol reforming for the production of hydrogen. *Quimica Nova* 37:850–856
- 228.Grenier JC, Bassat JM, Mauvy F (2012) Novel cathodes for solid oxide fuel cells. *Energy* 35:402–444
- 229.Ding D, Li X, Lai SY, Gerdes K, Liu M (2014) Enhancing SOFC cathode performance by surface modification through infiltration. *Energy Environ Sci* 7:552–575
- 230.Backhaus-Ricoult M (2008) SOFC—a playground for solid state chemistry. *Solid State Sci* 10:670–688
- 231.Yamamoto O (2000) Solid oxide fuel cells: fundamental aspects and prospects. *Electrochim Acta* 45:2423–2435
- 232.Huijsmans JPP, van Berkel FPF, Christie GM (1998) Intermediate temperature SOFC—A promise for the 21st century. *J Power Sources* 71:107–110
- 233.Singh P, Minh NQ (2004) Solid oxide fuel cells: technology status. *Int J Appl Ceramic Technol* 1:5–15
- 234.Veyo SE, Vora SD, Lundberg WL, Litzinger KP (2003) Tubular SOFC hybrid power system status. *ASME Turbo Expo: Power for Land, Sea & Air*, Atlanta, GA, United States, 708-714, 16–19 June 2003
- 235.Jones FGE, Casting T (2005) Co-Firing and Electrical Characterisation of Novel Design Solid Oxide Fuel Cell SOFCROLL PhD thesis, University of St Andrews
- 236.Tanner CW, Fung KZ, Virkar AV (1997) The effect of porous composite electrode structure on solid oxide fuel cell performance. 1. Theoretical analysis. *J Electrochem Soc* 144:21–30
- 237.Gorte RJ et al (2000) Anodes for direct oxidation of dry hydrocarbons in a solid-oxide fuel cell. *Adv Mater* 12:1465–1469
- 238.Zhou XD, Singhal SC, Fuel Cells—Solid Oxide Fuel Cells, pp 1–16
- 239.Amarasinghe S, Ammala P, Aruliah S, Mizusaki J (2005) Solid Oxide Fuel Cells IX (SOFC- IX). In: Singhal SC (ed) The Electrochemical Society, Inc, 184—190
- 240.Singhal SC, Kendall K (2003) High temperature solid oxide fuel cells: fundamentals, design and applications. Elsevier, Oxford
- 241.Suzuki M, Sogi T, Higaki K et al (2007) Development of SOFC residential cogeneration system at Osaka Gas and Kyocera. In: Eguchi K, Singhal SC, Yokokawa H, Mizusaki J (eds) Solid Oxide Fuel Cells-X, The Electrochemical Society, 27–30
- 242.Tanner CW, Fung KZ, Virkar AV (1997) The effect of porous composite electrode structure on solid oxide fuel cell performance: theoretical analysis. *J Electrochem Soc* 144:21–30
- 243.Vora SD (2007) Development of high power density seal-less SOFCs. In: Eguchi K, Singhal SC, Yokokawa H, Mizusaki J (eds) Solid oxide fuel cells-X. Electrochem Soc, New Jersey, pp 149–154

## **Chapter 2: Biohydrogen Production Processes**

### **2.1 Introduction**

In chapter 1 has been discussed as the world energy consumption is steadily rising with industrialization processes and population growth from 1900 [1]. Nowadays, fossil fuels are the predominant energy sources, approximately 80% of greenhouse gas emissions (GHG) originate from energy production and numerous action (COP 21-22, see par 1.2 and 1.3) have been adopted by worldwide countries to overcome global warming effect [2].

The environmental problems together with the increasing demand for energy and the forecasted depletion of fossil fuels has stimulated exploration for alternative sources and high efficient energy technologies [1]. In this perspective, renewable energy sources and fuel cells can help mitigate climate change and reduce dependence on fossil fuels [3].

Among renewable energy sources biomass are assuming growing interest and are considered highly promising alternatives to fossil-derived energy due to several inherent and significant merits [4, 5].

Biomethane production is a well consolidated process and some plants are nowadays in operation operating in many countries [1,6] that could be integrated to traditional endothermic devices [1,6] or FCs [1,6] for energy production. Biomethane is generally produced by anaerobic digestion of simple and complex biodegradable feedstocks, such as sewage sludge, manure, organic fraction of municipal solid waste, etc., into biogas (see par. 1.5.1).

Compared to other biofuels, biomethane has been shown to have a far better performance with regard to both agricultural land area efficiency and life cycle emissions [7] and has been used for energy production mainly by endothermal cycles engines.

A new challenge in biofuels research is the biohydrogen production. In comparison to biomethane nowadays biohydrogen appears more attractive principally because can be used in fuel cells to produce electricity [8-12].  $H_2$  has high energy capacity, with the largest amount of energy per mass unit than methane ( $H_2$ : 121.000 kJ/kg,  $CH_4$ : 5020 kJ/kg). The main advantages to the use of hydrogen as a biofuel are the absence of  $CO_2$  emission, its high energy content, and its combustion kinetics [7, 13,14].

An energetic economy fully based on biohydrogen/hydrogen appears still to be developed, but several countries are gearing to create the appropriate infrastructures. Approximately 1,500 miles of hydrogen pipelines are currently operating in the United States [1,2] while in Europe, Netherlands, Germany, Denmark, France and United Kingdom have been developed about 1000 km of pipelines for hydrogen transportation. [15-18]

In total, about 25,000 km of early highways will be required to connect the European user centers and enhance the distribution of hydrogen and vehicles based on FCs technology. In the next 10-15



years (2025-2030) the European Union has planned the large-scale deployment of hydrogen distribution stations that promote the widespread dissemination of a technology based on hydrogen [15-18].

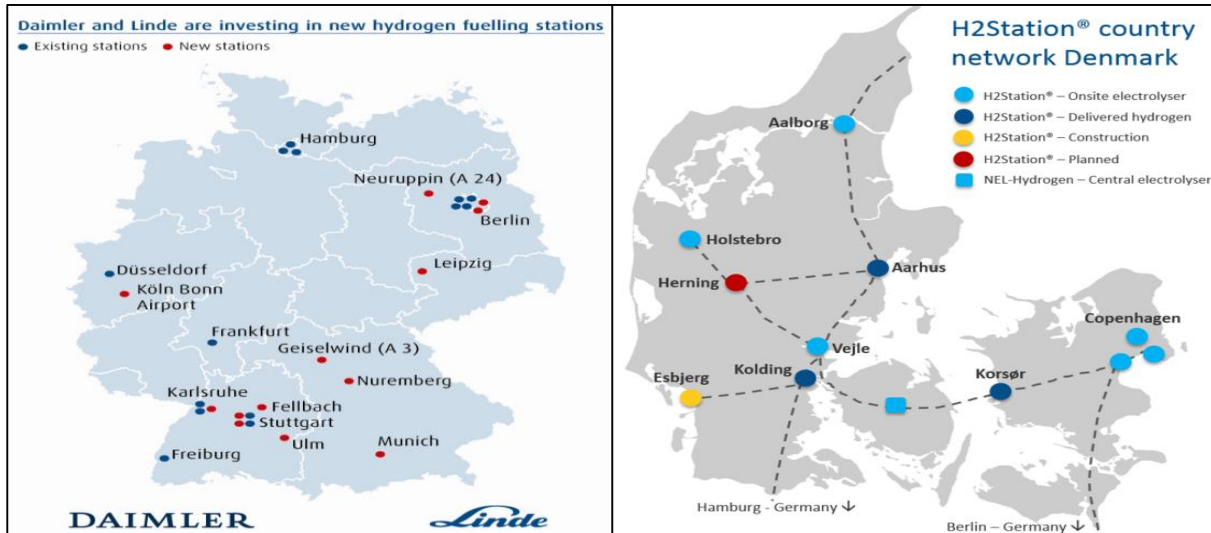


Fig. 2-1 Hydrogen stations in Germany and Denmark

## 2.2 Hydrogen from Renewable Sources

Biohydrogen can be produced from thermochemical or biological processes but differently from biomethane, biohydrogen production processes appear still a challenge that engages many researchers [19]. However, numerous benefits can be envisaged by the development of energy technologies based on biohydrogen (see par. 2.1).

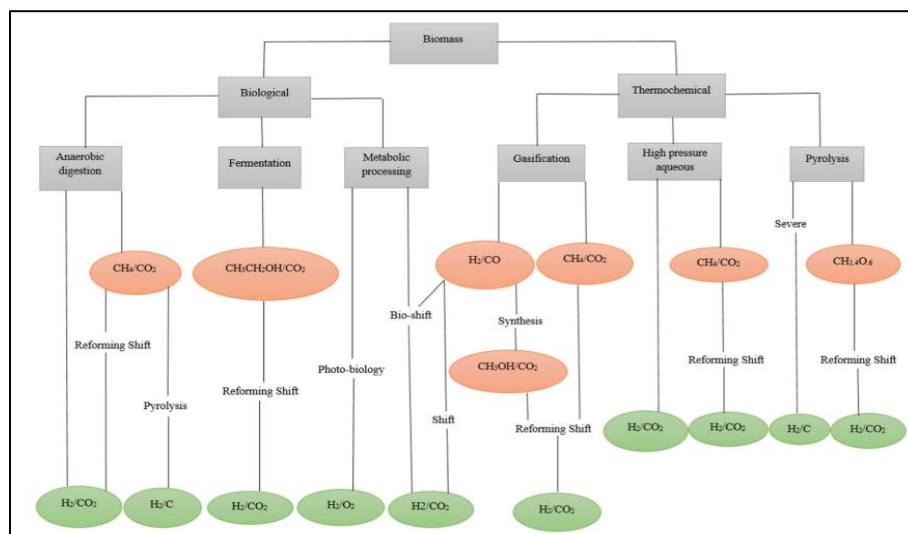


Fig. 2-2 Pathways of biomass based hydrogen production

In following paragraphs will be summarized the thermochemical and biological processes for biohydrogen production that represent the two main categories for hydrogen production from biomass.

Figure 2-2 depicts the major pathways of biomass based hydrogen production [19]. Hydrogen can be produced from biomass feedstock via gasification (steam gasification, supercritical water gasification (SCWG)), steam reforming of bio-oils and pyrolysis as thermochemical conversion processes. Dark fermentation and hybrid reactor system are the most well known biological hydrogen production processes although other technologies have been proposed such as photo-fermentation, biophotolysis of water using green algae and blue-green algae (cyanobacteria).

## **2.2.1 Biohydrogen Production by Thermochemical Processes**

### **2.2.1.1 Hydrogen from biomass pyrolysis**

Biomass pyrolysis is a route of gaseous, liquid (tar and other organics) and solid (char) production for generation of alternate sources of energy [20]. The required temperature range for pyrolysis in the absence of air is 273-500 °C at 0.1–0.5 MP [21]. With respect to the operating condition, the pyrolysis process is divided into fast pyrolysis and conventional (slow) pyrolysis. Low temperature tar and high temperature gas is generated in biomass fast pyrolysis, while slow pyrolysis is associated with high charcoal content [22]. Fast or flash pyrolysis in high temperatures and very short residence times is preferred for hydrogen production [23]. Slow pyrolysis is normally not taken into consideration for hydrogen production because the major product of this process is charcoal. In the fast pyrolysis process, the biomass feedstock is heated quickly in the absence of air (Eq. 2.1) to form vapor and condense to a dark brown mobile bio-liquid. The products of fast pyrolysis include gaseous products (CH<sub>4</sub>, H<sub>2</sub>, CO, CO<sub>2</sub> and other gases based on the organic nature of the biomass feedstock), liquid products (tar and oils such as acetic acid and acetone, which are liquid at room temperature), and solid products (composed of char and pure carbon plus other inert materials). Although pyrolysis processes are applied for biofuel production, biomass-based hydrogen can be generated directly through fast pyrolysis in high temperature circumstance and sufficient volatile phase residence time, according to Eq. (2.1)



The typical composition of biogas obtained is N<sub>2</sub> 40- 50%, H<sub>2</sub> = 15- 20%, CO = 10- 15%, CO<sub>2</sub> 10- 15%, CH<sub>4</sub> = 3- 5%. In order to increase the yield of hydrogen from fast pyrolysis mechanism, steam reforming of methane and other produced hydrocarbon vapors can be also performed followed by

water-gas shift reaction to enhance the rate of hydrogen production. Based on water solubility, the oily by-products of pyrolysis are separated into two fractions. The water-soluble by-products are applied for hydrogen production while the water-insoluble are used for adhesive production. Type of catalyst, temperature, heating rate and residence time are the most important parameters which control hydrogen yield from pyrolysis biomass process. The adjusting of these parameters is implemented by the selection of reactor types and heat transfer modes, such as solid–solid conductive heat transfers and gas–solid convective heat transfer [24]. In pyrolysis biomass hydrogen production, high temperature, high heating rate and long volatile phase residence time are crucial [25]. The yield of hydrogen from pyrolysis of biomass is augmented significantly when Ni-based catalyst is employed.

Due to difficulties of tar gasification, the influences of inexpensive catalytic dolomite and CaO [26] and some other catalysts such as Y-type zeolite [27], Ni-based catalysts [28], K<sub>2</sub>CO<sub>3</sub>, Na<sub>2</sub>CO<sub>3</sub> and CaCO<sub>3</sub> [19,28], on the breakup of hydrocarbon composition in tar were experimented. Furthermore, it was found that different oxides (Cr<sub>2</sub>O<sub>3</sub> [19,28] and Al<sub>2</sub>O<sub>3</sub>, SiO<sub>2</sub>, ZrO<sub>2</sub>, TiO<sub>2</sub> [1,19,28]) have excellent potential to decompose tar's hydrocarbon. Hydrogen production from pyrolysis of various biomass feedstock such as peanut shell [19-28], post-consumer wastes like plastics, trap grease, mixed biomass and synthetic polymers [21-29] rapeseed [21-29] and agricultural residue [21-29] was experimented by different researchers.

### 2.2.1.2 Biomass gasification

Biomass gasification is a thermal process that generates high gaseous products and small quantities of char. Generally gasification consists of combustion and pyrolysis processes to generate heat for the endothermic pyrolysis reactions. To enhance the rate of gas production, gasification is usually performed at high temperatures. A combination of hydrogen, methane, carbon monoxide, nitrogen and carbon dioxide is produced at the end of gasification process. In the biomass gasification systems, air or oxygen is employed in combustion or partial oxidation processes. Thermal decomposition of solid biomass takes place at temperatures around 600-1000 °C in which gas-phase products such as CH<sub>4</sub>, CO<sub>2</sub>, H<sub>2</sub>, H<sub>2</sub>O, CO and other gaseous hydrocarbons (CHs) are formed [19,29]. The combination of final produced gases in the gasification process is influenced by the composition of biomass feedstock, the gasifying agent and the gasification process. Equation 2.2 shows the biomass gasification process [19,29]:



The first step of the biomass gasification is the thermochemical decomposition of the cellulose, hemicelluloses and lignin compounds with production of volatiles and char [19,29]. Furtherly the char gasification and some other equilibrium reactions take place.

Biomass gasification is a form of pyrolysis implemented in higher temperatures resulting in a mixture of gases with hydrogen content ranging from 6–6.5% [19-29]. Biomass gasification has been known as a possible process for renewable hydrogen production, which is beneficial to develop environmentally friendly as well as highly efficient process for large-scale hydrogen production. Despite this high capacity, all process equipment required for biomass-based hydrogen production has been well established commercially, except gasifier equipment [19-29].

## 2.2.2 Biohydrogen Production by Biological Processes

### 2.2.2.1 Biophotolysis

The biological production of hydrogen (biohydrogen) is the microbiological conversion of organic substrates in  $H_2$  using metabolic enzymes such as hydrogenase (Hasi) and nitrogenase (Nasi). The biological production of  $H_2$  can be photobiological, using algae, photosynthetic bacteria or cyanobacteria, or it can take place by fermentation in the absence of light (Dark Fermentation), using heterotrophic bacteria [19,29].

Algae and cyanobacteria, known as blue-green algae are microscopic organisms that float in the water and performing the same type of plant photosynthesis, in which water is separated from the sunlight into  $O_2$  and a strong reducing agent, usually ferredoxin, normally used to reduce  $CO_2$  carbohydrate. However, under certain conditions, some microalgae produce  $H_2$  following the complete dissociation of the water, a process said biophotolysis (Fig. 2-3).

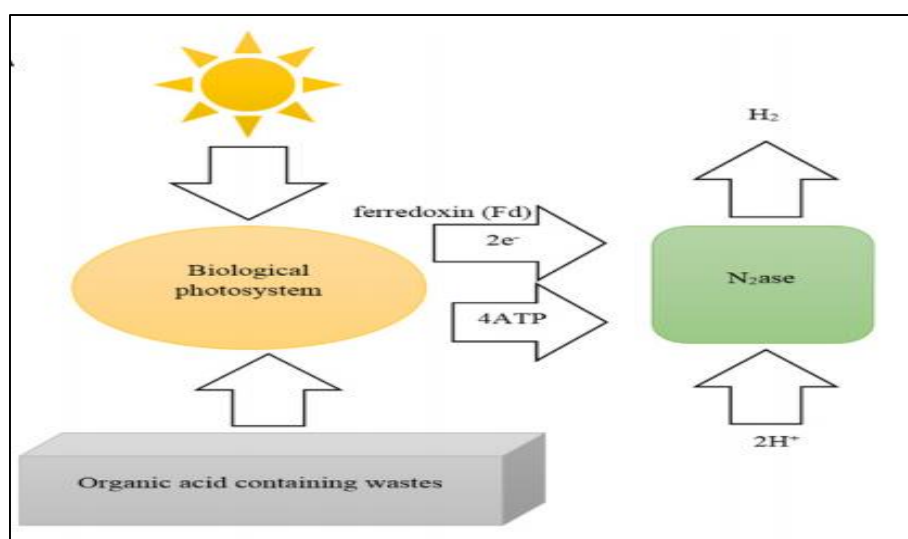


Fig. 2-3 Photo-fermentation process

### *Direct Biophotolysis*

If ferredoxin, produced by photosynthesis during the water splitting, is used to directly reduce manufacturers enzymes of  $H_2$ , hydrogenase or nitrogenase, without the intermediate  $CO_2$  fixation, the process is called direct biophotolysis. In theory, the direct biophotolysis is a very attractive process, but in practice is severely limited, among other factors, by the strong inhibition operated by  $O_2$  that simultaneously develops. One method to overcome this limitation is to remove the  $O_2$  product, for example by means of a breathing process using endogenous or exogenous substrates [19,29].

### *Indirect Biophotolysis*

The  $H_2$  can be also obtained from carbohydrates produced by microalgae during normal photosynthesis, a process called indirect biophotolysis. A mechanism for indirect biophotolysis is based on heterocystous cyanobacteria, filamentous species which exclude  $O_2$ , and reduce the nitrogen with the enzyme nitrogenase and subsequently produce  $H_2$ , coming to a complete water splitting. However, the *Nasi* is not an efficient enzyme and thus for practical purposes it would be necessary to replace it with hydrogenases. Another approach to the indirect biophotolysis consists in carrying out two reactions, sequentially and in separate stages: the first one is the production of  $O_2$  (with  $CO_2$  fixation) and then  $H_2$  production (with  $CO_2$  liberation). The second stage may be activated by light or conducted in the absence of light.

The photosynthetic bacteria, by using the light energy, are able to convert the organic acids and other organic substrates in  $H_2$  and  $CO_2$ , in the course of a photo-fermentation mediated by nitrogenase. On the contrary, the bacteria which carry out fermentation in the absence of light, the Dark Fermentation (DF), transform sugars, starches and other carbohydrates and easily fermentable organic substrates into  $H_2$  and  $CO_2$ , together with organic acids, alcohols and other by-products [19,29,30] (Fig. 2-4).

DF offers several advantages over other thermochemical and biochemical processes. Since the process does not depend on a light source, it is not affected by weather condition nor is land and cost demanding, there is no  $O_2$  limitation [19,29-36], residues or wastes can be used making  $H_2$  production advantageous either in economic and environmental aspects [29-36], produces valuable metabolites such as butyric, lactic and acetic acids as by products [19,29-36]. Moreover, biohydrogen production should contribute to the biorefinery concept since the wastes generated from biofuel production such as crude glycerol [19,29-36], deoiled algal cake [19,29-36] or cotton seed cake [19,29-36] can be utilized as a substrate.

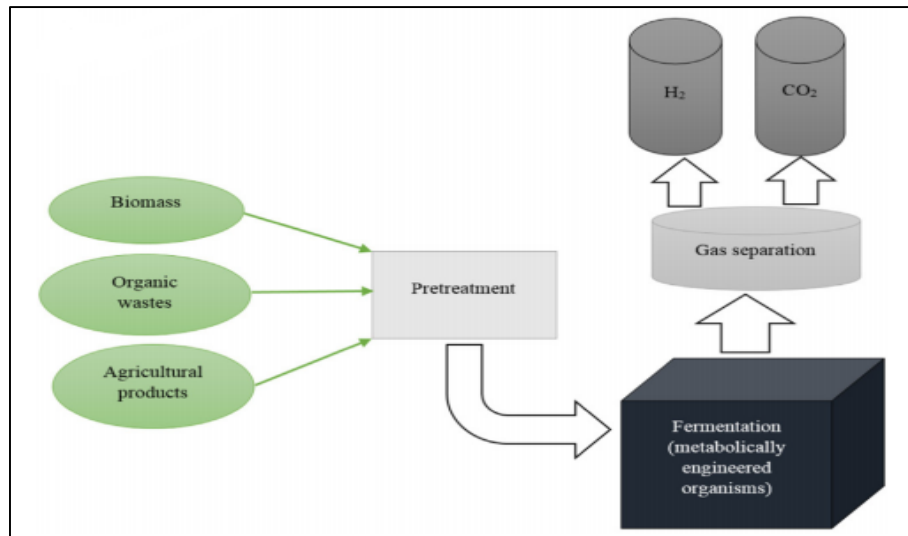


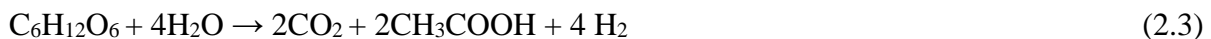
Fig. 2-4 Dark fermentation process

Most of studies on DF are addressed on investigating the role of hydrogen to the thermodynamic conversion of volatile fatty acids (VFAs) for the production of methane only [1,19,29]. The research for anaerobic bio-hydrogen production appears still lacking and reserves further efforts.

### 2.3 Dark Fermentation

The research applied in the field of biological production of  $H_2$ , at least until recently, it was concentrated mainly to the photo-biological process, forgetting almost completely the fermentation process in the absence of light. This is probably due in part to historical reasons: the first conference on this topic was directed by photosynthesis experts, determining the direction of this research [19,29,37]. The other reason has been the recognition that the anaerobic fermentations to  $H_2$ , in the absence of light, have a rather poor yield. Thauer et al. [37] pointed out that the conversion of glucose to  $H_2$  by anaerobic bacteria theoretically could produce up to four moles of  $H_2$  (Eq. 2.3), compared to the 12 theoretically possible moles (Eq. 2.4).

This value is called “Thauer’s limit” [37]:



Thauer’s limit is due to the thermodynamic of process: a yields of 4 moles of  $H_2$  and 2 moles of acetic acid per mole of glucose provides the higher variation of Gibbs’ free energy (215 kJ/mole at

25 °C and 1 bar of H<sub>2</sub>) [37]. This energy can be used form bacteria to produce 4 moles of ATP per mole of glucose and so used for anabolic metabolism [37].

The production of a stoichiometric quantity of 12 moles of hydrogen (Eq. (2.4)) is not thermodynamically favored and practically in DF process only the Eq. (2.3) occurs. In addition, Thauer et al. [37] showed that the yield in real DF process is about 2 moles of hydrogen per mole of glucose.

### **2.3.1 Dark Fermentation: Operating Conditions**

The production of hydrogen by Dark Fermentation is strongly dependent on the following parameters: pH, partial pressure of hydrogen, temperature and type of biomass used as substrates.

#### **2.3.1 pH**

Several studies were concerned the effect of pH on biohydrogen production by DF. Literature data indicate that the value of the optimum pH for DF process depends on the type of substrate used and in general, falls in the range 5-6.5, in which is favored the activity of hydrogenase [19,29,38].

A highly important aspect is related to the fact that the production of volatile organic acids during the process is different under different pH conditions. In particular, the routes that lead to the formation of hydrogen as low as butyrate and acetate are favored at pH comprised between 4.5 and 6 while at higher pH, also correspondending to the neutral pH value, there is an accumulation of ethanol and propionate. Several authors [19,29,38] studied the impact of pH on the activity and on the microbial metabolic diversity in the process of fermentation with glucose, xylose, glycerol at 30 °C. They also showed that for pH values lower than 6 the VOC products in larger quantities were butyrate and acetate while at higher pH values had yet acetate and ethanol. Furthermore, both in high pH conditions and low, the brewing process generally is dominated by Clostridia bacteria while at neutral pH is greater microbial diversity in [38] system. This suggests that the effects of pH involve not only a change of the metabolic sequences but also in large changes in the development of microbial communities.

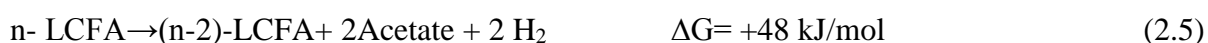
#### **2.3.2 Temperature**

The temperature is one of the most important parameters that affect the yield in the production of biohydrogen and the microbial metabolism in mixed cultures [38]. Due to the breadth of the types of substrates to be used in the DF, in the literature are not provided optimal temperature range for the process [19,29,38]. However, it is known by many literature studies that crop residues, food waste and cattle manure have higher yields hydrogen if the process is carried out in thermophilic

temperatures (50-70 °C) [7,19,29,38]. However the main disadvantage of the thermophilic anaerobic fermentation, is the energy cost for heating the reagent system. So, from industrial points of view, the mesophilic regime (30-40 °C), used in this PhD thesis, is the most attractive [38].

### 2.3.3 Hydrogen Partial Pressure

Hydrogen partial pressure has a significant influence since the increase of H<sub>2</sub> concentration causes a decrease of yields due to occurrence of the degradation reactions of volatile fatty acids through the oxidative beta-pathway (Eq. (2.5), (2.6)):



Eq. (2.5), (2.6) are characterized by positive values for the Gibbs free energy which are thermodynamically not favored [38]. Moreover it is noted that the reverse reaction to (2.6) is thermodynamically favored in fermentation processes and therefore reduces the performance of bioreactors due to the accumulation of acetate.

The growth of the hydrogen concentration due to microbial metabolism has effects not only on the production of hydrogen, but also on the metabolic pathway that shifts towards the solventogenesis or the production of lactate, ethanol, acetone and butanol. However some recent studies showed that, rather than an increase in the hydrogen partial pressure, it is the accumulation of volatile fatty acids which favors the solventogenesis [38]. Partial pressure of hydrogen during the DF can be reduced by properly stirring the digester, while ensuring a final production of greater biohydrogen. There are also alternatives to improve the extraction of gas as stripping of biohydrogen from the head of the reactor by means of an absorption membrane [38] or the bubbling of an inert gas such as N<sub>2</sub> within the [38] system. However, the above described techniques have disadvantages: the first technique develops a biofilm on the membrane which promotes the growth of methanogenic bacteria, while the second technique, regardless of the significant removal of biohydrogen.

Despite the various techniques available for reducing the hydrogen partial pressure, they required further research studies to develop the gas purification systems in order to maintain a low partial pressure of hydrogen in the reactant system.

### 2.3.4 Substrates and Inoculum

The substrate plays an important role in the H<sub>2</sub> yield, production rate and the overall economy of the process of biohydrogen production [39,40]. Characteristics of substrate are mainly dependent on the



carbohydrate content, bioavailability and biodegradation rate [39-44]. Carbohydrate rich substrates have been extensively used in DF studies, in particular pure glucose, sucrose and starch mixtures [38-44]. Monlau et al. [7] and Guo et al. [45] reported that the soluble and readily accessible sugars represent the main fraction of biomass that can be converted into hydrogen. In more recent dark fermentative studies, complex substrates have been considered, such as energy crops [38-44], organic fraction of municipal solid waste (OFMSW) [38,46-49], agro-industrial wastes like those from food processing industries (e.g. olive mill wastewater and cheese whey) [38-44], effluents from livestock farms and aquatic plants [38,40,42], the agricultural residues like lignocellulosic biomasses (e.g. rice straw, wheat straw and corn stalks) [19,29,38,45-48].

Various pretreatment steps have been employed prior DF digestion to facilitate bacterial access to the complex substrate and enhance hydrogen production: thermal [38] or microwave-assisted pretreatment [19,29,38], acid [19,29,38], alkaline [19,29,38] or enzymatic [19,29,38] hydrolysis [19,29,38].

Table 2-1 shows the biohydrogen production potential of different organic biomasses typically used by DF process and the pre-treatment methods of substrates and inoculum [45,50]. Several authors [19,29,38] have been used an acid hydrolysis of different types of biomass such as activate sludge, grass, beer, poplar leaves, food waste, cornstalk, obtaining a  $H_2$  yields up to  $100 \text{ mL } H_2 \cdot g^{-1} \text{ VS}$  [19,29,38]. Other authors used the alkaline hydrolysis (with NaOH) on tofu residue, beet-pulp, milled corncob, rice straw, maze straw, organic wastes obtaining  $H_2$  yields up to  $96 \text{ mL } H_2 \cdot g^{-1} \text{ VS}$ . Furtherly different types of treatment like Aqueous ammonia soaking (AAS), Ozone dosage ( $0.16 \text{ g } O_3/g \text{ TS}$ ) and high pressure (9bar) [19,38] have been recently reported.

Summarizing, the constructed microbial consortia for digestion of complex substrates require pretreatment to increase nutrient and seed formulation and enhance  $H_2$  production [38,51].

Biological pre-treatment of biomass is recently proposed. It consists of in enzymatic degradation of substrate to obtain easily fermentable sugars [52]. Compared to current thermal or chemical pretreatments, the biological offers the advantage of an environmental-friendly and energy-efficient process [52] although the substrate degradation occurs slowly and long pretreatment time is required.

Substrates	Pre-treatment	H <sub>2</sub> yields
Activated sludge	Acid: 0.5% (w/v) HCl; 24 hr, room T	Control: 9 mL g <sup>-1</sup> VS 24 h: 41 mL g <sup>-1</sup> VS $\Delta Y$ : +355.6%
Grass	Acid: 0.5-8% (w/v) HCl; 30 min boiling	Control: 4.39 mL 4.0% HCl: 72.21 mL $\Delta Y$ : +1544.9%
Grass	Alkali: 0.5-8.0% (w/v) NaOH, 30 min boiling	Control: 4.39 mL 0.5% NaOH: 19.25 mL $\Delta Y$ : +338.5%
Beer lees	Acid: 0.5-4% (w/v) HCl; 30 min boiling	Control: 3.16 mL g <sup>-1</sup> dry substrates 4.0% HCl: 53.03 mL g <sup>-1</sup> dry substrates $\Delta Y$ : +1578.2%
Poplar leaves	Acid: 0.5-8% (w/v) HCl; 30 min boiling	Control: 15.04 mL 4.0% HCl: 33.45 mL $\Delta Y$ : +122.4%
Food waste	Acid: 1.0 N HCl pH: 3.0, 24 h, 4 °C	Control: 42 mL g <sup>-1</sup> VS Treated: 55 mL g <sup>-1</sup> VS $\Delta Y$ : +31.0%
Food waste	Alkali: 1.0 N NaOH pH: 11.0, 24 h, 4 °C	Control: 42 mL g <sup>-1</sup> VS Treated: 46 mL g <sup>-1</sup> VS $\Delta Y$ : +9.5%
Food waste	Acid: pH 1.0, 1 day	Control: 4.4 mL g <sup>-1</sup> VS Treated: 89.5 mL g <sup>-1</sup> VS $\Delta Y$ : +1934.1%
Food waste	Alkali: pH 13.0, 1 day	Control: 4.4 mL g <sup>-1</sup> VS Treated: 50.9 mL g <sup>-1</sup> VS $\Delta Y$ : +1056.8%
Tofu residue	Acid: 0-2.0% (v/v) HCl, 30 min	Control: 0.3 mol mol <sup>-1</sup> hexose 1% HCl: 1.25 mol mol <sup>-1</sup> hexose $\Delta Y$ : +316.7%
Tofu residue	Alkali: 0-2.0% (v/v) NaOH, 30 min	Control: 0.3 mol mol <sup>-1</sup> hexose 1% NaOH: 1.09 mol mol <sup>-1</sup> hexose $\Delta Y$ : +263.3%
Beet-pulp	Alkali: 2 M NaOH pH: 12, 30 min	Control: 90.1 mL g <sup>-1</sup> COD Treated: 115.6 mL g <sup>-1</sup> COD $\Delta Y$ : +28.3%

Milled corncob	Acid: 0.1-2.0% (w/w) HCl, heating at 100 °C for 30 mins	Control: 13.1 mL g <sup>-1</sup> VS 1% HCl: 67.9 mL g <sup>-1</sup> VS ΔY: +418.3%
Milled corncob	Alkali: 0.1-2.4% (w/w) NaOH, 0.5% H <sub>2</sub> O <sub>2</sub> (w/w), heating at 100 °C for 30 min	Control: 13.1 mL g <sup>-1</sup> VS 2% NaOH: 14.3 mL g <sup>-1</sup> VS ΔY: +9.2%
Cornstalk	Acid: 0.1-4.0% (w/w) H <sub>2</sub> SO <sub>4</sub> , heating at 121 °C, 60 min	Control: 22.1 mL g <sup>-1</sup> VS 1.5% H <sub>2</sub> SO <sub>4</sub> : 103.3 mL g <sup>-1</sup> VS ΔY: +367.4%
Organic wastes	Acid: 1 N HCl pH: 2.0, 24 h	Control: 6.99 mL g <sup>-1</sup> VS Treated: 86.00 mL g <sup>-1</sup> VS ΔY: +1130.3%
Organic wastes	Alkali: 1 N NaOH pH: 12.5, 24 h	Control: 6.99 mL g <sup>-1</sup> VS Treated: 95.93 mL g <sup>-1</sup> VS ΔY: +1272.4%
Sludge	Acid: 6.0 M HCl pH: 2.0, 5 min, Initial pH: 7.0	Control: 1.21 mL g <sup>-1</sup> VS Treated: 3.25 mL g <sup>-1</sup> VS ΔY: +168.6%
Sludge	Alkali: 6.0 M NaOH pH: 12.0, 5 min, Initial pH: 7.0	Control: 1.21 mL g <sup>-1</sup> VS Treated: 1.46 mL g <sup>-1</sup> VS ΔY: +20.7%
Sludge	Alkali: 6.0 M NaOH pH: 12.0, 5 min, Initial pH: 11.5	Control: 7.57 mL g <sup>-1</sup> VS Treated: 11.68 mL g <sup>-1</sup> VS ΔY: +54.3%
Cattle dung slurry	1 mg/L Co, 2 mg/L Ni, 20 mg/L Fe and 20 mg/L Fe <sub>3</sub> O <sub>4</sub>	/
Rice straw	3% (w/v) NaOH, 35 °C, 48 h	/
Maize straw	NaOH (4% and 6%) (w/v) pretreatment, Fe dosage (50, 200, 1000 and 2000 mg/L)	/
Swine manure fibers	Aqueous ammonia soaking (AAS)	/
Organic solid waste	Ozone dosage (0.16 g O <sub>3</sub> /g TS)	/
A mixture of grass and maize silage	High pressure (9 Bar)	/

Tab 2-1 Substrates and pre-treatment used for biohydrogen production by DF

Biological pretreatment could be employed prior to physical or thermo-chemical pretreatment to effectively shorten the enzymatic pretreatment time and reduce the severity of thermo-chemical pretreatment. Other advantages could be the absence of the generation of toxic substances and the decrease of energy requirement. The enzymatic pre-treatment could be used essentially for the lignocellulosic materials that represent an enormous potential for biohydrogen production by dark fermentation. However up to now low hydrogen yields are obtained and various technologies belonging to inoculum or substrates pre-treatment have been investigated for enhancing biohydrogen production. Heat, acid and alkali pre-treatments are the most commonly studied technologies for both substrates and inoculum pre-treatment. Nevertheless, other techniques, like as ionic liquid, steam explosion, ammonia fiber-explosion, fungal and enzymatic, freezing and thawing, microwave irradiation, ultrasound irradiation have yielded positive findings [53].

The major obstacle for conversion of lignocellulosic material into fermentable sugar is the complex structure and the presence of inhibitor hemicellulose [53]. Mild alkali pretreatment has advantages in removing lignin with more effectiveness for agriculture residues and herbaceous crops [54]. Cheng and Zhu [55] proposed for sugarcane bagasse an optimized pretreatment at 80°C with 3% NaOH leading to hydrolysate containing pentose (xylose) and hexoses (glucose), xylose content influencing cell growth, substrate utilization, and product yield.

A culture of *Clostridium thermocellum* and *Thermoanaerobacterium aotearoense* have been used as inoculum due to the double benefit of low cost and the synergistic effect favouring the degradation of cellulose into H<sub>2</sub>. A yield of 50.05±1.51mmol H<sub>2</sub>/L was reported using a liquid-to-solid ratio of 25:1. Cellobiose, cellodextrins, and xylose were detected as by-products [54,55].

Hypothermal pretreatment of lignocellulosic biomass at dilute acid conditions generates inhibitors, such as phenolic compounds and aliphatic acids, but *Clostridium beijerinckii* exhibited resistance to these types of inhibitors.

Fermentation of the xylose-rich lignocellulosic hydrolysate with *C. beijerinckii* resulted into H<sub>2</sub> production of 2.72 mol H<sub>2</sub>/mol xylose [38,54,55]. The culture helped xylose utilization with improved metabolism and lowered acetate accumulation.

Li et al. [56] studied the digestion of Cornstalk, with a large lignocellulosic component and proposed a novel dynamic microwave-assisted alkali pretreatment (DMAP) to facilitate biomass digestion. It consists in supplying direct energy into the lignocellulosic material with an electromagnetic to achieve the removal of lignin and the increase of the soluble compounds release for easy access by microorganisms. Given amounts of cornstalk along with 2 L NaOH were mixed homogenously and circulated with periodic irradiation The hydrogen yield (105.61mL/g of

cornstalk) was 54.8 % higher, with increased hemicellulose (41–79%) and cellulose (71%) degradation rate in comparison with untreated cornstalk [38,53,54].

The biological treatment could be a promising methodology for fermentative conversion of lignocellulosic biomass to H<sub>2</sub>. [38,57].

The hydrogen producing seed inoculum or culture is crucial for hydrogen production [19,29,38,52-54,57]. Literature reports on the employment of pure [19,29,38,52-54,57] or mixed cultures [38]. Several pure cultures have been studied for digestion of different substrates and it appears that various strains species of Clostridia and Enterobacter are the mainly used pure cultures [38,57]. In Table 2-2 some recently literature results are summarized.

<b>Culture</b>	<b>Substrates</b>	<b>T (°C)</b>	<b>pH</b>	<b>Optimum H<sub>2</sub> yield (mol H<sub>2</sub>/mol glucose)<sup>a</sup></b>
Enterobacter cloacae IIT-BT08	Glucose	36	6	2.2
Clostridium thermolacticum DSM 2910	Lactose	58	7	1.5
Enterobacter cloacae DM 11	Malt, yeast extract & glucose	37	6	3.9
Thermotoga neapolitana DSM 4349	Hydrolyzed potato steam peels	80	6.9	3.3
C. thermocellum DSM 1237 and C. thermopalmarium DSM 5974	Cellulose	55	7	1.36
Clostridium thermocellum 7072	Corn stalk	55	7.2	1.2
Clostridium pasteurianum	HCl-pretreated grass	35	/	/
Clostridium sartagoforme FZ11	Corn stalk	35	/	/
Caldicellulosiruptor saccharolyticus DSM 8903	Switchgrass	65	/	11.2 mmol H <sub>2</sub> /g substrate

Tab 2-2 Biohydrogen production by DF with different substrates and cultures

The most commonly used are pure cultures of the *Clostridium* family in mesophilic or thermophilic conditions. However,  $H_2$  synthesizing bacteria exist commonly in environments such as soil, wastewater sludge, manure and compost. All these materials thus can be used as mixed cultures sources for fermentative  $H_2$  production [19,38,57].

Mixed cultures are generally preferred over pure ones for several advantages: practicability for engineering applications, economic benefits due to asepsis costs reduction, easiness in controlling microbial subgroups, broader feedstock choice [19,38,57].

The enrichment treatment of mixed cultures is however a necessary step to enhance biohydrogen production by inhibiting hydrogen consumer bacteria such as methanogens and homoacetogens, often present in mixed inocula [19,38,57]. Several authors (literature data) used different kinds of biomass inoculated with sewage sludge pretreated with different methods to enhance the growth of  $H_2$ -producer bacteria: heat-treatment (about 65-100 °C), immobilization of anaerobic microflora bacteria, ultrasonic pre-treatment at 100 KHz, DC (direct current) voltage application and alkaline pre-treatment [19,29,38,52-54,57].

The use of sewage sludge leads higher cumulative  $H_2$  production in comparison to other mixed culture sources, like as cow dung compost, chicken manure compost and river sludge [58].

The pretreatments of the inoculum proposed to this purpose often relies on the properties of the spore of  $H_2$  producing bacteria, such as *Clostridium*, which are ubiquitous in anaerobic sludge and sediments [19,29,38,58]. These organisms have a better chance to survive the harsh pretreatment conditions than the non-spore forming bacteria such as methanogens, as the spores can germinate again under favorable conditions [58]. Heat treatment of mixed cultures is largely used since it is a simple, inexpensive and effective method [38,58], although the effect might be different depending on the inoculum source [58]. Some studies reported a lower hydrogen yield by a heat shock treated seed inoculum than obtained by other pretreatment methods probably because the inhibition of other non-spore forming hydrogen producing bacteria might destabilize the main hydrogen production pathways [19,29,38,58]. Similarly, acid or base treatments of inoculum are widely employed. Generally, the activity of methanogens drops sharply at a pH below 6.3 or above 7.8 [58], whilst that of *Clostridium* spore and other hydrogen producers is not affected by mild acid conditions.

Other pretreatments, such as chemical or aeration pretreatment [19,29,38,58], are addressed aimed to obtain the selective inhibition of methanogens present in anaerobic sludge, which are strictly anaerobes [19,29,38,58] and sensitive to many chemicals [19,29,38,58]. Likewise, chemical inhibitors like sodium 2-bromoethanesulfonic acid (BESA), iodopropane, chloroform and acetylene are reported to inhibit  $H_2$  consumer methanogens growth [19,29,38,58]. In [19,29,38,58] is reported

that BESA inhibits the activity of co-enzyme M. reductase, which is a key co-enzyme of methanogenesis.

The selection of the best inoculum pretreatment for scaled-up systems must consider several parameters; such as operational costs, feasibility or complexity of the methods, time for the enrichment of the hydrogen producing seed, use of the DF residues in the post treatment processes. For example, BESA is not environmental friendly, expensive and is inadvisable when the DF residues are to be used in AD [38]. Likewise, heat shock treatment requires large energy inputs and is expensive for large scale applications. Conversely acid or shock load pre-treatment can be applied at large scale without net energy concerns [19,38,58].

Dark fermentation of wastes can be carried out by using the microorganisms spore contained in the waste itself [38,58] although. The fermentative hydrogen production took longer than supplying inoculum. The process start-up should be sped up by properly pretreating the inoculum or by applying appropriate reactor conditions [38,58] that enhance increase the growth rate of hydrogen producing microbial community.

### **2.3.5 Kinetics and Kinetic Models of Hydrogen Production**

Different factors such as substrate and inhibitor concentrations, temperature, pH and reactor type affect H<sub>2</sub> production rate by DF. Modeling of the H<sub>2</sub> production is very important to improve, analyze and predict H<sub>2</sub> production during fermentation. Mathematical models include the kinetic of cell growth and product(s) formation, substrate utilization and inhibition. In addition some models are developed to describe the effect of pH, temperature and dilution rate on H<sub>2</sub> production. The obtained model kinetic constants can be used in the design, operation and optimization of the fermentative H<sub>2</sub> production process. Different kinetic models have been proposed to describe growth of H<sub>2</sub> producing bacteria, substrate degradation and H<sub>2</sub> production.

Monod (or Michaelis–Menten equation) (Eq. (2.7)) [7,19,28,38] is an unstructured, non-segregated model of microbial growth, fits a wide range of data. The kinetic constants of this equation, K<sub>s</sub> and μ<sub>max</sub>, can be obtained by linear regression.

$$\mu = (1/X) \cdot (dX/dt) = \mu_{\max} (S / (K_s + S)) \quad (2.7)$$

where μ is the specific growth rate, X is the biomass concentration, S is the substrate concentration, K<sub>s</sub> is the saturation constant, μ<sub>max</sub> is the maximum specific growth rate.

Wang and Wan reported on previous studies using a Monod model to describe H<sub>2</sub> production with time in bio-H<sub>2</sub> fermentation [7,19,28,38].

Recently, the logistic model (Eq. (2.8)) became the most popular in describing cell growth because gives more detailed information on DF kinetic parameters. This equation has a sigmoidal shape that includes the lag phase, exponential and stationary phase of the batch growth:

$$\mu = (1/X) \cdot (dX/dt) = \mu_{\max} (1 - (X/X_m)) \quad (2.8)$$

where  $X_m$  is the maximum biomass concentration.

At high substrate concentration, the cell growth is inhibited and production of  $H_2$  is reduced.

Michaelis-Menten and logistic models cannot describe the inhibition phenomena, this drawback are overcome by more recent models. Different substrate inhibition models have been proposed. The Haldane-Andrew model (Eq. (2.9)) is widely used to describe the substrate dependence of the specific growth rate of  $H_2$  fermentations.

$$\mu = (1/X) \cdot (dX/dt) = \mu_{\max} (S / (K_s + S + (S^2/K_i))) \quad (2.9)$$

where  $K_i$  is the inhibition constant.

Some models have been proposed to describe the effect of inhibitors such as the modified Han-Levenspiel model (Equation (2.10)):

$$\mu = (1/X) \cdot (dX/dt) = \mu_{\max} (1 - (C/C_m)) \quad (2.10)$$

where  $C$  is the inhibitor concentration,  $C_m$  is the maximum inhibitor concentration or the concentration of inhibitor above which there is no biomass growth

The modified Gompertz model (Equation (2.11)) is widely used to describe the progress of cumulative  $H_2$  production in batch fermentations:

$$H = P \exp [- \exp [(\lambda - t)/B]] \quad (2.11)$$

where  $H$  is the cumulative production of  $H_2$  (L) in the range time  $t$ ,  $B$  is the final volume of hydrogen product (L) and  $\lambda$  is the lag phase (hr or day) and  $B$  is a parameter connected with the rate of  $H_2$ -production.

The Luedeking-Piret model (Equation (2.12)) has been widely used to describe the relation between cell growth rate and  $H_2$  production:



$$dP/dt = Y_{P/X} (dX/dt) + \beta X \quad (2.12)$$

where P is the product,  $Y_{P/X}$  is the growth associated yield coefficient;  $\beta$  is the non-growth associated product yield coefficient.

Wang and Wan reported that previous studies used the Luedeking-Piret model to relate cell growth rate and  $H_2$  production rate. The effect of temperature on the fermentative  $H_2$  production has been widely described using the Arrhenius model, while the effect of pH on the substrate consumption rate is described by an Andrew model using the concentration of  $H^+$  as the limiting substrate concentration. According to this model the rate of substrate consumption passes through maximum with increasing  $H^+$  concentration [7,19,28,38].

## 2.4 Content of Chapter

In this chapter have been studied different types of biomass for the  $H_2$  production by DF:

1) *Arundo donax* (AD) (Fig. 2-5) was studied as an example of lignocellulosic biomass. AD giant reed, also called domestic cane, is an herbaceous multiannual plant with long stem, robust and cable. It grows mainly in height reaching up to 8 meters.

It is very widespread in all the Mediterranean countries. Presents a very high growth rate and large amounts of fertilizers and pesticides are not necessary for the crop (so it return satisfactory values in terms of environmental sustainability). It also grows in marginal soils and with extreme conditions (high salinity, water scarcity). All these factors make this an excellent candidate for the cultivation of energy production from lignocellulosic biomass.

2) Organic Fraction of Municipal Solid Waste is another source of biomass with great potential. In fact in Italy it produces about 4411330 tons/a of waste per day. The energy recovery of such biomass would allow either to reduce the costs of disposal, both encouraging the recycling and then limit the environmental impact of landfills and low efficient disposal systems.

3) Litter: the disposal of soiled litter is a very important cost for the center and for this reason it is interesting to find an innovative methodology for the reutilization of this waste for energy purposes and reduce disposal costs.

4) Manure from cattle is widely available in Italy and more generally in Europe and worldwide. In Italy the number of cattle is about 6 million, disposal of manure is a significant cost and energy revaluation for this waste is a considerable plus for companies.

A synthetic medium based essentially on glucose was also considered as reference. Each substrate has been inoculated with a sewage sludge collected from wastewater treatment plant in Nola (Naples) that offers the benefit of higher potential  $H_2$  yields in comparison to other mixed cultures. All the tests have been carried out in mesophilic conditions (38 °C). For biohydrogen production

has been developed a different methodology to enhance the proliferation of hydrogen-producer bacteria to detriment of the methanogenic ones, the inoculum has been pre-treated with a medium of salt and nutrients at the same temperature of DF. This procedure is not commonly used in literature [19,29,38] but from an industrial applicative point of view, it is more convenient and less expensive than traditional pre-treatment methods and can be advantageous for the development of integrated plant anaerobic digester (biohydrogen Production)/Fuel Cells.

## **2.5 Materials**

### **2.5.1 Arundo Donax**

Arundo donax was collected from Torre Lama (Campania, Italy) agro-land. Leaves were separated from stems, washed, dried overnight at 80°C and minced with a chopper (Fig.2-6).



Fig. 2-5 Arundo donax

The tests were carried out with Arundo donax not treated (AD), and with Arundo donax treated by steam explosion at 210 °C for 6 min (ADexp, Fig 2-7) (supplied by ENEA in Trisaia (Matera, Italy)).

This treatment is aimed to separate the complex polymers (lignin, hemicellulose and cellulose) that characterize the biomass. The matrix of the biomass, then, is unstructured and more easily digested by the microorganisms for the biogas production.

This type of technique, however, also leads to the formation of by-products such as acetic acid, furfural, phenols, so these by-products may be toxic to the microorganisms and consequently for the process of anaerobic digestion.



Fig. 2-6 Arundo donax not treated used in DF tests



Fig. 2-7 Arundo donax treated by steam explosion used in DF tests

### 2.5.2 Organic Fraction of Municipal Solid Waste (OFMSW)

OFMSW has been prepared in laboratory (Fig. 2-8, Tab. 2-3) using food leftovers. Before being added to a bioreactor, it was grossly chopped, finely shredded with a home blender and finally pressed manually in a mortar to make a puree.



Fig. 2-8 OFMSW prepared in laboratory and used in DF tests

Component	% wt
Fruits	30
Cooked meat	5
Vegetable	30
Bread	35

Tab. 2-3 Laboratory OFMSW composition

### 2.5.3 Litter

Litter used in DF tests comes from an enclosure for mice. It consists mainly of beech wood chips mixed with mouse droppings. The litter (Fig. 2-9) has been collected from the research center BIOGEM s.c.a.r.l. in Ariano Irpino (AV). The center is equipped with one of the larger enclosures in Europe with a potential of 40,000 mice and 1,500 rats. Currently is present a population of about 7,000 mice and 200 rats.



Fig. 2-8 Litter used in DF tests

#### **2.5.4 Manure**

The last used biomass is represented by a manure coming from the cattle breeding “Cocca” located in San Marco de’ Cavoti (BN). The biomass is composed essentially from manure and some percentage of litter for cows. The farm has 8 heads (Cows “Marchigiane”), the average weight of single cow is about 400 kg. The cattle are located in a closed, stable free stall that involves the use of plentiful straw as bedding to ensure the comfort of the livestock. The barn cleaning is carried out by delivering the wastewater in the dung heap where it is stored for a period ranging between 4-6 months.

#### **2.5.5 Synthetic medium**

Synthetic medium has been prepared in a Pyrex glass vial (125 mL). The volume of liquid phase in the vial is 100mL. Synthetic medium was prepared with 19.6 mL of distilled water, 0.4 mL of resazurin solution 0.025% w/v; 10 mL of mineral solution ( $\text{Na}_2\text{HPO}_4$  7 g/L,  $\text{KH}_2\text{PO}_4$  3 g/L, NaCl 0.5 g/L,  $\text{NH}_4\text{Cl}$  1 g/L and trace elements). Resazurin is used as an indicator of anaerobiosis. After sterilization in autoclave (SMEG HV-85L) at 121°C for 20 minutes, 50 mL of solution 5 g/L of glucose (autoclaved separately); 250  $\mu\text{L}$  of saline solution 400x; 20 mL of inoculum were added to the medium.

### **2.6 Methods**

#### **2.6.1 Biomass Analysis**

Biomass composition, including the proximate (ASTM D5142), ultimate analysis (ASTM D3176), were analyzed using the TGA701-LECO Europe instrument (Table 2-4). For each biomass the moisture has been evaluated from 25°C to 107 °C in nitrogen flow until the constant weight; the



volatile in a ramp 107 °C to 950 °C in nitrogen flow for 7 min and ash in temperature range 600 to 750 °C in O<sub>2</sub> flow until the constant weight of the sample.

Biomass	C	H	N	Moisture	Volatile	Ash	Fixed carbon
	% dry ash free basis			% wt			
AD	47,32	5,92	0,33	8,39	72,6	14,85	4,14
ADexp	49,61	5,73	0,88	8,41	73,1	14,5	4
OFMSW	37,2	5,24	1,13	86,71	11,8	1,02	1,4
Manure	35,85	4,89	2,11	77,16	19,37	0,85	2,9
Litter	33,2	7	2,4	6,59	69,83	19,21	4,37

Tab. 2-4 Substrates analysis

### 2.6.2 Anaerobic Mixed Culture

Sewage sludge used as inoculum in DF tests was obtained from a primary wastewater digester of Nola (Naples). In the first fermentation the sludge was not subjected to treatments and used directly as inoculum, with a filtration to remove coarse particles, to obtain biomethane.

For the production of biohydrogen, the sludge was treated with a nutrient medium to support the growth of bacteria hydrogen producer (such as *Clostridium*) and to eliminate the methanogenic bacteria.



Fig. 2-9 Sewage sludge used as inoculum

### 2.6.3 Preparation of Nutrient Medium

The sludge has been treated with a nutrient medium to support the growth of hydrogen producer bacteria (such as *Clostridium*) and to eliminate the methanogenic ones. Nutrient medium was

prepared by dissolution in water (1L) of  $\text{NH}_4\text{Cl}$  (1 g),  $\text{K}_2\text{HPO}_4$  (0.3 g),  $\text{KH}_2\text{PO}_4$  (0.3 g),  $\text{MgCl}_2 \cdot 6\text{H}_2\text{O}$  (0.2 g),  $\text{CaCl}_2 \cdot 2\text{H}_2\text{O}$  (0.1 g),  $\text{NaCl}$  (10 g),  $\text{KCl}$  (0.1 g), cysteine (0.5 g),  $\text{CH}_3\text{COONa}$  (0.5 g), yeast extract (2 g), tripeptone (2 g),  $\text{NaOH}$  solution at pH 11 (10 mL), resazurin (0.1 g).

Before the fermentation tests, the inoculum has been pre-treated at 38 °C for 48 h with nutrient medium, in anaerobic conditions, with a ratio sewage sludge/medium of 1:1 v/v.

#### 2.6.4 Biomass Hydrolysis

The pre-treatment of biomass is essential to obtain reducing sugars easily fermentable by microbial consortium to increase the biomethane and biohydrogen yields, as discussed in par. 2.3.4. The biomass utilized in this PhD thesis have been subjected to enzymatic hydrolysis by the action of cellulase (Celluclast 1.5L, from Novozymes) and cellobiase (Novozyme 188, from Novozymes). Hydrolysis has been performed at 50°C for 72 h by contacting 20 g of biomass with 200 mL of deionized water, 2.48 mL of cellulase and 0.625 mL of cellobiase. The hydrolyzate has been filtered and the pH adjusted to 5.5-6 with 1M  $\text{NaOH}$  solution before the inoculation. For each substrate the concentration of reducing sugars has been evaluated. The only exception is the organic fraction of municipal solid waste. This type of biomass has not been subjected to hydrolysis because it already has monomers digestible by the microbial pool and because the enzymatic hydrolysis step is not is not very efficient on OFMSW.

Table 2-5 summarizes the results obtained.

<b>Biomass</b>	<b>Reducing sugars (g/l)</b>
AD	5
ADexp	5
Litter	2,59
Manure	2,14

Tab. 2-5 Reducing sugars content of different substrates after hydrolysis

#### 2.6.5 Fermentation Tests

Fermentation tests on, AD, ADHexp, litter and manure were carried out, in a vial of 125 mL (Fig. 2-10), with a composition of each batch reactor of 70 mL of hydrolysate supplemented with 0.4 mL of 0.025% w/v resazurin solution (indicator of anaerobiosis), 10 mL of mineral solution ( $\text{Na}_2\text{HPO}_4$  7 g/L,  $\text{KH}_2\text{PO}_4$  3 g/L,  $\text{NaCl}$  0.5 g/L,  $\text{NH}_4\text{Cl}$  1 g/L), 20 mL of inoculum (see Par 2.6.2).

For the OFMSW fermentation tests the following conditions have been adopted: 20 g of biomass (not hydrolysate) mixed in 80 mL of  $\text{H}_2\text{O}$  deionized, 20 mL of inoculum.

The vial is clamped with butyl rubber stopper pierced equipped with an aperture ring and the anaerobic conditions were obtained keeping the vial under stream of nitrogen for 30 min. A synthetic medium (see Par. 2.7.5), essentially based on glucose, has been used as comparison.



Fig. 2-10 Vials used in DF tests

### 2.6.6 Analytical Techniques

In all tests Microbial Biomass (MB) growth, reducing sugars, pH, volatile acids, ethanol and composition of the biogas have been monitored according to standard anaerobic procedures [59]. The biomass concentration was monitored by measuring the optical absorbance of liquid samples at 600 nm. After centrifugation at 3000 rpm for 5 minutes and filtration with 0.2  $\mu\text{m}$  cut-off filters, the liquid sample was analyzed for residual substrate content (glucose or total reducing sugars) and soluble fermentation products (organic acids, alcohols).

The concentration of glucose was measured following a modified Nelson-Somogyi method for reducing sugars [59]. Concentration of acetic, butyric, propionic acids and ethanol was measured by GC technique, using a Shimadzu instrument GC-17A equipped with FID detector and a capillary column containing a PEG stationary phase (BP20, 30 m by 0.32 mm i.d., 0.25  $\mu\text{m}$  film thickness, from SGE).

$\text{CH}_4$ ,  $\text{H}_2$  and  $\text{CO}_2$  concentrations were measured by GC technique, using a HP 5890 series II equipped with a TCD detector and a double packed molecular sieves-porapak column.

### 2.6.7 Nelson-Somogyi method

The analysis of the reducing sugars was carried out with the colorimetric method of Nelson-Somogy [59]. For the calibration of the method, a glucose standard solution was prepared (1 mg / ml) by dissolving 100 mg glucose in 100 ml of distilled water. Later they were taken from the



solution 10 ml and so added 90 ml of water (so as to have a concentration of 0.1 mg/ml). Subsequently, 0.1, 0.2, 0.3, 0.4 and 0.5 ml of this solution were taken and placed in test tubes of 10 ml, and in each was added distilled water to obtain a final volume of 2 ml. Subsequently, after adding 1 ml of alkaline copper tartrate solution, the tubes were placed in a boiling water bath for 10 min. After cooling down it was added 1 ml of Arseno-molybdate reagent and then distilled water so as to obtain a final volume of 10 ml. Finally, for each sample was measured the absorbance (Abs) at 620 nm.

Following has been reported the experimental procedure used for the analysis of samples: 200 microliter of sample; 1 mL of reactant A&B; 1.8 mL of H<sub>2</sub>O deionized;

After heating up to 100 °C and cooled the tube has been added 1 mL of reactant C and H<sub>2</sub>O distilled up to a final volume of 10 mL.

In following lines has been reported the composition of reactants A, B and C:

Reactant A: In a 100 mL flask has been mixed 80 mL of deionized water, 2.5 g of Na<sub>2</sub>CO<sub>3</sub>, 2.5 g of Rochelle Salt (KNaC<sub>4</sub>H<sub>4</sub>O<sub>6</sub>·4H<sub>2</sub>O), 20 g of Na<sub>2</sub>SO<sub>4</sub>. After the complete mixing has been added deionized water up to a final volume of 100 mL.

Reactant B: In a 100 mL flask has been mixed 80 mL of deionized water, 15 g of CuSO<sub>4</sub>\*5 H<sub>2</sub>O, mixed and added H<sub>2</sub>O up to a final volume of 100 mL and after the completely dissolution of the salt added 2 drops of H<sub>2</sub>SO<sub>4</sub> (97 % wt).

Reactant C: this reactant is the sum of 2 solutions; the first one is prepared added 45 mL of H<sub>2</sub>O, 2.5 g of (NH<sub>4</sub>)<sub>6</sub>Mo<sub>7</sub>O<sub>24</sub>\*4H<sub>2</sub>O and 2.1 of H<sub>2</sub>SO<sub>4</sub> (97%wt); the second solution is prepared dissolved in 25 mL of H<sub>2</sub>O 0.3 g of Na<sub>2</sub>HAsO<sub>4</sub>\*7H<sub>2</sub>O. After the preparation the two solution has been mixed and so added H<sub>2</sub>O up to final volume of 100 mL. Before use the final solution has been heat at 37 °C for 48 h in a continuous stirred mixed.

Reactant A&B: 24 mL of reactant A and 1 mL of reactant B.

### 2.6.8 Microbial biomass measurement

The biomass concentration has been monitored by turbidimeter measures, through the use of a Shimadzu double beam spectrophotometer, with a tungsten and a deuterium lamps. For not too high concentration of microbial biomass suspended (corresponding to values of Abs> 1.2), it is possible to apply the Lambert-Beer equation [59]:

$$\text{Abs} = \epsilon * c * l \quad (2.13)$$

where: Abs is optical density (or absorbance);  $\epsilon$  extinction coefficient; c concentration; l: the optical path length (usually uniform).

Therefore, it was possible to assess the growth of the microbial biomass measuring the absorbance of each sample at 600 nm at regular time intervals.

### 2.6.9 Biogas Volume Measurement

The crimped vial is a standard technique in anaerobic studies, even though it does not allow an easy evaluation of biogas volumes. The culture medium contained in the vial is placed in continuously stirring (800 rpm), inside an electrical oven at a constant temperature of 38 °C.

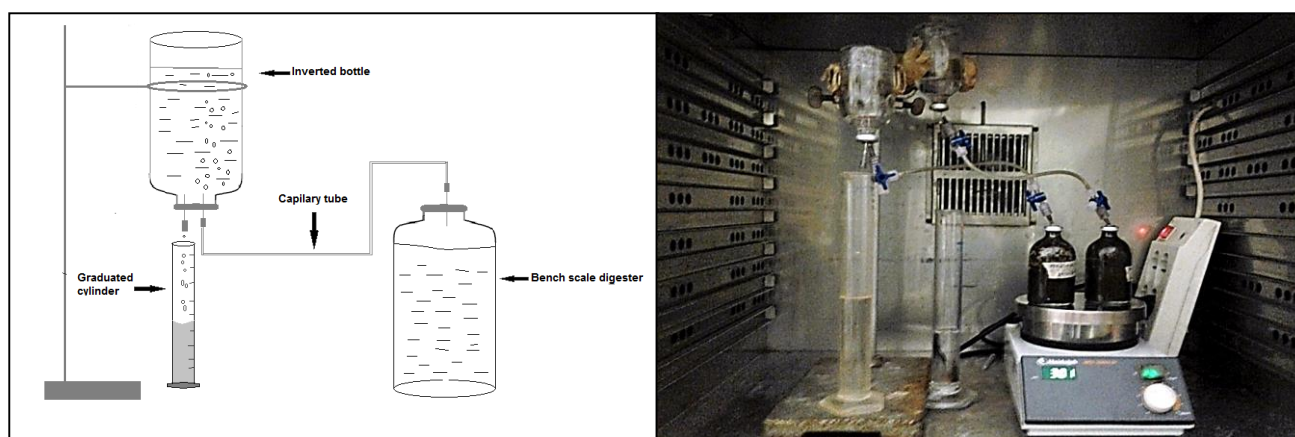


Fig. 2-11 Experimental apparatus for the evaluation of biogas obtained

A capillary tube connects the vial to an overturned vial which contains 100 mL of distilled water (Figure 2). The tubular connection allows the flow of the biogas produced from the first to the second vial where it accumulates in the top of the vial, thus allowing the dripping of the liquid phase through a bullet hole. The volume of liquid that is collected corresponds to the volume of biogas produced according to the Mariotte's law (volume of liquid dripped = volume of gas produced) [60,61].

### 2.6.10 Selection of H<sub>2</sub>-Producers Bacteria

The inoculum used for DF tests is a mixed culture containing H<sub>2</sub>-producer and CH<sub>4</sub>-producer bacteria. For the production of CH<sub>4</sub> the inoculum is not treated (it is only filtered to remove coarse particles) and used directly in anaerobic digestion tests following the standard procedure described in several literature papers [1-8,19,38]. The novelty of this work is the procedure based on the selection of hydrogen producer bacteria to enhance H<sub>2</sub> yields in biogas. For this purpose, the inoculum has been treated for a specific medium of salt and nutrient (see par. 2.6.3). Figure 2-12

summarizes the procedure adopted in DF tests for biohydrogen production. For simplicity, in the figure, are indicated only the AD, ADexp and SM (not subject to hydrolysis). Obviously, this procedure has been followed also for other biomass examined in this work (OFMSW, manure and litter).

The adapted inoculum (AI) has been used in the first fermentation tests on hydrolysate biomass, SM or OFMSW (ADH I, ADHexp I and SM I) under the conditions previously described.

Subsequently 20 mL of ADH I, ADHexp I and SM I digestate has been taken and treated with the same medium of nutrient used in step 1 with the ratio digestate: nutrient medium of 1:1 v/v to achieve a further adaptation. The new adapted inoculum has been used for second fermentation tests (ADH II, ADHexp II, SM II) (step 2).

Finally, the fermentation on ADH III, ADHexp III, SM III was carried out following the same procedure employed in the second one.

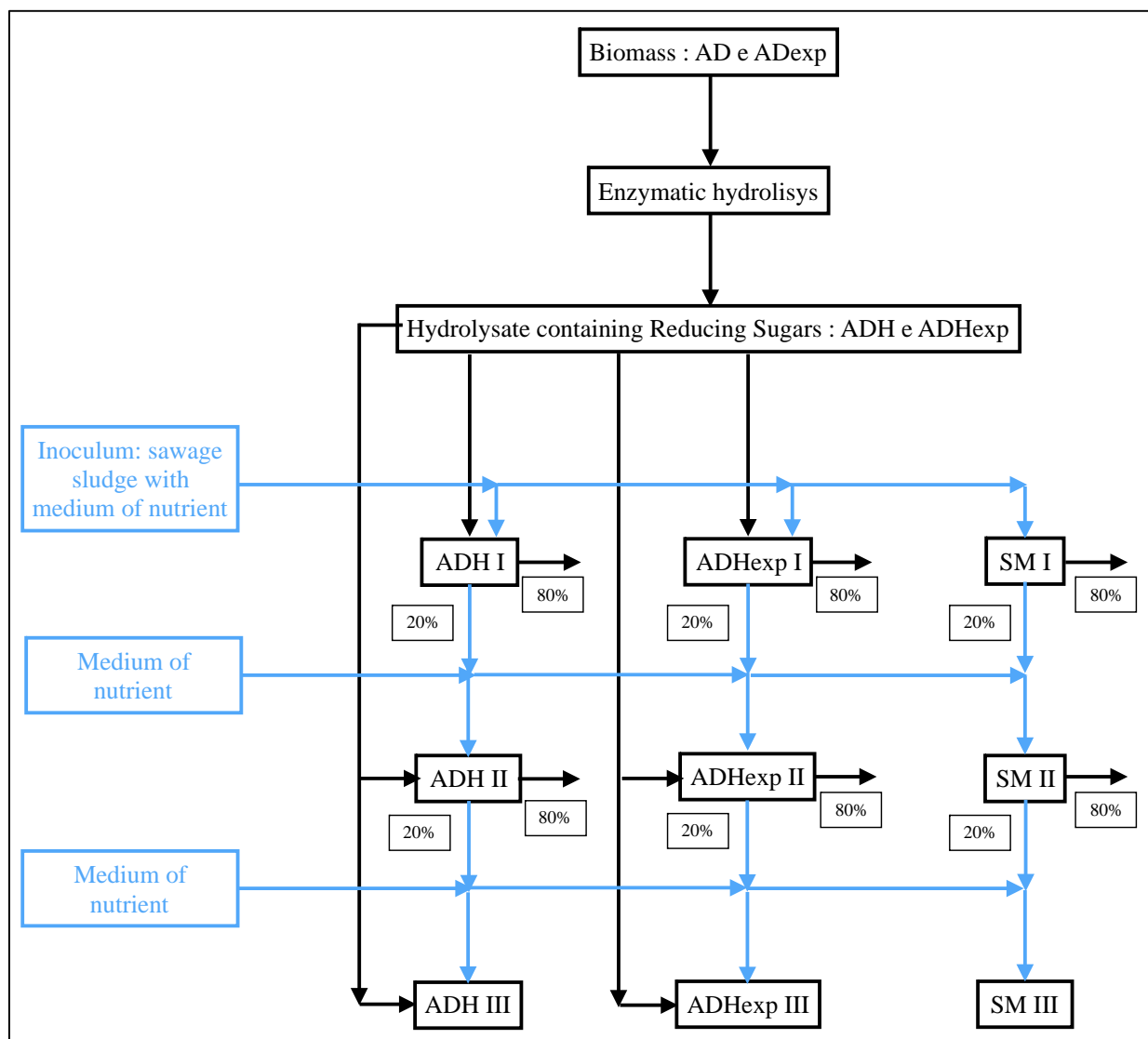


Fig. 2-12: Tests carried out to enhance the  $H_2$ -producer bacteria

This procedure has been adopted in optical of industrial application, in fact, after the third adaption the microbial consortium is composed essentially of  $H_2$  producer bacteria. During the experimental procedure has been noted that after 3 adaptations the results not change significantly, so it is possible hypothesize that the procedure is stabilized and the yields of  $H_2$  is constant.

## 2.7 Results and Discussion

### 2.7.1 Biomethane Production

Preliminary tests were carried out on all substrates in order to verify the presence of methanogenic bacteria inside the inoculum from sewage sludge. These tests were carried out only as a check, since the scope of the experimental activity is the biohydrogen production.

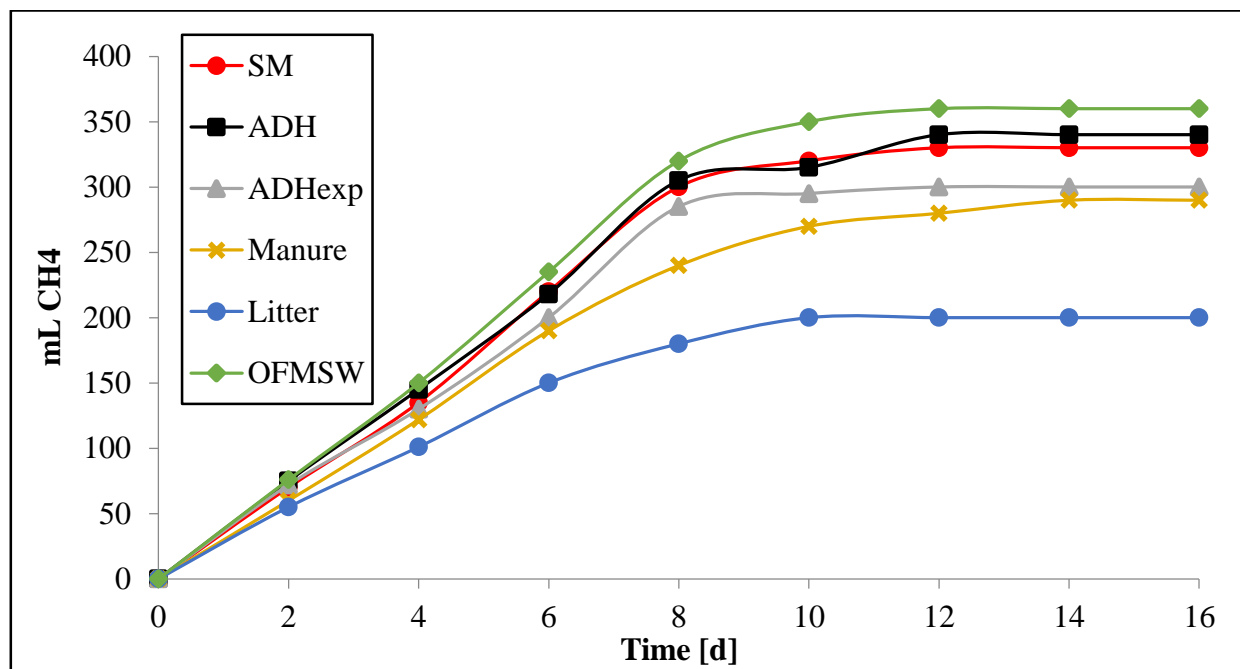


Fig. 2-13 Cumulative Biomethane production vs Time (days)

The experimental apparatus used for anaerobic digestions tests have been described in par. 2.8.9. The tests have been carried out in the following conditions:  $T=38^{\circ}\text{C}$ , inoculum/Biomass hydrolysate ratio: 1:4 v/v, 16 days of retention time. Each 2 days  $\text{CH}_4$  has been analyzed until its complete disappearance.

Figure 2-13 shows the results obtained in terms of cumulative volume of  $\text{CH}_4$  produced vs time. It can be noted that the higher volume of  $\text{CH}_4$  has been obtained with OFMSW (360 mL) while the lower amount of  $\text{CH}_4$  has been obtained with the litter (about 200 mL). These results are not surprising because the OFMSW has more available nutrients for microbial consortia, especially the methanogenic ones, while the litter, being essentially composed of lignin, possess lower amount of

easily digestible reducing sugars (see par. 2.6.4). Interesting case is represented by *Arundo donax* that shows relevant production of CH<sub>4</sub>. This confirms the potential of this lignocellulosic biomass for the utilization in anaerobic digestion and Dark Fermentation tests [19,29,38]. The comparison of ADH and ADHexp data indicates that steam explosion treatment disadvantages CH<sub>4</sub> production. This could be explained by the presence of inhibitory compounds, such as phenols and furfurals, which are produced during the steam explosion treatment. As regards the synthetic medium, a methane production of 330 mL has been obtained. This value is slightly lower than that obtained with the OFMSW and with the ADH, probably because in the synthetic medium is present only glucose, while in the hydrolysate of *Arundo donax* and in the OFMSW other types of sugars (i.e. pentose) that may be more easily digested by the microbial consortium are present. Ultimately, the anaerobic digestion of manure, leads to CH<sub>4</sub> production of 290 mL. This result may be surprising, given that the initial concentration of reducing sugars is the lowest (2,14 g/L, see tab. 2-5) among the biomass used. This can be justified by the fact that in the manure is already an amount of methanogenic bacteria. In several works the use of manure co-digestion with other substrates is reported to significantly enhance CH<sub>4</sub> yields. Table 2-6 summarizes CH<sub>4</sub> production on the different substrates.

Sample	CH <sub>4</sub> Volume (mL /g biomass )*
ADH	17
ADHexp	15
Manure	14,5
Litter	10
OFMSW	18

Tab. 2-6 Biomethane production on different substrates

\*For each anaerobic digestion test have been used 20 g of biomass

### 2.7.2 Biohydrogen Production

The biohydrogen production using ADH, ADHexp, manure, litter and OFMSW as substrate has been investigated and compared to a synthetic medium as reference. In the first adaptation the microbial consortium contains both methanogenic and hydrogen-forming bacteria. The focus of this work is to enhance the growth of the latter bacteria to the detriment of the methanogenic ones. To this purpose successive adaptations of the substrates and inoculum were required. In particular, every fresh substrate (see paragraph 2.6.10) was inoculated with a microbial consortium deriving from the previous adaptation. Each new inoculum from a previous adaptation has been subjected to

treatment with a nutrient medium (see paragraph 2.6.3) to promote the growth of H<sub>2</sub>-producer bacteria. Fermentation tests have shown that this procedure gives an improvement and stabilization of dark fermentation after three adaptations for each substrates with the stabilization of H<sub>2</sub> yields.

In each DF test it has been monitored the pH, the microbial biomass, reducing sugars, volatile fatty acids and bioethanol for the liquid phase and for the gas phase the biogas production and composition.

In subsequent figures it will report the trends for each substrate highlighting the increase in the hydrogen yields while in table 2-13 will be summarized the results pointing out the ml of hydrogen obtained per gram of reducing sugars and biomass utilized.

#### **2.7.2.1 Synthetic Medium (SM)**

Figures 2-14 and 2-15 show the trend of liquid phase analysis for SM. The glucose concentration (Figure 2-14) decreases to zero reaching negligible contents after 48 h. Consequently, the biogas production is essentially limited to the first two days of fermentation as showed in Fig. 2-16. This can be due to the depletion of glucose and to the acidification of the solution since dark fermentation takes place optimally with a pH of about 5.5-6 [19,29,38]. In fact, as shown in the Figure 2-15, the concentration of VFA (in particular acetic acid and butyric acid) in the culture medium increases with time leading to the acidification of the solution, that inhibits the H<sub>2</sub> production. This is confirmed by the microbial biomass trend reported in Figure 2-14, showing that the microorganisms growth increases in the first 24 h (value of microbial biomass equal to 5,59) reaching a maximum, after which slowly decrease (value of 4 after 72 h).

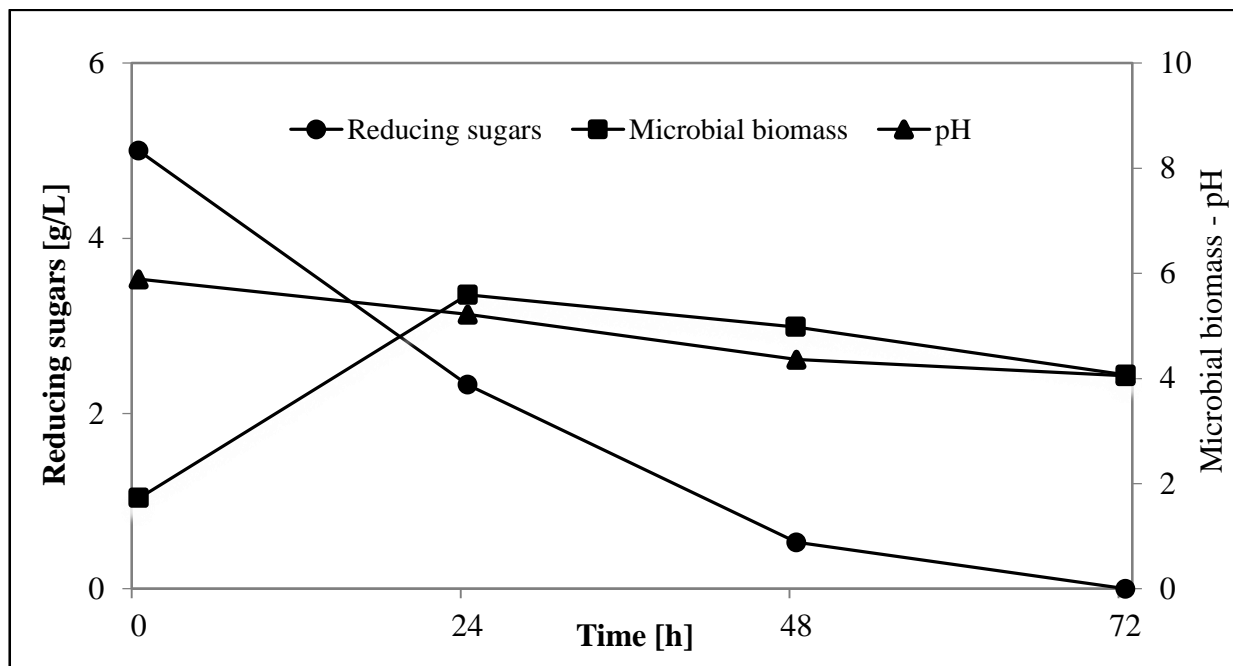


Fig. 2-14 Concentration of glucose, biomass and pH for SM as function of time

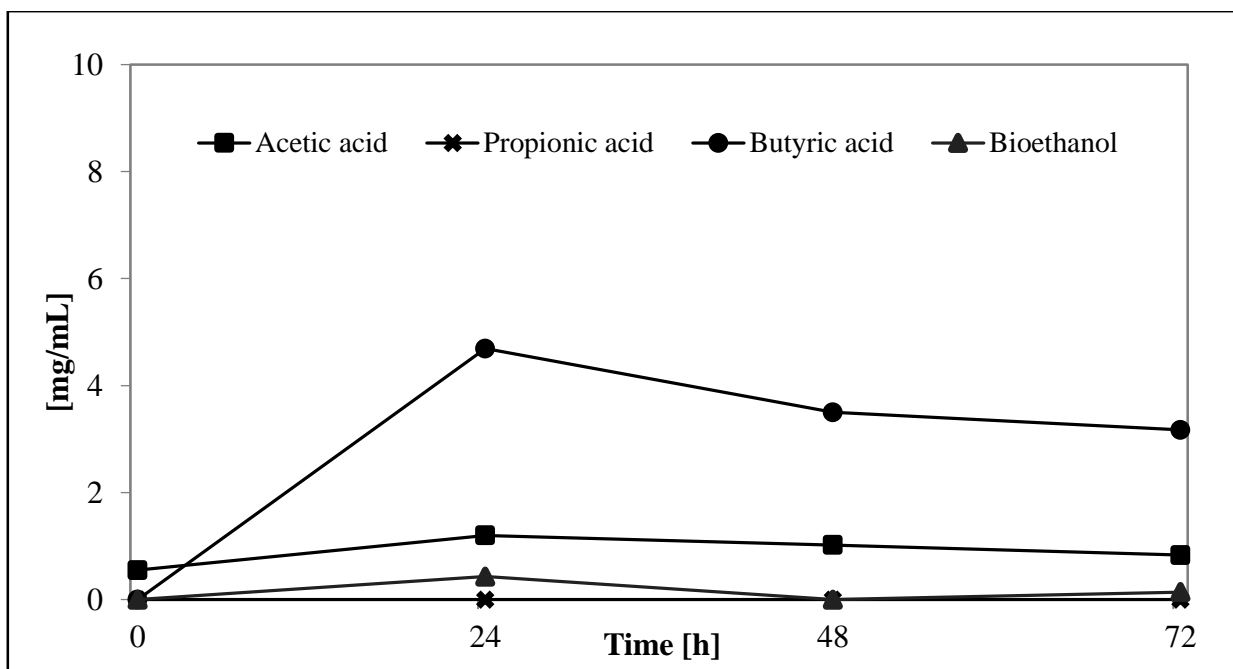


Fig. 2-15 Concentration of VFA and ethanol for SM as function of time

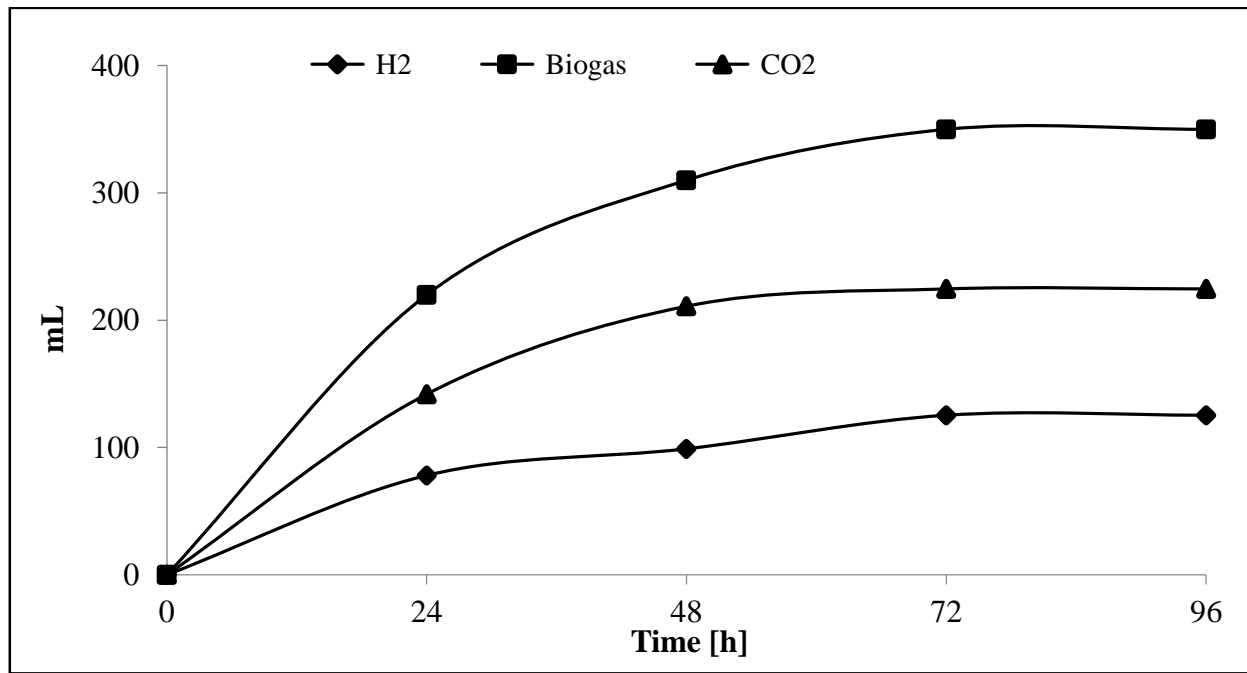
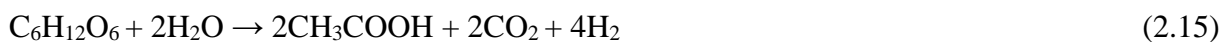


Fig. 2-16 Cumulative biogas production for SM as function of time

The analysis of the liquid phase (Fig. 2-15) showed the presence of acetic acid ( $\text{CH}_3\text{COOH}$ ), butyric acid ( $\text{CH}_3(\text{CH}_2)_2\text{COOH}$ ), propionic acid ( $\text{CH}_3\text{CH}_2\text{COOH}$ ) and ethanol ( $\text{C}_2\text{H}_5\text{OH}$ ), the main product for all substrates being butyric acid (3,2 mg/mL at 72h). The total concentration of VFA and ethanol in SM dark fermentation, is 4,28 mg/mL.

On the basis of liquid phase analysis data, the following reactions can be hypothesizing occur during DF process [38]:



Reactions (2.14) and (2.15), producing butyric and acetic acid respectively, lead both to the formation of hydrogen; although, reaction (2.15) occurs with a higher  $\text{H}_2$  yield (4 moles per mole of glucose). Moreover, reactions (2.16) and (2.17), producing propionic acid and ethanol respectively, indicate that degradation of sugar occurs without  $\text{H}_2$  formation. Therefore, the best reaction network for biohydrogen production should exclude the formation of ethanol and propionic acid, and should favour reaction (2.15) in comparison to reaction (2.14).



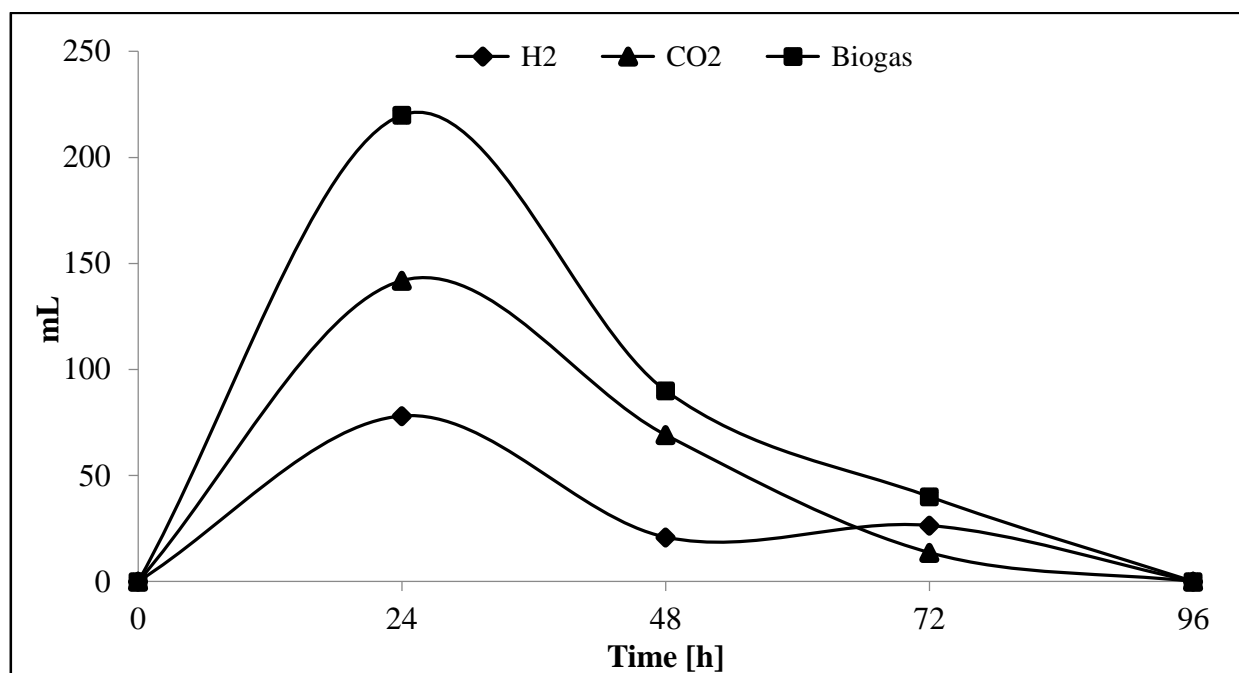


Fig. 2-17 Daily biogas production for SM as function of time

Figures 2-16 and 2-17 show the daily and cumulative biogas production, respectively. It can be noted, as previously said, that the production of biogas is limited in firstly 2 days of fermentation and the total volume of biogas is 350 mL with 125,4 mL of H<sub>2</sub> (36% vol). After 72 h the biogas production goes to zero, because the nutrients of microbial consortium are depleted and so the microorganism are coming to phase death (Fig. 2-14), according to several literature data [38,39,40].

Sample	Microbial Biomass (ABS at 600 nm)	VFA-Ethanol (mg/mL)	H <sub>2</sub> Volume (mL)
SM I	2,98	8,8	53,4
SM III	5,59	4,28	125,4

Tab. 2-7 MB, VFA-Ethanol and H<sub>2</sub> production for SMI and SMIII tests

Tab 2-7 shows the results from SMI and SM III (experimental conditions are reported in par. 2.8.10). It is possible noted that the values of microbial biomass and the production of H<sub>2</sub> strongly increase from the first to third adaption. In particular, the production of hydrogen goes from 53,4 mL to 125,4 with an increase of 70%. These results parallel to liquid phase analysis data showing a strong reduction (about 50%) of VFA and ethanol concentration.

These values confirm the success of the experimental procedure adopted and described in par. 2.7.13.

### 2.7.2.2 Arundo Donax not treated (ADH)

Figures 2-18 and 2-19 show the trend of liquid phase analysis for ADH. Also for this biomass the reducing sugars concentrations goes to zero after 72 h and the microbial biomass has firstly the initial phase of exponential growth (maximum value of 8,45 at 24 h) followed by a strong decrease up to a value of 5,83, after 72 h. Compared to SM the values of microbial biomass and consequently hydrogen yields are increased. The VFA and ethanol concentrations amount to 5,15 mg/mL, a value slightly higher than SM, due to lignocellulosic characteristics of the arundo donax. The trends of VFA and ethanol confirm the occurrence of reactions (2.14-2.17) described above.

Figures 2-20 and 2-21 show the trend of biogas production for ADH. It is possible note that the biogas production is higher in the first day of DF and decrease in the following 2 days of test. The cumulative volume of biogas corresponds to 285 mL and it is remarkable the high amount of H<sub>2</sub> produced, equal to 190,1 mL (67% vol). This value is in agreement with to the microbial biomass trend and confirm that the procedure adopted is suitable for this type of biomass.

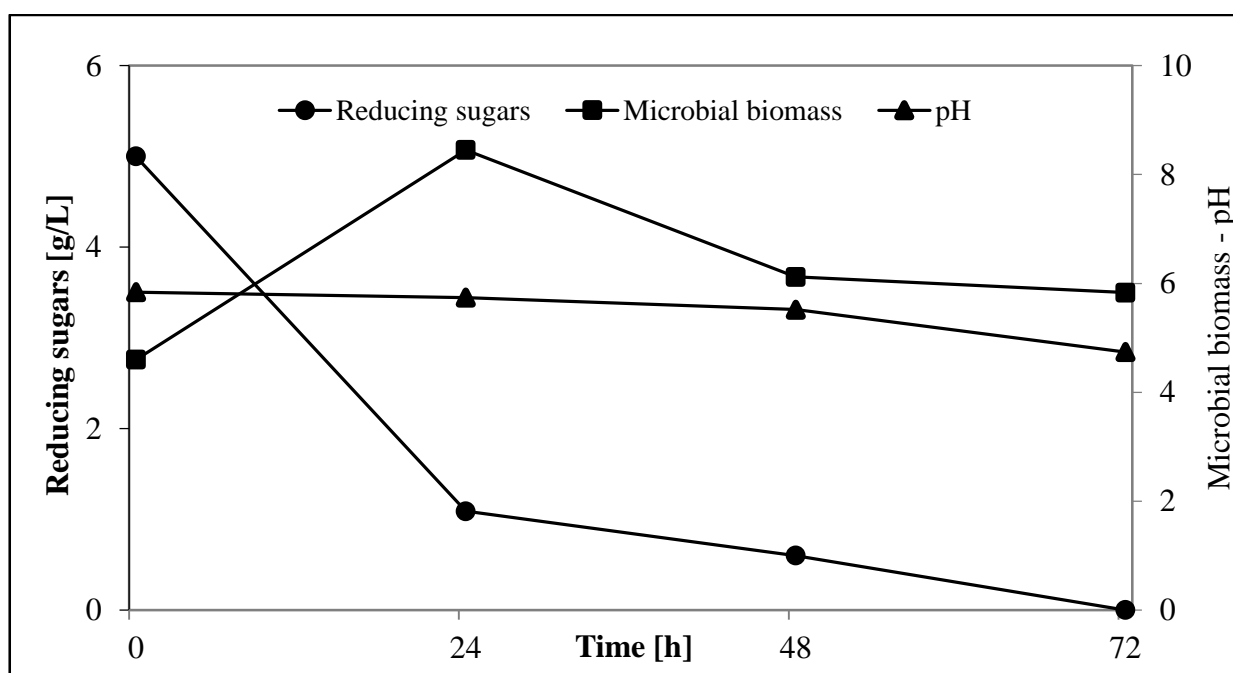


Fig. 2-18 Concentration of glucose, biomass and pH for ADH as function of time

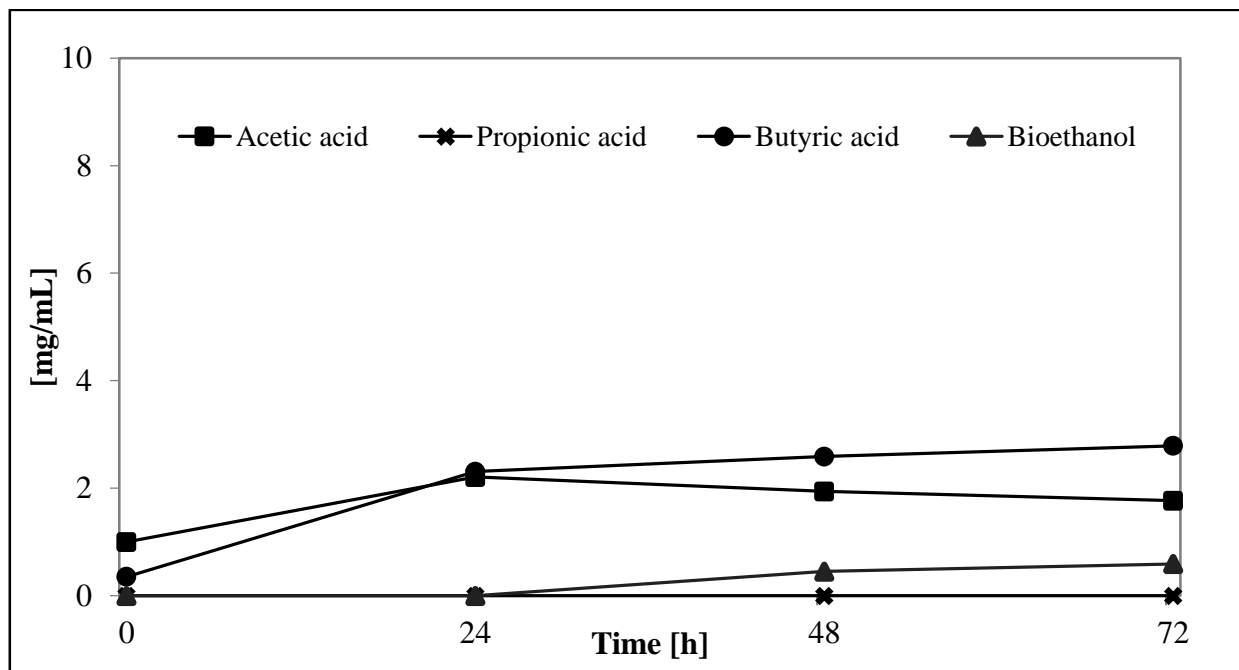


Fig. 2-19 Concentration of VFA and ethanol for ADH as function of time

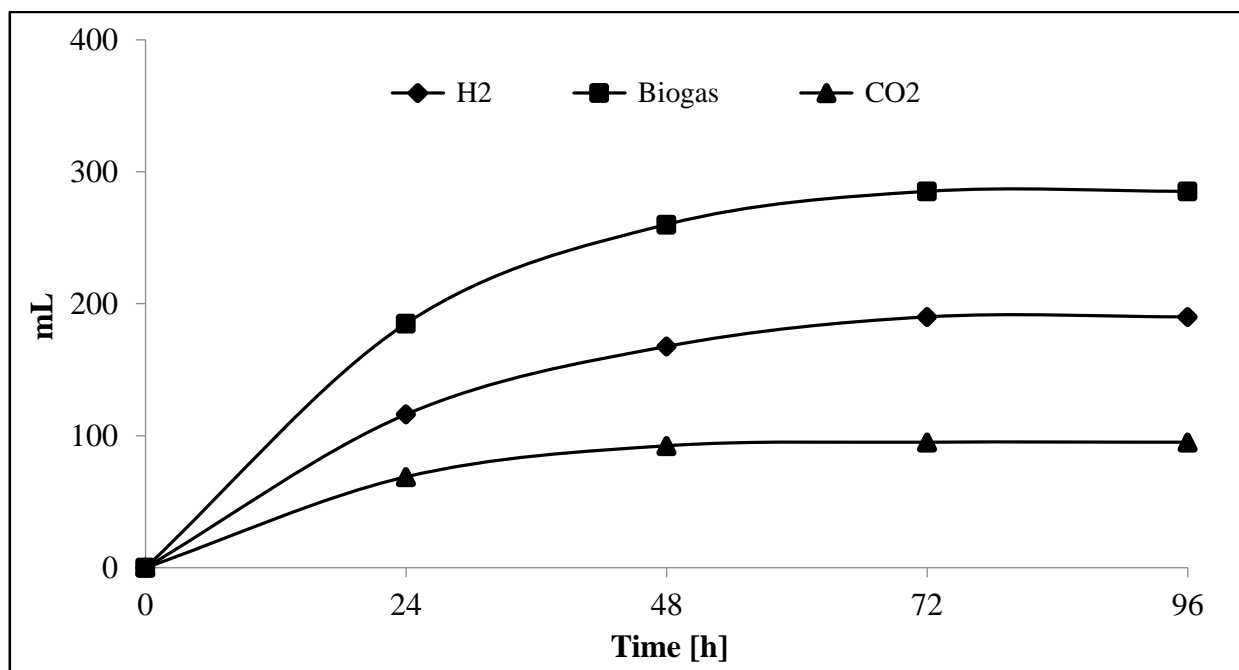


Fig. 2-20 Cumulative biogas production for ADH as function of time

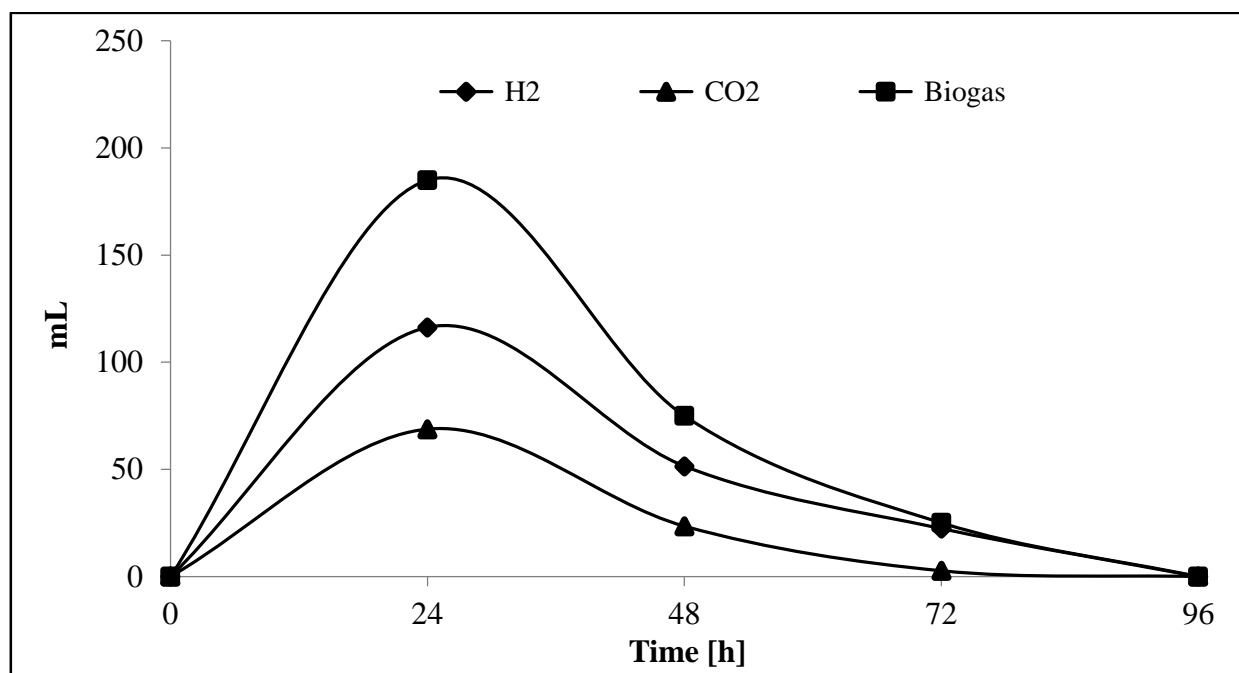


Fig. 2-21 Daily biogas production for ADH as function of time

Table 2-8 reports the differences between the first and the third ADH fermentations tests. It is possible noted that the increase of microbial biomass (from 5,98 to 8,45) and H<sub>2</sub> (from 127,1 mL to 190,1) is less marked than in SM, with an increase of H<sub>2</sub> production of 33% and in both cases the amount of H<sub>2</sub> is higher than SM. This is due to the hydrolysis pretreatment of ADH that leads to the formation of monomers and reducing sugars that can be separated and digested more easily than the glucose present in synthetic medium does enhancing the fermentation.

Sample	Microbial Biomass (ABS at 600 nm)	VFA-Ethanol (mg/mL)	H <sub>2</sub> Volume (mL)
ADH I	5,98	10,65	127,1
ADH III	8,45	5,15	190,1

Tab. 2-8 MB, VFA-Ethanol and H<sub>2</sub> production for ADHI and ADHIII tests

### 2.7.2.3 Arundo donax treated with Steam Explosion (ADHexp)

Figures 2-22 and 2-23 show the trend of liquid phase analysis for ADHexp. The trends are similar to those obtained for ADH: in fact, the reducing sugars concentration goes to zero after 72 h and the microbial biomass has firstly the initial phase of exponential growth (maximum value = 5,77 at 24 h) followed by the death phase of microorganism with a value after 72 h of 4,77. The values of microbial biomass are lower than ADH, suggesting a lower production of biogas. The VFA and ethanol concentration amount to 6,7 mg/mL and this value is slightly higher than ADH and SM.

Also for ADHexp, the trends of VFA and ethanol confirm the occurrence of reactions (2.14-2.17) reported above.

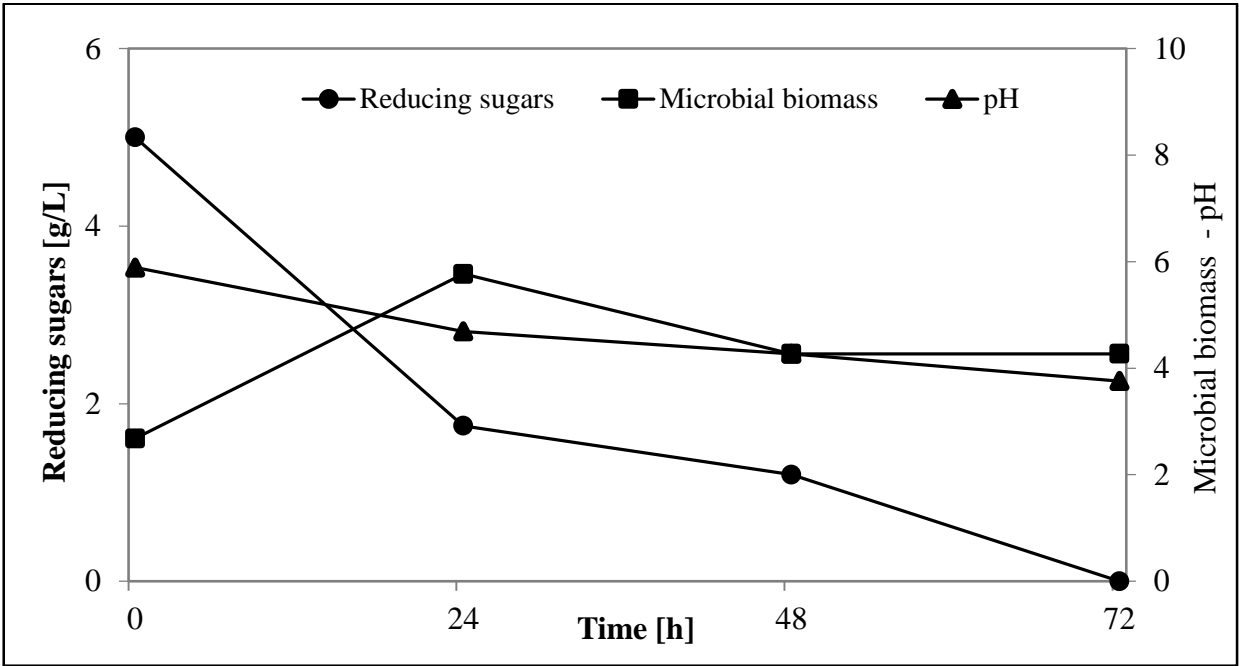


Fig. 2-22 Concentration of glucose, biomass and pH for ADHexp as function of time

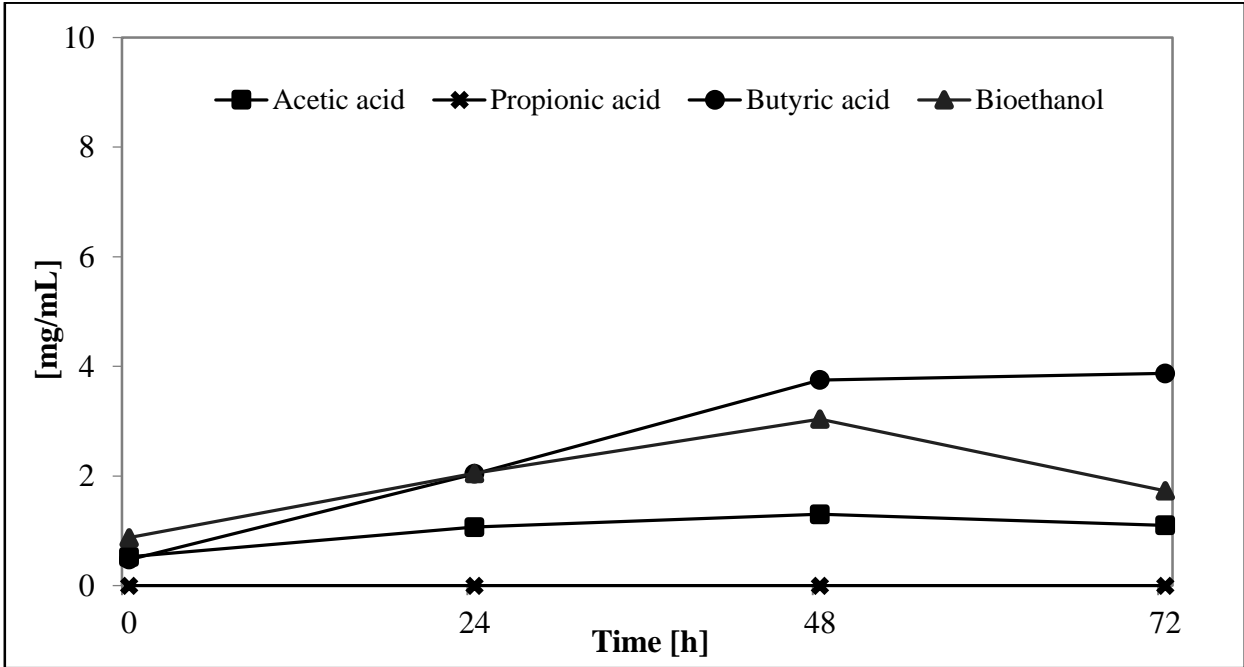


Fig. 2-23 Concentration of VFA and ethanol for ADHexp as function of time

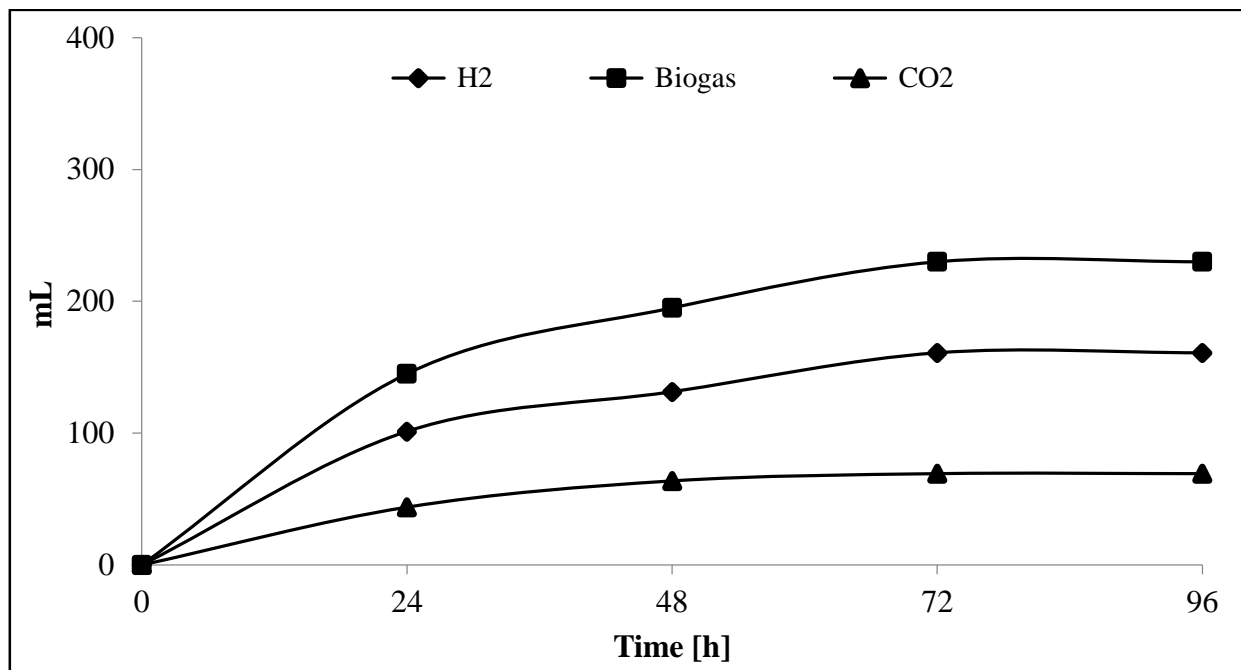


Fig. 2-24 Cumulative biogas production for ADHexp as function of time

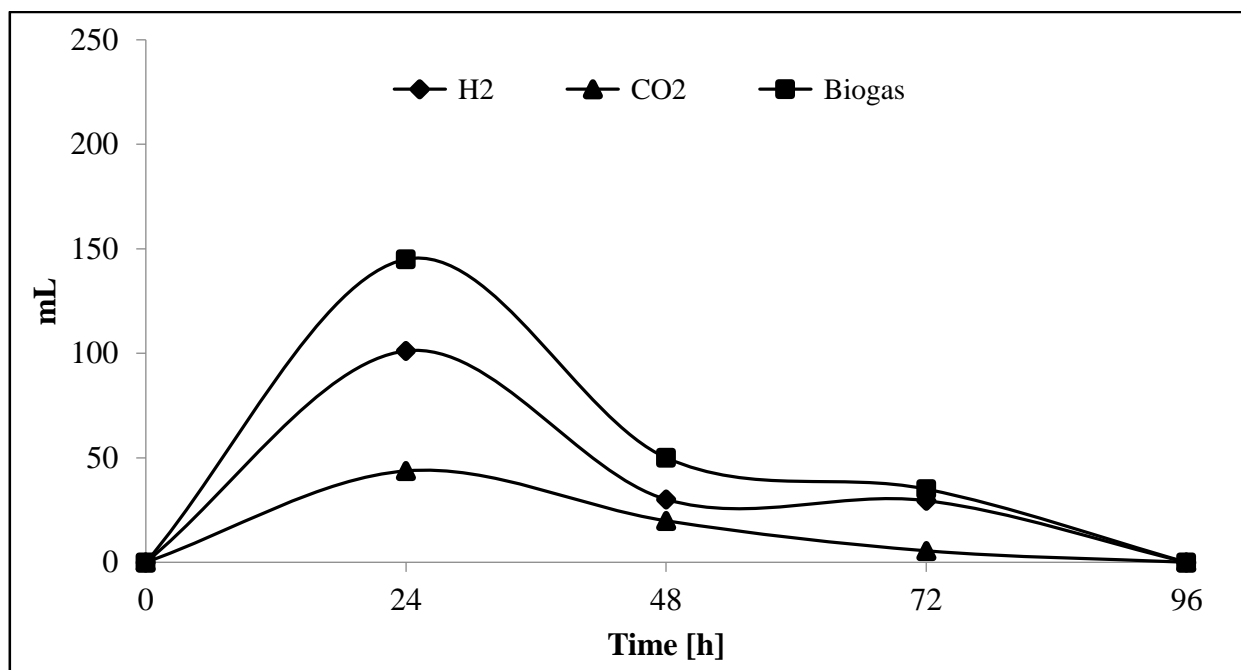


Fig. 2-25 Daily biogas production for ADHexp as function of time

The trends of biogas production of ADHexp (Figures 2-24 and 2-25) are similar to ADH although the volume of biogas (230 mL) and the volume of H<sub>2</sub> (160,8 mL, 69% vol) are lower. The cumulative volume of H<sub>2</sub> product with the ADHexp is lower than ADH but the H<sub>2</sub> concentration in biogas is very close to ADH. The lower cumulative biogas production is due to the presence of

inhibitory substances (i.e. phenols) as previously discussed: probably during the process of steam explosion there is an accumulation of this substances that can inhibit the DF process.

<b>Sample</b>	<b>Microbial Biomass (ABS at 600 nm)</b>	<b>VFA-Ethanol (mg/mL)</b>	<b>H<sub>2</sub> Volume (mL)</b>
<b>ADHexp I</b>	3,53	13,33	71,8
<b>ADHexp III</b>	5,77	6,70	160,8

Tab. 2-9 MB, VFA-Ethanol and H<sub>2</sub> production for ADHexpI and ADHexpIII tests

Table 2-9 reports the values of microbial biomass (MB), VFA, ethanol and H<sub>2</sub> production. Also in this case the production is considerable enhances with the inoculum treated by salts and nutrient medium, increasing from 71,8 to 160,8 mL. In addition, it is possible noted that The MB increase from 3,53 to 5,77 and the VFA and ethanol concentration is halved, in agreement with biogas production.

#### **2.7.2.4 Manure**

Figures 2-26 and 2-27 show the trend of liquid phase analysis for manure. These data appear quite different compared to other biomass examined until now (SM, ADH and ADHexp). In fact, the concentration of reducing sugars starts from a lower value (equal to 2,14 g/l), suggesting that the enzymatic hydrolysis has had a worse effect for this type of biomass (see par. 2.6.4). Moreover, the reducing sugars concentrations goes to zero more rapidly (after 48 h) since they are in lower amount in manure. As aspected the microbial biomass trends has firstly the initial phase of exponential growth (maximum value equal to 1,47) with a subsequent decrease to 0,34 after 72 h.

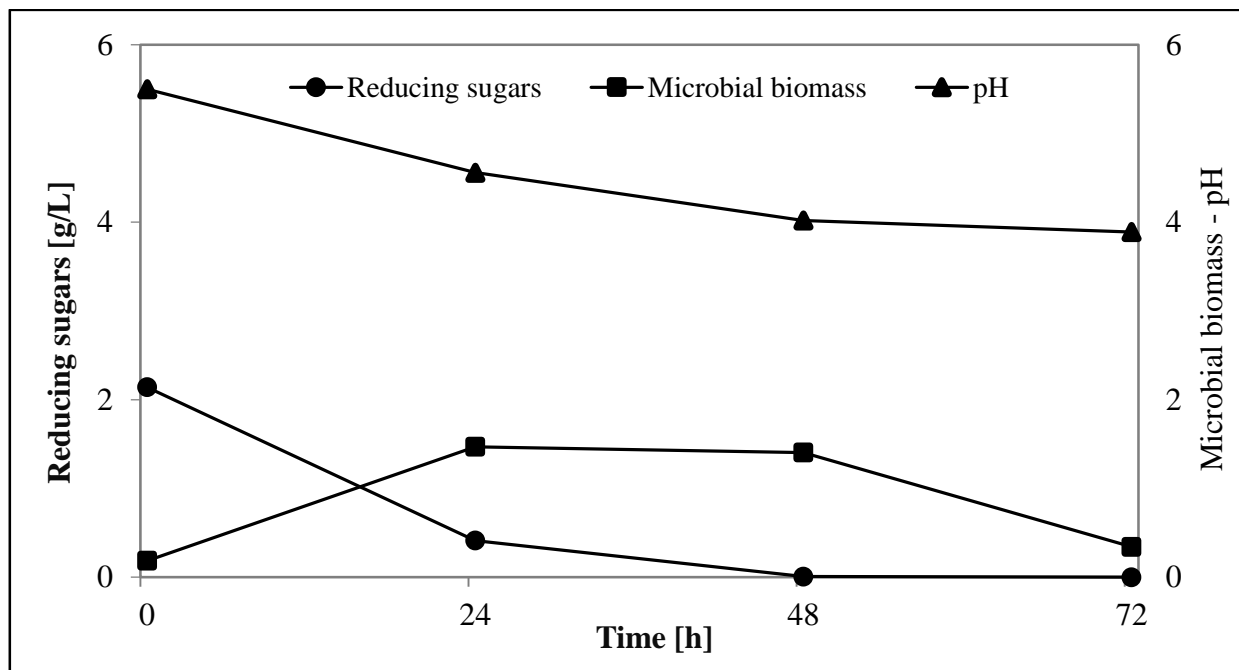


Fig. 2-26 Concentration of glucose, biomass and pH for manure as function of time

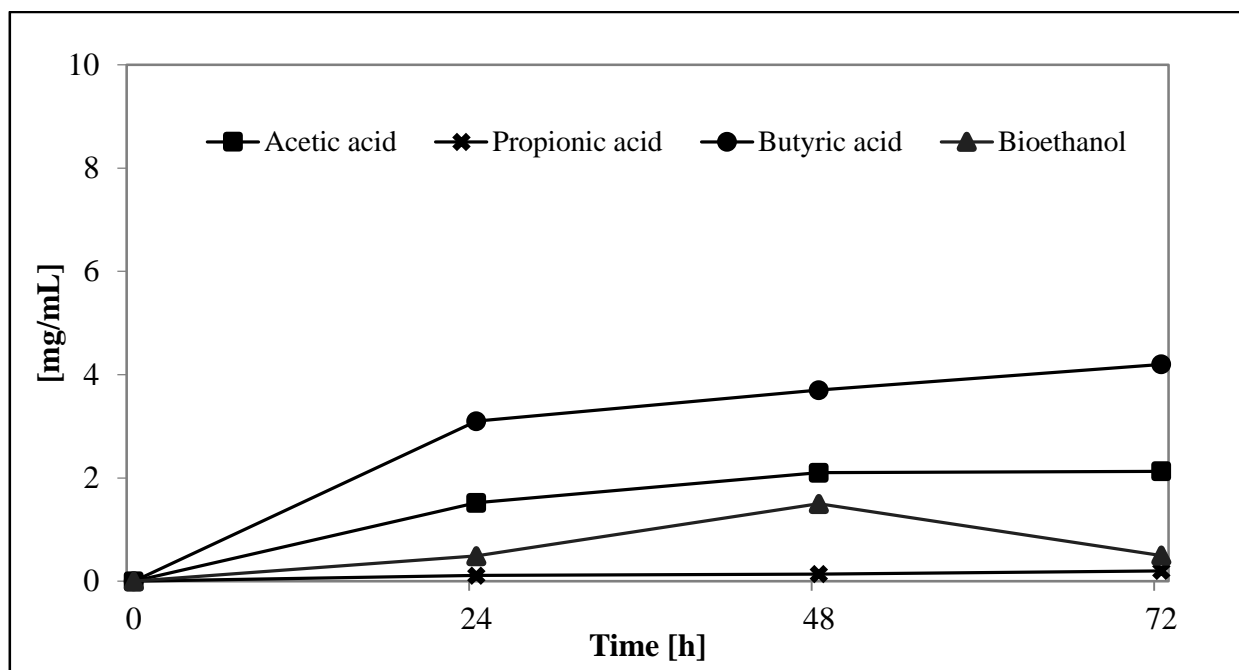


Fig. 2-27 Concentration of VFA and ethanol for manure as function of time

The VFA and ethanol concentration is 7,3 mg/mL: this value is comparable to that observed with other biomass, confirming the occurrence of reactions (2.14-2.17) described above and a consequently increase of the solution acidification can explain the lower biogas production. It must be remembered that the manure is a more complex biomass compared to the lignocellulosic ones



due to the presence of a more dilute phase and methanogenic bacteria derived from cow digestion process that lead more difficult the growth of H<sub>2</sub> producer bacteria.

Figures 2-28 and 2-29 show the daily and cumulative biogas production. It is possible observed that for this biomass, the production of biogas and H<sub>2</sub> is lower in comparison to ADH, ADHexp and SM. The total volume of biogas is equal to 106 mL with 64% vol of H<sub>2</sub> (68 mL).

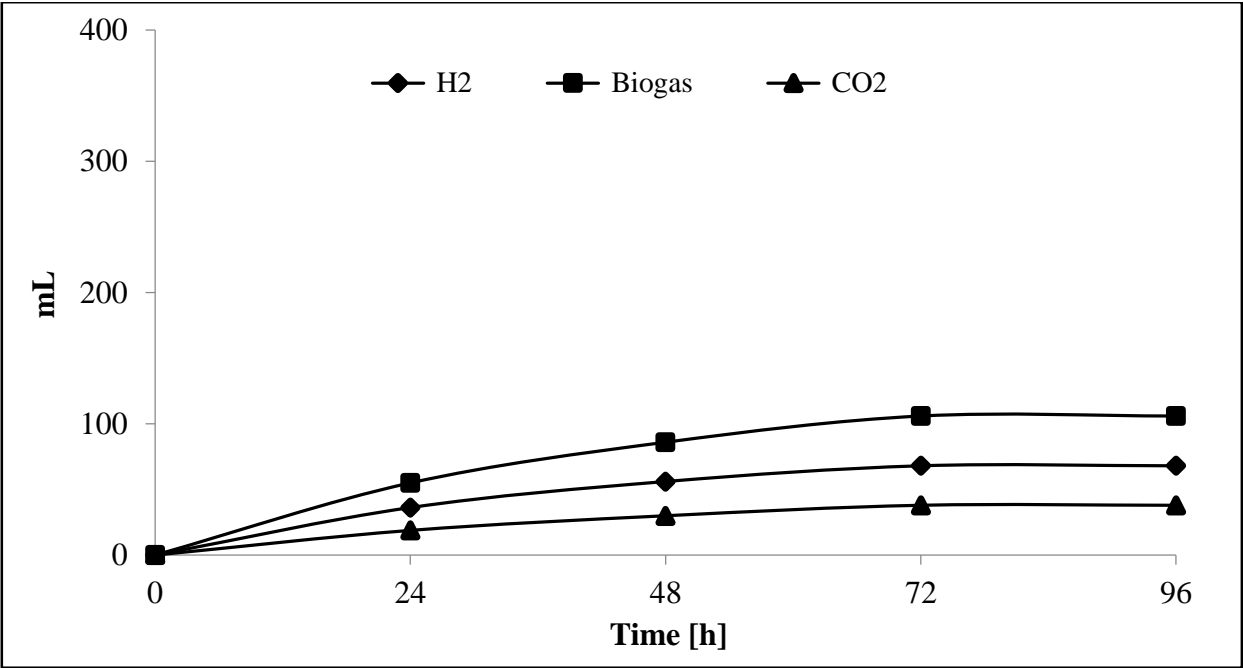


Fig. 2-28 Cumulative biogas production for manure as function of time

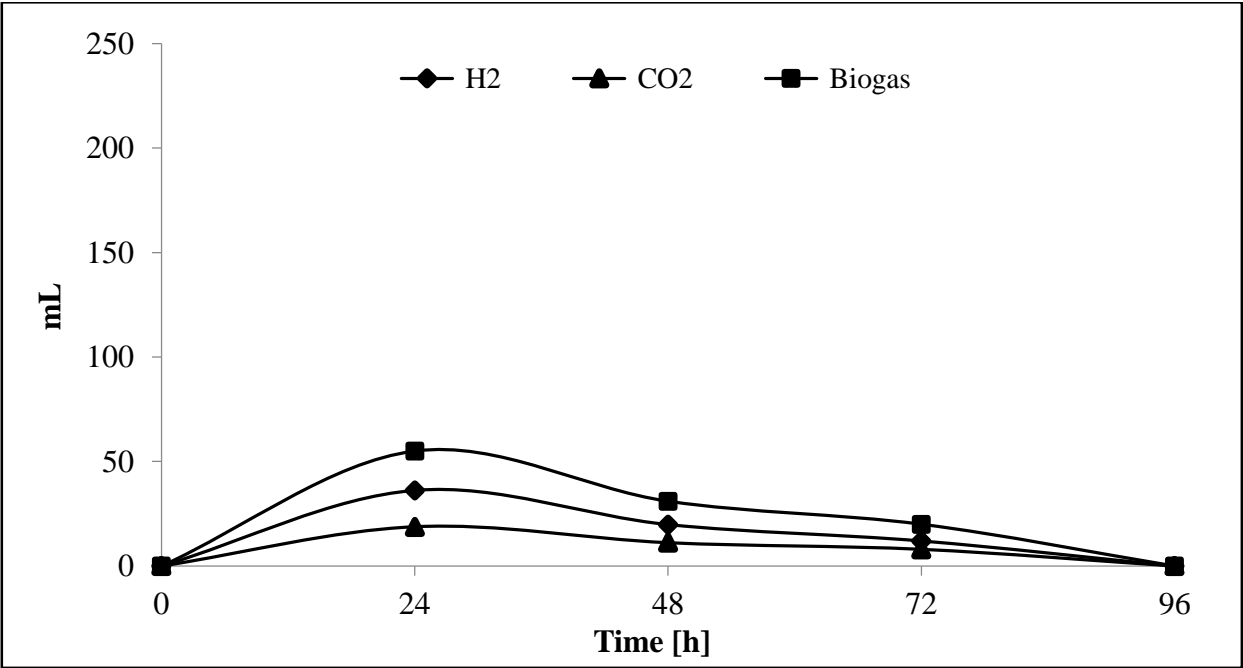


Fig. 2-29 Daily biogas production for manure as function of time

This behavior can be explained by the lower growth of the microbial biomass and appreciable production of VFA and ethanol.

The volume of H<sub>2</sub> is significantly increased from 15 mL to 68 (table 2-10) pointing the efficiency of the procedure used to promote the growth of bacteria hydrogen producers. This is confirmed by the growth of microbial biomass from first and third tests. VFA and ethanol amount do not change significantly, suggesting that this parameter has lower effect on H<sub>2</sub> production.

<b>Sample</b>	<b>Microbial Biomass (ABS at 600 nm)</b>	<b>VFA-Ethanol (mg/mL)</b>	<b>H<sub>2</sub> Volume (mL)</b>
<b>Manure I</b>	0,31	8	15
<b>Manure III</b>	1,47	7,3	68

Tab. 2-10 MB, VFA-Ethanol and H<sub>2</sub> production for Manure I and Manure III tests

#### 2.7.2.5 Litter

Figures 2-30 and 2-31 show the trend of liquid phase analysis for litter. The value of initial reducing sugars value is similar to that of manure (2,59 g/L) but concentration goes to zero more rapidly, after 24 h. Microbial biomass trend is similar to other biomass, with the initial phase of exponential growth with a maximum value equal to 1,93 and the death phase (up to 0,65 after 72 h). The VFA and ethanol concentration is 9,12 mg/mL. These values are slightly higher than those obtained for the manure. It is important noted the presence of urine and feces of mice in the litter which represent a limit for the dark fermentation process because represents a fraction not digestible for H<sub>2</sub>-producer microbial consortium.

Figures 2-32 and 2-33 show the cumulative and daily biogas production. The biogas production is essentially concentrated in the first day of fermentation because the reducing sugars goes to zero after 24 h while the values of the acids maintains high values (6,37 g/L).

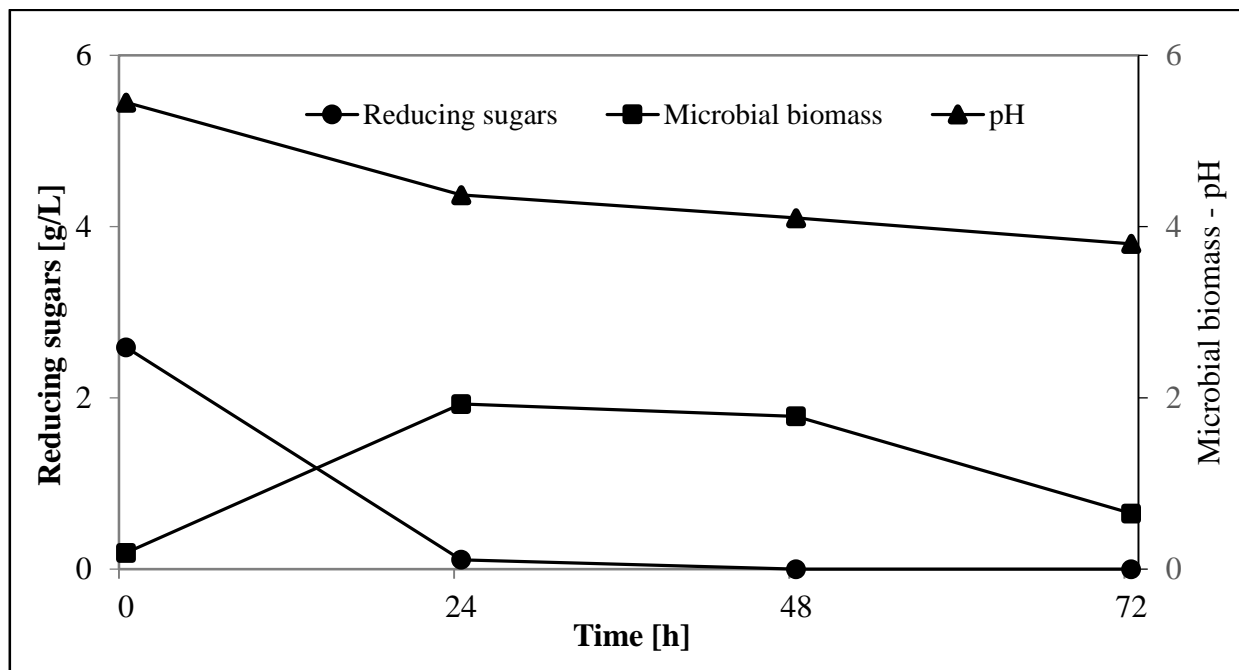


Fig. 2-30 Concentration of glucose, biomass and pH for litter as function of time

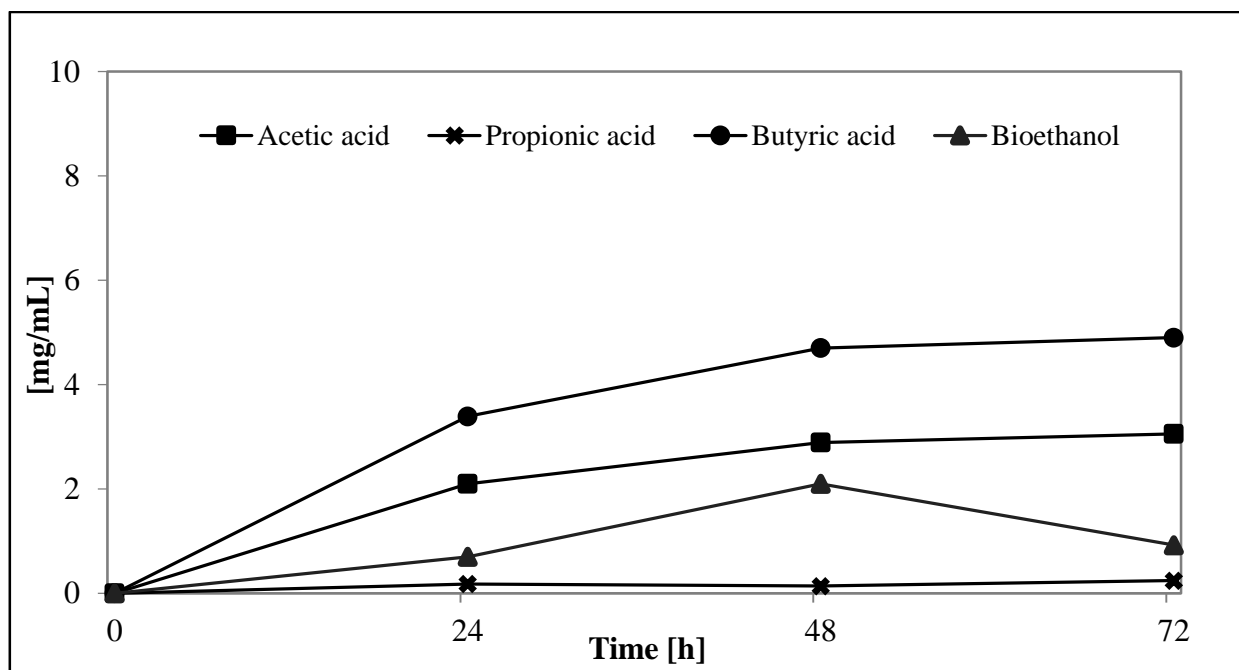


Fig. 2-31 Concentration of VFA and ethanol for litter as function of time

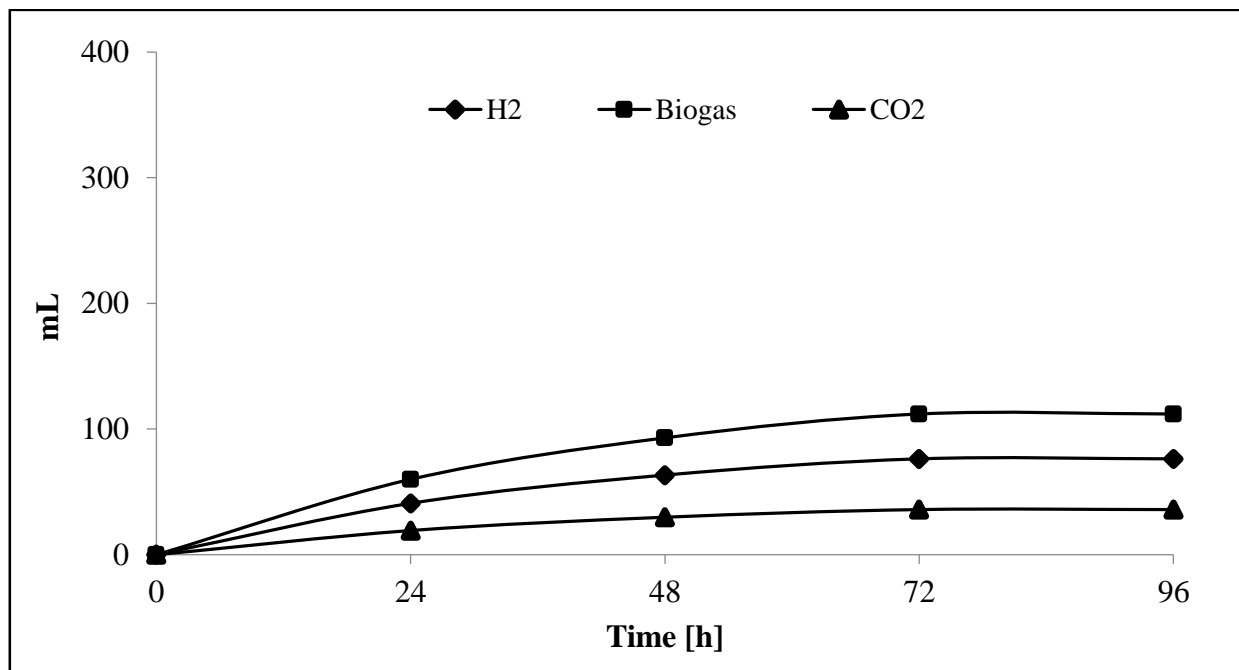


Fig. 2-32 Cumulative biogas production for litter as function of time

The cumulative volume of biogas is 112 mL with 76,16 mL of H<sub>2</sub> corresponding to 68% vol. This behavior could be to the lower reducing sugars content and the presence of compounds hardly digestible as observed for the manure.

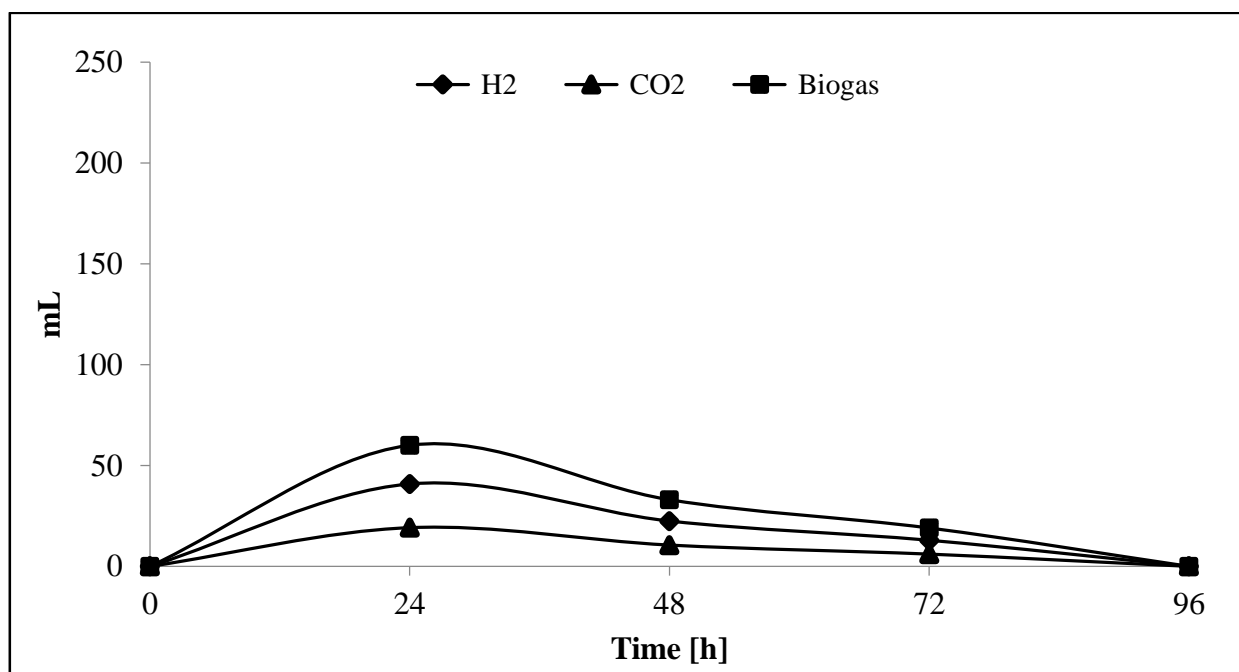


Fig. 2-33 Daily biogas production for litter as function of time

Sample	Microbial Biomass (ABS at 600 nm)	VFA-Ethanol (mg/mL)	H <sub>2</sub> Volume (mL)
Litter I	0,33	13,9	19
Litter III	1,93	9,12	76,16

Tab. 2-11 MB, VFA-Ethanol and H<sub>2</sub> production for Litter I and Litter III tests

Table 2-11 shows the differences between the first and the third adaption of culture: it can be noted the increase of H<sub>2</sub> production (from 19 to 76,16 mL) with an increase of the production of biohydrogen of 75%.

#### 2.7.2.6 OFMSW

Figures 2-34 and 2-35 show the trends of liquid phase for OFMSW. It is important noted that the concentration of sugars, although is practically the same in comparison to ADH, ADHexp and SM (5 g/L), but goes to zero less rapidly. This is due to the fact that the OFMSW is a more heterogeneous biomass compared to the others, and contains substances that are digested more slowly by H<sub>2</sub>-producer bacteria. Also for OFMSW the higher value of microbial biomass is at 24 h with a value of 7,83 and 5,41 at 72 h.

The VFA and ethanol concentration is about 7 mg/mL, value comparable with the results obtained for the other biomass analyzed.

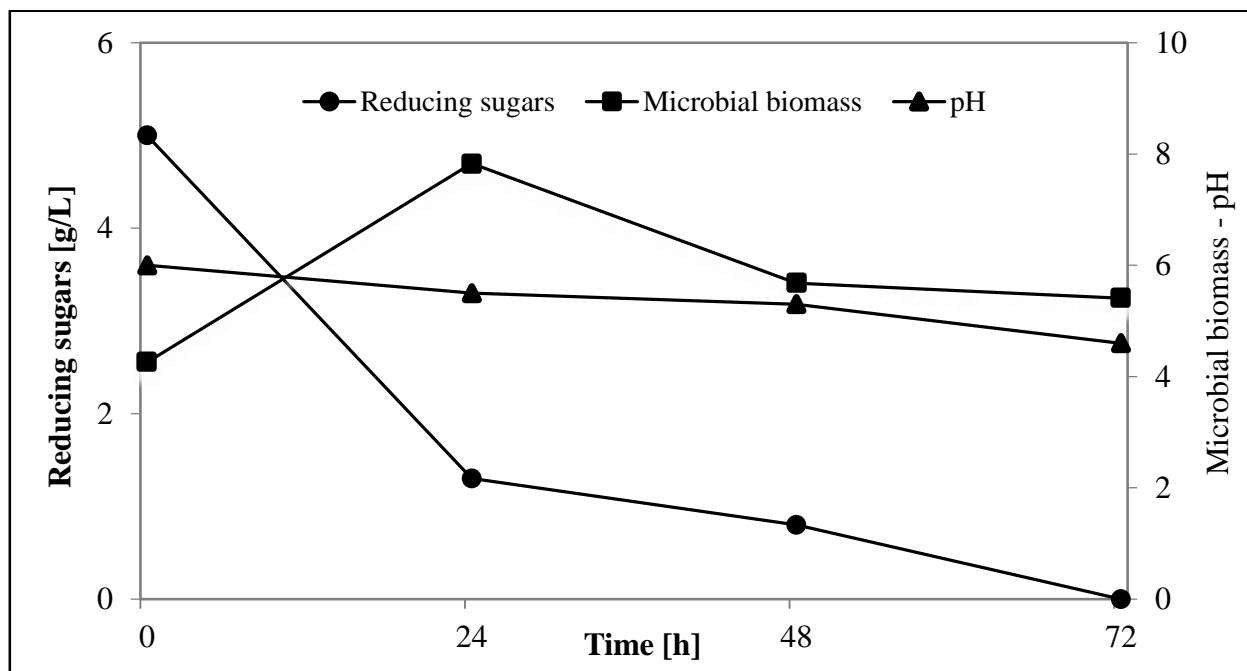


Fig. 2-34 Concentration of glucose, biomass and pH for OFMSW as function of time

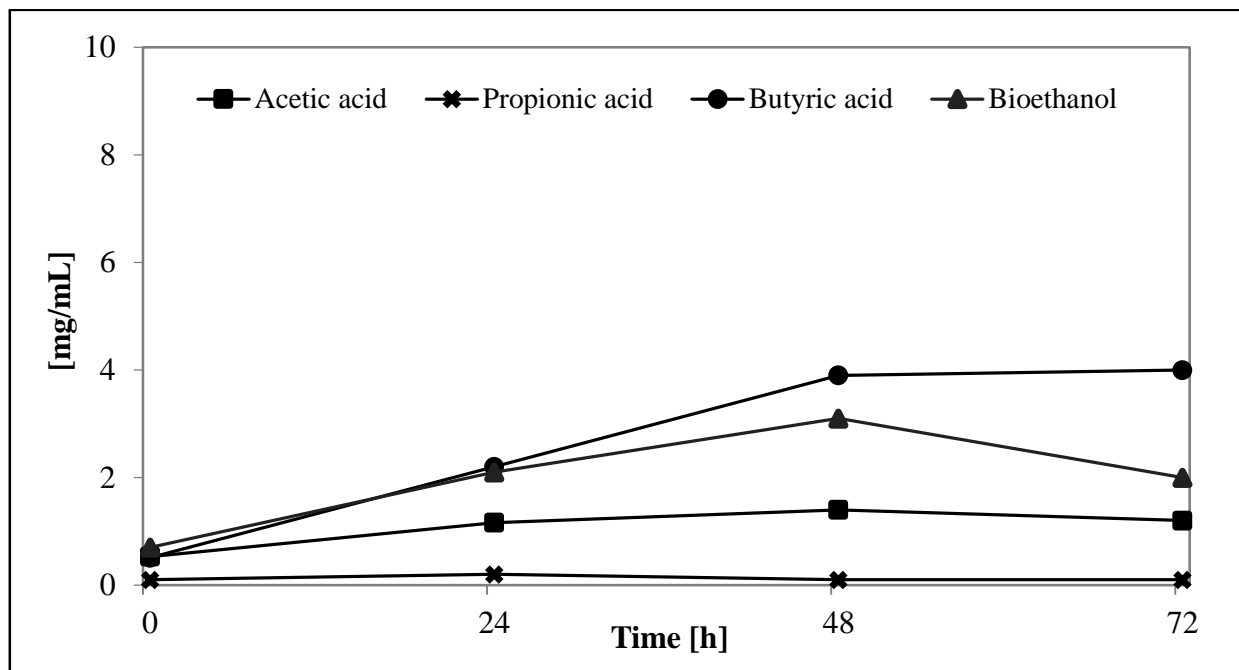


Fig. 2-35 Concentration of VFA and ethanol for OFMSW as function of time

Figures 2-36 and 2-37 show the cumulative and daily biogas production. The total volume of biogas product is 264 mL, with 176,4 mL of  $H_2$  (67 % vol). It must be remarked that for the OFMSW, unlike the other biomasses analyzed, the production of a significant amount of biohydrogen up to the third day of fermentation (88 mL). This result is in agreement with the trend of reducing sugars and microbial biomass.

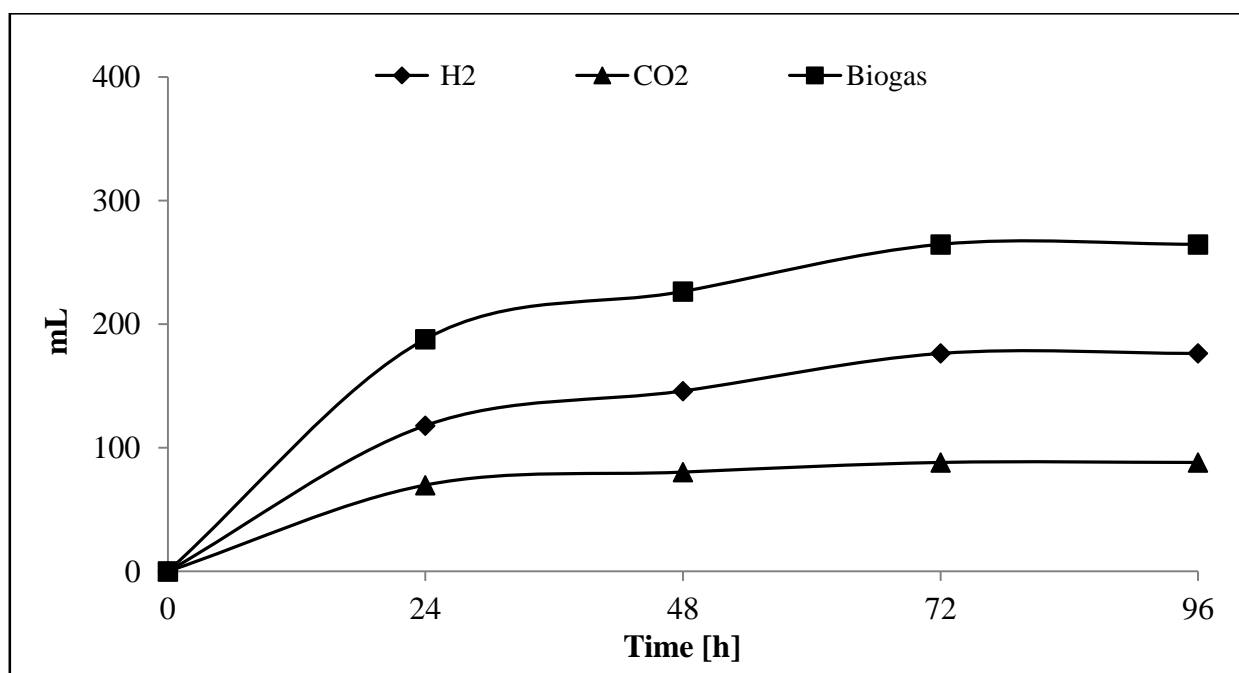


Fig. 2-36 Cumulative biogas production for OFMSW as function of time

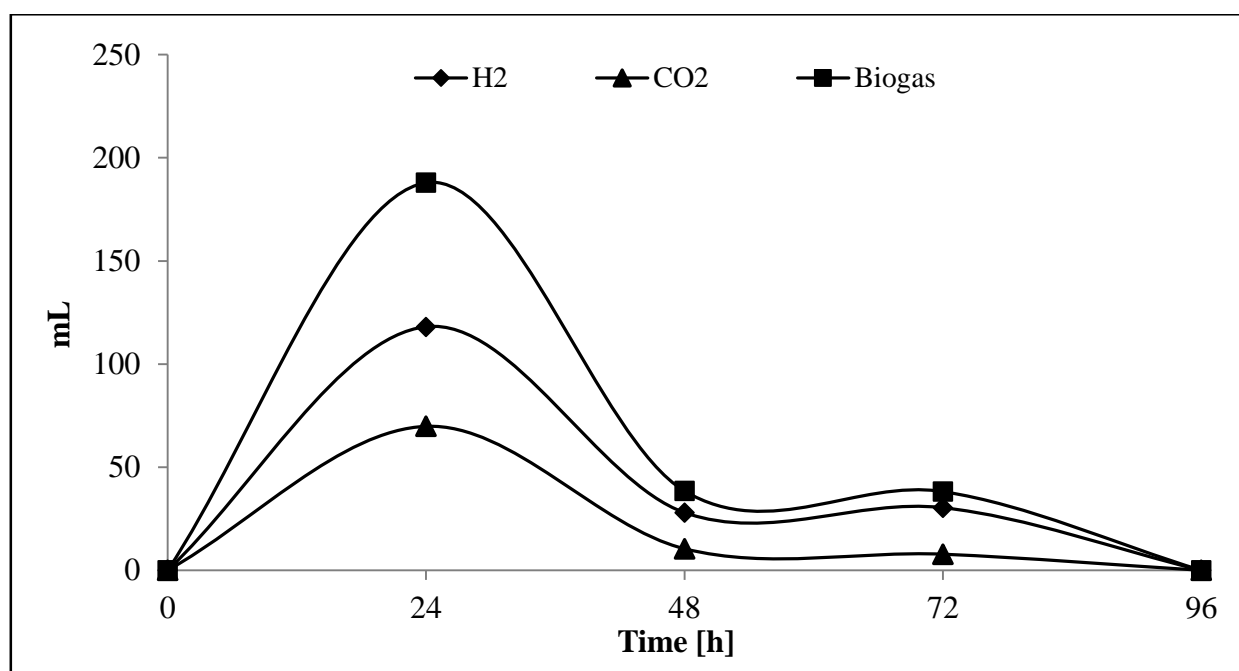


Fig. 2-37 Daily biogas production for OFMSW as function of time

Sample	Microbial Biomass (ABS at 600 nm)	VFA-Ethanol (mg/mL)	H <sub>2</sub> Volume (mL)
OFMSW I	5,10	12,6	98
OFMSW III	7,83	7	176,4

Tab. 2-12 MB, VFA-Ethanol and H<sub>2</sub> production for OFMSW I and OFMSW III tests

Table 2-12 report compares the results obtained in the first and third adaptions. It is possible noted the large increase of H<sub>2</sub> volume produced (from 98 mL to 176,4) with an increment of 44%. The percentage increase is lower than manure and litter being comparable to ADH and ADHexp. This could be due to the presence of a wide variety of compounds present in OFMSW, making more difficult the microbial consortium to adapt to the substrate does hindering in some extent the H<sub>2</sub> production.

## 2.8 Conclusions

Figures 2-38 shows the cumulative biohydrogen production obtained with the biomass utilized in this PhD thesis. The best result has been obtained with ADH with 190 mL of H<sub>2</sub>. Manure gives the lower volume of H<sub>2</sub> (68,4 mL). Table 2-13 summarize the results obtained. The comparison among the biomass is done by normalizing the production of hydrogen per unit mass and reducing sugars (columns 1,2,4,6 table 2-13).

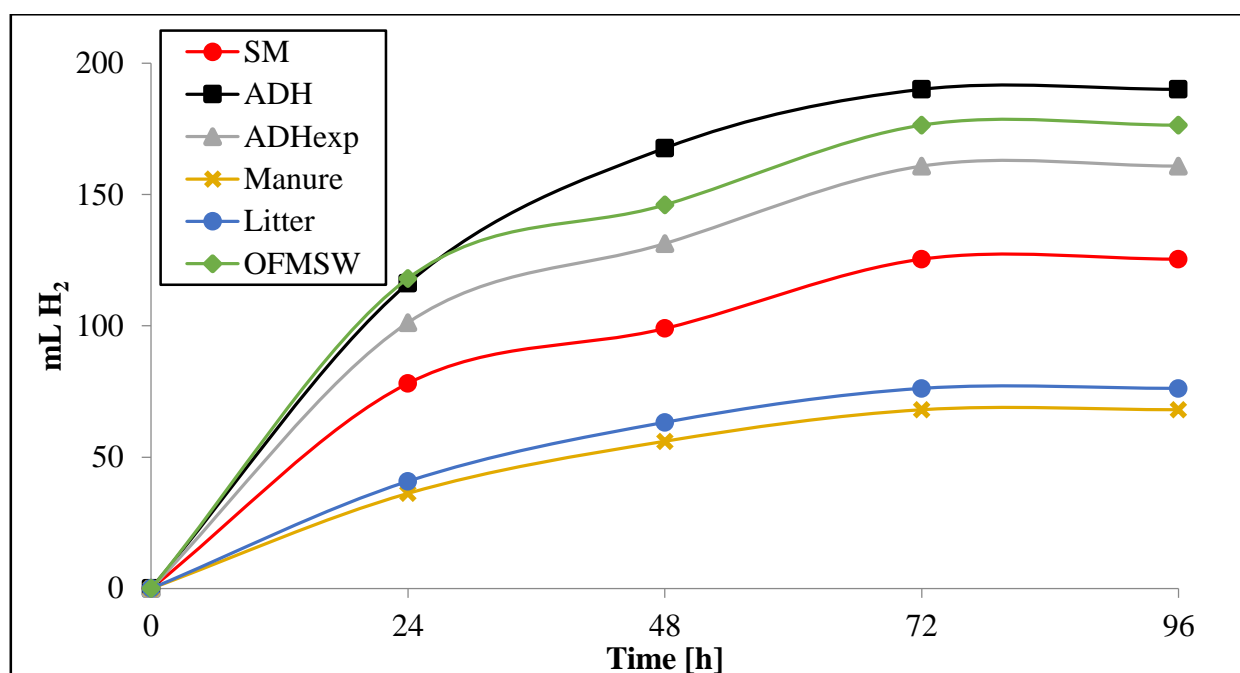


Fig. 2-38 Cumulative Biohydrogen production vs Time (h) for biomass utilized

Sample	Reducing Sugars (g/L)	H <sub>2</sub> Volume (mL)	mL H <sub>2</sub> /g Red.Sugars	Biomass (g)	mL H <sub>2</sub> /g Biomass
SM	5,0	125,4	25,08	/	/
ADH	5,0	190,1	38,02	20	9,50
ADHexp	5,0	160,8	32,16	20	8,04
Manure	2,14	68,04	31,79	20	3,40
Litter	2,59	76,16	29,40	20	3,81
OFMSW	5,0	176,4	35,28	20	8,82

Tab. 2-13 Results obtained by DF of biomass utilized

For each biomass can be observed a significative production of hydrogen per gram of reducing sugars, the range is 25,08 (SM)-38,02 (ADH), and for the volume of H<sub>2</sub> per gram of biomass the data are in the range of 3,4 (Manure)-9,50 (ADH).

The following conclusion can be drone from the results of DF tests:

- the production of hydrogen via DF is concentrated mainly in the first 24 h of fermentation, while in the subsequent 48 h decreases up to run out to 96 h, according to several literature data [19,29,38]. The only exception is represented by the organic fraction, but this was to be expected, because as explained in section 2.7.15.6, the organic fraction presents more complex monomers to digest;



- the best results have been obtained with ADH, this type of biomass is very promising because it allows to obtain good yields of hydrogen, but also because it can be used in marginal lands, as well as having a lower cost compared to other lignocellulosic biomass;
- the manure and the litter showed a lower production of biohydrogen. This could be due to the presence in the manure of a larger amount of methanogenic bacteria which inevitably lower the yield and in the litter of rat droppings that go to inhibit the DF process;
- it has been successfully developed an experimental procedure able to enhance the growth of H<sub>2</sub>-producer bacteria to the detriment of methanogenic ones, and all the substrates utilized have been showed good results getting considerable increase in the production of hydrogen in the dark fermentation process.

## References

1. Turco M, Ausiello A, Micoli L (2016) Treatment of Biogas for Feeding High Temperature Fuel Cells, Springer International Publishing Switzerland, Green Energy and Technology, DOI 10.1007/978-3-319-03215-3\_1
2. Cui W, Cheng J J. Growing duckweed for biofuel production: a review. *Plant Biology* 2015; 17:16-23
3. Scarlat N, Dallemand J F, Monforti-Ferrario F, Banja M, Motola V. Renewable energy policy framework and bioenergy contribution in the European Union – An overview from National Renewable Energy Action Plans and Progress Reports. *Renewable and Sustainable Energy Reviews* 2015;51:969–985
4. Cherubini F, Strømman AH. Life cycle assessment of bioenergy systems: state of the art and future challenges. *BioresourTechnol* 2011;102:437–451
5. Kaparaju P, Serrano M, Thomsen A B, Kongjan P, Angelidaki I. Bioethanol, biohydrogen and biogas production from wheat straw in a biorefinery concept. *Bioresour. Technol.* 2009;100:2562–2568
6. Cheng C L, Lo Y C, Lee K S, Lee D J, Lin C Y, Chang, J S. Biohydrogen production from lignocellulosic feedstock. *Bioresour. Technol.* 2011; 102:8514–8523
7. Monlau F, Barakat A, Trably E, Dumas C, Steyer J P, Carrère H (2013) Lignocellulosic Materials Into Biohydrogen and Biomethane: Impact of Structural Features and Pretreatment, *Critical Reviews in Environmental Science and Technology*, 43:3, 260-322, DOI: 10.1080/10643389.2011.604258
8. Helton J A, Cicero B J, Rafael R N, Elisandro P F, Michelle S F, Coimbra-Araujo C H (2010) *Int J Hydrogen Energy* 2010
9. Levin DB, Chahine R. Challenges for renewable hydrogen production from biomass. *Int J Hydrogen Energy* 2010;35:4962-9
10. Papadiaz DD, Ahmed S, Kumar R. Fuel quality issues with biogas energy e an economic analysis for a stationary fuel cell system. *Energy* 2012;44:257-77.
11. Hotza D, Da Costa JCD. Fuel cells development and hydrogen production from renewable resources in Brazil. *Int J Hydrogen Energy* 2008;33:4915-35.
12. Herle JV, Membrez Y, Bucheli O. Biogas as a fuel source for SOFC co-generators. *J Power Sources* 2004;127:300-12.
13. Koroneos, C., Dompros, A., Roumbas, G., and Moussiopoulos, N. (2004). Life cycle assessment of hydrogen fuel production processes. *International Journal of Hydrogen Energy*, 29, 1443–1450.
14. Sierens, R., and Rosseel, E. (2000). Variable composition hydrogen/natural gas mixtures for increased engine efficiency and decreased emissions. *Journal of Engineering for Gas Turbines and Power-Transactions of the Asme*, 122, 135–140.
15. <http://www.osti.gov/scitech/biblio/1068610> Accessed 11 Feb 2017
16. <http://energy.gov/eere/fuelcells/hydrogen-pipelines> Accessed 11 Feb 2017
17. [http://gofuelcellbus.com/uploads/11.\\_Mossa\\_Hydrogen\\_Refueling\\_Solutions\\_for\\_Buses\\_FCB\\_WS2013.pdf](http://gofuelcellbus.com/uploads/11._Mossa_Hydrogen_Refueling_Solutions_for_Buses_FCB_WS2013.pdf) Accessed 11 Feb 2017
18. [http://cordis.europa.eu/pub/fp7/energy/docs/hyways-roadmap\\_en.pdf](http://cordis.europa.eu/pub/fp7/energy/docs/hyways-roadmap_en.pdf) Accessed 11 Feb 2017
19. Hosseini S E, Wahid M A (2016) Hydrogen production from renewable and sustainable energy resources: Promising green energy carrier for clean development, *Renewable and Sustainable Energy Reviews*, 57:850-866
20. Yaman S. Pyrolysis of biomass to produce fuels and chemical feedstocks. *Energy Conversion and Management* 2004; 45(5):651–671.
21. Zhang Q, Chang J, Wang T, Xu Y. Review of biomass pyrolysis oil properties and upgrading research. *Energy Conversion and Management* 2007; 48(1): 87–92.
22. Wang D, Czernik S, Montané D, Mann M, Chornet E. Biomass to hydrogen via fast pyrolysis and catalytic steam reforming of the pyrolysis oil or its fractions. *Industrial & Engineering Chemistry Research* 1997; 36(5):1507–1518.
23. Bridgwater AV. Principles and practice of biomass fast pyrolysis processes for liquids. *Journal of Analytical and Applied Pyrolysis* 1999; 51(1–2):3–22.
24. Demirbaş A. Gaseous products from biomass by pyrolysis and gasification: effects of catalyst on hydrogen yield. *Energy Conversion and Management* 2002; 43(7):897–909.
25. Chen G, Andries J, Spliethoff H. Catalytic pyrolysis of biomass for hydrogen rich fuel gas production. *Energy Conversion and Management* 2003; 44(14): 2289–2296.

26. Williams PT, Brindle AJ. Catalytic pyrolysis of tyres: influence of catalyst temperature. *Fuel* 2002; 81(18):2425–2434.
27. Sutton D, Kelleher B, Ross J. Catalytic conditioning of organic volatile products produced by peat pyrolysis. *Biomass and Bioenergy* 2002; 23(3): 209–216.
28. Abedi J, Yeboah Y, and Realff M. An integrated approach to hydrogen production from agricultural residues for use in urban transportation. *Proceedings of the 2001 DOE Hydrogen Program Review, NREL/ CP, 2001; 570–30535.*
29. Hosseini S E, Mazlan A W, Jamil M M, Anis A M Azli, Misbah M. F. A review on biomass-based hydrogen production for renewable energy supply *Int. J. Energy Res.* 2015; 39:1597–1615
30. Debabrata Das, T.Nejat Veziroglu, 2008, “Advances in biological hydrogen production processes”, *International Journal of Hydrogen Energy* 33, 6046–6057.
31. Khanna N, Das D. Biohydrogen production by dark fermentation. *Wiley Interdisciplinary Reviews: Energy and Environment* 2013; 2(4):401–421.
32. Tao Y, Chen Y, Wu Y, He Y, Zhou Z. High hydrogen yield from a two-step process of dark- and photo-fermentation of sucrose. *International Journal of Hydrogen Energy* 2007; 32(2):200–206.
33. Rittmann S, Herwig C. A comprehensive and quantitative review of dark fermentative biohydrogen production. *Microbial Cell Factories* 2012; 11(1):115.
34. Mariakakis I, Bischoff P, Krampe J, Meyer C, Steinmetz H. Effect of organic loading rate and solids retention time on microbial population during bio-hydrogen production by dark fermentation in large lab-scale. *International Journal of Hydrogen Energy* 2011; 36(17):10690–10700.
35. Hay JXW, Wu TY, Juan JC, Jahim MJ. Biohydrogen production through photo fermentation or dark fermentation using waste as a substrate: overview, economics, and future prospects of hydrogen usage. *Biofuels, Bioproducts and Biorefining* 2013; 7(3): 334–352.
36. Valdez-Vazquez I, Sparling R, Risbey D, Rinderknecht-Seijas N, Poggi-Varaldo HM. Hydrogen generation via anaerobic fermentation of paper mill wastes. *Bioresource Technology* 2005; 96(17): 1907–13.
37. Thauer R. et al., 1977, “Energy conservation in chemotrophic anaerobic bacteria”, *Bacteriological Reviews*, 41, 100-180.
38. Ghimire A, Frunzo L, Pirozzi F, Trably E, Escudie R, Lens P N L, Esposito G A review on dark fermentative biohydrogen production from organic biomass: Process parameters and use of by-products *Applied Energy* 144 (2015) 73–95
39. Ren N, Guo W, Liu B, Cao G, Ding J. Biological hydrogen production by dark fermentation: challenges and prospects towards scaled-up production. *Curr Opin Biotechnol* 2011;22:365–70.
40. Hawkes F, Hussy I, Kyazze G, Dinsdale R, Hawkes D. Continuous dark fermentative hydrogen production by mesophilic microflora: principles and progress. *Int J Hydrogen Energy* 2007;32:172–84.
41. Kapdan IK, Kargi F. Bio-hydrogen production from waste materials. *Enzyme Microb Technol* 2006;38:569–82.
42. Ntaikou I, Antonopoulou G, Lyberatos G. Biohydrogen production from biomass and wastes via dark fermentation: a review. *Waste Biomass Valorizat* 2010;1:21–39.
43. Guo XM, Trably E, Latrille E, Carrère H, Steyer J-P. Hydrogen production from agricultural waste by dark fermentation: a review. *Int J Hydrogen Energy* 2010;35:10660–73.
44. Chong M, Sabaratnam V, Shirai Y, Ali M, Hassan MA. Biohydrogen production from biomass and industrial wastes by dark fermentation. *Int J Hydrogen Energy* 2009;34:3277–87.
45. Guo XM, Trably E, Latrille E, Carrere H, Steyer J. Predictive and explicative models of fermentative hydrogen production from solid organic waste: role of butyrate and lactate pathways. *Int J Hydrogen Energy* 2013;39:1–10.
46. Valdez-vazquez I, Riosleal E, Esparzagarcia F, Cecchi F, Poggivaraldo H. Semi- continuous solid substrate anaerobic reactors for H<sub>2</sub> production from organic waste: mesophilic versus thermophilic regime. *Int J Hydrogen Energy* 2005;30:1383–91.
47. Zhang M-L, Fan Y-T, Xing Y, Pan C-M, Zhang G-S, Lay J-J. Enhanced biohydrogen production from cornstalk wastes with acidification pretreatment by mixed anaerobic cultures. *Biomass Bioenergy* 2007;31:250–4.
48. Nissilä ME, Tähti HP, Rintala Ja, Puhakka Ja. Thermophilic hydrogen production from cellulose with rumen

- fluid enrichment cultures: effects of different heat treatments. *Bioresour Technol* 2011;102:1482–90.
49. Tawfik , El-Qelish M. Continuous hydrogen production from co-digestion of municipal food waste and kitchen wastewater in mesophilic anaerobic baffled reactor. *Bioresour Technol* 2012;114:270–4.
  50. Choi J, Ahn Y. Characteristics of biohydrogen fermentation from various substrates. *Int J Hydrogen Energy* 2013;39:3152–9.
  51. Fang HHP, Zhang T, Liu H. Microbial diversity of a mesophilic hydrogen- producing sludge. *Appl Microbiol Biotechnol* 2002;58:112–8.
  52. Nan-Qi R, Lei Z, Chuan C, Wan-Qian G, Guang-Li C A review on bioconversion of lignocellulosic biomass to H<sub>2</sub>: Key challenges and new insights *Bioresource Technology* 215 (2016) 92–99
  53. Zumar Bundhoo M A, Mohee R, Ali Hassan M Effects of pre-treatment technologies on dark fermentative biohydrogen production: A review *Journal of Environmental Management* 157 (2015) 20-48
  54. Pachapur V L, Sarma S J, Brar S K, Le Bihan Y, Soccol C R, Buelna G, Verma M Co-culture strategies for increased biohydrogen production *Int. J. Energy Res.* 2015; 39:1479–1504
  55. Cheng J, Zhu M. A novel anaerobic co-culture system for bio-hydrogen production from sugarcane bagasse. *Bioresource Technology* 2013; 144:623–631.
  56. Li Q, Guo C, Liu CZ. Dynamic microwave-assisted alkali pretreatment of cornstalk to enhance hydrogen production via co-culture fermentation of *Clostridium thermocellum* and *Clostridium thermosaccharolyticum*. *Biomass and Bioenergy* 2014; 64:220–229.
  57. Kotay SM, Das D. Microbial hydrogen production from sewage sludge bioaugmented with a constructed microbial consortium. *International Journal of Hydro- gen Energy* 2010; 35:10653–10659.
  58. Kumar G R, Chowdhary N Biotechnological and bioinformatics approaches for augmentation of biohydrogen production: A review *Renewable and Sustainable Energy Reviews* 56 (2016) 1194–1206
  59. Strobel H., 2009, Basic laboratory culture methods for anaerobic bacteria. In Mielenz, J. R., editor, *Biofuels*, Vol. 581 of *Methods in Molecular Biology*, 247–261. Humana Press c/o Springer Science+Business Media, LLC, New York, USA. ISBN 978-1-60761-213-1 DOI 10.1007/978-1-60761- 214-8\_16.
  60. Toscano G, Ausiello A, Micoli L, Zuccaro G, Pirozzi D (2014), Anaerobic digestion of residual lignocellulosic materials to biogas and biohydrogen, *Chemical Engineering Transactions* 32, 487-492.
  61. Ausiello A, Micoli L, Pirozzi D, Toscano G and Turco M (2015), Biohydrogen production by Dark Fermentation of *Arundo Donax* for feeding Fuel Cells, *Chemical Engineering Transactions*, 43, 385-390.

## **Chapter 3: The Use of Biogas in Fuel Cells Technology: Adsorption Processes and Adsorbent Materials for Removal of Noxious Compounds**

### **3.1 Introduction**

Fuel cells are highly efficient, cost effective, and ultra-low emission power generation systems. The major application for FCs are stationary electric power plants, including cogeneration units, as motive power for vehicles and as on-board electric power for space vehicles or other closed environments [1]. The most promising progress on which European or worldwide programs [2–8] have concentrated concerns mainly polymer membranes fuel cells (PEMFCs). Nevertheless the molten carbonate (MCFCs) and solid oxide fuel cells (SOFCs) are competitors for the development of high power units due to the possibility of heat and electricity cogeneration. They can be fed with different kinds of fuels: natural gas, LPG, gaseous carbon, and liquid fuels (such as gasoline and diesel) and biogas [9, 10]. European environment agency (EEA) identified and prioritized five environmental and sectorial areas for energy production which the European Union has included in its Sixth Environment Action Programme as well as in its sustainable development strategy. Regarding climate change, there is a great interest to reduce greenhouse gases as well as to enhance the rational use of fossil fuels (energy efficiency and renewable and sustainable energy sources) [11].

One of the main guide lines for renewable energy in the European Union is the Renewable Energy Roadmap [12] which has the goal of raising the share of renewable energy in total energy consumption to 20 % by 2020. In 2004 that share amounted to 109 million tons oil equivalent (MTOE), or 6.25 % of the 1747 MTOE of energy consumed in the 25 EU member states, about two thirds of that, or 72 MTOE coming from biomass mainly the agricultural ones.

Biomethane may play an important role in an integrated strategy to achieve ambitious targets for biofuels within Europe (25 % of total road transport in 2030) and worldwide. European market of the biomethane production is essentially developed in Germany where the first plants were started in 2007 and there were more efforts for regulatory the technical standard for its grid injection, furthermore other countries, as Austria, Switzerland, Sweden and the Netherland, have developed several plants for biomethane production [13]. Biomethane can be obtained from anaerobic decomposition of organic matter, and the most important sources are digestors (manure and agro-forest matter) and landfills (municipal solid waste). Biogas composition is strongly dependent on the source and is within (50–75) %  $\text{CH}_4$ , where the main contaminants are  $\text{CO}_2$  (up to 50 %) which lowers the calorific value of the gas and sulphuric acid ( $\text{H}_2\text{S}$ ) which could cause several problems on the plants and for human health: on the plants it causes corrosion (compressors, gas storage tank

and engines), while it is toxic after its inhalation [14–19]. Feedstocks used for biogas production and the corresponding composition and type of contaminants are reported in Table 3-1.

Plant size	Installed power	Biogas Substrate
Small size	10–100 kW <sub>el</sub>	livestock effluents energy crops agricultural waste organic waste
Medium size	<1 MW <sub>el</sub>	livestock effluents + energy crops + agricultural waste agro-industrial waste small wastewater treatment units
Large size	1–10 MW <sub>el</sub>	large-scale wastewater treatment units landfills

Tab. 3-1 Classification of Biogas Substrate According to Power Plant Capacity [20]

### 3.2 Substrates for biogas production and impurities

Three different plant categories are identified and classified as a function of installed power capacity of the biogas user. Connected to each category substrates considered for biogas production varied: the larger the power rating, the larger the biogas resources which have to be harvested.

In the following, the different substrates are specified in more details:

- Livestock effluents: manure from farm animals is used in most agricultural biogas plants; in practice manure is mixed with straw, bedding material fodder, and other residues from animal husbandry;
- Energy crops; such crops are grown to be specifically used for energetic valorization whereas anaerobic digestion is one option; energy crops include (among others) cereals, corn, and grasses;
- Agricultural waste: any kind of biological residue and green waste generated on a farm is considered in this substrate group; more precisely it includes plant residues, side products of agricultural production processes, sawdust, and other wastes;
- Organic waste: small municipalities gather and separate waste from restaurants, abattoirs, other small-scale businesses, and households in order to utilize the organic waste fraction.

Depending on the substrate used for biogas production the type and amount of impurities vary largely, according to Tables 3-2 and 3-3.

The main contaminants in biogas produced from agricultural wastes and biological substrates are sulphur compounds among which hydrogen sulphide (H<sub>2</sub>S) is the most dominant one [22–24].

In biogas stemming from food and animal waste as well as waste water halogenated compounds are present in very small trace amounts. Organic silicon compounds are only detected in landfill gas and from WWTU [24, 25]. Sulphur is present in nearly all biological compounds as part of amino acids such as methionine and cysteine [26]. In addition, biomass itself is made by up to <2 % (on weight basis of dry and ash-free biomass) of sulphur taken up through soil and air [27]. During digestion sulphur is converted into gaseous compounds including H<sub>2</sub>S, carbonyl sulphide (COS), mercaptans, and disulphides among which H<sub>2</sub>S is the most common one [24].

Concentration levels of H<sub>2</sub>S in biogas along with the overall chemical buildup of biogas vary significantly depending not only on substrate but also on operating conditions. Sklorz et al. [28] observed the H<sub>2</sub>S concentration fluctuations in a 45 kWe biogas plant using a gas engine for power generation due to microorganism or chemical reactions of H<sub>2</sub>S in coordination with galvanized steel tubing, mechanical stirring, to the injection of new batch of fresh sulphur-containing matter.

Not only H<sub>2</sub>S is present in biogas but other sulphur compounds [29] such as methanethiol (CH<sub>3</sub>SH) propanethiol (C<sub>3</sub>H<sub>7</sub>SH), butanethiol (C<sub>4</sub>H<sub>9</sub>SH), and dimethylsulphide (DMS), with levels that at time even surpass those of H<sub>2</sub>S. As a consequence, at least two gas-cleaning steps are needed for effective biogas cleaning: one step to remove bulk H<sub>2</sub>S concentration and a second step to remove remaining sulphur compounds because H<sub>2</sub>S removal should be not enough to remove other sulphur compounds [24]. Halogens are contained in waste in the form of kitchen salts and polymers (polytetrafluoroethylene PTFE polyvinyl chloride PVC) As such these compounds are mostly found in biogas from landfills [24,25, 30]. The presence of halogens in biological substances is due to the uptake by the plants through salts which are washed out of the soils. On average chlorine build up in plants amounts to < 1% wt. The quantities of halogens reported in literature are below 1 ppm [18,29,31,32].

<b>Composition</b>	<b>Natural Gas</b>	<b>Waste Water</b>	<b>Food Waste</b>	<b>Animal Waste</b>	<b>Landfill</b>
CH <sub>4</sub> (vol %)	80–100	50–60	50–70	45–60	40–55
CO <sub>2</sub> (vol %)	<3	30-40	25-45	35-50	35-50
N <sub>2</sub> (vol %)	<3	<4	<4	<4	<20
O <sub>2</sub> (vol %)	<0.2	<1	<1	<1	<2
H <sub>2</sub> S (ppm)	<0.1	<400	<10000	<100	<200
Non H <sub>2</sub> S sulphur (ppm)	<10	<1	<1000	<30	<30
Halogens (ppm)	<0.1	<0.2	<0.2	<0.2	<100
Moisture (%)	<0.02	~ 3	~ 3	~ 3	~ 3

Tab. 3-2 Biogas Composition for Different Biogas Plant Types [21]

Species	Contaminants	Average value (ppm)	Maximum value (ppm)
Sulphur compounds	H <sub>2</sub> S	400	2987
Siloxanes	D4	0.825	20.144
	D5	1.689	18.129
Halogens	Dichloromethane	0.082	0.052
	Chlorobenzene	0.255	0.693
	Dichlorobenzene	0.254	0.610

Tab. 3-3 Average and Maximum Values of the main contaminants in biogas from WWTU [20]

### 3.3 Biogas to biomethane

The biogas has different applications, such as a source for heat, steam, and electricity, household fuel for cooking, fuel cell, and can be further upgraded to vehicle fuel, or for production of chemicals and is a very promising technology for generating bioenergy [17,33,34].

The presence of CO<sub>2</sub> is a major problem in the biogas and its removal is needed to improve the calorific value and the relative density according to the specifications of the Wobbe index [35]. However, it is well assessed that the removal of H<sub>2</sub>S (that can be performed both during digestion (in situ) or after digestion) [36] can be of crucial point to the technological and economic feasibility of upgrading process of the gas.

The removal of CO<sub>2</sub> from biogas to obtain biomethane with purity above 98% is the most expensive step in the upgrading. Depending on the extraction method employed in landfills, nitrogen can also be found as a contaminant with contents up to 10%. Water washing, amine scrubbing, pressure swing adsorption (PSA), and membranes are commercial technologies already available to remove CO<sub>2</sub> from biogas, although it is recognized that the energy consumption of actual technologies can be improved.

In order to convert biogas into biomethane two major steps are performed: (1) a cleaning process to remove the trace components and (2) an upgrading process to adjust the calorific value. Upgrading is generally performed in order to meet the standards for use as vehicle fuel or for injection in the natural gas grid [18].

The basic gas upgrading steps include: water vapor removal, H<sub>2</sub>S removal, CO<sub>2</sub> removal, and siloxane and trace gas removal.

A number of techniques have been developed to remove H<sub>2</sub>S from biogas. Air dosing to the biogas and addition of iron chloride into the digester tank are two procedures that remove H<sub>2</sub>S during digestion. Techniques such as adsorption on probe materials or absorption in liquids remove H<sub>2</sub>S after digestion. Subsequently, trace components like siloxanes, hydrocarbons, ammonia, oxygen,



carbon monoxide and nitrogen can require extra removal steps, if not sufficiently removed by other treatment steps. Finally, CH<sub>4</sub> must be separated from CO<sub>2</sub> using pressure swing adsorption, membrane separation, physical or chemical CO<sub>2</sub>-absorption [18]

### **3.4 Biogas Upgrading**

#### **3.4.1 Removal of oxygen/air**

Oxygen and in part also nitrogen indicate that air has intruded the digester or landfill gas collector. This occurs quite often in landfills where the gas is collected through permeable tubes by providing a slight vacuum. Small concentrations (0-4%) of oxygen are harmless. Biogas in air with a methane content of 60% is explosive between 6 and 12%, depending on the temperature [18].

#### **3.4.2 Removal of water**

##### *Physical drying methods (condensation)*

The simplest way of removing excess water vapor is the refrigeration. This method can only lower the dewpoint to 0.5 °C due to problems with freezing on the surface of the heat exchanger. To achieve lower dewpoints the gas has to be compressed before cooling and then later expanded to the desired pressure. The lower the dew point, the higher pressure is needed to be applied [35].

The condensed water droplets are entrapped and removed. The physical drying methods prevent water contact with downstream equipment like compressors, pipes, activated carbon beds and other parts of the process, thus avoiding the problem of corrosion.

Techniques using physical separation of condensed water include: demisters in which liquid particles are separated with a wired mesh (0.5-2 mm). A dewpoint of 2-20 °C (atmospheric pressure) can be reached; cyclone separators in which water droplets are separated using centrifugal forces; moisture traps in which the condensation takes place by expansion, causing a low temperature that condenses the water; water taps in the biogas pipe from which condensed water can be removed [18,37].

##### *Chemical drying methods (adsorption or absorption)*

These techniques are usually applied at elevated pressures. At atmospheric pressure only a small amount of water is removed by the absorption and adsorption techniques.

Adsorption using alumina or zeolites/molecular sieves is the most common technique [38-42]

Methods based on gas drying include: adsorption of water vapour on silica [43] or alumina [44, 45] or equal chemical components that can bind water molecules (adsorption dryer).

The gas is pressurized and led through a column filled with silica. Usually two columns are used in parallel: one column adsorbs water, while the other is being regenerated. Regeneration is achieved by evaporating the water through decompression and heating.

#### *Absorption of water in triethylene glycol*

Drying takes place by using the water binding component triethylene glycol. Used glycol is pumped into a regeneration unit, where a temperature of 200° C is used to regenerate the glycol. Dew points from -5 to -15°C (atmospheric pressure) can be reached [37].

#### *Absorption of water with hygroscopic salts*

The salt is dissolved as it absorbs water from the biogas. The saturated salt solution is withdrawn from the bottom of the vessel. The salt is not regenerated and new salt granules have to be added to replace the dissolved salt [35].

### **3.4.3 Removal of CO<sub>2</sub>**

Upgrading biogas to natural gas quality needs the removal of CO<sub>2</sub> in order to obtain the quality that meets the Wobbe Index [18,35].

Depending on its use (pipeline or vehicle fuel), biomethane consists typically of 97-99% methane and 1-3% CO<sub>2</sub>. Typical pipeline specifications require a CO<sub>2</sub> content of less than 3% whereas vehicle fuel specifications require a combined CO<sub>2</sub>N<sub>2</sub> content of 1.5-4.5% [37]. One of the following techniques can be used to remove CO<sub>2</sub> from the biogas: (1) physical and chemical CO<sub>2</sub>-absorption, (2) Pressure Swing Adsorption (PSA) and Vacuum Swing Adsorption (VSA), (3) membrane separation, (4) cryogenic separation and (5) biological methane enrichment (Table 3-4) [17, 35,37,46-57].

#### *Physical and chemical CO<sub>2</sub>-absorption*

This technique is based on the separation of CO<sub>2</sub> and CH<sub>4</sub> by using an absorbent. One of the methods is the use of water as physical absorbent: CO<sub>2</sub> is separated from the biogas by washing with water at high pressure. Alternatively, biogas can be upgraded by chemical absorption with amines. CO<sub>2</sub> is absorbed in the liquid and reacts at quasi atmospheric pressure with the chemical substance in the absorption column [58,59].

Method	Advantages	Disadvantages
Absorption with water	High efficiency (>97% CH <sub>4</sub> ) Simultaneous removal of H <sub>2</sub> S When H <sub>2</sub> S < 300 cm <sup>3</sup> m <sup>-3</sup> Easy in operation Capacity is adjustable by changing pressure or temperature	Expensive investment Expensive operation Clogging due to bacterial growth Foaming possible Low flexibility toward variation of input gas

	Regeneration possible Low CH <sub>4</sub> losses (<2%) Tolerant for impurities	
Absorption with polyethylene glycol	High efficiency (>97% CH <sub>4</sub> ) Simultaneous removal of organic S components, H <sub>2</sub> S, NH <sub>3</sub> , HCN and H <sub>2</sub> O Energetic more favorable than water Regenerative Low CH <sub>4</sub> losses	Expensive investment Expensive operation Difficult in operation Incomplete regeneration when stripping/vacuum (boiling required) Reduced operation when dilution of glycol with water
Chemical absorption with amines	High efficiency (>99% CH <sub>4</sub> ) Cheap operation Regenerative More CO <sub>2</sub> dissolved per unit of volume (compared to water) Very low CH <sub>4</sub> losses (<0.1%)	Expensive investment Heat required for regeneration Corrosion Decomposition and poisoning of the amines by O <sub>2</sub> or other chemicals Precipitation of salts Foaming possible
PSA/VSA Carbon molecular sieves Molecular sieves (zeolites) Alumina silicates	Highly efficient (95-98% CH <sub>4</sub> ) H <sub>2</sub> S is removed Low energy use: high pressure, but regenerative Compact technique Also for small capacities Tolerant to impurities	Expensive investment Expensive operation Extensive process control needed CH <sub>4</sub> losses when malfunctioning of valves
Membrane technology Gas/gas Gas/liquid	H <sub>2</sub> S and H <sub>2</sub> O are removed Simple construction Simple operation High reliability Small gas flows treated without proportional increase of costs Gas/gas Removal efficiency: <92% CH <sub>4</sub> (1 step) or > 96% CH <sub>4</sub> H <sub>2</sub> O is removed Gas/liquid Removal efficiency: > 96% CH <sub>4</sub> Cheap investment and operation Pure CO <sub>2</sub> can be obtained	Low membrane selectivity: compromise between purity of CH <sub>4</sub> and amount of upgraded biogas Multiple steps required (modular system) to reach high purity CH <sub>4</sub> losses Little operational experience
Cryogenic separation	90-98% CH <sub>4</sub> can be reached CO <sub>2</sub> and CH <sub>4</sub> in high purity Low extra energy cost to reach liquid biomethane (LBM)	Expensive investment and operation CO <sub>2</sub> can remain in the CH <sub>4</sub>
Biological removal	Removal of H <sub>2</sub> S and CO <sub>2</sub> Enrichment of CH <sub>4</sub> No unwanted end products	Addition of H <sub>2</sub> Experimental e not at large scale

Tab. 3-4 Advantages and disadvantages of techniques for removal of CO<sub>2</sub> [18]

### *Pressure swing adsorption (PSA), vacuum swing adsorption (VSA)*

PSA and VSA use a column filled with a molecular sieve, typically activated carbon, silicagel, alumina or zeolite, for differential adsorption of the gases CO<sub>2</sub> and H<sub>2</sub>O, allowing CH<sub>4</sub> pass through [47,49]. The molecules are adsorbed loosely in the cavities of the molecular sieve and not irreversible bound [46]. It is a cyclic batch process where adsorption is performed on a relatively higher pressure (around 800 kPa) and desorption (regeneration) at lower pressure [51]. H<sub>2</sub>S, adsorbing irreversibly, must be removed before the PSA or VSA unit to prevent poisoning of the molecular sieve. PSA and VSA are similar systems, but VSA has a supplementary vacuum pump: the differential pressure is situated at lower absolute pressure. Adsorption takes place on a gas under pressure, desorption at vacuum [50].

### **3.5 Membrane separation**

Membrane separation is based on the selective permeability property of membranes. Two systems are proposed: (1) gas-gas separation with a gas phase at both sides of the membrane and (2) gas-liquid absorption separation with a liquid absorbing the diffused molecules. Due to imperfect separation, multiple stages may be required [46]. Because of this, an increase in methane loss is obtained. This can be partly prevented by recirculation [60].

A demonstration plant that use membranes for biogas upgrading through has been installed at Bruck/Leitha in the south of Austria [61]; the membranes used are hollow fiber type and the operative pressure is of about 8–9 bar. The process is carried out in two stages and biomethane concentration was of about 98% in volume that is injected into the local gas grid. This technology is capable of removing also small concentrations of H<sub>2</sub>S.

Several literature studies show the industrial applicability of the processes in polymeric membranes for the separation of carbon dioxide from biogas [62-79]. At the actual state polymeric membranes show a good level of competitiveness with conventional technologies for CO<sub>2</sub> and H<sub>2</sub>S separation from biogas. Biogas upgrading plant and other equipment used are located at the ENEA Trisaia (Italy) research centre [80]. The polymer membranes are PEEK and works up to 48 bar, with a differential pressure 41 bar in a range of temperature 5–70 °C in line with the operational regimes of the biogas plants. The H<sub>2</sub>S presence in the biogas do not represents a problem in term of separation stage using PEEK polymeric membrane, but its selectivity was of about 50%. Best performing could be carried out using multiple stage separation processes where is possible to work with low operative pressure in the feed stream.

### **3.6 Cryogenic separation**

Taking into account that  $\text{CH}_4$ ,  $\text{CO}_2$  and other impurities liquefy in different temperature/pressure areas, it is possible to produce biomethane by cooling and compressing the biogas. The liquid  $\text{CO}_2$  should also dissolve and thus separate the remaining impurities from the gas. The raw biogas is compressed till 8000 kPa. Compression is done in different stadia with interim refrigeration. The compressed gas needs to be dried in advance, to prevent freezing in the following cooling steps. The dried and compressed biogas is eventually cooled till  $-45\text{ }^\circ\text{C}$ . The condensed  $\text{CO}_2$  is removed and treated in a next step to recover the remaining  $\text{CH}_4$ . The biogas is cooled further to  $-55\text{ }^\circ\text{C}$  and afterward expanded to 800 1000 kPa in an expansion tank, reaching a temperature of about  $-110\text{ }^\circ\text{C}$ . In these conditions, there is a gas-solid phase balance, with the solid phase being  $\text{CO}_2$  and the gaseous phase containing more than 97%  $\text{CH}_4$ . The  $\text{CH}_4$  gas stream is collected and heated before leaving the plant [35,81].

### **3.7 Biological methane enrichment**

Biological methane enrichment was recently studied [57,82, 83].

Strevett et al. [57] investigated the mechanism and kinetics of chemo-autotrophic biogas upgrading. Different methanogens using only  $\text{CO}_2$  as a carbon source and  $\text{H}_2$  as an energy source were examined. The selection between mesophilic and thermophilic operation temperatures must be properly chosen. Thermophilic methanogens exhibit rapid methanogenesis, while mesophilic bacteria give more complete conversion of the available  $\text{CO}_2$  [57]. The authors selected *Methanobacterium thermoautotrophicum* that works optimally at temperatures of  $65\text{--}70\text{ }^\circ\text{C}$  and has a specific requirement for  $\text{H}_2\text{S}$ , so leading to the removal of further unwanted compounds.

### **3.8 Removal of $\text{H}_2\text{S}$**

Due to the damage that  $\text{H}_2\text{S}$  can cause in several parts of the plants, it is typically removed in an early state of the biogas upgrading process. Several techniques are applied: (1) removal of  $\text{H}_2\text{S}$  during digestion and (2) removal of  $\text{H}_2\text{S}$  after digestion (Table 3-5) [35,46-50,81].

Method	Advantages	Disadvantages
Biological with O <sub>2</sub> /air (in filter/scrubber/digester)	Cheap investment and exploitation: low electricity and heat requirements, no extra chemicals or equipment required Simple operation and maintenance	Concentration H <sub>2</sub> S still high (100-300 cm <sup>3</sup> m <sup>-3</sup> ) Excess O <sub>2</sub> /N <sub>2</sub> in biogas implies difficult upgrading or additional cleaning. Overdosing air results in explosive mixture
FeCl <sub>3</sub> /FeCl <sub>2</sub> /FeSO <sub>4</sub> (in digester)	Cheap investment: storage tank and dosing pump Low electricity and heat requirements Simple operation and maintenance Compact technique H <sub>2</sub> S not in biogas wire No air in biogas	Low efficiency (100-150 cm <sup>3</sup> m <sup>-3</sup> ) Expensive operation (iron salt) Changes in pH/temp not beneficial for the digestion process Correct dosing is difficult
Fe <sub>2</sub> O <sub>3</sub> /Fe(OH) <sub>3</sub> -bed	High removal efficiency: >99%	Sensitive for water
Rust steel wool impregnated wood chips or pellets	Mercaptanes are also captured Cheap investment Simple	Expensive operation costs, Regeneration is exothermic: risk of ignition of chips Reaction surface reduced each cycle Released dust can be toxic
Absorption in water	H <sub>2</sub> S <15 cm <sup>3</sup> m <sup>-3</sup> Cheap when water is available (not regenerative) CO <sub>2</sub> is also removed	Expensive operation: high pressure, low temperature Difficult technique Clogging of the absorption column possible
Chemical absorption NaOH FeCl <sub>3</sub>	Low electricity requirement Smaller volume, less pumping, smaller vessels (compared to absorption in H <sub>2</sub> O) Low CH <sub>4</sub> losses	Expensive investment & operation More difficult technique Not regenerative
Chemical absorption Fe(OH) <sub>3</sub> Fe-EDTA Cooab	High removal efficiency: 95-100 % Cheap operation Small volume required Regenerative Low CH <sub>4</sub> losses	Difficult technique Regeneration through oxygenation CO <sub>2</sub> → H <sub>2</sub> CO <sub>3</sub> (using EDTA) leads to precipitation Build up of thiosulfates from chelates + H <sub>2</sub> S (using EDTA)
Membranes	Removal of >98 % is possible CO <sub>2</sub> is also removed	Expensive operation and maintenance Complex
Biological filter	High removal possible: >97 % Low operational cost	Extra H <sub>2</sub> S-treatment to reach pipeline quality; O <sub>2</sub> /N <sub>2</sub> in biogas implies difficult and additional upgrading steps
Adsorption on activated carbon (Impregnated with KI 1-5 %)	High efficiency (H <sub>2</sub> S <3 cm <sup>3</sup> m <sup>-3</sup> ) High purification rate Low operation temperature Compact technique High loading capacity	Expensive investment and operation CH <sub>4</sub> losses H <sub>2</sub> O and O <sub>2</sub> needed to remove H <sub>2</sub> S H <sub>2</sub> O can occupy the binding places of H <sub>2</sub> S; Regeneration at 450 °C Residue present till 850 °C

Tab. 3-5 Advantages and disadvantages of techniques for removal of H<sub>2</sub>S [18]

### 3.9 Removal of H<sub>2</sub>S during digestion

To choose an appropriate technique for H<sub>2</sub>S removal, the technique to remove CO<sub>2</sub> should be considered first. A technique such as absorption in water or selexol, membranes or PSA/VSA that removes H<sub>2</sub>S as well as CO<sub>2</sub>, will make an additional technique for the removal of H<sub>2</sub>S unnecessary, unless H<sub>2</sub>S is present in high concentrations (>300 cm<sup>3</sup>m<sup>-3</sup>). A CO<sub>2</sub> removal technique such as absorption with amines, that does not explicitly eliminate H<sub>2</sub>S, will necessitate an additional removal step such as absorption in a NaOH-solution, absorption on hygroscopic salt and reaction in a Fe<sub>2</sub>O<sub>3</sub>-bed. H<sub>2</sub>S can be treated directly in the digester vessel. The sulphide either reacts with a metal ion to form an insoluble metal sulphide or is oxidized to elementary sulphur [35,81].

#### *Air/oxygen dosing to the biogas system*

This technique is based on the biological aerobic oxidation of H<sub>2</sub>S to elemental sulphur by a group of specific bacteria [18].

Most of sulphide oxidizing micro-organisms (Thiobacillus) are autotrophic [84-87] and use CO<sub>2</sub> from the biogas as source of carbon. They grow on the surface of the digestate or on the framework of the digester and do not require inoculation. The following reaction occurs in the biogas:



not only elemental sulphur, but also sulfate is formed, which can cause corrosion in solutions. A certain amount (2-6%) of O<sub>2</sub> required for the reaction, is introduced in the biogas. A reduction of H<sub>2</sub>S concentrations down to 20-100 cm<sup>3</sup>m<sup>-3</sup> and a removal efficiency of 80-99% can be achieved [46,47] but the remaining concentrations may still be too large [37]. Safety measures have to be taken to avoid overdosing of air since biogas in air (6-12%) is an explosive mixture. Moreover, care has to be taken to guarantee anaerobic conditions.

#### *Addition of iron chloride into the digester*

Commonly FeCl<sub>2</sub>/FeCl<sub>3</sub> is added during digestion to reduce the concentration of H<sub>2</sub>S to a few hundred cm<sup>3</sup>m<sup>-3</sup>. Precautions should be taken to prevent O<sub>2</sub> and N<sub>2</sub> from entering the biogas, rather than to remove them [35,46,47,81].

Iron chloride can be dosed directly into the digester or through the influent mixing tank. It reacts with the H<sub>2</sub>S present in the biogas to form FeS (particles) according to Eqs (3.2) and (3.3). The precipitation reaction of the iron salt can be written as follows:





This method is very efficient in reducing high concentrations of  $\text{H}_2\text{S}$ , since a reduction of  $\text{H}_2\text{S}$  concentration down to  $100 \text{ cm}^3 \text{ m}^{-3}$  can be achieved [37], but does not allow the attainment of a low and stable level of hydrogen sulphide [47].

### 3.10 Removal of $\text{H}_2\text{S}$ after digestion

#### *Adsorption using iron oxide or hydroxide*

Hydrogen sulphide reacts easily with iron oxide, iron hydroxide and zinc oxide and forms iron sulphide or zinc sulphide respectively [18]. This process is often referred to as “iron sponge” because rust-covered steel wool may be used to form the reaction bed.

Iron oxide and iron hydroxide react with  $\text{H}_2\text{S}$  in the biogas according to following reactions



The reaction is slightly endothermic: a temperature minimum of about  $12^\circ\text{C}$  is required, but the optimal conditions are between  $25$  and  $50^\circ\text{C}$ . Condensation of water on the iron oxide should be avoided since the iron oxide material will link together with water which reducing the surface [3].

The iron oxide can be regenerated with oxygen according to the following reaction:



#### *Physical and chemical absorption with liquids*

Physical absorption removes  $\text{H}_2\text{S}$  by absorption in water or an organic solvent [18,37,88-90]. The most common solvent is water although operational problems due to the growth of micro-organisms on the packing occur.

Two types of water absorption processes are commonly used for the upgrading of biogas: single pass absorption and regenerative absorption [48]. A high consumption of water is needed in the case of absence of regeneration steps.

Chemical absorption liquids that can be used are diluted  $\text{NaOH}$ -solution:  $\text{NaOH}$  reacts with  $\text{H}_2\text{S}$  to form  $\text{Na}_2\text{S}$  or  $\text{NaHS}$  which precipitates. The formed sodium salts are not regenerative and have to be disposed of  $\text{FeCl}_2$ -solution:  $\text{FeCl}_2$  f reacts with  $\text{H}_2\text{S}$  to form insoluble  $\text{FeS}$  that needs to be

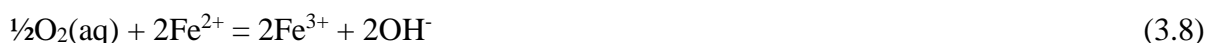


removed; Fe(OH)<sub>3</sub>-solution: H<sub>2</sub>S is removed using Fe(OH)<sub>3</sub> resulting in the formation of Fe<sub>2</sub>S<sub>3</sub>. Regeneration is done with oxygen or air (closed system) [18,37,91,92].

Horikawa et al. [93] investigated chemical absorption of H<sub>2</sub>S in an Fe(III)-EDTA catalyst solution. In this process, H<sub>2</sub>S is dissolved in an aqueous solution and catalytically removed by a chelated iron according to the following reaction:



The sulphur produced is easily separated by sedimentation or filtration from the Fe-EDTA-solution. Regeneration of the aqueous Fe-EDTA-solution is done by oxygenation according to Eq. (3.8):



The regeneration the Fe-EDTA-solution allows a large consumption of chemicals. The process can be carried out at ambient temperature and is highly selective in removing H<sub>2</sub>S: the volumes CH<sub>4</sub> and CO<sub>2</sub> present in biogas remain nearly constant. A removal of 90-100% can be obtained for biogas containing 2.2% H<sub>2</sub>S at a gas flow of 1 dm<sup>3</sup> min<sup>-1</sup>, and at a solution flow of 83.6 cm<sup>3</sup> min<sup>-1</sup> and an inlet biogas pressure of 220 kPa [93]. At lower catalytic solution flow, lower absorption efficiency is obtained. At lower inlet H<sub>2</sub>S concentration higher absorption efficiency is obtained. Therefore, the total removal of H<sub>2</sub>S depends on the use of the adequate ratio of gas to liquid flow rates [93].

### 3.11 Separation of H<sub>2</sub>S with Membrane

H<sub>2</sub>S can be separated from the gas by the use of semi-permeable membranes. H<sub>2</sub>S (and CO<sub>2</sub>) can pass the membrane whereas CH<sub>4</sub> cannot [18,37]. In addition, gas-liquid absorption membranes can be used. The membranes are micro porous and have hydrophobic properties: the molecules in the gas stream, flowing in one direction, diffuse through the membrane and are absorbed on the other side by the liquid, flowing in counter current. At a temperature of 25-35°C the H<sub>2</sub>S concentration of the raw gas of 2% could be reduced to less than 250 cm<sup>3</sup>m<sup>-3</sup> thus yielding an efficiency of more than 98%. NaOH is used as the absorb in liquid [18,46].

### 3.12 Biological filter

This method is similar to the technique where air/O<sub>2</sub> was added to the digestion tank. It is based on the use of specific bacteria that are able to oxidize H<sub>2</sub>S. Air (4-6%) is added to the biogas the filter bed; H<sub>2</sub>S is absorbed in the liquid phase, that is gas condensate and liquid from effluent slurry

separation. After absorption,  $\text{H}_2\text{S}$  is oxidized by the bacteria, growing on the filter bed. The temperature is about  $35^\circ\text{C}$  that promotes the biological process. Sulphur is retained in the liquid of the filter [18,35,37,79]. Biological filtration is required in several plants for removing odors (oxygen rich situation) [47] and in some cases to remove  $\text{H}_2\text{S}$  from biogas. This technique has the advantage of low costs in comparison to chemical cleaning. The method is also able to remove ammonia from the biogas. With addition of air to the biological filters, the  $\text{H}_2\text{S}$  content can be decreased from 2000-3000 to 50-100  $\text{cm}^3 \text{ m}^{-3}$ . Some works reported  $\text{H}_2\text{S}$  reduction from 800 to 10  $\text{cm}^3 \text{ m}^{-3}$  [35,79].

Among the several gas purification processes proposed to eliminate  $\text{H}_2\text{S}$ , such as chemical scrubbing, physical adsorption [92], electrochemical treatment [93], and biofiltration [94,95] the physical and chemical treatments suffer the disadvantages of high costs and secondary pollutants production although are rapid and efficient. On the contrary biological treatment that directly metabolize  $\text{H}_2\text{S}$  into sulfate has receiving increasing attention. It is reported that the drop in pH caused by sulfate accumulation has negative effects [96-101], therefore, studies on biological processes have focused on removing low  $\text{H}_2\text{S}$  concentrations (10–50 ppm) to prevent rapid pH drop [102-106].

Other studies that combined chemical and biological processes for both  $\text{H}_2\text{S}$  elimination and ferric iron regeneration by *Acidithiobacillus ferrooxidans* have been reported [107-109]. These processes are based on two reactions as follows: the inlet  $\text{H}_2\text{S}$  is first oxidized with a ferric iron solution and yields elemental sulphur, and the reduced ferrous iron is then reoxidized by *A. ferrooxidans* in the biological process.

Separate studies that focused on chemical absorption [110,111] and biological oxidation [109,112] were proposed. For instance, when the inlet  $\text{H}_2\text{S}$  concentration is lower than 300 ppm, the rate-limiting step for the chemical absorption process is the mass-transfer limitation, as revealed by model validation [113]. When the system has a high inlet  $\text{H}_2\text{S}$  concentration (e.g., above 1500 ppm), the  $\text{H}_2\text{S}$  removal efficiency is significantly maintained via long GRT (gas retention time) and stable ferric iron concentration in the chemical reactor [114]. In the biological reaction, Mesa et al. [115] investigated the continuous oxidation efficiency of ferrous iron by using immobilized *A. ferrooxidans*. However, studies that focused on the combined and continuous operation are limited. In the present study, the chemical absorption reactor and the biological oxidation reactor with immobilized *A. ferrooxidans* CP9 were connected and then examined in both laboratory and pilot scales to evaluate the performance of  $\text{H}_2\text{S}$  elimination. In the laboratory-scale study, optimal operating parameters such as GRT, temperature, and  $\text{H}_2\text{S}$  inlet loading were examined. In the pilot-scale study, the biogas with an average  $\text{H}_2\text{S}$  concentration of 1645 ppm was introduced into the

chemical–biological system. The long-term performance was examined, and the results demonstrate that the chemical–biological process effectively removed H<sub>2</sub>S from the biogas.

Biotrickling filters work by passing a stream of contaminated air through a chemically inert packing material over which an aqueous phase is continuously trickled. Microorganisms grow as biofilms on the surface of the packing material by using pollutants transferred from the gas to the biofilm as energy and/or carbon sources. The effect of CH<sub>3</sub>SH in the removal of H<sub>2</sub>S in biogas in biotrickling filters has not been explored yet although there are few references in the co-treatment of low loads of CH<sub>3</sub>SH and H<sub>2</sub>S for odour removal [106,116].

The biological oxidation of H<sub>2</sub>S in aerobic (Eqs. 3.9 and 3.10) and anoxic (Eq. 3.11) biotrickling filters occurs according the following scheme [100,117]



Eq. (3.3) involves both complete and partial denitrification coupled to complete and partial H<sub>2</sub>S oxidation [118]. In both cases the principal products are sulphate and elemental sulphur. The risk of clogging by elemental sulphur formation is the most important bottleneck for stable, long-term operation in biotrickling filters.

The ratio between the available electron acceptor and H<sub>2</sub>S i.e. O<sub>2</sub>/H<sub>2</sub>S and NO<sub>3</sub><sup>3-</sup>/H<sub>2</sub>S in aerobic and anoxic biotrockling filter are the key parameters to end up with a certain SO<sub>4</sub><sup>-2</sup>/S<sup>°</sup> produced ratio [100,119].

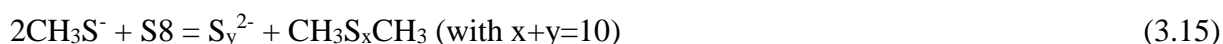
The biological oxidation of CH<sub>3</sub>SH under aerobic conditions produces formaldehyde and H<sub>2</sub>S intermediate product [120]. The overall reaction can be expressed by Eq. (3.12) [121]



Chemical oxidation of CH<sub>3</sub>SH to DMDS in an aerobic reactor has been reported according to Eq. (3.13) [122]



Recently van Leerdaam [122,123] have found that CH<sub>3</sub>SH also reacts chemically with biosulphur particles at pH 8.7 to form DMDS and other polysulphided according to



The main product of these reactions are dimehyl polisulphides (DMDS and dimehyl trisulphide (DMTS)) and some longer-chain dimehyl polysulphides.

DMDS and DMTS are less inhibitory than  $\text{CH}_3\text{SH}$  on biological (poly)sulphide oxidation [124].

$\text{H}_2\text{S}$  and methylmercaptan ( $\text{CH}_3\text{SH}$ ) are the most common sulphur compounds found in biogas. Montebello et al [99] studied the simultaneous removal of  $\text{H}_2\text{S}$  and  $\text{CH}_3\text{SH}$  was tested at neutral pH in two biotrackling filters one operated under aerobic conditions and the other one under anoxic conditions. Both reactors were run for several months treating  $\text{H}_2\text{S}$  concentration of around 2000 ppm and  $\text{CH}_3\text{SH}$  in the range 10-75 ppm. Maximum removal capacities of around 1.8 g S- $\text{CH}_3\text{SH}$   $\text{m}^{-3}\text{h}^{-1}$  were observed by stepwise increasing  $\text{CH}_3\text{SH}$  concentrations from 0 to 75-90 ppm(v) at a constant  $\text{H}_2\text{S}$  loading rate of 53-63 gS- $\text{H}_2\text{S}$   $\text{m}^{-3}\text{h}^{-1}$ . Maximum  $\text{H}_2\text{S}$  elimination capacities for both reactors were between 100 and 140 gS- $\text{H}_2\text{S}$   $\text{m}^{-3}\text{h}^{-1}$ .

A negative influence was found in the elimination capacities of  $\text{CH}_3\text{S}$  by the presence of high  $\text{H}_2\text{S}$  in both biotrackling filters.  $\text{CH}_3\text{SH}$  chemically reacts with elemental sulphur at neutral pH enhancing the overall reactors performance by reducing the impact of sulphur accumulation. Both reactors were also able to treat  $\text{CH}_3\text{S}$  without prior inoculation because of the already existing sulphide-oxidizing microorganisms grown in the reactors during  $\text{H}_2\text{S}$  treatment. Co-treatment of  $\text{H}_2\text{S}$  and  $\text{CH}_3\text{SH}$  under aerobic and anoxic conditions was considered as a feasible operation for concentrations commonly found in biogas (2000 ppm of  $\text{H}_2\text{S}$  and below 20 ppm of  $\text{CH}_3\text{SH}$ ).

A chemical–biological process has been proposed by Ho et al. [107] to remove a high concentration of  $\text{H}_2\text{S}$  in biogas. The high iron concentration tolerance (20 g  $\text{L}^{-1}$ ) of *Acidithiobacillus ferrooxidans* CP9 provided sufficient ferric iron level for stable and efficient  $\text{H}_2\text{S}$  removal. The results showed that the  $\text{H}_2\text{S}$  removal efficiency reached 98% for 1500 ppm  $\text{H}_2\text{S}$ . The optimal ferric iron concentration was kept between 9 and 11 g  $\text{L}^{-1}$  with a cell density of 108 CFU  $\text{g}^{-1}$  granular activated carbon and a loading of 15 g S  $\text{m}^{-3}$   $\text{h}^{-1}$ . In pilot-scale studies for biogas purification, the average inlet  $\text{H}_2\text{S}$  concentration was 1645 ppm with a removal efficiency of up to 97% for a 311 operation days and an inlet loading 40.8 g S  $\text{m}^{-3}$   $\text{h}^{-1}$ .

Removal of  $\text{H}_2\text{S}$  up to <100 ppm by in situ precipitation was reported by several authors [20,125,126]. The remaining content of  $\text{H}_2\text{S}$  which is not removed by bacterial activity is cleaned by adsorption on ZnO ideally reaching concentrations levels of <1 ppm [127].

Trace impurities are removed in a final step by an adsorption bed of activated carbon aiming for concentration levels <1 ppm [128].

### 3.13 Adsorption on activated carbon

H<sub>2</sub>S can also be removed by using activated carbon, which is often dosed with KI or sulphuric acid (H<sub>2</sub>SO<sub>4</sub>) to increase the reaction rate. Before entering the carbon bed 4-6% air is added to the biogas and H<sub>2</sub>S is catalytically converted to elemental sulphur and water in biological filters, according to Eq. (3.16):



The elementary sulphur is adsorbed by the activated carbon. Best efficiency is obtained at pressures of 700-800 kPa and temperatures of 50-70°C that can be achieved through heat generation during compression. In continuous process the system consists of two vessels [35,46,79]: one vessel for adsorption and the other for regeneration. Regeneration can be performed with hot nitrogen (inert gas) or steam. The sulphur is vaporized and, after cooling, liquefied at approximately 130°C. Typically, the activated carbon is replaced rather than regenerated [18,35,46,79].

### 3.14 Ammonia stripping

Anaerobic digestion effluent typically contains high amounts of ammonium, phosphate, suspended solid (SS), and persistent organic substrate, which has been generally applied as a fertilizer for recycling the nutrients in agricultural field [129]. However, the excessive application of digested effluent in agricultural areas is the probable cause of nitrogen pollution in farming areas [130]. The high ammonia, phosphate and SS contents of anaerobic digestion effluent are generally difficult of access to conventional biological treatment processes such as activated sludge process [131,132], soil trench system, etc. [133]. In addition, the relatively low chemical oxygen demand/total nitrogen (COD/TN) ratio [129-131] is insufficient to facilitate efficient TN removal. Meinhold et al. [134] suggested that the COD/TN ratio for efficient TN removal by nitrification and denitrification in an activated sludge process should be between 4 and 5. Hence, physico-chemical pre-treatments such as ammonia stripping, ion exchange, membrane processes, and chemical precipitation are required to lower the concentration of ammonia, phosphate, and SS prior to application to biological treatment processes. Ammonia stripping has been successfully applied in pretreating pig slurry [135,136], landfill leachate [137], urea fertilizer plant wastes [138], etc. However, researches on the application of ammonia stripping to anaerobic digested effluent are limited. Further, the optimal

Ca(OH)<sub>2</sub> dosage must also be studied because of the different C, N, and P concentrations and pH buffer capacity of anaerobic digested effluent.

Lei et al. [139] showed that an overdose of calcium hydroxide, i.e., 27.5 g/L wastewater, achieved higher ammonia, phosphorus, chemical oxygen demand, suspended solids, and turbidity removal efficiency. The pH of the anaerobic digestion effluent can be increased from about 7 to about 9 by CO<sub>2</sub> stripping. It was roughly estimated that 43 m<sup>3</sup> of biogas (CH<sub>4</sub>:CO<sub>2</sub> ≈60%:40%) produced daily could be purified to CH<sub>4</sub>:CO<sub>2</sub> ≈74%:26% by neutralizing the pH of the 5m<sup>3</sup> anaerobic digestion effluent pretreated by ammonia stripping.

### **3.15 Materials for Sulphur Removal: Activate carbons and Zeolites**

At present adsorption technology is recognised to be the most common technology applied to reach ultra-low sulphur levels for fuel cells applications. Activated carbon is one of the most versatile adsorbents known with high removal efficiency, low costs reusability and possible product recovery [16,140-155]. However there are many other commercial adsorbents used for fuels desulphurization at ambient temperature and pressure such as silica, alumina, zeolites and some metal oxides [156-166].

Aslam et al. [147] reported the study of activated carbon (AC) made from waste oil fly ash (OFA) which is produced in large quantities from power generation plants through combustion of heavy fuel oil. OFA contains ~80 % C that makes it suitable for producing AC by physicochemical treatments using a mixture of HNO<sub>3</sub>, H<sub>2</sub>SO<sub>4</sub>, and H<sub>3</sub>PO<sub>4</sub> acids to remove non-carbonaceous impurities. The physicochemical treatments of OFA increased the surface area from 4 to 375 m<sup>2</sup>/g. The materials are characterized by combined SEM and EDX techniques. The AC is further treated with HNO<sub>3</sub> and NH<sub>4</sub>OH solutions in order to attach the carboxylic and amine groups on the surface, respectively. FTIR characterization is used to confirm the presence of the functional groups on the surface of AC at different stages of its development. The performance of functionalized AC samples is tested for the removal of H<sub>2</sub>S from a synthetic natural gas by carrying out breakthrough curves. The results showed maximum adsorption capacity of 0.3001 mg/g for NH<sub>4</sub>OH functionalized AC with 86.43% regeneration efficiency. The NH<sub>4</sub>OH-treated AC is more effective for H<sub>2</sub>S removal than acid-treated AC.

Phooratsamee et al. [146] reported the preparation of activated carbon from palm oil shells by chemical activation using ZnCl<sub>2</sub> impregnated with NaOH, KI and K<sub>2</sub>CO<sub>3</sub> for H<sub>2</sub>S absorption from biogas. The production of activated carbon involved three stages; (1) carbonization of raw material at 600°C; (2) activation of char product from the first stages; (3) alkali impregnation of activated carbon NaOH, KI and K<sub>2</sub>CO<sub>3</sub> solutions. The result showed that the highest surface area and the pore

volume ( $741.71 \text{ m}^2/\text{g}$  and  $0.4210 \text{ cc g}^{-1}$ ) was obtained on  $\text{K}_2\text{CO}_3$ -AC activated carbon. The best performances were obtained with  $\text{K}_2\text{CO}_3$ -AC in comparison to KI-AC and NaOH. Therefore,  $\text{K}_2\text{CO}_3$ -AC impregnated activated carbon has a high surface area and showed be an efficient adsorbent for removal of  $\text{H}_2\text{S}$  from biogas product.

The influence of modification conditions and operation conditions on the  $\text{H}_2\text{S}$  adsorption performance on AC samples was also study by Liang et al. [150]. The authors reported that a combinatory method of high-pressure hydrothermal treatment followed by alkaline solution impregnation could promote the  $\text{H}_2\text{S}$  adsorption performance remarkably.

Monteleone et al. [153] studied anaerobic  $\text{H}_2\text{S}$  adsorption on activated carbons, with particular attention to the influence of thermal treatment on adsorption capacity, to feasibility of regeneration and the competitive adsorption of  $\text{H}_2\text{S}$  and  $\text{CO}_2$ . The selected materials were characterized before and after adsorption tests, using sorption of N, XRPD, TGA-DTA, SEM and EDX. All tested carbons showed a better adsorption capacity before thermal treatment, confirming the crucial role of  $\text{H}_2\text{O}$  in absorption mechanism. Activated C impregnated with metal salts, revealed the highest adsorption capacity due to the combination of microporosity and oxidative properties.

Osorio et al. [167] reported a study dealing with biogas purification coming from the anaerobic digestion of sludge in a wastewater treatment plant. The purification apparatus contains scrubbing towers and filters of activated carbon at the end of the line. The  $\text{H}_2\text{S}$  inflow concentrations were quite high (up tp 2000ppm). The effluent biogas from the scrubbing towers presented an  $\text{H}_2\text{S}$  concentration less than 1 ppm and zero or undetectable values after adsorption of active carbons filters.

An et al. [151] investigate the performance of activated carbon fiber (ACF) modified by impregnation with transition metals. The differences of the performance between original and modified ACF and the effects of type and concentration of impregnants were studied. It was observed that the adsorption capacity of ACF was significantly improved by modification and that sulphur capacity increased with the concentration of impregnant initially, and then decreased. The adsorption of  $\text{H}_2\text{S}$  was in the order: 5%  $\text{Cu}(\text{NO}_3)_2$ -ACF>5%,  $\text{Co}(\text{NO}_3)_2$ -ACF>5%,  $\text{Mn}(\text{NO}_3)_2$ -ACF. The modified ACF by 5%  $\text{Cu}(\text{NO}_3)_2$ -3%  $\text{Co}(\text{NO}_3)_2$  solutions has the best performance with the sulphur capacity of 166.7 mg/g. The modified ACF by 5%  $\text{Cu}(\text{NO}_3)_2$ -3%  $\text{Co}(\text{NO}_3)_2$ -1%  $\text{Mn}(\text{NO}_3)_2$  solution has the worst performance with a sulphur capacity of 83.3 mg/g

Huang and Chen [152] propose a dynamic adsorption model to simulate removal of  $\text{H}_2\text{S}$  by a fixed-bed packed with copper impregnated activated carbon (IAC). After diffusion into the interior of a pellet,  $\text{H}_2\text{S}$  species either may be physical adsorbed on carbon surface or may react with the copper impregnated on the IAC.

Hernandez et al [141] studied a system for both the desulphurization and dehalogenation of landfill biogas at ambient temperature. The principal aim of the work was to identify a multifunctional adsorption bed that would be able to purify the landfill biogas to sulphur and chlorine concentrations of below 1 ppmv, with a high removal efficiency ( $> 99\%$ ). Two commercial activated carbons were studied. Moreover, activated carbon, functionalized by ZnO nanoparticles, was tested at ambient temperature for the simultaneous removal of  $\text{H}_2\text{S}$  and organochlorinated mols. The biogas desulphurization results have shown that the ZnO (10%) modified commercial active carbon has a higher adsorption capacity than the commercial material due to the presence of well dispersed ZnO nanoparticles on the surface. Moreover, the biogas dehalogenation results confirm that the use of two adsorbent beds in series improves the performance of the abatement of high molecular weight halogenated.

Riberio et al. [14] reported a study of adsorption of carbon dioxide, methane, and nitrogen on an activated carbon honeycomb monolith supplied by Mast Carbon (United Kingdom). A very interesting property of honeycomb monoliths is that the pressure drop is almost negligible [168]. Kinetics of adsorption (diffusion rates) of pure gases was measured by diluted breakthrough curves of the pure gases diluted in helium. A mathematical model using one lumped resistance was employed to determine diffusivity coefficients from experimental data. The results were correlated with the Langmuir and multisite Langmuir models.

Chang [142] reported the study of high silica/alumina ratio ( $>10$ ) zeolite including MCM-4 and Y-type zeolite or high-silica zeolite and  $\text{Mg}^{2+}$  or  $\text{Cu}^{2+}$  modified activated carbons.

Yazdanbakhsh et al. [158] reported the  $\text{H}_2\text{S}$  breakthrough capacity of copper-exchanged Engelhard Titanosilicate-2 (ETS-2). The adsorbent efficiency remains unchanged up to  $950^\circ\text{C}$ . Below  $750^\circ\text{C}$ , the adsorption capacity at breakthrough is 0.7 mol of  $\text{H}_2\text{S}$  per mol of copper while  $>750^\circ$  the capacity of the adsorbent is halved. The change in  $\text{H}_2\text{S}$  capacity is due to  $\text{Cu}^{2+}$  reduction by the  $\text{H}_2$  which is formed through the thermal dissociation of  $\text{H}_2\text{S}$ .

Liu et al. [157] studied an efficient hybrid adsorbent/photocatalytic composite ( $\text{TiO}_2/\text{zeolite}$ ) for the  $\text{H}_2\text{S}$  removal and  $\text{SO}_2$  capture by coating  $\text{TiO}_2$  on the surface of cheap natural zeolite with an ultrasonic-calcination way. The  $\text{TiO}_2/\text{zeolite}$  showed the highest  $\text{H}_2\text{S}$  removal capacity and lowest  $\text{SO}_2$  emission, compared with the single zeolite adsorption and  $\text{TiO}_2$  photocatalysis.  $\text{H}_2\text{S}$  removal capacity and  $\text{SO}_2$  capture capacity of  $\text{TiO}_2/\text{zeolite}$  were enhanced in the presence of moisture in the biogas.

Papurello et al [29] reported the use of with Na-X zeolites combined with a ZnO guard bed (heated at  $300^\circ\text{C}$ ) before feeding the reformer unit in order to guarantee a durable and stable operation.



Tomadakis et al. [162] proposed pressure swing adsorption method using as adsorbent materials 4A, 5A, and 13X molecular sieves. It was found that 13X and 5A materials give high purity methane (98% or more) of zero or nearly zero H<sub>2</sub>S concentration for short periods of time. High methane recovery rates were obtained in most adsorption experiments, averaging at 60-70% for all sieves, and topped by 100% in certain 13X runs. Similarly, high H<sub>2</sub>S recovery rates were typically achieved in desorption tests averaging at 72% with sieve 4A, and reaching 100% in some 13X and 4A runs.

A theoretical approach to describe the adsorption phenomena of H<sub>2</sub>S on zeolites was reported in literature. Shah et al. [156] studied the adsorption behavior of binary mixtures of H<sub>2</sub>S and CH<sub>4</sub> on different all-silica zeolite frameworks using Gibbs ensemble Monte Carlo simulations at 25 and 70°C and pressures in the range 1-50 bar. The simulations demonstrate high selectivities that increase with increasing H<sub>2</sub>S concentration due to favourable sorbate-sorbate interactions. The simulations indicate significant inaccuracies using unary adsorption data and ideal adsorbed theory. Cosoli et al. [160] used Coupled Grand Canonical-Canonical Monte Carlo and mol. dynamics (MD) simulation techniques to investigate in details the adsorption of low-pressure hydrogen sulphide (H<sub>2</sub>S) in zeolites, and the selective adsorption behavior towards carbon dioxide and methane, the main biogas constituents. Results from Monte Carlo (MC) simulations indicated, among many others, zeolite NaY as the best option for H<sub>2</sub>S removal. Thermodynamic evaluations confirm the results obtained from Monte Carlo simulations, evidencing the greater affinity for H<sub>2</sub>S to NaY zeolite framework.

A theoretical approach was also reported by Qiu et al. [161] to investigate the interactions between H<sub>2</sub>S and HZSM-5 zeolites. The results showed that the nature of interactions lead to the formation of the zeolite cluster-H<sub>2</sub>S and silanol-H<sub>2</sub>S complexes was van der Waals force confirmed by a little change of geometric structures and properties.

Recently the removal of sulphur and chlorinated compounds has received more and more attention but only few reports are focused on the selectivity of different adsorbent materials respect to these different molecules [15].

Ryckebosch et al [18] described the removal of halogenated carbon hydrates that are mainly found in landfill gas. These compounds cause the corrosion in engines and can be removed with activated carbon. Generally, are used two tubes in parallel for the treatment and for the regeneration respectively. Regeneration is done by heating the activated carbon to 200 °C, thus evaporating the adsorbed components which are thereafter removed by an inert gas flow [46].

Hernandez et al. [141] report a study on the removal of sulphur and halogenated compounds from a model landfill biogas through adsorption. SCL3 Recently Papapdias et al. [30] performed a detailed

analysis of impurities contained in digester and landfill gas combined with a sensitivity analysis of electricity costs of a fuel cell system focusing on establishing a fitting gas-cleaning unit SC L3. The landfill was in Pianezza (Turin) performed with the company Asja Ambiente Italia S.p.A. The authors [141] reported the results obtained on six commercial adsorbents (Table 3-6) to compare their selectivity and their uptake capacity towards nine different sulphur compounds (including mercaptans). In Table 3-7 the analysis of the biogas is reported.

Use	Active component	Supplier	Product name
Desulphurisation	Activated carbon with Cr and Cu salts	Norit	RGM-3
	Zeolite 13X	Grace Davison	554HP
	Molecular sieve	Grace Davison	Sylobead 522
	Molecular sieve	Grace Davison	Sylobead 534
	Metal oxides	Non disclosable	ST
	Metal oxides	ECN	SulfCath
Dehalogenation	Activated carbon	Norit	R1540W
	Activated carbon	Norit	RB4W

Tab. 3-6 Adsorbents tested [145].

Norit activated carbon presented the highest adsorption capacities for COS MM, EM tBM and sBM. Conversely zeolite 13X had the highest uptake capacity for DMS and iPM and the ST material showed the highest capability to adsorb MES and THT; almost the same performance was observed for MES adsorption on zeolite 13X.

Moisture and other sulphur-free hydrocarbons (C2 to C5) are indeed present in the real biogas and may influence the adsorption process. Since activated carbons and zeolites can adsorb water this capability can significantly reduce their selectivity and uptake capacity towards sulphur compounds [169-172]. When RGM3 was tested in the presence of moisture its uptake capacity towards some sulphur compounds was greatly reduced (from 58.892 to 22.164%). Reduction of up to 100% for COS, 57% for DMS-iPM, 89% for MES and 60% for THT were observed.

It was found that each halogenated compound is adsorbed on the activated carbon in a different manner: Norit R1540W and Norit RB4W could remove the majority of the chlorinated species but with different breakthrough times.

The adsorptive capacity for the smaller molecular weight species (chloromethane and chloroethane) is practically zero but it is the highest for the 1,1,2,2-tetrachloroethane (6.79 and 7.76 wt%, for the R1540W and RB4W respectively). Hence, these activated carbons have an uptake capacity that increase with the molecular weight (MW) of the halogenated molecules, although this trend is not

absolute: the adsorption capacity can be explained as a function of the adsorbate molecular weight, degree of unsaturation, polarisation and symmetry as well.

Parameter	Measure unit	Minimum value	Maximum value
Temperature	°C	9	26
Humidity	% v	0.6	1.1
O <sub>2</sub>	% v t.q.	1.5	2.8
CO <sub>2</sub>	% v t.q.	34	40.9
CO	% v t.q.	. < 0.001	0.003
N <sub>2</sub>	% v t.q.	11.4	16.0
H <sub>2</sub>	% v t.q.	< 0.1	< 0.1
CH <sub>4</sub>	% v t.q.	42.8	50.2
Hydrocarbons > C5 (as hexane)	mg/m <sup>3</sup>	337.3	1178.0
Aromatic hydrocarbons	mg/m <sup>3</sup>	101.4	128.0
Total organic carbon (as C)	mg/m <sup>3</sup>	306	790.1
Siloxanes	mg/m <sup>3</sup>	< 0.05	< 0.2
NH <sub>3</sub>	mg/m <sup>3</sup>	< 0.5	15.7
HCl	mg/m <sup>3</sup>	< 0.6	2.0
Organochlorurated compounds	mgCl/m <sup>3</sup>	20	30.6
Total chlorine	mgCl/m <sup>3</sup>	17.4	32.0
HF	mg/m <sup>3</sup>	< 0.5	0.8
Organofluorinated compounds	mgF/m <sup>3</sup>	1.2	6
Total fluorine	mgF/m <sup>3</sup>	1.2	< 6,6
H <sub>2</sub> S	p.p.m.	114.3	205
H <sub>2</sub> SO <sub>4</sub>	p.p.m.	< 0.3	1.0
Mercaptanes (C <sub>2</sub> H <sub>5</sub> SH)	p.p.m.	0.7	27.7

Tab. 3-7 Analysis of the Pianezza MSW landfill biogas [175]

The authors concluded that none the tested adsorbents could remove the wide variety of sulphur compounds and the chlorinated compounds with low molecular weight that could be present into the landfill biogas such as chloromethane and chloroethane.

The authors [141] proposed a multistep desulphurization process with two adsorption beds so that the species not adsorbed in the first bed could be trapped in the second one. The first bed is based on molecular sieves; the second one contains activated carbons that are able to remove all the S-compounds present in the biogas. Tests that have been performed on the SOFC Power Generation System at the Turbocare site in Turin [171]. A two component arrangement of 130 kg Zeolite-X followed by 90 kg activated carbon provided an acceptable solution for large scale SOFC unit. After four months of operation no sulphur breakthrough was observed.

### **3.16 Removal of sulphur compounds in fuels by adsorption processes**

Organic sulphurs in natural gas and liquid fuels are poison to both the reforming catalyst and fuel cell's electrocatalysts. Many zeolites adsorb organic sulphurs and can efficiently remove these impurities from fuels. Sulphur removal by adsorption has obvious advantages over hydrodesulphurization. The process can be carried out at room temperature and does not require hydrogen, which is an important advantage. Table 3-8 lists some zeolites and mesoporous materials used for the removal of sulphur compounds. Yang and co-workers [173,174] prepared Ag and Cu ion-exchanged NaY zeolites that selectively adsorbed sulphur compounds via  $\pi$ -complexation between thiophene and the ion-exchanged metals. Other researchers reported high degree of desulphurization using Ni/KY [175], AgNO<sub>3</sub>/Beta [176] and CuZn/Y [177] adsorbents. These adsorbents were regenerated by washing with solvents at room temperature without loss of capacity. Feng and coworkers [178] used Ce(IV)Y zeolite to produce diesels with unprecedented low S (i.e., <0.01 ppm S). Mesoporous materials with their extremely high surface area and highly accessible pores are also efficient adsorbents [179-188]. Metal oxides and salts supported on mesoporous materials [189-196] had been used to remove sulphur from fuels, but were less able to attain the same level of ultra-deep desulphurization seen in the zeolite counterparts. Metal cations in zeolite appear to be the key in achieving ultra-deep desulphurization and it might be possible to replicate the same zeolite environment in mesoporous silica by incorporating zeolite framework structure on the pore wall, which has been demonstrated by several researchers [197-210].

Material	Sulphur compounds or fuel	Temperature (K)	Results Sulphur content (ppm)	Results Adsorption capacity (mg S g <sup>-1</sup> )	Regeneration method
Cu(I)Y, AgY	Commercial diesel	RT	430 → <0.2	N	Air-calcination at 623 K and at 723 K, washing with dimethylformamide or carbon tetrachloride
Cu(I)Y	Commercial gasoline	RT	335 → <0.28	12.5	N
Ni/KY	Benzothiophene, 2-methylbenzothiophene, 5-methylbenzothiophene	RT and 353	510 → <1	5	Air-calcination at 573 K
AgNO <sub>3</sub> /BEA, AgNO <sub>3</sub> /MCM-41, AgNO <sub>3</sub> /SBA-15	Tetrahydrothiophene, tert-butylmercaptane	RT-353	80 → 0.1	41.1 (AgNO <sub>3</sub> /BEA)	N
AgY CuZnY	Thiophene, dibenzothiophene, 4,6-dimethyldibenzothiophene	293–353	700 → 22 (Ag-Y) 700 → 36 (CuZn-Y)	44.9 (at 1500 ppm) 17.5 (at 500 ppm)	Air-calcination at 723 K
Ce(IV)Y	HDS-treated diesel	353	1.87 → <0.01	N	N
Ga/AlY	Thiophene, tetrahydrothiophene, 4,6-dimethyldibenzothiophene	293–333	500 → 15	7.0, 17.4, 14.5	Air-calcination at 573 K N <sub>2</sub> -calcination at 623 K
CuY, NiY, NaY, and USY	Benzothiophene	303	N	54.1(NaY), 53.8(USY), 57.6(NiY), 63(CuY)	N
Cu(I)Y	Thiophene, benzothiophene, dibenzothiophene,	RT	300 → <0.1	3.1	N

Cu(I)Y	Commercial jet fuel	RT	364 → 0.071	25.5	Air-calcination at 623 K calcination in 5 vol. % H <sub>2</sub> /He at 504 K
Cu(I)Y Cu(I)/ZSM-5	Commercial diesel	RT	297 → 0.06 AC/Cu(I)Y	12.2 (Cu(I)Y) 2.6 (Cu(I)/ZSM-5)	Air-calcination at 700–923 K
Ni(II)X, Ni(II)Y	Commercial diesel	RT and 353	297 → 0.22	10.6	Air-calcination at 623 K
AgBeta CuBeta	Dimethyl disulphide	333	20 → 1	7.1 8.7	N
Cu(I)/ETS-10	Tert-butylmercaptan tetrahydrothiophene	303	N	80	N
Cu <sub>2</sub> O/MCM-41	JP-5 light fraction	RTa	841 → 50	12.8	Air-calcination at 723 K He-calcination at 973 K
Ni/SBA-15	Commercial diesel	RT-473	240 → 10 11.7 → 0.1	1.7 (at 240 ppm) 0.47 (at 11.7 ppm)	N <sup>b</sup>
CuCl(PdCl <sub>2</sub> )/MCM-41(SBA-15)	JP-5 light fraction	RT	841 → 50 (PdCl <sub>2</sub> /SBA-15)	38.4 (PdCl <sub>2</sub> /SBA-15)	Purge with benzene at 343 K
Cu(I)/Mesoporous aluminosilicate	Diesel	303	315 → 54	N	N
AgNO <sub>3</sub> /mesoporous silica	Benzothiophene, dibenzothiophene, 4,6-dimethyldibenzothiophene	RT	N	20.5	Purge with diethyl ether
CuO/SBA-15	Thiophene	RT	N	6.4	N

Ni/MCM-41	4-Methyldibenzothiophene	RT	N	1.5	H <sub>2</sub> calcination at 773 K
Fe <sub>3</sub> O <sub>4</sub> /MAS Fe <sub>3</sub> O <sub>4</sub> /MCM-41	Hydrotreated diesel	303	37 → 6	N	N

Table 3-8: Zeolites and mesoporous materials used for the removal of sulphur compounds [214].

### 3.16 The effect of sulphur compounds on MCFC

#### 3.16.1 Sulphur poisoning on the MCFC components

Molten carbonate fuel cells (MCFC) are composed of a porous nickel based anode, a porous nickel oxide-based cathode and molten carbonate salts as electrolyte within a porous lithium aluminate matrix. Molten carbonate fuel cells with internal reforming can be fed directly with light hydrocarbons rich gas such as biogas.

Though MCFCs have the advantage of not requiring noble metal catalysts for the electrochemical reactions, some species have a poisoning effect on the catalytic properties of the electrodes.

The harmful effect of impurities may depend on the partial pressure of other species in the gas (e.g. hydrogen, water, carbon dioxide), the current density at which the fuel cell is operated, the temperature and the fuel utilization.

Hydrogen sulphide is the most important contaminant and even few parts-per-million concentrations the fuel gas at the anode side strongly affect cell performance. H<sub>2</sub>S has an immediate effect on cell performance, also at 1 ppm [211]. The effect of sulphur poisoning was observed at the initial H<sub>2</sub>S addition, even though the concentration was very low.

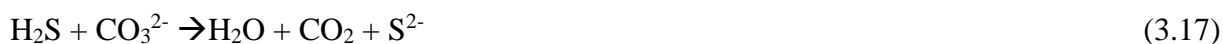
The limit of H<sub>2</sub>S concentration accepted for fuel gas is less than 1 ppm. Sulphur poisoning of the electrode is irreversible upon long-term exposure to concentrations of more than about 10 ppm since surface structure changes take place and cause permanent damage and deactivation of the anode [212-221]. At low concentrations the effects of H<sub>2</sub>S are generally reversible by passing over H<sub>2</sub>S-free hydrogen and water vapour.

Poisoning mechanisms depend on many factors, such as applied current density, inlet anodic gas composition, operating temperature and pressure.

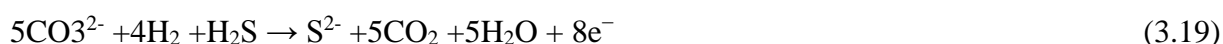
In many studies various causes have been identified for the immediate decrease in MCFC performance upon introduction of H<sub>2</sub>S [221-226]. This problem has been widely studied but no assessment on the mechanisms of the poisoning by H<sub>2</sub>S has been reached.

There are two main interactions of H<sub>2</sub>S with cell components, with the electrolyte and with the anode and catode [221].

H<sub>2</sub>S can react chemically with carbonates of the electrolyte to form either sulphide or sulphate ions (Eqs. 3.17 and 3.18) reducing electrochemically active charge carriers which would otherwise be available for the hydrogen oxidation mechanism [215,223,227], The cell performances decay, even if the ion conductivity of the electrolyte does not appreciably change because carbonate ions are replaced by the same equivalent number of sulphur-based anions.



H<sub>2</sub>S can react with carbonates also via electrochemical processes [215,224,228], (Eqs.3.19 and 3.20) yielding harmful, ionised sulphate compounds forming either sulphide S<sup>2-</sup> or sulphate SO<sub>4</sub><sup>2-</sup> ions.



Standard potentials of above reactions are respectively -1.037V and -0.986V with respect to O<sub>2</sub>:CO<sub>2</sub> = 33:67 vol% reference electrode.

When the above reactions occur instead of the hydrogen oxidation, the overall cell reactions are respectively as follows:



where M is a metal such as lithium or potassium.

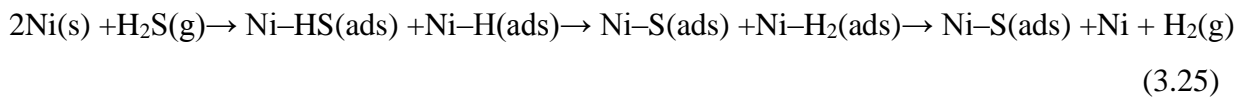
Hydrogen sulphide is a poison for the nickel catalyst and the negative effect on fuel cell performance is well documented [213,218,219,223,228].

H<sub>2</sub>S reacting with nickel can block electrochemically active sites for the hydrogen oxidation, can change the wettability of the anode toward carbonates, can modify the anode surface and its porous structure, can alter the anode conductivity, can change the carbonate conversion to sulphate and can poison catalytic sites for the water gas shift reaction.



The affected sites give rise to morphological changes in the anode structure, and can thereby cause further deterioration of cell performance through secondary effects like impeded gas diffusion, volume change or reduced wetting by the electrolyte [230].

Possible reactions of hydrogen sulphide with nickel can have different natures: formation of bulk nickel sulphides via chemical reactions, reaction (3.23); surface sulphuration either via physical adsorptions of hydrogen sulphide molecules, reaction (3.24), or via chemisorptions of sulphur atoms, reaction (3.25) [228].



With the anode,  $\text{H}_2\text{S}$  can be chemisorbed on nickel surfaces or can react chemically with nickel to form nickel sulphide. Nickel sulphides can be formed also electrochemically by oxidation of sulphide ions in the electrolyte.



Electrochemical poisoning reactions occur when the anodic potential reach electrode potentials for nickel sulphides formation: the standard electrode potential for the half-reaction forming  $\text{NiS}$  and  $\text{Ni}_3\text{S}_2$  are respectively  $-0.756\text{V}$  and  $-0.829\text{V}$  [223,228]. At open circuit voltage conditions, the anodic potential is more negative than electrode potentials necessary for either  $\text{NiS}$  or  $\text{Ni}_3\text{S}_2$  formation.

At low  $\text{H}_2\text{S}$  levels just two poisoning reaction types occur: physical and chemical absorptions on nickel surface by reactions (3.23) and (3.24); replacement of carbonate ions with sulphide and sulfate ions. In fact, formations of bulk nickel sulphides by reaction (3.27) are thermodynamically forbidden.

Devianto et al. [231] investigated the poisoning effect of  $\text{H}_2\text{S}$  on Ni-based anodes in MCFC at low  $\text{H}_2\text{S}$  concentrations, simulating biogas impurity. A conventional Ni-Cr anode was coated with ceria using dip coating to form a rare earth metal oxide thin layer on the surface of the anode. Electrochemical studies of the Ni-based samples were performed in symmetric cells under anode

atmosphere (H<sub>2</sub>, CO<sub>2</sub>, H<sub>2</sub>O and N<sub>2</sub> as balance) with 2, 6, 12, and 24 ppm of H<sub>2</sub>S by means of electrochemical impedance spectroscopy.

The results showed that the poisoning resistance was enhanced at low coating percentages of ceria; the effects depend on H<sub>2</sub>S concentration and the applied load. These results were confirmed by electrochemical impedance tests where the cerium oxide addition appears through stable polarization behaviour up to 6 ppm of H<sub>2</sub>S, particularly in the mass transfer region. The protection is explained by the depression of poisoned Ni active sites and formation of a layer to the metal surface. The ceria coating layer is a potential solution to reduce H<sub>2</sub>S poisoning of MCFCs fuelled with biogas.

Higher water content accelerated the effect of corrosion and the poisoning resistance was enhanced at low coating percentages of ceria; effects depend on H<sub>2</sub>S concentration and the applied load. The ceria coating layer is a potential solution to reduce H<sub>2</sub>S poisoning of MCFCs fuelled with biogas.

The research to obtain new advanced anode materials with high sulphur tolerance and effective recovery capability is largely discussed in literature [217,227,232] the Zaza et al. [228] studied the H<sub>2</sub>S poisoning mechanisms of conventional nickel-based anode MCFCs in order to determine sulphur tolerant advanced anodes for MCFC fed with biogas Proposed anode materials include two different categories: anodes made of an electrocatalyst and a hydrogen sulphide trap such as NiCr covered with either CeO<sub>2</sub> or CeO<sub>2</sub>-ZrO<sub>2</sub>; anodes made of a hydrogen sulphide resistance electrocatalyst such as NiAl.

### 3.16.2 Effect of SO<sub>2</sub> on cathode and H<sub>2</sub>S on anode

Recently Rexed et al. [233] studied the effect of contamination of MCFC with low concentrations of both SO<sub>2</sub> at the cathode and H<sub>2</sub>S at the anode. The poisoning mechanism of SO<sub>2</sub> is due to sulphur transfer through the electrolyte and formation of H<sub>2</sub>S at the anode. Measurements were performed with SO<sub>2</sub> in the oxidant gas at concentrations up to 24 ppm, for short-term (90 min) and long-term (100 h) contaminant exposure. The poisoning effect of H<sub>2</sub>S (up to 12 ppm) was studied for gas compositions with high- and low concentration of H<sub>2</sub> in fuel gas. Sulphur poisoning by SO<sub>2</sub> of MCFC has been considered as a result of anode exhaust gas recirculation to the anode. Any H<sub>2</sub>S present in the exhaust gas will be oxidized to SO<sub>2</sub> together with residual fuel in a catalytic burner before entering the cathode.



H<sub>2</sub>S causes poisoning of the Ni-anode surface by formation of NiS which kinetically hinders the oxidation of hydrogen [213,217,228]. It may react chemically to form NiS (reaction 3.30), or electrochemically as sulphide in the electrolyte (reaction 3.31), with the nickel anode to form nickel sulphide.



SO<sub>2</sub> added to the cathode immediately affects also the anode, indicating a transfer mechanism of sulphur from anode to cathode. It can be hypothesized that SO<sub>2</sub> dissolves into the electrolyte as sulfate ions which migrate to the cathode where are released as H<sub>2</sub>S, causing the poisoning of the anode catalyst by interactions with nickel H<sub>2</sub>S. Increased polarization of both anode and cathode was observed after long-term exposure to 8 ppm SO<sub>2</sub> at the cathode increasing at high current density. The short-term tests show anode polarization for concentrations higher than 12 ppm SO<sub>2</sub> suggesting that the transfer mechanism of sulphur from the cathode to the anode is fast, although no detailed data on transfer kinetics are reported. The anode poisoning effects were largely reversible by regeneration with clean gas. However the cathode evidenced irreversible polarization. The increase in cell resistance after long-term exposure was attributed to the cathode. This could be due to carbonate being replaced by sulfate by reaction with SO<sub>2</sub> dissolved in the electrolyte, or the formation of a layer at the electrode-current collector interface.

Ciccoli et al. [215] discuss the possibility of regeneration of the fuel cell.

In fact in the case of nickel transformation to nickel sulphide (reaction 3.31), passing pure gas over the poisoned anode can regenerate the electrochemically inert metal sulphide to the original, active catalyst:

The conditions and limits for the above reaction to be reversible are under investigation in and could provide a crucial, added operating parameter to guarantee long-term reliability of the MCFC stack. In this study [215], it is observed that, at different currents and concentrations of H<sub>2</sub>S, the cell voltage drops can be partially recuperated. At higher degrees of poisoning and current load, the performance degradation is permanent.

Zaza et al. [228] reported that cell performances recovery levels depend on water vapor amounts in inlet anode gas. Irreversible poisoning effects are due to stable nickel sulphide formations, Ni<sub>3</sub>S<sub>2</sub>.

### 3.17 The effect of biogas impurities on SOFC

Biogas contains several substances (Table 3-9) that have negative impact on the process converting the biogas into energy. So the biogas should be converted into biomethane stream having proper characteristics.

The treatment of biogas generally aims at: (1) a cleaning process, in which the trace components harmful to the natural gas grid, appliances or end-users are removed, (2) an upgrading process, in which CO<sub>2</sub> is removed to adjust the calorific value and relative density in order to meet the specifications of the Wobbe Index. This latter parameter is dependent on both the calorific value and the relative density [234,235].

After transformation, the final product is referred to as 'biomethane', typically containing 95-97% CH<sub>4</sub> and 1-3% CO<sub>2</sub>. Biomethane can be used as an alternative for natural gas. In general, the type of end use of the biogas sets its quality demands [236].

Impurity	Possible Impact
Water	Corrosion in compressors, gas storage tanks and engines due to reaction with H <sub>2</sub> S, NH <sub>3</sub> and CO <sub>2</sub> to form acids Accumulation of water in pipes Condensation and/or freezing due to high pressure
Dust	Clogging due to deposition in compressors, gas storage tanks
H <sub>2</sub> S	Corrosion in compressors, gas storage tanks and engines Toxic concentrations of H <sub>2</sub> S (>5cm <sup>3</sup> m <sup>-3</sup> ) remain in the biogas SO <sub>2</sub> and SO <sub>3</sub> are formed due to combustion, which are more toxic than H <sub>2</sub> S and cause corrosion with water
CO <sub>2</sub>	Low calorific value
Siloxanes	Formation of SiO <sub>2</sub> and microcrystalline quartz due to combustion; deposition at spark plugs, valves and cylinder heads abrading the surface
Hydrocarbons	Corrosion in engines due to combustion
NH <sub>3</sub>	Corrosion when dissolved in water
O <sub>2</sub> /air	Explosive mixtures due to high concentrations of O <sub>2</sub> in biogas
Cl <sup>-</sup>	Corrosion in combustion engines
F <sup>-</sup>	Corrosion in combustion engines

Tab.3-9 Biogas impurities and their consequences [237].

An interesting alternative to conventional technology can be based on SOFC due to their high biogas to electricity conversion efficiency (around 50-60%). Conversely to thermal engines, SOFC can operate with diluted biogas, differently from while internal combustion engines (ICE) that cannot operate if the CH<sub>4</sub> content in biogas falls below 40-45%. Essentially two main concerns come from direct biogas feeding in an SOFC: carbon deposition and the detrimental effects of contaminants on the Ni anode electrode [238-242]. Carbon deposition can be easily managed provided that a proper steam-to-carbon or oxygen ratio is guaranteed at the SOFC inlet so that C build up is thermodynamically unfeasible. Carbon deposition has been investigated by several authors [237,243-246]. Memelstein et al [243] reported that thermodynamic calculations do not indicate C deposition from a typical biomass gasification syngas at SOFCs operating temperatures >750 °C. However, intermediate temperatures <650° C require threshold current densities well above what is achievable to inhibit the effects of C deposition. Zheng et al. [244] observed that C deposition depends on temperature, gas composition, (CO or CH<sub>4</sub>), and presence of Ce<sub>0.8</sub>Gd<sub>0.2</sub>O<sub>1.9</sub> electrolytes in the composite-type electrode. Stable fuel cell performance, without C deposition, was obtained for SrFe<sub>0.75</sub>Mo<sub>0.25</sub>O<sub>3-δ</sub>-based SOFC in 10 vol.% of CO in CO<sub>2</sub>. Also for SOFC operating with CH<sub>4</sub> at temperatures ≤700 °C no coking was obtained. Singh et al [245] reported thermodynamic analysis of the carbon deposition in a SOFC fuelled by a biomass gasifier. The carbon deposition is shown to decrease with steam in the feed stream, whilst the amount of carbon first decreases and then increases with temperature. Gunji et al. [246] studied a SOFC using Ni/scandia-stabilized zirconia (Ni-ScSZ) anodes under internal reforming conditions. A single cell achieved a maximum power density of 0.64 W/cm<sup>2</sup> at 900° with a 97% CH<sub>4</sub>/3% H<sub>2</sub>O fuel. With this fuel composition the cell voltage during power generation at 0.5 A/cm<sup>2</sup> was stable at 900°C for ≥150 h. However, under the same conditions degradation of anode performance and C deposition occurred at 800°C.

The as produced biogas from AD contained several contaminants like as sulphur, aromatic, siloxane and halogenated compounds that can in principle affect the SOFC performance and the electrode stability. Sulphur compounds are present in the range from tens to thousands of ppm(v) (sulphur) while halogens and siloxanes vary from 0.1 to 10 ppm(v). Sulphur compounds are generally the most abundant in biogas and decompose to H<sub>2</sub>S at the SOFC operating temperature. Moreover, H<sub>2</sub>S is a poison for Ni-based ceramic cells [239,247]. Sulphur compounds decompose to H<sub>2</sub>S at the SOFC operating temperature as shown from equilibrium thermodynamic calculation [238]. H<sub>2</sub>S adsorbs on the Ni active sites preventing H<sub>2</sub> and CO oxidation as well as also methane reforming [248]. The effect of chlorine compounds, generally decomposed to HCl in the H<sub>2</sub> rich anode environment, is less understood than sulphur compounds. However a deactivation mechanism

similar to that of sulphur (dissociative chemisorption on the Ni surface) but less severe was generally observed [249]. Aromatic compounds are probably the less dangerous ones as they are catalytically converted to H<sub>2</sub> and CO within the SOFC. Siloxanes are instead the most critical ones for durability of the fuel cell. For instance, a study by Ruokomaki et al. [250] showed how the siloxane compounds already affect the SOFC performance at 10 ppb(v) whereas chlorine compounds concentration above 5000 ppb(v) are required. Haga et al. [251] also showed how an amount of 10 ppm(v) of D5 in the H<sub>2</sub> feed quickly led to a cell failure.

### 3.18 Effect of halogenated compounds

Halogenated compounds lead to corrosion in delicate power plant components and measures have to be taken in order to keep low the concentrations [237]. In connection to SOFC the effect of chlorine gas has been analyzed in several articles: experiments show that fuel gas containing 5 ppm of Cl does not cause cell degradation or voltage drop in the SOFC [252-254]. Blesznowski et al. [254] investigated the effect of HCl-contaminated fuel gas and concluded that at 10 ppm a recoverable voltage drop is identified. When increasing concentration levels to 1000 ppm the cell voltage starts to decrease continuously at a rate of 9.4% over 100 h.

Recently Trembly et al. [255] have investigated the effect of HCl on the SOFC at 800 and 900°C. The study has indicated that introduction of 20–160ppm HCl leads to a performance loss of about 13–52%. It was also shown that the cell performance loss at 800°C is mostly associated with the increase in charge-transfer resistance whereas at 900°C the performance losses are affected by increases in the ohmic resistance and charge-transfer resistance across the SOFC [255,256].

In the chlorine poisoning, the reaction of Ni with chlorine is crucial to understand the poisoning mechanism. According to Haga et al. [251] the formation of NiCl<sub>2</sub> may be described by Eq. (3.32):



Haga et al. [251] observed low but still measurable degradation in cell voltage for H<sub>2</sub>-based fuels containing 5 ppm Cl<sub>2</sub>, whereas fuels containing 100 ppm and 1000 ppm Cl<sub>2</sub> caused continuous degradation of cell voltage with an almost constant degradation rate. The degradation rates were 1.7% and 13% per 100h for H<sub>2</sub>-based fuels containing 100 ppm and 1000 ppm Cl<sub>2</sub>, respectively. In addition, significant microstructural change of cermet anode surfaces was confirmed by the FESEM observations.

Haga et al [251] suggested that contrary to sulphur, chlorine can easily react with Ni: nickel chloride (NiCl<sub>2</sub>) is stable even when only ca. 100 ppb and 10 ppm Cl<sub>2</sub> are contained in fuel gases at

800°C and 1000°C, respectively. Furthermore the formation of NiCl<sub>2</sub> should be paid careful attention in durability of SOFC anodes, as the sublimation temperature of NiCl<sub>2</sub> is 985°C, near the typical SOFC operational temperatures [251].

The interaction of Cl<sub>2</sub> with Ni was also proposed by Tjaden et al. [257] that suggested the subliming of NiCl<sub>2</sub> at Cl concentration >100 ppm. Low levels of halogens compound typically observed in biogas are not dangerous for the SOFC system. However halogen compounds have to be considered when applying adsorptive gas-cleaning methods: adsorption efficiency of active carbon decrease in the presence of halogenated and aromatic co-vapours. Absolute breakthrough times of various sulphur compounds decrease by up to 14% when halogen containing co-vapours are added to the gas stream [258].

Poisoning effects by various fuel impurities, including H<sub>2</sub>S, CH<sub>3</sub>SH, COS, Cl<sub>2</sub>, and siloxane, to Ni–ScSZ cermet anodes have been analyzed and compared by Haga et al. [251] with the aim to study the poisoning mechanisms for typical SOFC fuel impurities (sulphur compounds, chlorine, and siloxane).

Haga et al. [251] studied degradation of cell performance by measuring cell voltage and anode polarization at a constant current density of 0.2 A cm<sup>-2</sup> for humidified H<sub>2</sub> and CH<sub>4</sub> fuels. Cell voltage was measured at a constant current density of 0.2 A cm<sup>-2</sup>, at temperatures 800-1000°C and, by changing the carrier gas from pure N<sub>2</sub> to impurity-containing N<sub>2</sub>. Gradual and continuous degradation was verified in Cl<sub>2</sub> poisoning, associated with a microstructural change to form Ni precipitates in the Ni-Sc-SZ cermet anodes. Poisoning for hydrogen-based fuels containing 5 ppm sulphur compounds, H<sub>2</sub>S, CH<sub>3</sub>SH, and COS, caused an initial cell voltage drop of about 15 mV at 1000°C. The initial voltage drop was independent of the kind of sulphur compounds, whereas in the case of poisoning by CH<sub>3</sub>SH, an additional gradual decrease in cell voltage was clearly detected after the initial voltage drop. It is known that a few ppm levels of H<sub>2</sub>S as well as sulphide based odorants are typically contained in commercial natural gas [259], and thus the major impurity in SOFC anode poisoning may be H<sub>2</sub>S so far [252,260-265].

### **3.19 Effect of sulphur compounds on SOFC**

Depending on its production source and the stage of the up-grading process biogas can contain a number of sulphur compounds that have the capability to corrode processing equipment and gas pipeline, to inhibit the performance of vehicle catalysts and to damage fuel cells.

It is widely recognized that sulphur compounds are the major poisons for fuel cell systems [266-272] Most common reduced sulphur compounds found in biogas are H<sub>2</sub>S and methylmercaptan (CH<sub>3</sub>SH) Also ethylmercaptan, dimethyl sulphide (DMS) and dimethyldisulphide (DMDS) are

found [273-275]. Brown et al. [273] reported as an example a study measuring sulphur-containing compounds in biogas from a plant in Linköping, Sweden [275]: the biogas before upgrading contained hydrogen sulphide (at a volume fraction of up to 32.4  $\mu\text{mL L}^{-1}$ ) carbonyl sulphide (1.2  $\mu\text{mL L}^{-1}$ ) methanethiol (up to 0.75  $\mu\text{mL L}^{-1}$ ) dimethyl sulphide (up to 9.2  $\mu\text{mL L}^{-1}$ ) carbon disulphide (up to 0.02  $\mu\text{mL L}^{-1}$ ), 2-propanethiol (up to 0.05  $\mu\text{mL L}^{-1}$ ) ethylmethyl sulphide (up to 1.2  $\mu\text{mL L}^{-1}$ ) diethyl sulphide (up to 0.58  $\mu\text{mL L}^{-1}$ ) and dimethyl disulphide (up to 1.0  $\mu\text{mL L}^{-1}$ ).

Typically  $\text{H}_2\text{S}$  content in biogas ranges 1000 to 20000 ppm, while  $\text{CH}_3\text{SH}$  is normally present in trace levels of around 1-20 ppm, with maximum values reported around 100 ppm [277-279].

In terms of process performance impact Van de Bosch et al. [276] reported that  $\text{CH}_3\text{SH}$  severely inhibits biological sulphideoxidation (50% reduction of the biological oxidation rate) at concentrations above 0.05 mM under natron-alkaline-aerobic conditions. Complete inhibition was found at  $\text{CH}_3\text{SH}$  of concentration of 0.65 nM. Thus potential accumulation of  $\text{CH}_3\text{SH}$  in aerobic and anoxic biotrickling filters may hinder  $\text{H}_2\text{S}$  removal.

### **3.20 Levels of sulphur containing compounds in biogas**

The accurate quantification of low concentration of sulphur containing compounds in gases is essential to ensure compliance with legislation in a number of industrial and environmental sectors. These measurements are very arduous due to the reactivity of such compounds [274]. The actual European Directives of promote the diversification gas supply [280-281] and European Commission targets specify that 20% of EC energy consumption should come from renewable sources by 2020 [282]. As a direct result of these drivers the European biogas industry has strongly increased starting from 2012, more than 20 Mtoe of biogas was produced in the European Union [283]. The key uses for biogas (as biomethane) are for the injection into natural gas network and for vehicle fuel [274].

CEN (The European Committee for Standardization) Technical Committee 408 (Natural gas and biomethane for injection in the natural gas grid) is currently working in response to the ECs Mandate M/475 [284] to develop specifications for the permissible levels of a range of compounds.

The concentrations of sulphur containing compounds in biogas can vary substantially depending on the source of the gas, but mass concentrations of hydrogen sulphide as high as 7000  $\text{mg m}^{-3}$  are possible [285]. However typically hydrogen mass concentrations are <600  $\text{mg m}^{-3}$  for biogas produced by anaerobic digestion and <100  $\text{mg m}^{-3}$  for biogas from landfill [286]. Biogas is usually desulphurized whilst still in the bioreactor in order to avoid damage to downstream processing equipment [274].



The maximum gas concentrations of sulphur-containing compounds permissible in European countries [287] are shown in Table 3-10.

Country	Maximum mass concentration [mg m <sup>-3</sup> ]		
	Total sulphur containing compounds	Hydrogen sulphide	Thiols
Austria	100	5	15
Belgium	150	5*	15
France	30	5*	6
Germany	30	5	6
Italy	150	6.6	15.5
Netherland	45	5	-
Poland	40	7	16
Spain	50	15*	17
Sweden	23	10	-
Switzerland	10	5	-
United Kingdom	50	5	-

Tab. 3-10 Maximum mass concentrations of sulphur containing compounds specified in European gas transmission network. An Asterix (\*) indicates the specification is for the sum of hydrogen sulphide and carbonyl sulphide; a dash (-) indicates that no specification exists [274].

H<sub>2</sub>S is the most stable sulphur compound under SOFC operational conditions and the equilibrium concentration of other sulphur compounds such as COS is relatively low [251].

Tjaden et al. [257] reported chemical equilibrium calculations showing that H<sub>2</sub>S is the most stable sulphur compound at the operating temperature of SOFC [257,266].

Sasaki et al. [266] reported equilibrium concentration of minor sulphur based impurities in the fuel cell fuels in the temperature range 400-1000°C. As sulphur-based impurities in the fuel cell gases, H<sub>2</sub>S, elementary sulphur, inorganic sulphur compounds, mercaptans alkyl (di-)sulphides, thiophenes, and related compounds have been taken into account.

The authors considered various types of fuels including H<sub>2</sub>, H<sub>2</sub>-CO, CO, CH<sub>4</sub>, biogas, LPG, gasoline kerosene and diesel fuel. COS can also coexist, but even in CO riche gases and in hydrocarbon based fuels COS concentration in equilibrium is one order of magnitude lower than H<sub>2</sub>S concentration. Other sulphur compounds such as CH<sub>4</sub>S at intermediate temperatures and HS<sub>(g)</sub> and SO<sub>2</sub> at high temperature are also expected to coexist but their concentrations are less than 1 ppb assuming thermochemical equilibrium. As a solid carbon, only the graphite was taken into account for simplicity. Thermochemical calculations at 400-1000°C clearly indicates that H<sub>2</sub>S is the

predominant sulphur species at the elevated temperatures the typical operational temperatures of fuel processors for low temperature fuel cells PEFC as well as of high temperature fuel cell such as SOFCs.

As the poisoning by  $\text{H}_2\text{S}$  with a concentration less than approximately 100 ppm, a typical sulphur concentration of practical fuel, is associated with an increase in anodic overvoltage: the tolerance concentration of sulphur can be determined by the tolerant cell voltage drop. Concentration of sulphur will also be limited by irreversible poisoning process such as oxidation of Ni to NiO and Ni sulphide in SOFC [259].

Initial cell voltage drop due to sulphur contamination is temperature dependent and decrease with increasing temperature [257,288]. The extent and nature of cell degradation is dependent on applied cell materials and microstructural characteristics and thus the phenomenon of degradation cannot be generalized. It is assumed that any kind of sulphur compound has to be removed to a level  $< 1$  ppm to ensure long term performance of the SOFC.

Haga et al. [251] studied the poisoning by sulphur compounds and observed that it occurs generally in the following way: cell voltage decreases rapidly after adding each impurity to fuel gas, followed by a steady-state with a constant cell voltage [252,261]. In this study, the initial voltage drops by three types of sulphur impurities were compared under various conditions. Similar results are reported by Tjaden et al. [257] that concluded that long term exposure to mercaptanes can be however more critical than  $\text{H}_2\text{S}$  or COS contamination.

The initial voltage drops by  $\text{CH}_3\text{SH}$  and COS were almost identical to the initial voltage drop by  $\text{H}_2\text{S}$ . Initial voltage drops at a constant current density of  $0.2 \text{ A cm}^{-2}$  were approximately 80, 35, and 15 mV at 800 °C, 900 °C, and 1000 °C.

Degradation behavior by  $\text{CH}_3\text{SH}$  was different from that by  $\text{H}_2\text{S}$ , as cell voltage gradually decreased with time after operation beyond ca. 2 h.

Ni particles with the size of 50–70 nm<sup>ϕ</sup> were deposited on ScSZ surfaces in the anodes.

In a recent paper [288] SOFC cells with YSZ electrolyte and anodes of LaSrCrMn oxide (LSCrM perovskite) or LSCrM impregnated with Ni/CeO<sub>2</sub> are tested with H<sub>2</sub> fuel containing 50 ppm H<sub>2</sub>S. Ni and CeO<sub>2</sub> particles with diameter of about 100 nm are distributed on the surface of LSCrM. XRD, XPS measurements showed that the anode poisoned with H<sub>2</sub>S is covered by adsorbed sulphur, metal sulphides and sulphate radical. Sulphides are produced by the reaction of sulphur with the anode rather than the direct reaction between H<sub>2</sub>S gas and anode. This seems to contradict previous studies on Ni/YSZ anodes [290], where absorbed sulphur is the sole poisoning product. According to thermodynamic analysis [291], the sulphide Ni<sub>3</sub>S<sub>2</sub> can be formed only when H<sub>2</sub>S concentration (in H<sub>2</sub>) is higher than 3600 and 4700 ppm at 750 and 800°C, respectively. Formation

of other sulphides such as NiS and Ni<sub>3</sub>S<sub>4</sub> need a higher equilibrium pressure of H<sub>2</sub>S. However Ni<sub>3</sub>S<sub>2</sub> is detected on the anode with a low H<sub>2</sub>S concentration of 50 ppm. The formation of sulphides can take place at a lower H<sub>2</sub>S concentration through the reaction of absorbed sulphur with nickel considering the higher adsorption energy of S compared to H<sub>2</sub>S on the anode surface, as confirmed by DFT calculations.

Thermodynamic calculations [292-294] were reported on the stability of nickel sulphides as a function of temperature, PO<sub>2</sub> (or P(H<sub>2</sub>)/P(H<sub>2</sub>O)), and H<sub>2</sub>S content. At low H<sub>2</sub>S conc. (~10 ppm), sulphides were not observed [295-297]. For higher (100 ppm) H<sub>2</sub>S concentrations, nickel sulphides were generally observed [298-300]. Ni sulphide formed in H<sub>2</sub> containing 100 ppm H<sub>2</sub>S at 727°C [298] although it is not thermodynamically stable. Haga et al. [251] reported no formation of Ni sulphide under the condition with 5 ppm sulphur compounds.

These results outline the importance of in situ techniques to study the sulfidation process.

Thi et al. [290] studied the kinetics of the reactions between H<sub>2</sub>S and Ni or Ni-CGO (ceria doped with gadolinium) by using Raman spectra in situ. Ni<sub>3</sub>S<sub>2</sub> is formed at low temperature (200–500°C) and remains stable at 800°C while no Ni<sub>3</sub>S<sub>2</sub> is formed on clean nickel at 800 °C. It is important to avoid contact of a working SOFC with H<sub>2</sub>S during heating and cooling. Probably the first step of Ni<sub>3</sub>S<sub>2</sub> formation is adsorption of sulphur onto Ni, that is fast at low temperature, but much more difficult at high temperature [301-302]. At high temperature, a Ni<sub>3</sub>S<sub>2</sub> film is formed at the surface of the Ni-CGO pellet, due to a diffusion of nickel toward the H<sub>2</sub>S atmosphere. Moreover H<sub>2</sub>S reacts with the support CGO to produce Ce<sub>4</sub>O<sub>5</sub>S<sub>2</sub>.

SOFC anodes Ni-gadolinium doped ceria (Ni/GDC) are studied for sulphur poisoning under operando conditions by Nurk et al. [295]. The molecular structure of sulphur species formed on the anodes in the temperature range 250-550°C is studied by XANES (K shell). With H<sub>2</sub> fuel containing 5 ppm H<sub>2</sub>S, several sulphur species in different oxidation states (6+, 4+, 0, -2) are detected: the species could either relate to -SO<sub>4</sub><sup>2-</sup> or SO<sub>3</sub> (g), -SO<sub>3</sub><sup>2-</sup> or SO<sub>2</sub> (g), S<sub>2</sub> (g) or surface-adsorbed S atoms, and Ni or Ce sulphides. These results don't agree with thermodynamic phase calculations, in particular the formation of sulphate species is not expected at the highest temperatures: this can be related to the difference between equilibrium conditions and the steady state conditions in the fuel cell that are determined by kinetic-controlled processes.

Ni anodes exposed to H<sub>2</sub>S undergo a reversible or partially reversible degradation for few minutes, followed by a slow non-reversible degradation [273,295,303]. It is generally accepted that the initial rapid decrease of performance is due to adsorption of sulphur species with inhibition of the three-phase-boundary (TPB) for hydrogen oxidation [273,303]. On the other hand, different hypotheses have been proposed to explain the following slow degradation: 1) the formation of a volatile Ni<sub>x</sub>S<sub>y</sub>

phase, leading to degradation of the electrode structure [290,294,304]; 2) adsorption of sulphur on nickel particles that are in less accessible sites, such as pores with bottlenecks [304]; 3) surface reconstruction of Ni that leads to catalytically less active form [304]; 4) bulk phase diffusion of sulphur into Ni grains [304].

Nickel sulphide formation is reported with  $\text{H}_2\text{S} > 2500$  ppm at  $850^\circ\text{C}$  with 50%  $\text{H}_2$  fuel and therefore cannot explain the generally observed power degradation of SOFCs with few ppm  $\text{H}_2\text{S}$ : the sulphur poisoning of nickel based anodes is generally explained by dissociative adsorption of  $\text{H}_2\text{S}$  on nickel [297]. Two stage poisoning of Ni/8YSZ (8 mol %  $\text{Y}_2\text{O}_3$  doped  $\text{ZrO}_2$ ) anodes was reported [273,294,306]. Singhal [304] found that at  $1000^\circ\text{C}$  with constant current density, adding  $\text{H}_2\text{S}$  to the fuel, the cell voltage decreased rapidly (11.5% with 10 ppm  $\text{H}_2\text{S}$ ). A slow decrease of cell voltage (3.5%) occurred in the following 100 h. The effect of  $\text{H}_2\text{S}$  was reversible. Sasaki et al. [272] also found a two phase poisoning with 5 ppm  $\text{H}_2\text{S}$  in 5%  $\text{H}_2\text{O}/95\%$   $\text{H}_2$  fuel at  $1000^\circ\text{C}$ . The cell voltage was almost recovered after removing  $\text{H}_2\text{S}$ . The poisoning was more severe and not reversible when the temperature was lowered to  $850^\circ\text{C}$ . It was hypothesized that the chemisorption of sulphur caused a decrease of electrochemical sites thus increasing the anodic polarization. Increasing  $\text{pH}_2\text{S}$  to 20 ppm led to increased chemisorption of sulphur on nickel and thus further increase in anodic polarization and cell voltage loss. However no sulphur but NiO traces were found in the poisoned anode. Wang et al. [292] studied the effect of adding 2-50 ppm  $\text{H}_2\text{S}$  to a fuel containing 50%  $\text{H}_2/1.5\%\text{H}_2\text{O}$  in  $\text{N}_2$ . The cell voltage dropped rapidly in the first minutes and slowly in the next 120 h. After removing  $\text{H}_2\text{S}$ , the cell voltage was recovered to 96% in 50 h. The irreversible poisoning was explained with a microstructural change of the nickel surface. Fewer studies are reported on the poisoning of Ni/CGO ( $\text{Gd}_2\text{O}_3$  doped  $\text{CeO}_2$ ) anodes. Tests with syngas (34.8%  $\text{H}_2/35.7\%\text{N}_2/40\%\text{CO}$ ) containing 207 ppm  $\text{H}_2\text{S}$  at  $850^\circ\text{C}$  showed a rapid drop of power of 6-8% then a slow degradation up to 10-12.5% (Tremblay et al. [263]). The power recovered to 97% after  $\text{H}_2\text{S}$  removal. After the tests the amount of nickel decreased and morphological change was observed. NiS formation was the proposed mechanism. Lohsoontorn et al. [294] reported that the performance of a Ni-CGO/YSZ/Ni-CGO symmetrical cell decreases with decreasing  $\text{pH}_2$  (9.7% - 97%), decreasing temperature (600 –  $557^\circ\text{C}$ ) and increasing  $\text{pH}_2\text{S}$  (1 - 3 ppm). The recovery of the cell after removal of  $\text{H}_2\text{S}$  increased with increasing  $\text{pH}_2$ . The performance loss was due to the increase of the resistance due to charge transfer. Zhang et al. [305] compared Ni/YSZ and Ni/10CGO anodes in the presence of  $\text{H}_2\text{S}$  (5- 00 ppm in  $\text{H}_2$ ) at  $800^\circ\text{C}$ . The drop of cell voltage was much higher with Ni/YSZ than with Ni/CGO anode. The positive effect of CGO was attributed to its mixed ionic electronic conductivity. Ni surface of both anodes appeared rougher after contamination with  $\text{H}_2\text{S}$  but no sulphur was found with EDX. Smaller CGO particles were observed after the experiment.

In the work of Schubert et al. [303] Ni/YSZ and Ni/10CGO anodes are compared for the effect of H<sub>2</sub>S, using an H<sub>2</sub>/H<sub>2</sub>O/N<sub>2</sub> fuel mixture at 850°C. The degradation of cell voltage is noticeable even with 2 ppm H<sub>2</sub>S. The cell with Ni/8YSZ anode showed two poisoning stages: the first stage occurred in few minutes while the following degradation was slower and lasted more than 10 h. The degradation of cell with Ni/10CGO occurred in one step and was slighter. The drop of performance cannot be explained by sulphide formation because it is not thermodynamically possible under these conditions. Dissociative H<sub>2</sub>S adsorption on Ni is assumed on the base of DFT calculations (Eq. 3.33) [306]:



where the subscript (s) indicates species on the surface of metallic Ni. The heat of adsorption of H<sub>2</sub>S on different forms of metallic Ni was found more favourable than the heat of formation of Ni sulphides [307,308]. The authors propose a Temkin like equation to describe the adsorption of H<sub>2</sub>S and a mechanism of poisoning that explains the time progress of sulphur contamination of the Ni anode. On the basis of this mechanism, it is possible to calculate the nickel anode surface area from the duration of the first step of decrease of the cell voltage. The higher sulphur resistance of Ni/10CGO compared to Ni/YSZ is explained with the high mixed ionic electronic conductivity of the CGO phase and its ability to adsorb H<sub>2</sub>.

SOFC degradation due to H<sub>2</sub>S is studied by a mathematical modelling approach by Vahc et al [309]. Electrolyte-supported and anode-supported SOFC are considered. Both contain five layers: anode gas diffusion layer (AGDL), anode active layer (ACL), electrolyte (ELEC), cathode active layer (CCL), and cathode gas diffusion layer (CGDL). The electrochemical reaction occurs at each active layers and the internal reforming reaction occurs only at AGDL. The model is based on a Temkin-like isotherm of sulphur adsorption. The sulphur coverage and cell polarization are related to the cell temperature, H<sub>2</sub>S concentration and electrochemical performance. Vahc et al. [309] concluded that the effect of sulphur poisoning on the internal reforming reaction is dominant over its impact on the electrochemical reaction.

### 3.21 Materials and Methodology

Microporous materials used for HCl and H<sub>2</sub>S adsorption tests, supplied by Norit, Calgon Carbon and Union Carbide are summarized in Table 3-11. They consist of commercial activated carbons and 13X zeolites. In the same table the morphological characteristics are also reported.

	<b>Filtrisorb</b>	<b>RGM3</b>	<b>RBAA1</b>	<b>Zeolite 13X</b>
<b>Supplier</b>	Calgon Carbon	Norit®	Norit®	Union Carbide
<b>Geometry</b>	Pellet, d = 2 mm	Pellet, d = 3 mm	Pellet, d = 2 mm	Sphere, d = 1.6 mm

Tab. 3-11 Adsorbent materials used in experimental tests

### 3.21.1 Preparation of Activated Carbon

The adsorbing capacity of the materials can be improved by physical/chemical treatments that allow the introduction of more functional groups reactive towards HCl and H<sub>2</sub>S, in comparison to those initially present as discussed in par. 3.15.

For this reason, the activated carbons have been treated with basic solutions of NaOH, KOH and Na<sub>2</sub>CO<sub>3</sub>, widely used in the literature for this purpose [310,311].

The vacuum impregnation technique is used to functionalize the active carbon.

The procedure involves three steps: sample degassing in He stream; vacuum impregnation with solutions of NaOH (10% w/w), KOH (10% w/w) and Na<sub>2</sub>CO<sub>3</sub> (10% w/w); heat treatment at 250 °C of the impregnated activated carbons [310,311].

### 3.21.2 Degassing

Before the impregnation process, the sample is subjected to a degassing treatment by vacuum pump. The sample is placed inside a burette, externally covered with a heating jacket that allows to adjust the temperature at the following conditions:

Pressure: 5 µmHg

Temperature: 250 °C

Time of treatment: 2 h

Sample mass : 300 mg

Such treatment is carried out to remove all the impurities present in the pores, so that the entire volume is provided for the impregnating solution.

### 3.21.3. Impregnation

The activated carbon samples, previously degassed, are placed inside a flask to create the vacuum conditions, less stringent than the previous (about 50/100 mmHg), which allows a better contact between the impregnating solution and the pores of the activated carbon.

The impregnation is carried out with 10% by weight, NaOH, KOH, Na<sub>2</sub>CO<sub>3</sub> solutions. The experimental apparatus for materials impregnation (Figure 3-1), consists of a 100 cm<sup>3</sup> flask connected via a non-return valve to a Venturi tube which realizes the vacuum exploiting the passage of water to the its inside.



Fig. 3-1 Plant used for impregnation of activated carbons

A sample mass of 300 mg was placed in the flask the solution is fed through a burette connected to the flask with a fitting silicone to prevent air infiltration. The vacuum is maintained for about 15 min before the introduction of solution (2 cm<sup>3</sup>) by dripping. After introducing the alkaline solution, the mixture is stirred for about 30 minutes to ensure that all of the test solution to penetrate into the pores of activated carbon. It must avoid stirring too strong not to damage the support.

Finally, by means of a valve it is restored the atmospheric pressure in the flask and the activated carbons are subsequently filtered to remove the excess solution.

#### 3.21.4 Heat treatment

Heat treatment is carried out in an electric oven Heraeus (Figure 3-2) under air flow of 6 l/h. The sample is heated from room temperature up to 250 °C, with a heating rate of 10 °C/min, for 2 hours. The treatment allows to remove water from the sample and to improve the precipitation of NaOH, KOH and Na<sub>2</sub>CO<sub>3</sub> (in excess).



Fig. 3-2 Oven used for heat treatment of activated carbons

### 3.21.5 Preparation of Zeolites

Zeolites are important ion exchanger materials. In the presence of electrolytic solutions are able to exchange the ions present in their framework with those present in the aqueous phase. This property is determined by the fact that the cations, present in the channels to balance the negative charge of the framework resulting from the presence of aluminum in tetrahedral coordination, are bound rather weakly to anionic scaffolding of the zeolite. The ionic bonds existing between the zeolite and the cations, in fact, are being undermined by the action dielectric exerted by water molecules; this makes possible the replacement of such cations with other present in the solution phase. The maximum amount of such substitution represents the cation exchange capacity that is the number of milliequivalents of cations that can be exchanged for gram of zeolite. This quantity is a function of the Si/Al ratio, being greatest when this ratio assumes a unit value.

It should be noted that the actual exchange capacity of a zeolite towards a given cation depends, firstly, on the concentration of competing ions in solution, but also and especially by the affinity of the zeolite towards each of them. Such affinity is definable only in relation to that shown for another cation, which acts as antagonist in the exchange. The measure of the preference that one performs for an ion exchanger with respect to another is called selectivity.

Modified zeolites were prepared by ion exchange or impregnation methods. Ion exchange was obtained by treating 3 g zeolite with 250 mL of 0.1 M solution of  $\text{Cu}(\text{NO}_3)_2 \cdot 2.5\text{H}_2\text{O}$  or  $\text{Zn}(\text{NO}_3)_2 \cdot 6\text{H}_2\text{O}$  under stirring at 80 °C for 2 h (Figure 3-3).



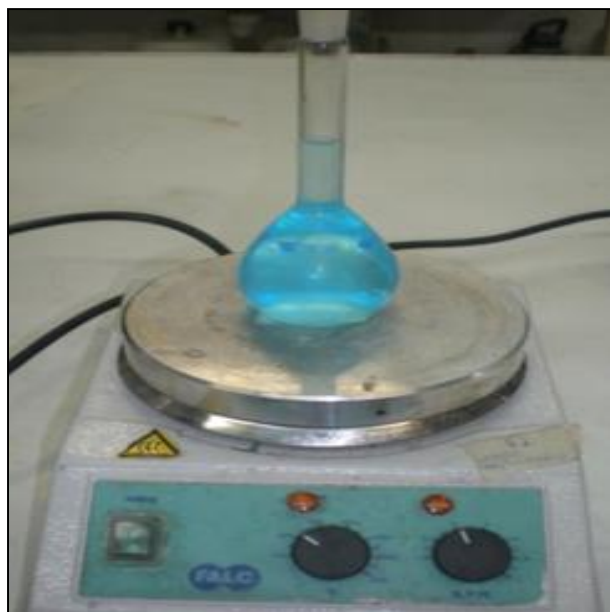


Fig. 3-3 System used for ion exchange of zeolites

Afterwards the sample was separated from the solution and dried at 120°C for 2 h, then thermally treated in air flow at 250 °C for 2 h. The impregnation of the zeolite was carried out under vacuum conditions obtained with a Venturi tube to enhance the penetration of the solution into the material pores. The sample (3 g) was impregnated to incipient wetness with 3 mL of 0.1 M solution of  $\text{Cu}(\text{NO}_3)_2 \cdot 2.5\text{H}_2\text{O}$  or  $\text{Zn}(\text{NO}_3)_2 \cdot 6\text{H}_2\text{O}$  at 40 °C under stirring conditions. The sample was dried at 120 °C for 2 h and thermally treated in air flow at 250 °C for 2 h. The thermal treatment leads to the decomposition of the nitrates and the formation of zinc or copper oxide, as follows:



Fig 3-4 Zeolite 13X not modified (white) and modified with  $\text{Cu}(\text{NO}_3)_2 \cdot 2.5\text{H}_2\text{O}$

### 3.21.6 Chemical-physical characterization

#### 3.21.6.1 Surface area measurements

It defines the total surface area of particles of material contained in the unit of mass or volume area. Generally, the data is supplied in  $\text{m}^2/\text{g}$ . The evaluation of this area is not direct, but is done experimentally by measuring the adsorption capacity of the surface for each sample.

The chemical-physical adsorption is the mechanism by which molecules, atoms or ions form a chemical bond or establish an interaction of physical chemical type, through Van der Waals forces, on the surface of the interphase. The interphase involved, in the separation surface between two different phases, it is often solid-liquid or solid-gas type.

The most widely used technique for surface area measurements is  $\text{N}_2$  adsorption at 77 K, the B.E.T. (Brunauer, Emmett and Teller) method [311].

A Micromeritics ASAP 2020 (Fig. 3-5) apparatus was used. It is based on technique of adsorption of gases based on the principle of static-volumetric operation to generate experimental data of high value, usable both in research applications and in those of quality control.

The instrument uses the physical adsorption and desorption of nitrogen at liquid nitrogen temperature. The specific volume of adsorbed nitrogen allows the determination of the specific surface area, the specific volumes of mesopores and micropores. At this temperature, it creates a vacuum and with a  $\text{N}_2$  gas stream that begins to adsorb until equilibrium is reached. While nitrogen is adsorbed, the partial pressure decreases: therefore, it is possible to evaluate a pressure difference between the initial and the equilibrium pressure conditions. In this way the adsorption isotherm is obtained.



Fig. 3-5 Micromeritics ASAP 2020

#### 3.21.6.2 BET model

The BET theory is a model describing the physical adsorption of gas molecules on a solid surface and can be used for the measurement of the specific surface area of a material. This model is due to

Stephen Brunauer, Paul Hugh Emmett and Edward Teller that in 1938 published the results of the modeling of physical adsorption isotherms. The B.E.T. theory, that takes its name from their initials hypothesizes a multilayer adsorption involving two possible fundamental interactions: surface-adsorbate and adsorbate-adsorbate "vertical" (attraction interaction). The vertical adsorbate-adsorbate interaction is independent of the considered layer, while the adsorbate-adsorbate interaction in the same monolayer (horizontal) is considered negligible compared to the interaction adsorbate-surface. The system is composed then by endless monolayers that follow the Langmuir model.

BET model is used to calculate the volume of the monolayer from which you can derive the number of particles that make it up and consequently the surface area through the Eq. (3.34):

$$\frac{1}{v[(P_0/P)-1]} = \frac{c-1}{v_m c} \left( \frac{P}{P_0} \right) + \frac{1}{v_m c} \quad (3.34)$$

where P and P<sub>0</sub> are the pressures at dynamic equilibrium and at saturation pressure of the adsorbate at the adsorption temperature, V is the amount of gas adsorbed, V<sub>m</sub> is the amount adsorbed in a monolayer and c is the B.E.T. constant:

$$c = \exp \left( \frac{E_1 - E_L}{RT} \right) \quad (3.35)$$

in which: E<sub>1</sub> is the enthalpy of adsorption of the first layer, E<sub>L</sub> is the enthalpy for all other layers and is equivalent to the enthalpy of liquefaction.

The B.E.T. equation can be approximated to the equation of a straight line of the type y = ax + b and then represented, whereas, on the x axis the ratio P/P<sub>0</sub> (partial pressure of nitrogen and its vapor pressure at the liquid nitrogen temperature) and on the y axis the ratio 1/V [(P<sub>0</sub>/P) - 1].

In particular, it is proved that the relation is linear in the range 0.05 < P/P<sub>0</sub> < 0.35.

Since the slope of the straight line and the intercept value on the ordinate it is possible to estimate the amount of vapor adsorbed for monolayer V<sub>m</sub> and constant c of B.E.T. theory.

From the value of the monolayer volume, it is possible obtain the number of particles in the monolayer n<sub>m</sub> and surface area value can be evaluated using the following equation:

$$A.s. = N_m N_a A_{N_2} \quad (3.36)$$

where: n<sub>m</sub> is the number of moles of the monolayer, N<sub>a</sub> is Avogadro's number, A<sub>N<sub>2</sub></sub> is the area of single particle of nitrogen.

### 3.21.6.3 Electron Microscopy (SEM) and Elementary Analysis (EDS)

Scanning Electron Microscopy (SEM) allows to meet a collection of high-definition images, Energy Dispersive X-ray Spectrometry (EDS) allows to obtain an estimation of the chemical composition of the species present on the surface going up, therefore, the amount of substance deposited on the support in phase segregated, during the preparation.

SEM-EDS were performed using Philips XL30 instrument.

#### *Scanning electron microscopy*

In the SEM analysis, a very fine probe of electrons with energy up to 30 keV is focused on the surface of the sample inside of the microscope and it is induced to exert a scan in the form of a succession of parallel lines. Some phenomena occurring on the surface subjected to the impact of the electrons; the most important are: the emission of secondary electrons with energies of about 10-20 eV; remission or reflection of high-energy electrons or backscattered belonging to the primary radius.

The configuration and the arrangement of the detectors of the two types of emitted electrons are able to use the peculiarities of the emission mechanism. In particular, the secondary electrons are used for the construction of magnified images and resolved up to 5 nm due to the fact that the low energy of which they are provided, these electrons come from the superficial layers of the sample. Instead, the primary electrons are used to identify the presence of different compounds in a heterogeneous sample being the intensity with which they occur, a direct function of the average atomic number of the substance invested by the primary ray.

The emitted electron current is collected by the detectors and amplified simultaneously with the scanning of the electron beam on the sample, the variations in the strength of the resultant signal are used to vary the brilliance of the trace of the electron beam which makes a scan on a fluorescent screen synchronic with the electron beam on the sample.

#### *Elementary analysis*

The microanalysis or chemical analysis, in the electron microscope (SEM) is performed by measuring the energy and distribution of the intensity of X-rays generated by the electron beam on the sample using a scatter detector energy of EDS (energy dispersive spectrometry). The analysis produced can be either the area that is enlarged at that time, or, stopping the scan of the electron beam, of a point of interest on the sample surface (microanalysis).

Since the portion of space excited by the electron beam, which produces the spectrum X is a neighborhood of a few microns, the SEM-EDS is a powerful means of investigation of solids chemically inhomogeneous at a microscopic scale.

### 3.21.7 Experimental Apparatus for Adsorption tests

#### 3.21.7.1 H<sub>2</sub>S adsorption tests

H<sub>2</sub>S adsorption tests were carried out in a laboratory scale plant, showed in Fig. 3-6.

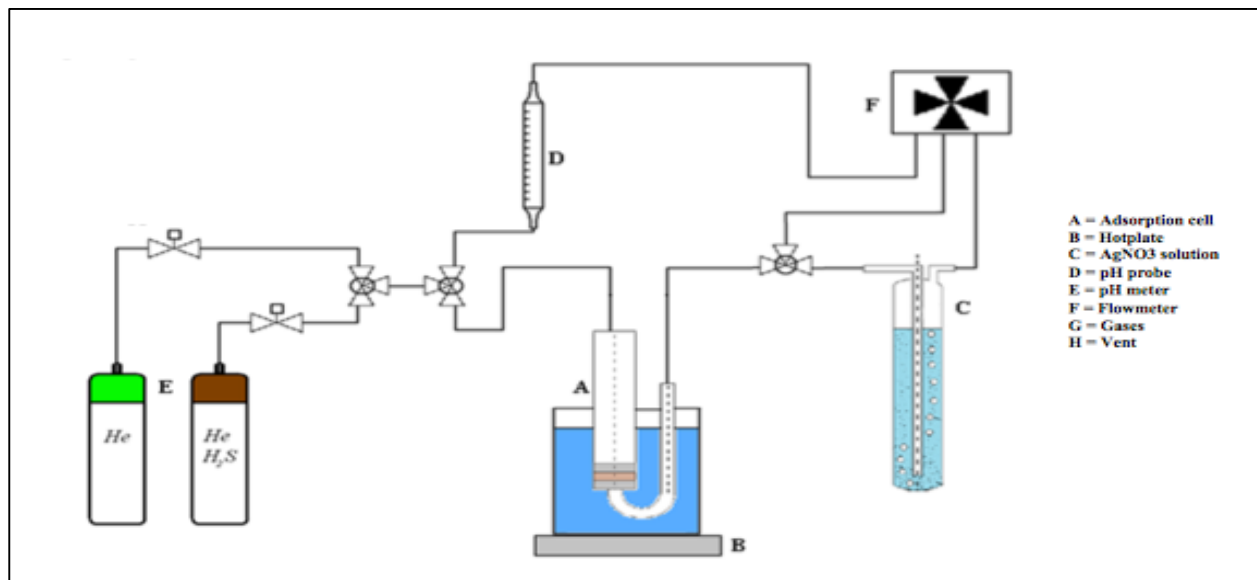


Fig. 3-6 Plant used for H<sub>2</sub>S adsorption tests

This is an innovative apparatus that permit very fast, reproducible and accurate measurements properly designed to the purpose. In this apparatus, a stream ( $0.1 \text{ L min}^{-1}$ ) of a gaseous mixture containing 8 ppm of H<sub>2</sub>S in He is flowed through a fixed bed of the sample (20 mg) immersed in a water bath at 40 °C. The samples are treated at 250 °C for 2 h in air flow ( $0.1 \text{ L min}^{-1}$ ) before the tests. H<sub>2</sub>S effluent from the adsorption cell (Fig.3-7) is analyzed using a procedure based on potentiometric measurement.



Fig.3-7 Detail of the adsorption cell used in H<sub>2</sub>S clean up plant

The stream effluent from the adsorption cell is bubbled through a 0.01 M AgNO<sub>3</sub> solution in H<sub>2</sub>O (volume = 40 cm<sup>3</sup>). H<sub>2</sub>S is absorbed in the solution and dissociates according to Eqs. (3.37) and (3.38):



where K<sub>1</sub> and K<sub>2</sub> are the first and second ionization constants of H<sub>2</sub>S respectively. The S<sup>2-</sup> ions react with Ag<sup>+</sup> forming the highly insoluble Ag<sub>2</sub>S precipitate according to Eq. (3.39):



where K<sub>3</sub> is the solubility product of Ag<sub>2</sub>S. Due to the high value of K<sub>3</sub>, the formation of Ag<sub>2</sub>S<sub>(s)</sub> shifts the equilibrium of (3.37) and (3.38) towards right, therefore the H<sub>2</sub>S dissociation can be considered complete and the amount of H<sup>+</sup> produced corresponds to twice that of H<sub>2</sub>S dissolved into the solution. The tube containing the AgNO<sub>3</sub> solution was designed to obtain the quantitative dissolution of H<sub>2</sub>S, as ascertained by analyzing the exhausted gas in preliminary tests.

The amount of H<sup>+</sup> produced, and thus the amount of H<sub>2</sub>S dissolved in the AgNO<sub>3</sub> solution at a given time, was determined by a pH measurement. using a Hanna HI3220 pH meter. The amount of H<sub>2</sub>S dissolved at a given time corresponds to the amount not adsorbed by the material. In this way, the

H<sub>2</sub>S concentration exiting from the adsorption cell was obtained as a function of time (breakthrough curve) for each sample. In this way the breakthrough curves have been obtained.

The accuracy of the method was checked by blank tests with the adsorption cell filled with inert glass powder. The method allowed to achieve a remarkable sensitivity of 0.1 ppm H<sub>2</sub>S in the gaseous phase (by the way, with a simple, low cost set-up).

### 3.21.7.2 HCl adsorption tests

HCl adsorption tests were carried out in an original experimental apparatus based on potentiometric analysis procedure similar to H<sub>2</sub>S adsorptions tests (Fig. 3-8).

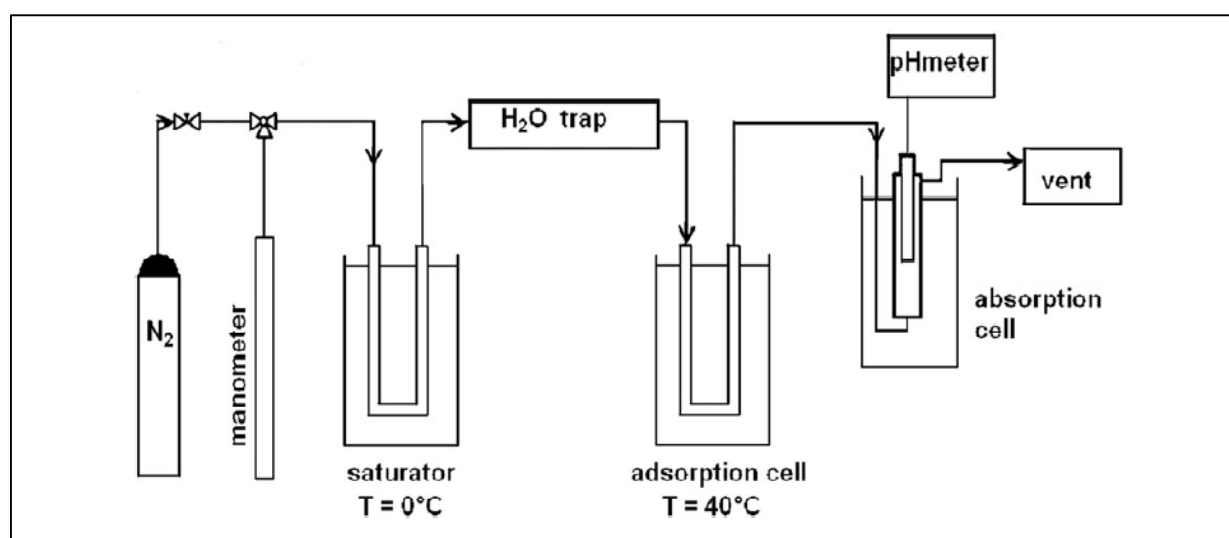


Fig. 3-8 Plant used for HCl adsorption tests

The apparatus operates at atmospheric pressure under flow conditions. It consists of three main sections: the feeding system, the adsorption cell containing the material under test and the analysis system. The gaseous feed containing 100 ppm HCl was obtained by bubbling pure N<sub>2</sub> (100 cm<sup>3</sup> min<sup>-1</sup>) through a 22% w/w HCl solution at constant temperature of 0 °C. Water vapour was removed from the gaseous stream by a P<sub>2</sub>O<sub>5</sub> trap (Sicapent, Merck). The saturation of the gaseous mixture was ascertained by titration after HCl dissolution in a Na<sub>2</sub>CO<sub>3</sub> solution. The adsorption cell containing the material under test (200 mg) consisted in a U glass tube (i.d. = 0.4 cm, Fig. 3-9)) maintained at 40 °C by a water bath equipped with a PID thermal controller.

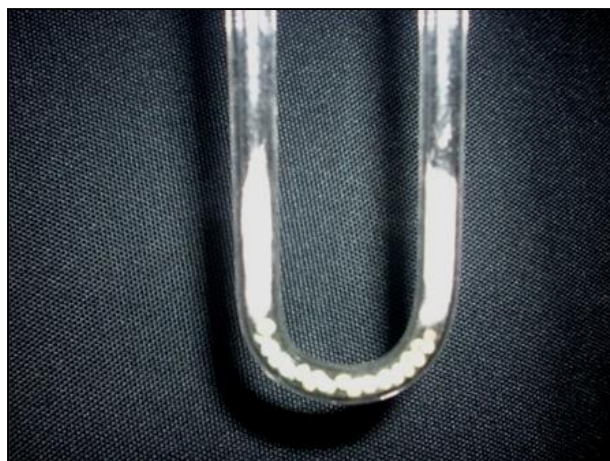


Fig. 3-9 Detail of the adsorption cell used in H<sub>2</sub>S clean up plant

The samples were treated at 250 °C for 2 h in air flow (100 cm<sup>3</sup>min<sup>-1</sup>) before the tests. HCl effluent from the adsorption cell, was analyzed using potentiometric measurement. The stream effluent from the cell was bubbled through a test tube containing distilled water (40 cm<sup>3</sup>) in which HCl dissolved. The test tube was properly designed to guarantee the complete HCl dissolution in the water. Preliminary tests with different amounts of water and depth of the bubbling point allowed to optimize the operating conditions for the complete HCl dissolution. A pH probe HI1131B connected to a Hanna HI3220 pH meter was immersed in the solution. The pH value measured at a given time allowed to determine the amount of HCl dissolved in water until that time, that corresponds to the amount not adsorbed by the material: from these data, by a derivative procedure, the HCl concentration in the effluent from the cell was obtained as a function of time. In this way the breakthrough curve was obtained. Preliminary blank tests with the cell filled with an inert material were carried out to check the accuracy of the method. The sensitivity was as low as 1 ppm HCl.

### 3.21.7.3 Analytical procedure

The adsorption measurements associated to those of pH represent an experimental innovation that deserves a thorough discussion. Figure 3-10 shows a typical pH curve obtained in the adsorption tests for HCl and H<sub>2</sub>S removal.



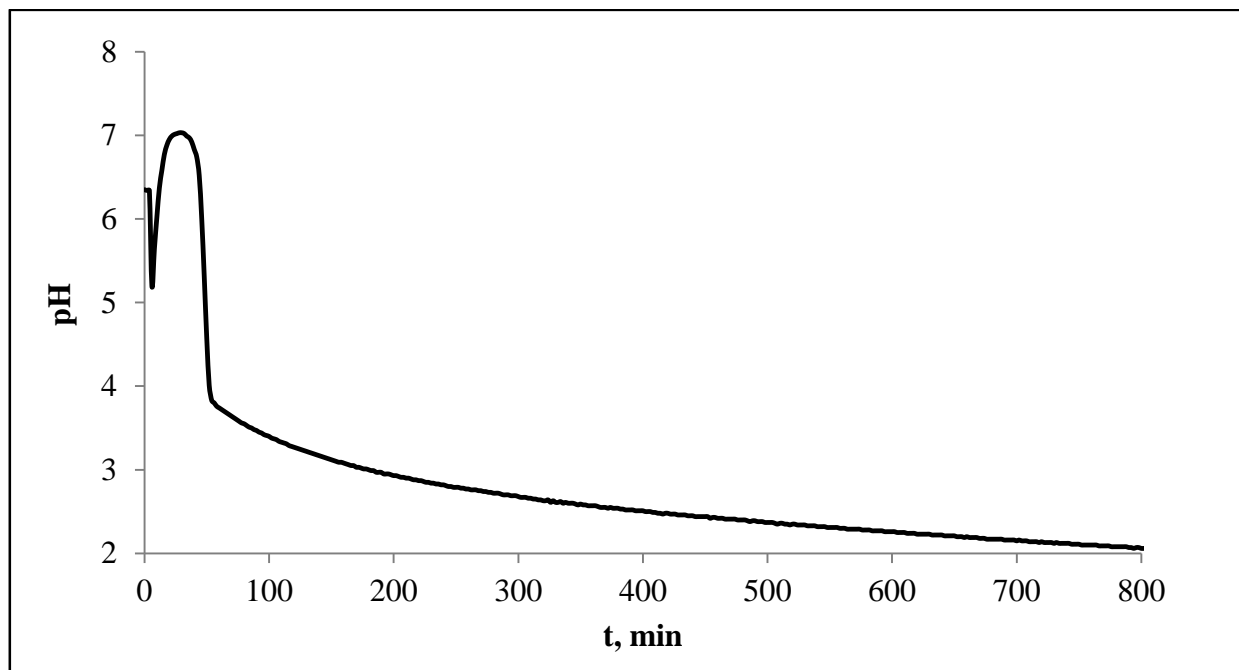


Fig.3-10 Example of pH vs Time curves obtained with experimental procedure

The pH trend on time presents an initial peak due to the presence of dissolved  $\text{CO}_2$  in distilled water and subsequent stripping that leading to the initial pH increase which ends after about 30 min. In fact,  $\text{H}_2\text{S}/\text{He}$  or  $\text{HCl}/\text{He}$  flow in the absorption cell generates a turbulent flow and a strong mixing with consequent separation of dissolved  $\text{CO}_2$ , resulting in an increase of pH. Subsequently, the pH starts to decrease due to absorption of  $\text{H}_2\text{S}$  or  $\text{HCl}$  in solution.

The concentration of  $\text{H}^+$  ions can be calculated from pH value according to:

$$pH = -\text{Log}[H^+] \quad (3.40)$$

It is possible to obtain:

$$[H^+] = 10^{-(pH)} \quad (3.41)$$

From the volume of the test solution it is possible to obtain the number of moles of  $\text{H}^+$ :

$$mol = [H^+] * V \quad (3.42)$$

Since during the test part of the solvent is inevitably entrained from the gas stream, according to the balance due to Raoult's law, it must be considered the change in the volume (V) in order to obtain a more accurate value of the number of moles.

For this reason, a measurement is taken of the downstream volume of the test, approximating the reduction from the initial volume, 40 cc, according to a linear law over time. Now a small distinction must be made for the adsorption of H<sub>2</sub>S and HCl.

For H<sub>2</sub>S, note the volume and the initial concentration of H<sup>+</sup> ions (by pH measurement of the initial Ag nitrate solution), can be evaluate the number of moles present in the initial solution. This value will be subtracted from the calculated during the experimental measurements, in fact, the assessment of the number of moles of H<sub>2</sub>S absorbed by the solution is evaluated on the basis of the variation of pH from the initial value.

In the solution occur respectively the dissociation reactions of H<sub>2</sub>S, reactions (3.37) and (3.38), and the reaction (3.39) of formation of silver sulphide Ag<sub>2</sub>S, which is deposited on the bottom, extremely favored, which moves the balances (3.37) and (3.38) towards the formation of products ensuring the full absorption of H<sub>2</sub>S in solution. From the stoichiometry, the ratio between the H<sub>2</sub>S moles sent and H<sup>+</sup> ions released (Eq. (3.37) and (3.38)) is 1: 2, and the number of initial moles calculated can be traced back to H<sub>2</sub>S moles absorbed by the solution:

$$mol_{H_2S} ads = \frac{(V*[H^+] - mol_{H^+_{t=0}})}{2} \quad (3.43)$$

For HCl adsorption tests the measuring cell was designed with the purpose that the acid present in the gas stream (if present), is completely dissolved in water: this is possible because HCl has a high solubility in H<sub>2</sub>O (720 g / l).

The output current from the measuring cell will contain N<sub>2</sub> and a small percentage of water due to phenomena of dragging and evaporation. The volume of liquid, on which are made the measurements of pH, is reduced, and then, progressively about 1 ml every 2 hours, then the calculation of the moles of H<sup>+</sup> present considers the actual volume (V) at time t of measurement:

$$V = V_{in} - V_{evaporated} \quad (3.44)$$

From the variation of the pH of the solution contained in the measuring cell, it is possible obtain the moles of HCl absorbed in the water and the moles of HCl adsorbed by the material analyzed:

$$\text{mol H}^+ = V * 10^{-\text{pH}} \quad (3.45)$$

$$\text{mol H}^+ \sim \text{mol HCl ads} \quad (3.46)$$

Figures 3-11 and 3-12 shows a typical curve (mol ads vs t) obtained by both of the experimental procedures.

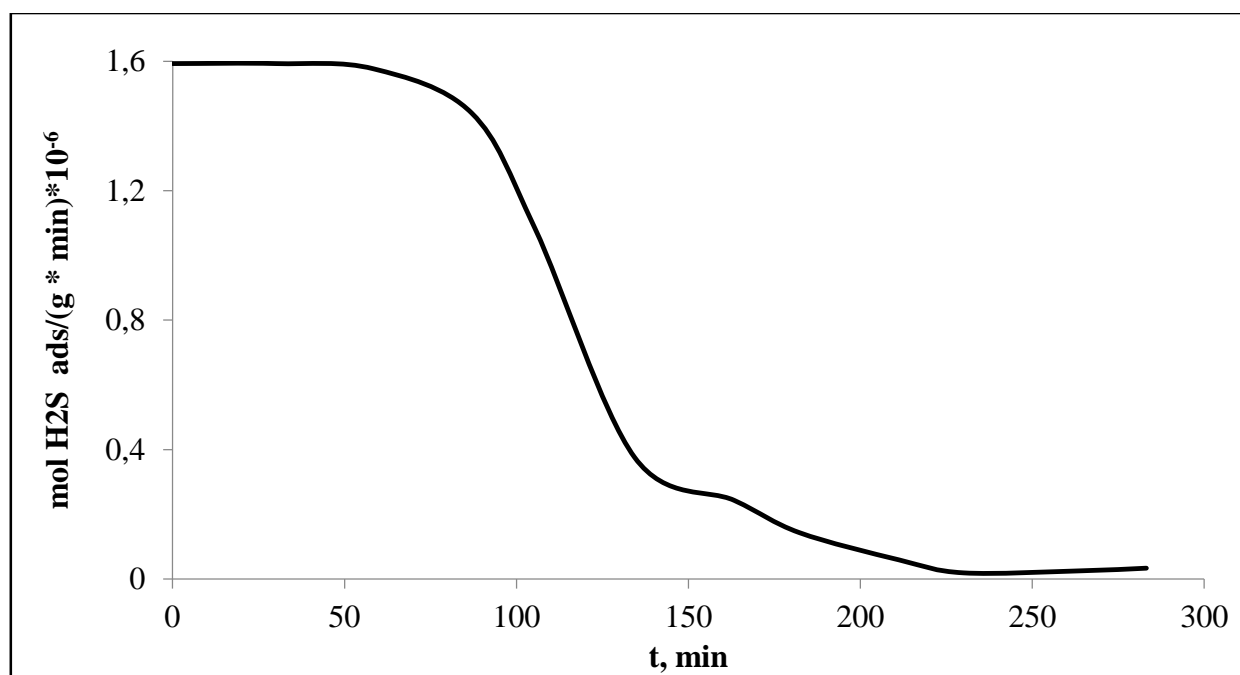


Fig. 3-11 Example of mol of H<sub>2</sub>S vs Time curves obtained with experimental procedure

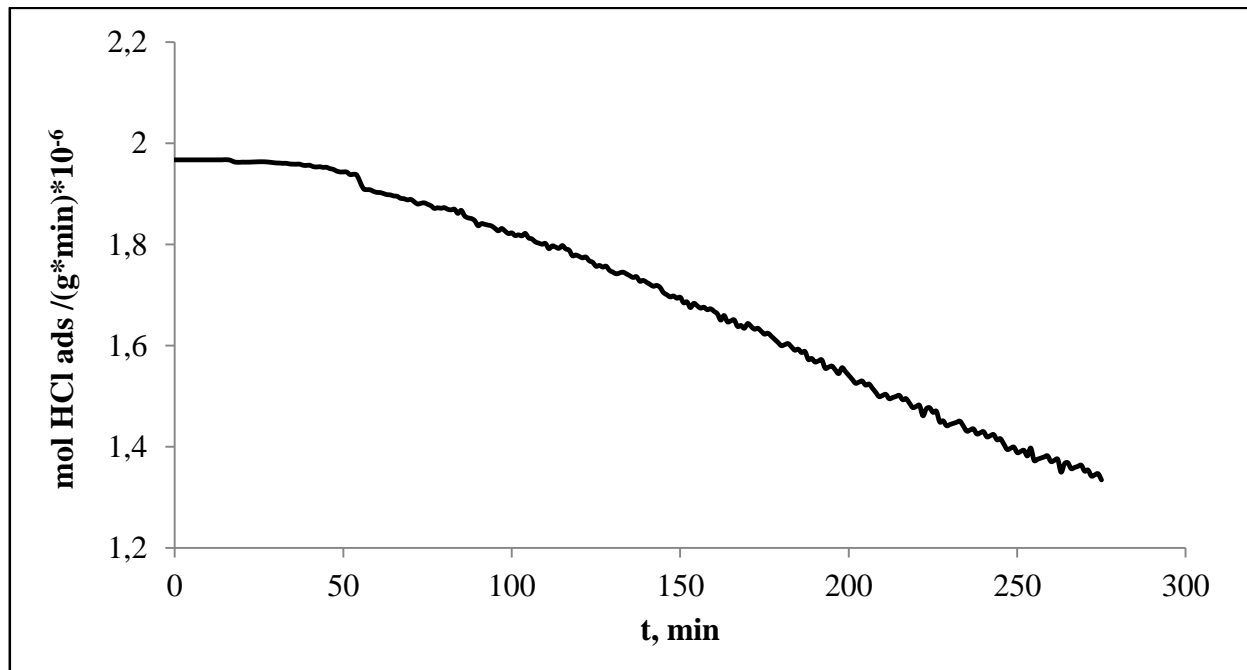


Fig. 3-12 Example of mol of HCl vs Time curves obtained with experimental procedure

Finally, to obtain the curve of breakthrough of the material expressed in terms of ppm of H<sub>2</sub>S or HCl in the output against time must be considered the following equation:

$$H_2S \text{ ppm} = 10^6 \cdot \left( \frac{\frac{\text{mol } H_2S \text{ ads}}{\text{min}}}{\frac{\text{mol tot in}}{\text{min}}} \right) \quad (3.47)$$

$$HCl \text{ ppm} = 100 * \left( 1 - 1 * \frac{\text{mol } HCl \text{ in} - \text{mol } HCl \text{ ads}}{\text{mol } HCl \text{ in}} \right) \quad (3.48)$$

Figure 3-13 shows an example of breakthrough curves obtained with the experimental procedure previously described.

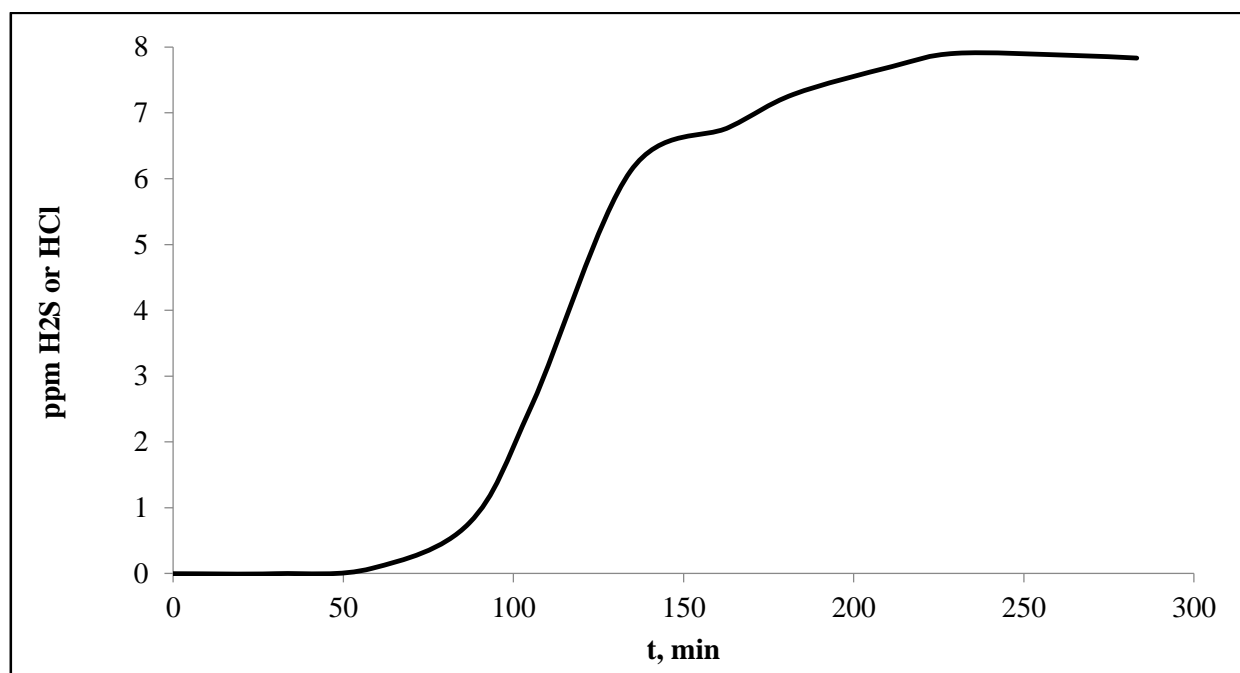


Fig. 3-13 Example of breakthrough curves obtained with experimental procedure

### 3.22 Results and Discussion

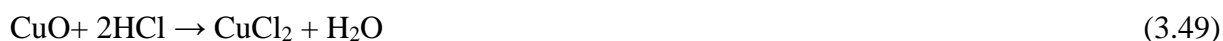
#### 3.22.1 SEM-EDS measurements

The EDS analysis results provide information on surface elementary composition of the samples, while SEM show materials morphology on microns scale.

The following table 3-12 shows the results of EDS analysis for untreated activate carbons and zeolite 13X.

13 X zeolite contains mainly Si, Al, Na, since the zeolite is the Na form, with traces of magnesium ions, potassium, chlorine, calcium and iron resulting from the production process of the zeolite itself. Si/Al ratio (about  $1.65 \text{ mol mol}^{-1}$ ) measured is close to theoretical value of 13X Zeolites suggesting the accuracy of such measurement. Na content is in agreement with charge neutrality of the zeolite.

The main component of all activated carbons is C of course. Norit RGM3 also contains chromium and copper oxides deriving from the treatment used by the supplier to promote the adsorption/oxidation mechanism according to the reaction:



RBAA1 contains K with an amount of 24% due to the treatment with a KOH solution of effected by the supplier. Traces of other compounds, such as Al and Si, are present in all the activated carbons,

while other compounds, such as Fe, Ca, etc. are more frequently present in activated carbons treated, probably as a residue of the treatment of the precursor materials.

Element (wt%)	Samples			
	13X	Norit RGM3	RBAA1	Filtrisorb
Si	25.24	0.33	2.17	0.82
Al	14.7	0.20	-	0.88
O	46.93	6.25	9.87	6.48
Cu	-	3.65	-	-
Na	8.39	-	0.32	-
Mg	1.82	0.44	0.62	-
Cl	0.33	0.25	-	-
K	0.87	0.12	23.91	-
Ca	0.5	0.43	9.49	-
Fe	1.22	0.20	1.03	-
C	-	86.48	52.59	91.81
S	-	0.57	-	-
Cr	-	1.01	-	-
Mn	-	0.06	-	-

Table 3-12 Chemical composition of Zeolite 13X and Activated Carbons

SEM micrographs are able to provide detailed images of the sample surface. In the following images the SEM obtained for the samples used in the adsorption tests have been reported.

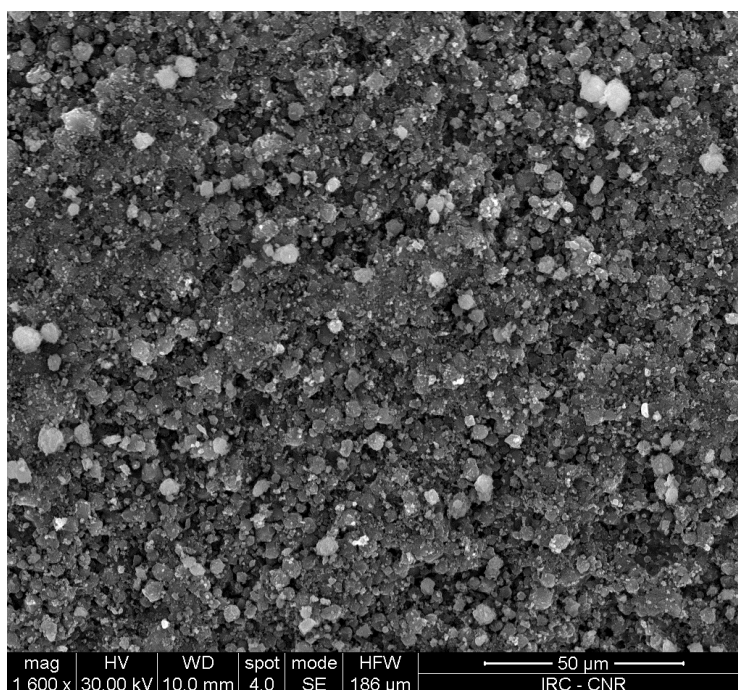


Fig. 3-14 Zeolite 13X SEM

In the micrograph (Fig. 3-14) on the zeolite 13 X can be detect the presence of regular crystalline particles, characteristics of the morphology of the zeolites.

As regards the active carbon, the SEM images are shown in figures 3-15:3-17

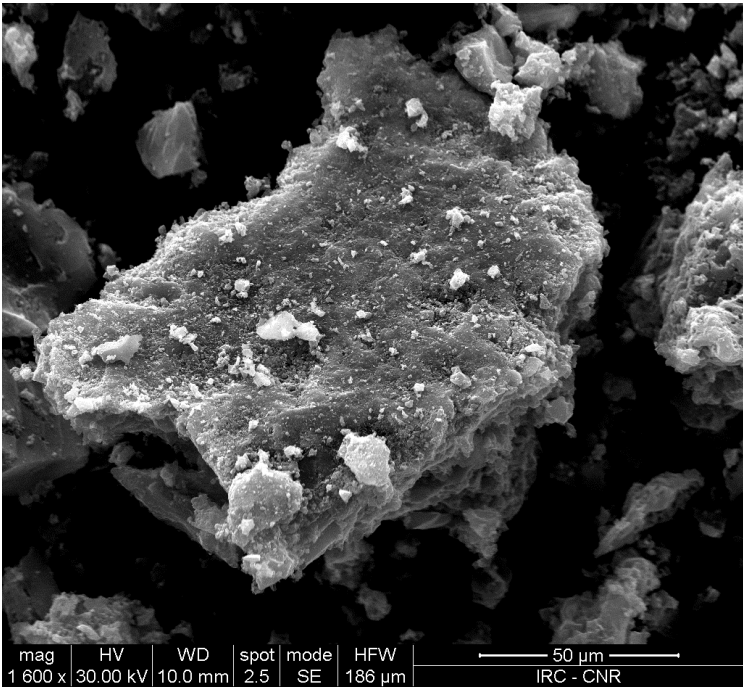


Fig. 3-15 RGM3 SEM

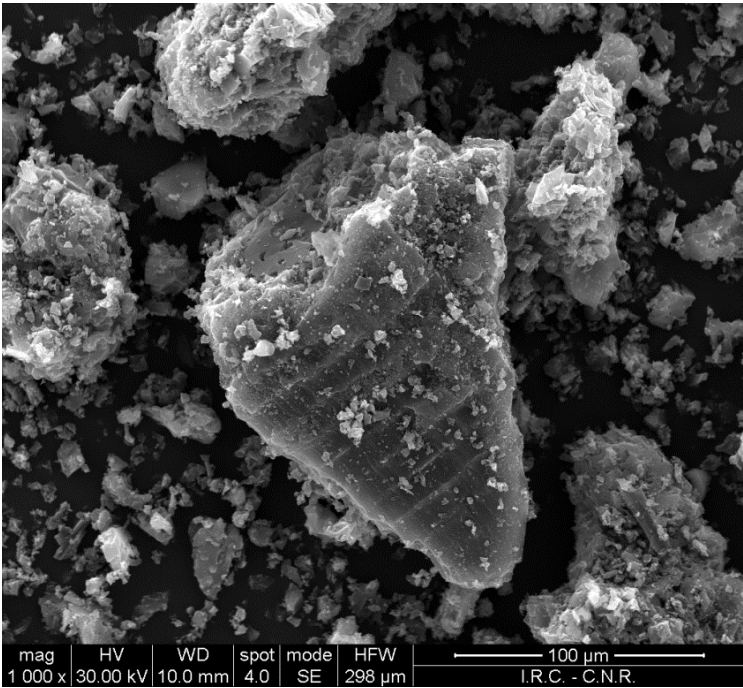


Fig. 3-16 RBAA1 SEM

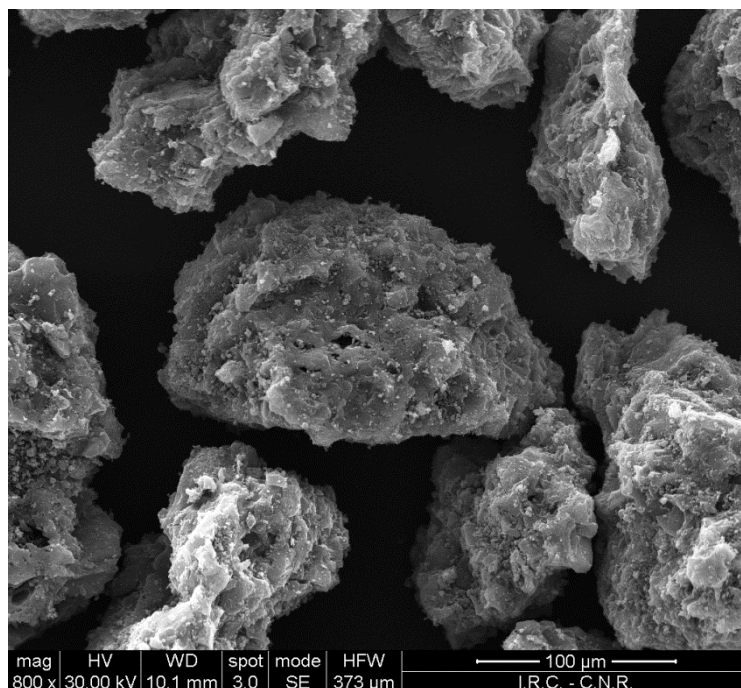


Fig. 3-17 Filtrasorb SEM

The images of activated carbons show the classic "creased" area and a morphology clearly less crystalline in comparison to zeolite 13X.

### 3.22.2 Surface area measurements

The surface area is a critical feature for a sorbent, since it affects the adsorbent capacity. Through the technique of nitrogen adsorption at 77 K, illustrated previously, the surface areas, the porosimetric distribution and the pore volume have been obtained. The results are summarized in the following table 3-13:

Sample	13X	RGM 3	RBAA1	Filtrasorb
Surface Area (m <sup>2</sup> /g)	581.2	1110	815.8	1050
Pore Volume (cm <sup>3</sup> /g)	0.325	0.409	0.450	0.593
Average pore size (Å)	22.41	19.55	22.10	27.22

Tab. 3-13 Surface Area and Pore volume of Zeolite 13X and Activated Carbons not treated

Active carbons have specific surface areas in the range 815-1110 m<sup>2</sup>/g as expected from literature data (ref libro, clark, sing) that are significantly higher than 13 X zeolite (580 m<sup>2</sup>/g).

The following figures (3-18:3-21) shows the N<sub>2</sub> adsorption isotherms obtained for the samples not functionalized.



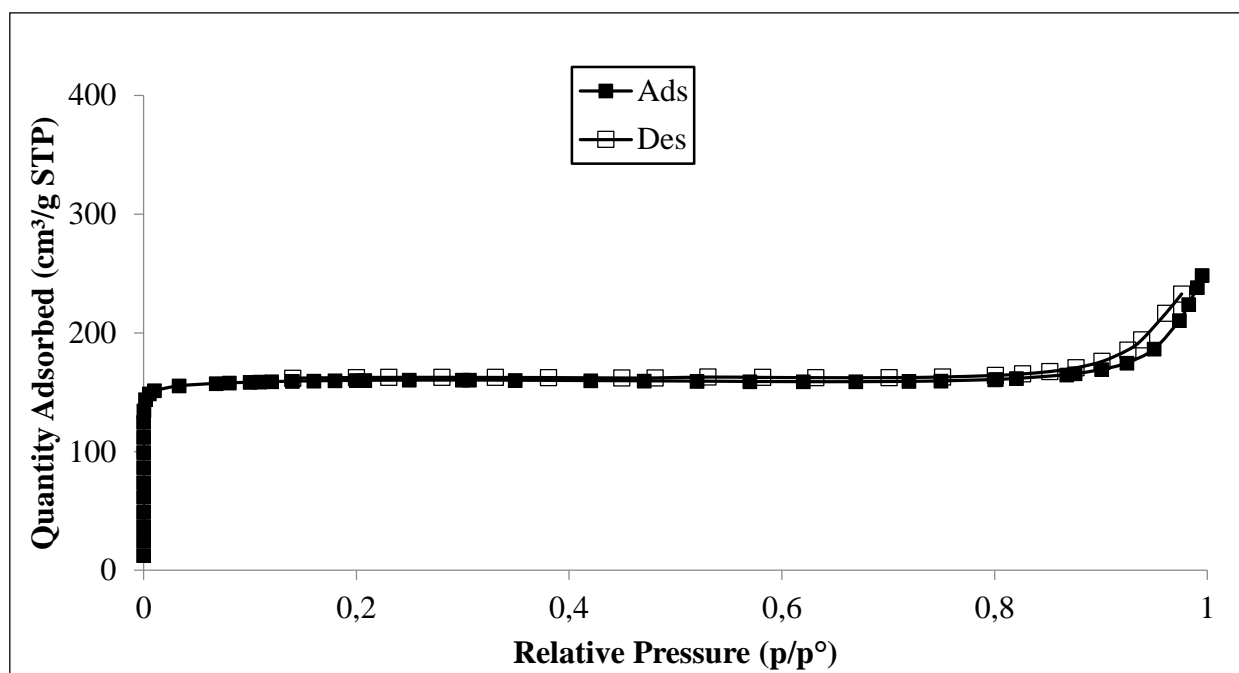


Fig. 3-18 Isotherm of N<sub>2</sub> adsorption at 77K for Zeolite 13X

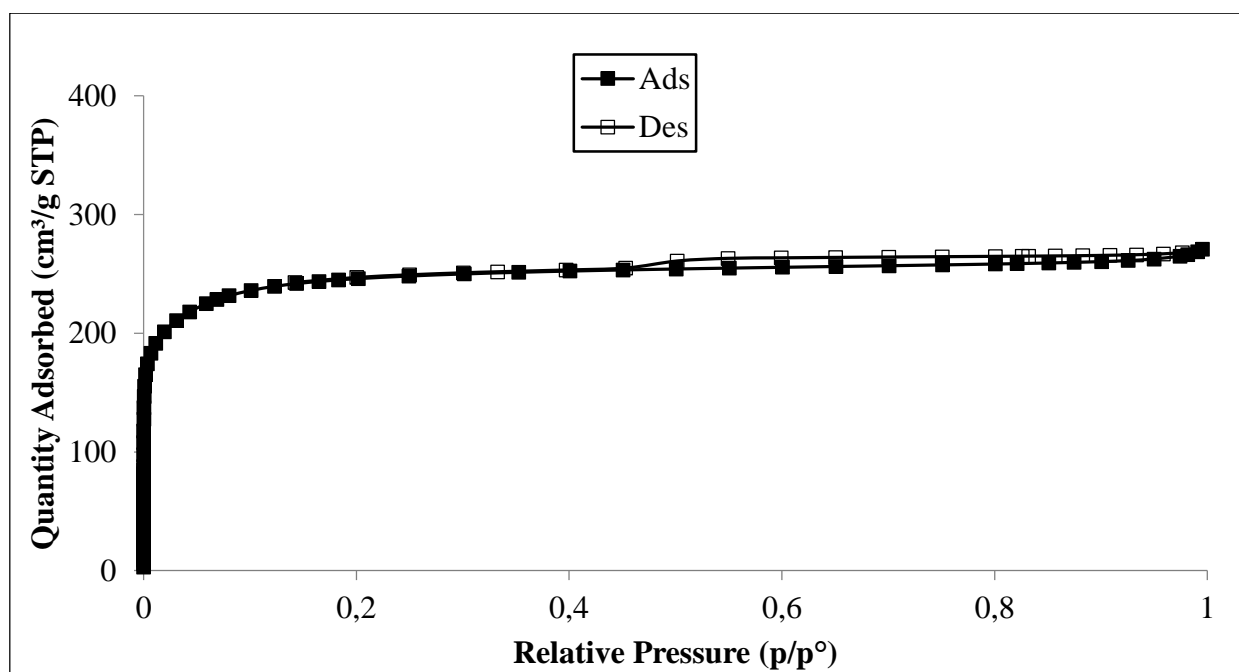


Fig. 3-19 Isotherm of N<sub>2</sub> adsorption at 77K for Norit RGM3

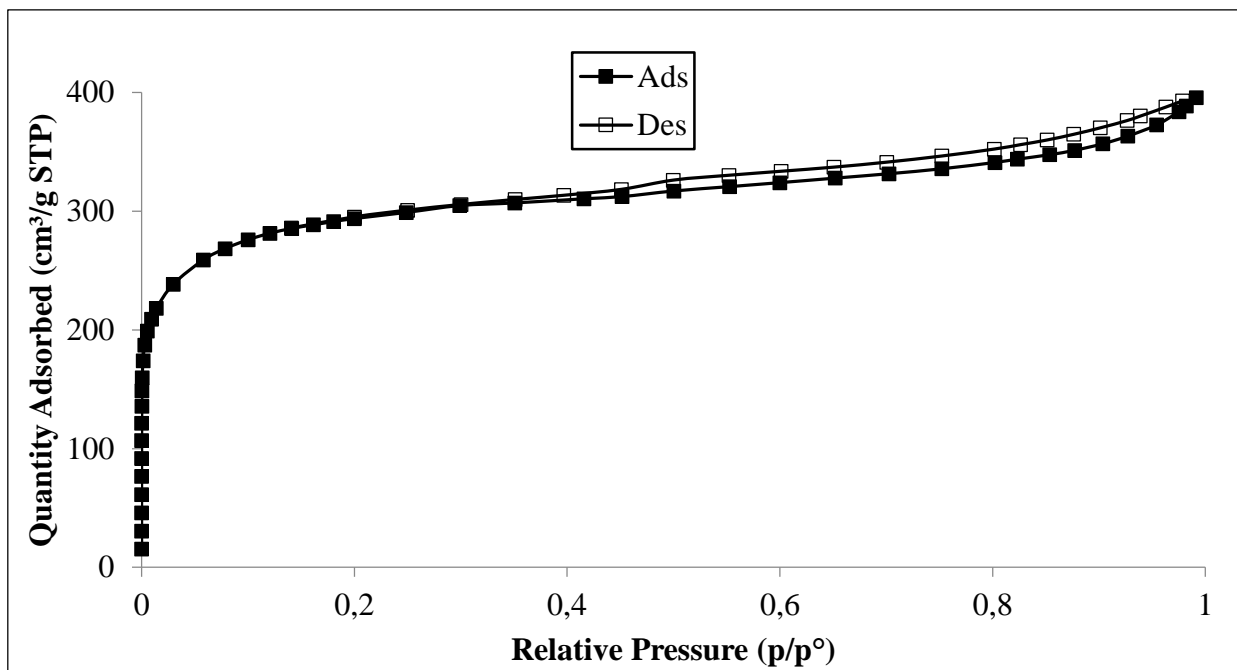


Fig. 3-20 Isotherm of N<sub>2</sub> adsorption at 77K for Filtrasorb

All isotherms are of type I according to the IUPAC classification [310,311] and are typical of microporous materials. Adsorption occurring in microporous materials is essentially a pore-filling process, possible for the molecules whose dimensions are compatible with those of the pores themselves. The most distinctive feature of a type I isotherm is a fast increase of adsorbate volume at low  $p/p_0$  values up to an almost constant value which extends across most, if not all, of the multilayer range up to  $p/p_0 \rightarrow 1$ .

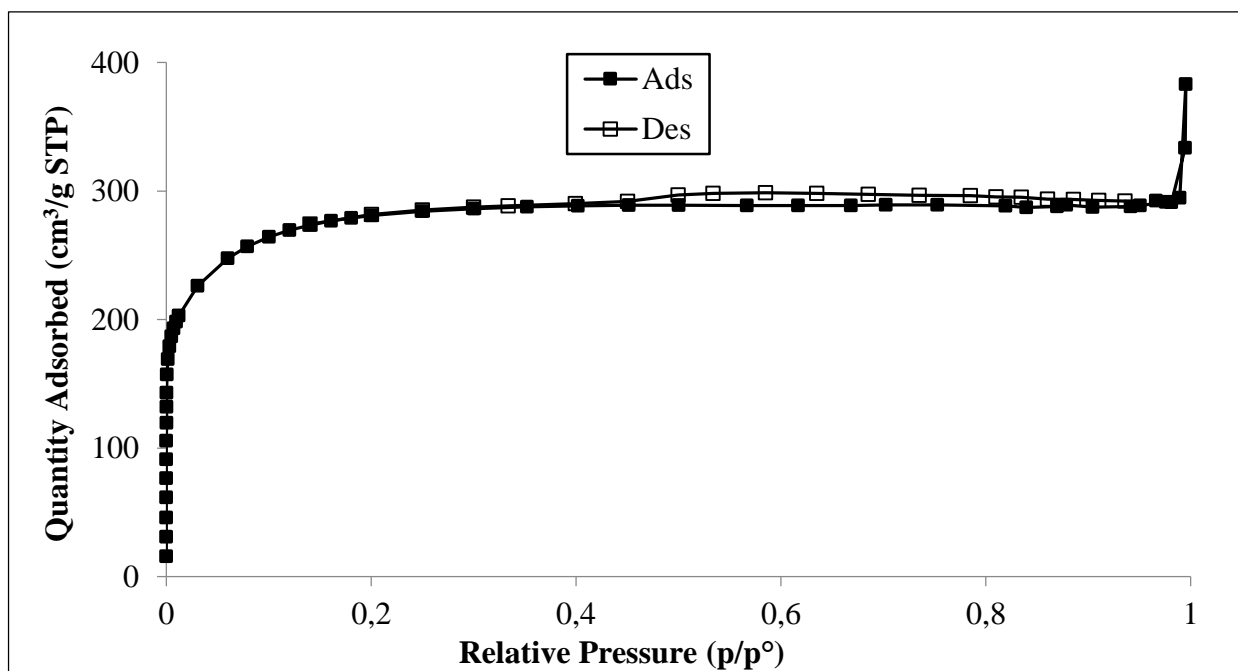


Fig. 3-21 Isotherm of N<sub>2</sub> adsorption at 77K for RBAA1

That micropores are filled reversibly in the  $p/p^0$  range below the normal onset of capillary condensation is now indisputable, but the mechanism involved in micropore filling are still under discussion-as they have been for over 40 years. However, it is now apparent that the micropore filling process is dependent on both the ratio of the pore width to the molecular diameter ( $w/d$ ) and the pore shape.

This mechanism was studied by Dubinin who developed a model based on the above considerations [311]. B.E.T. model can be approximated without problems to microporous materials (2-3% error), especially when the surface areas involved are high ( $>200 \text{ m}^2/\text{g}$ ).

In the case of mesopores and macropores the specific surface area also plays an important role, since the solute-sorbent interaction occurs only at a certain distance between them and not in any part of the pore void volume. It is also possible to have a multi-layer adsorption, but while for the mesopores is conceivable an adsorption mechanism due to capillary condensation, the small specific surface area of the macropores limits its influence on the adsorption capacity, relegating the macropores to the role of transportation of adsorbate in the micropores [312].

Furthermore, a hysteresis should be observed in the isotherms but his contribution is irrelevant and the presence of mesoporosity should be excluded. Definitively, pore volume and pore size distribution has a profound influence on the adsorbing characteristics of active carbons and zeolites because they have an influence in the solute-sorbent interactions.

Table 3-14 shows the surface areas for the modified samples, and the corresponding percentage change, compared to the material not treated.

<b>Sample</b>	<b>Surface Area (<math>\text{m}^2/\text{g}</math>)</b>
FT NaOH	1009
FT KOH	1133
FT $\text{Na}_2\text{CO}_3$	1049
RGM3 NaOH	1039
RGM3 KOH	1322
RGM3 $\text{Na}_2\text{CO}_3$	1106
13X_Ex_Cu	370
13X_Ex_Zn	356
13X_Im_Cu	575
13X_Im_Zn	585

Tab. 3-14 Surface Area for Zeolite 13X and Activated Carbons modified

The treatment of the activated carbons with the impregnation method causes an increase in the surface area of the sample modified by alkaline solution of KOH, while a surface area decreases are

found for the sample impregnated with NaOH solution. Finally, no change was detectable for the sample functionalized with Na<sub>2</sub>CO<sub>3</sub> solution. This results are in agreement with several literature data [310].

For the zeolite 13X, ion exchange, but not impregnation, causes a decrease of surface area, that however is still high (356-370 m<sup>2</sup>/g). Such a reduction of surface area generally occurs when zeolites are modified with metal ions and is probably due to the formation of clusters of metal oxides that partially occlude micropores [310].

Sample	Metal Content (mmoleq g <sup>-1</sup> )			
	Cu <sup>2+</sup>	Zn <sup>2+</sup>	Na <sup>+</sup>	Others (K <sup>+</sup> , Ca <sup>2+</sup> , Mg <sup>2+</sup> )
13X	-	-	3.65	1.92
13X_Ex_Cu	4.66	-	0.22	1.48
13X_Ex_Zn	-	5.46	0.16	1.10
13X_Im_Cu	1.80	-	3.44	1.90
13X_Im_Zn	-	0.50	3.60	1.89

Tab. 3-15 Metal Content in Zeolite 13X and 13X modified samples

Table 3-15 shows the metal content for 13X not modified and modified samples. It can be observed that 13X zeolites modified by ion exchange show higher metal contents compared to those modified by impregnation suggesting the presence of the metals in zeolites framework. This can be related to the large excess of solution employed in the exchange method. The metal content of exchanged samples is close to the amount corresponding to total exchange (5.8 mmol eq g<sup>-1</sup>). It must be noted that besides Na<sup>+</sup> other cations are exchanged (such as K<sup>+</sup>, Ca<sup>2+</sup> and Mg<sup>2+</sup>). A similar value can be assumed for exchanged zeolites, where Na<sup>+</sup> is substituted by equivalent amount of Cu<sup>2+</sup> or Zn<sup>2+</sup>, while for the impregnated zeolites a higher value is expected due to the presence of the basic oxides CuO or ZnO.

Samples	FT NaOH	FT KOH	FT Na <sub>2</sub> CO <sub>3</sub>	RGM3 NaOH	RGM3 KOH	RGM3 Na <sub>2</sub> CO <sub>3</sub>	RBAA1
Active Phase	Na <sup>+</sup>	K <sup>+</sup>	Na <sup>+</sup>	Na <sup>+</sup>	K <sup>+</sup>	Na <sup>+</sup>	K <sup>+</sup>
(mmol eq/g)	2.10	2.10	5.5	7.98	2.60	5.01	1.92

Tab. 3-16 Active phase Content in modified Active Carbons

Table 3-16 shows the results obtained, regarding the active phase, for modified active carbons. For all the samples the impregnation with  $\text{Na}_2\text{CO}_3$  involves a content approximately double of active phase compared to the other samples, with a values of approximately 5-5.5 mmol eq/g. The only exception is given by Norit RGM3 impregnated with NaOH solution that showing a higher active phase content equal to 7.98 mmol eq/g. Recall, also, that for RBAA1 the active phase has been introduced by the supplier, such content is comparable (1.92 mmol eq/g for RBAA1, 2.1-2.6 for other samples) to the modified carbons impregnated with KOH.

### 3.22.3 Tests of HCl Adsorption capacity

The adsorption tests have been carried out with the experimental apparatus previously described in the paragraph 3.21.7.2.

Figure 3-22 shows the breakthrough curves for the active carbons not modified. HCl concentration range of interest is limited taking into account that 1 ppm is the maximum limit tolerated by SOFCs and MCFCs. Figure 3-22 shows that the best performance is obtained with the Norit RGM3 that shows the slowest increase of HCl concentration, compared to the other samples leading to the highest breakthrough time at 1 ppm. The higher affinity with HCl due to the presence of Cu in the sample not treated. In Table 3-17 are summarized the adsorbed moles and the breakthrough time at 1 ppm and 10 ppm for each samples used in HCl adsorption tests (treated and not treated).

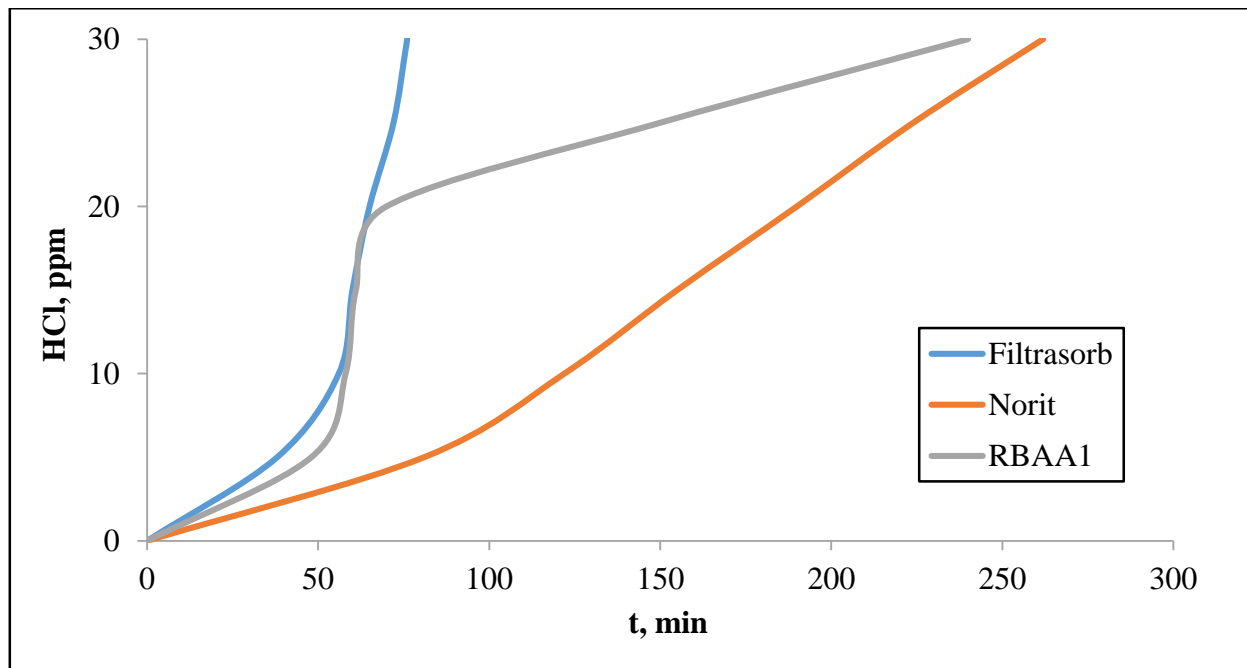


Fig. 3-22 HCl Breakthrough curve of activated carbon not modified

Figure 3-23 shows the breakthrough curves for the active carbons filtrasorb not treated compared to the samples treated with NaOH, KOH and  $\text{Na}_2\text{CO}_3$ .

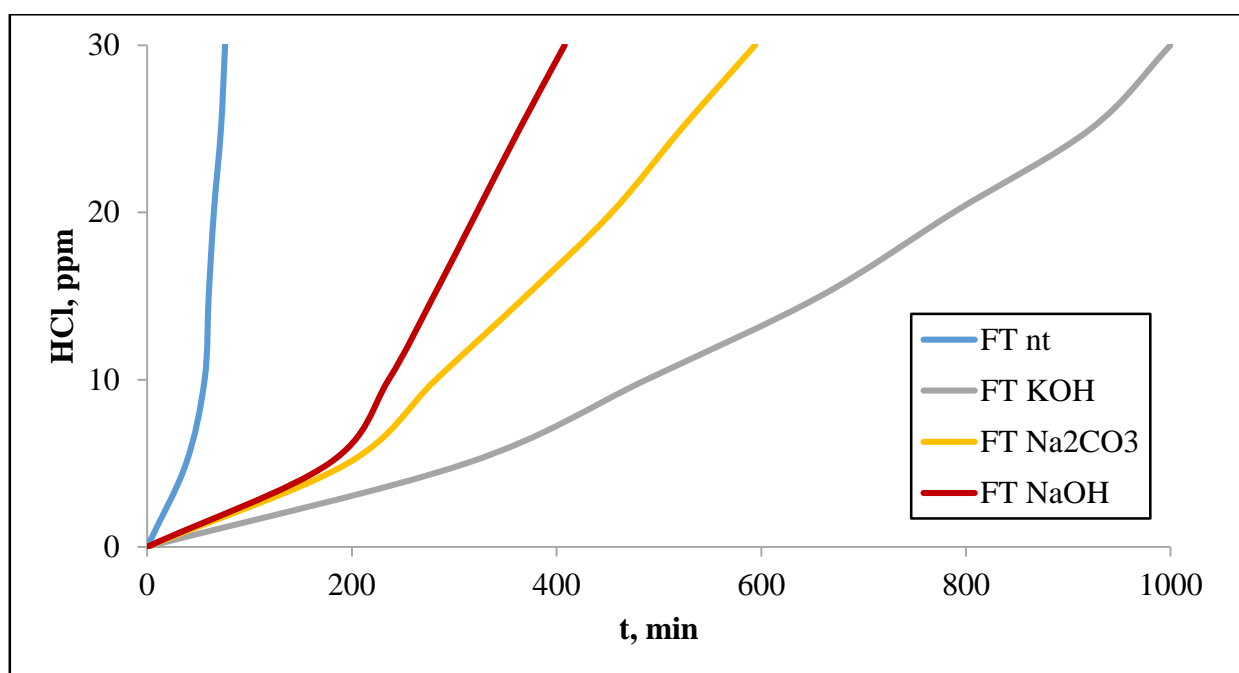


Figure 3-23 HCl Breakthrough curve for Filtrasorb not treated and modified

From the analysis of breakthrough curves it can be observed that functionalization by impregnation improves at all the performance of the coal itself. In particularly the best results are obtained with Filtrasorb treated with KOH that shows a breakthrough time of 212 min at 1 ppm and an adsorption capacity of 0.45 mmol HCl/g. This result can be justified by the higher surface area of the sample, since the other parameters do not play a decisive role. In fact, the amount of active phase is the same for the samples modified with KOH and NaOH (2.1 mmol/g) while the sample treated with Na<sub>2</sub>CO<sub>3</sub> has a higher active phase, but lower performance probably due to the higher steric hindrance of Na<sub>2</sub>CO<sub>3</sub> molecule that obstructing partially the pores of activated carbons.

Figure 3-24 shows the curves obtained for the samples Norit RGM3 not treated (nt) and treated with NaOH, KOH and Na<sub>2</sub>CO<sub>3</sub>, similarly to filtrasorb sample.

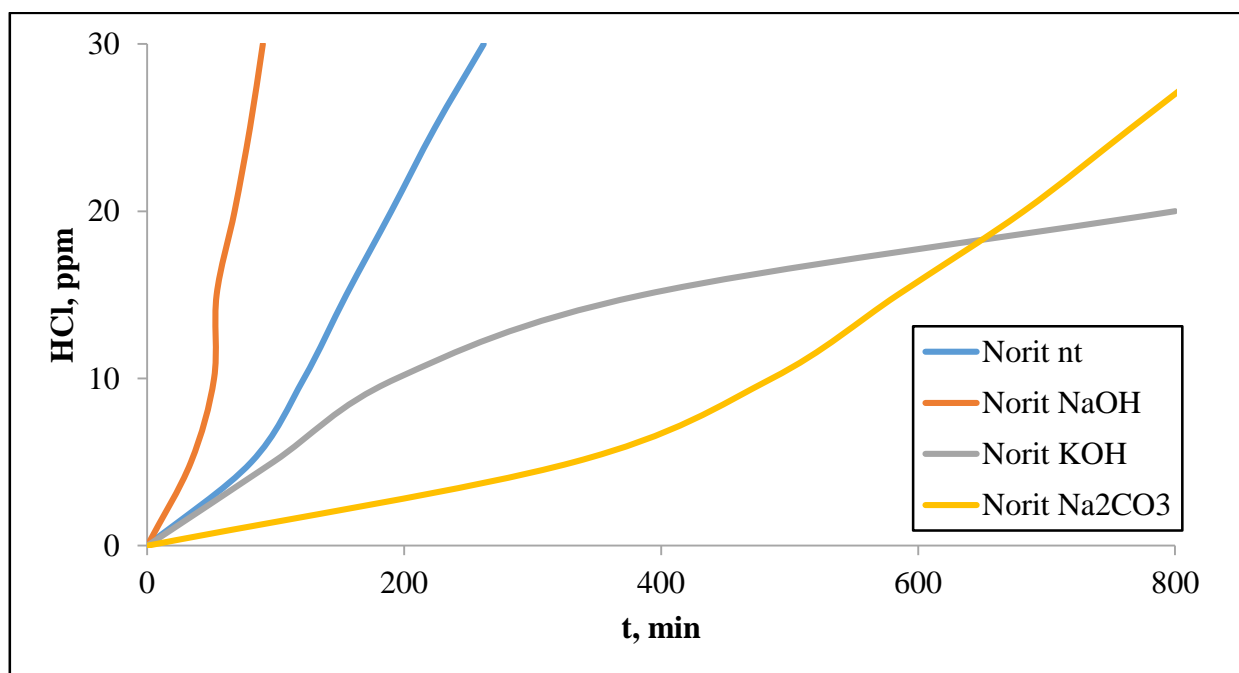


Fig. 3-24 HCl Breakthrough curve for Norit RGM3 not treated and modified

It should be noted that sample treated with NaOH initially shows lower performance compared to the sample not treated, but after about 200 min performance become better. This result is not satisfactory for our purposes, since the range of interest is for low values of adsorbed HCl ppm, up to 10.

For RGM3 samples impregnated with  $\text{Na}_2\text{CO}_3$  and KOH the adsorbent capacity increase with a values of 0.52 mmol HCl/g adsorbed at 1 ppm ( $t = 252$  min) for Norit  $\text{Na}_2\text{CO}_3$  and with values of 0.18 mmol HCl/g adsorbed at 1 ppm ( $t = 84$  min) for Norit KOH.

The activated carbons impregnated with NaOH, which have the highest content of active phase, show a very low adsorption capacity, which is also lower than not modified sample.

This unexpected behavior could be related to an excessive content of Na, which leads to occlusion of micropores with the consequent reduction of the surface, and which therefore reduces the amount of HCl adsorbed.

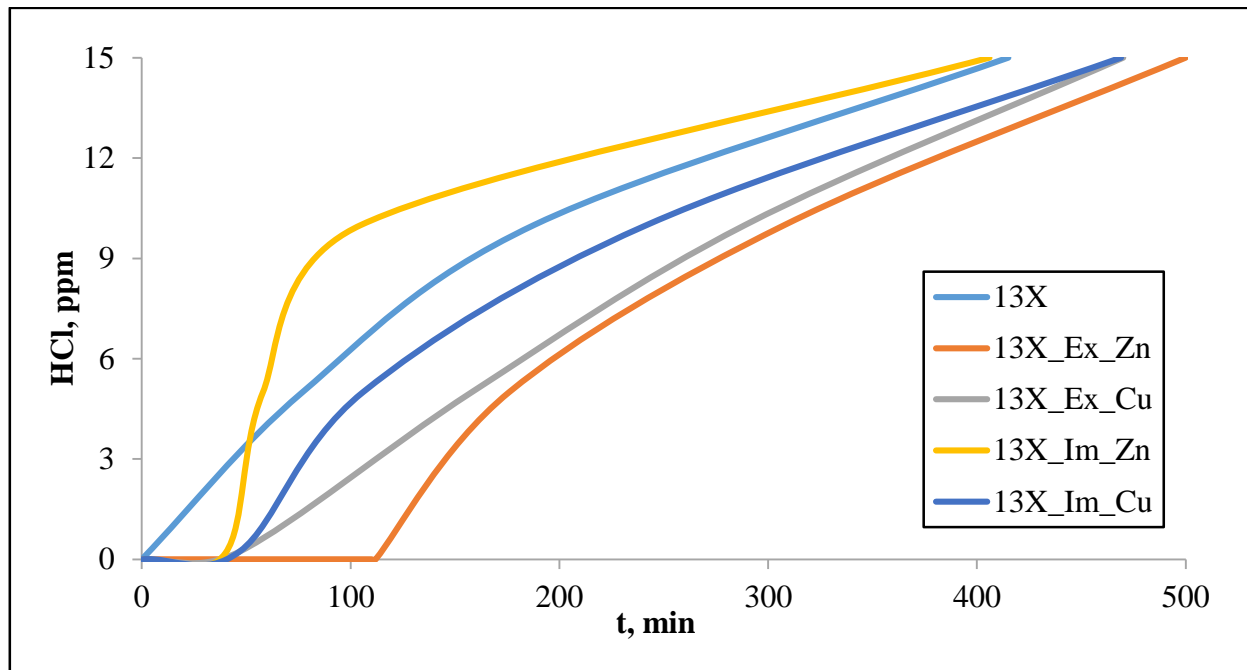


Fig. 3-25 HCl Breakthrough curve for Zeolite 13X not treated and modified

Breakthrough curves of the zeolite 13X and modified samples are reported in Fig. 3-25. The shapes of the breakthrough curves of the materials appear quite different from activated carbons. This suggests different kinetics of HCl adsorption. [310-312].

The curve of not modified 13X, shows a steady increase of HCl concentration with time up to about 120 min, then the slope reduces. The breakthrough curves of Cu modified zeolites, 13X\_Ex\_Cu and 13X\_Im\_Cu, are quite similar, showing a delay time of about 55 min, after which HCl concentration increases steadily.

As regards the zeolites modified with Zn, a noticeable difference can be observed between the samples prepared by impregnation and by ion exchange. The former gives a breakthrough curve with a delay of about 40 min before the appearance of HCl, after which HCl concentration increases rapidly to values higher than 10 ppm. The latter shows a much longer delay of about 110 min before HCl detection, then HCl concentration increases steadily and approaches the values of the other samples at the end of the test.

The shape of the curves suggests that the rate of adsorption is gradually reduced with time: this behaviour is probably related to diffusive resistance in the narrow pores of the zeolite ( $d = 8 \text{ \AA}$ ). Obviously this resistance increases with time due the increase of the amount of adsorbate in the pores. For the not modified zeolite it can be hypothesize that HCl is chemisorbed according to Eq. (3.50)





As showed in Fig. 3-25 for the zeolites the best results are obtained with samples modified by ion exchange and this is in according to the higher active phase content (see Tab. 3-15).

Table 3-17 summarize the adsorption properties as derived from breakthrough curves for all samples studied.

The results show that, with the exception of Norit NaOH sample, treatment with basic solutions, improves the adsorption properties of activated carbons.

In the case of Filtrasorb, all treatments lead to an increase of the performance compared to sample not treated. The best results are obtained for the sample Filtrasorb KOH, which presents a breakthrough time at 1 ppm of 212 minutes with a total amount of HCl adsorbed approximately 0.45 mmol/g, almost double value than the other two treated samples and about 7 times greater compared to not treated Filtrasorb.

For the activated carbons Norit RGM3, it can be noted that the impregnation with KOH and  $\text{Na}_2\text{CO}_3$  improves the HCl adsorption properties due to the increase of basic sites.

The sample with  $\text{Na}_2\text{CO}_3$ , at 1 ppm, shown a breakthrough curve with an about triple adsorption value in comparison to RGM3 impregnated with KOH (0.52 vs 0.18 mmol/g). However, the activated carbons impregnated with NaOH, which have the highest content of active phase, show a very low adsorption capacity, which is also lower than not modified sample.

Ultimately for Norit RGM3 samples, the best performances have been obtained with  $\text{Na}_2\text{CO}_3$  treatment, which leads to a breakthrough time at 1 ppm of about 5 times higher than the untreated Norit and an HCl adsorption uptake of 0.52 mmol/g.

As regards the other sample considered as a comparison sample, the RBAA1 (modified by supplier with a KOH solution at 15% wt), it presents a breakthrough time at 1 ppm equal to 44 min with HCl adsorbing capacity of 0.08 mmol/g.

For Zeolite 13X the results have shown improved performances of modified 13X zeolites compared to the untreated zeolite: the best results have been obtained with the zeolite ion exchanged with  $\text{Zn}^{2+}$ , that gives a breakthrough time of 110 min at 1 ppm (0.23 mmol HCl/g) compared to a breakthrough time of 28 min of the not treated zeolite (0.08 mmol HCl/g).

This confirms the efficiency of the procedure developed in this PhD thesis.

<b>Sample</b>	<b>t @ 1 ppm (min)</b>	<b>t @ 10 ppm (min)</b>	<b>mmol HCl ads @ 1 ppm (mmol g<sup>-1</sup>)</b>
<b>FT tq</b>	27	55	0.06
<b>FT NaOH</b>	102	236	0.22
<b>FT KOH</b>	212	498	0.45
<b>FT Na<sub>2</sub>CO<sub>3</sub></b>	122	282	0.26
<b>RGM3 tq</b>	48	123	0.10
<b>RGM3 NaOH</b>	23	50	0.05
<b>RGM3 KOH</b>	84	186	0.18
<b>RGM3 Na<sub>2</sub>CO<sub>3</sub></b>	252	480	0.52
<b>RBAA1</b>	44	57	0.08
<b>13X</b>	28	188	0.06
<b>13X Ex Cu</b>	56	306	0.12
<b>13X Ex Zn</b>	110	287	0.23
<b>13X Im Cu</b>	54	242	0.11
<b>13X Im Zn</b>	46	62	0.10

Tab. 3-17 Breakthrough times and adsorbed moles at 1 ppm for 13X zeolites and active carbons not treated and modified

### 3.22.4 Tests of H<sub>2</sub>S Adsorption

The same materials used for HCl removal have been also studied for H<sub>2</sub>S adsorption in order to ascertain their ability to obtain the purification of biohydrogen stream up to the tolerance limits of the fuel cell and to check the possible utilization of a unique adsorbing bed in the clean-up system. In this paragraph results of H<sub>2</sub>S adsorption tests are reported. It must be taken into account that the MCFCs and SOFCs tolerance limit for H<sub>2</sub>S is lower than 0.5 ppm [310,313] and more stringent removal properties are required for H<sub>2</sub>S purification sorbent materials, so in this PhD thesis will be investigated the limit of 0.5 ppm.

Firstly, have been reported the performances of commercial activated carbons: Filtrasorb, Norit RGM3 and RBAA1, which will be taken as a reference for the results of the functionalized carbon.

Figure 3-26:3-28 show, time trends of H<sub>2</sub>S concentration, outgoing from the adsorption cell.

RBAA1 sample, (figure 3-28) gives the best results among the commercial materials since it presents highest breakthrough time at 0.5 ppm (1070 min), suggesting that, it is able to adsorb H<sub>2</sub>S for a longer time, before saturation, than Norit RGM3 (t at 0.5 ppm equal to 725 min) and even more than the Filtrasorb (t at 0.5 ppm equal to 33 min).

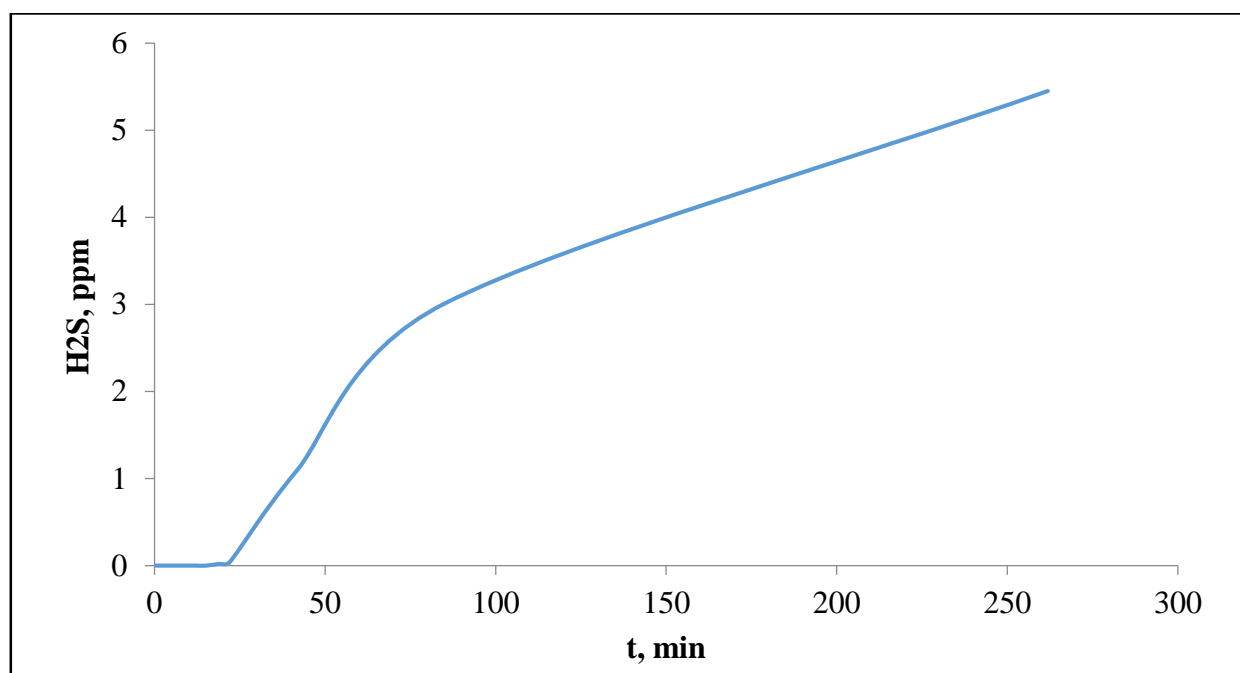


Fig. 3-26 H<sub>2</sub>S Breakthrough curve of Filtrasorb not modified

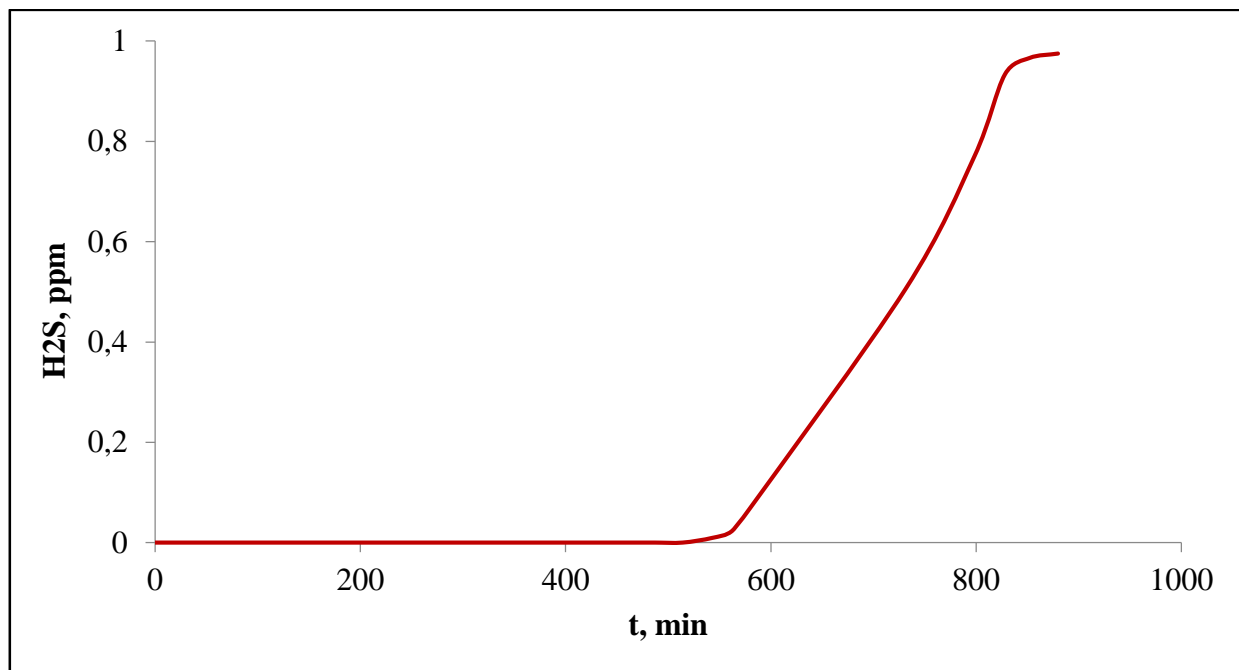


Fig. 3-27 H<sub>2</sub>S Breakthrough curve of Norit RGM3 not modified

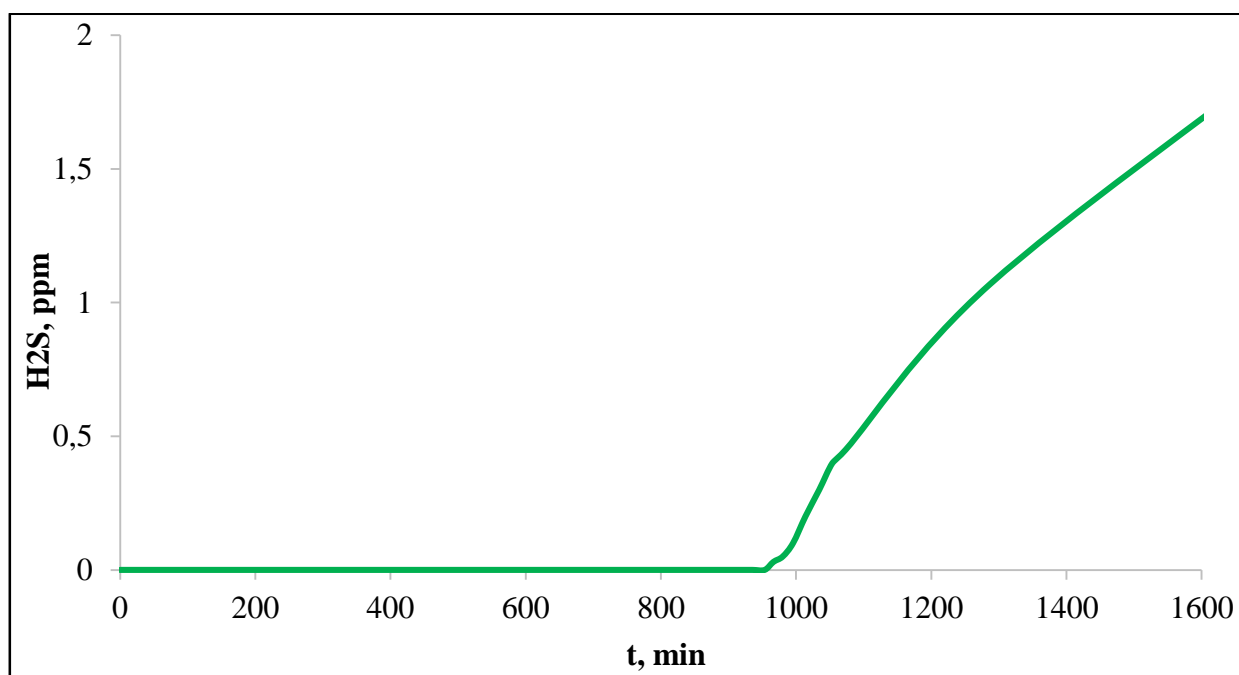


Fig. 3-28 H<sub>2</sub>S Breakthrough curve of RBAA1 not modified

These results point to the beneficial effects of the basic alkaline treatments: Filtrasorb has the lower adsorption capacity because it is an activated carbon free of additives and so with lower basic properties which favor the adsorption of H<sub>2</sub>S (see Tab 3-1).

In fact, the presence of metal ions, such as copper and chromium, in the sample Norit RGM3 enhance H<sub>2</sub>S adsorption capacity promoting the adsorption/oxidation mechanism. Moreover the presence of Cu, in the form of CuO oxide, favors the formation of sulphides according to equation:



Furthermore, copper ions eventually also present, can contribute to the improvement by the equation:



The best performance is obtained with the sample RBAA1 modified with 15% wt of KOH solution, because the basic sites favor the chemical adsorption of  $\text{H}_2\text{S}$  according to the equation:



Figure 3-29 shows the breakthrough curves of the samples Filtrasorb not treated and treated with a  $\text{Na}_2\text{CO}_3$ ,  $\text{NaOH}$  and  $\text{KOH}$  solutions.

The best performances, in terms of breakthrough time at 0.5 ppm (101 min) and moles of  $\text{H}_2\text{S}$  adsorption capacity (0.2 mmol/g), are obtained for the Filtrasorb treated with  $\text{KOH}$ .

However, it appears that the functionalization with alkaline solutions, significantly improves the adsorbing capacity. Performance improvement through the impregnation with the sodium hydroxide can be explained by assuming its catalytic action in the formation of the intermediate  $\text{HS}^-$ . Bagreev and Bandoz [314] have proposed the following mechanism:



Similar considerations can be made for the sample Filtrasorb impregnated with  $\text{KOH}$  solution.

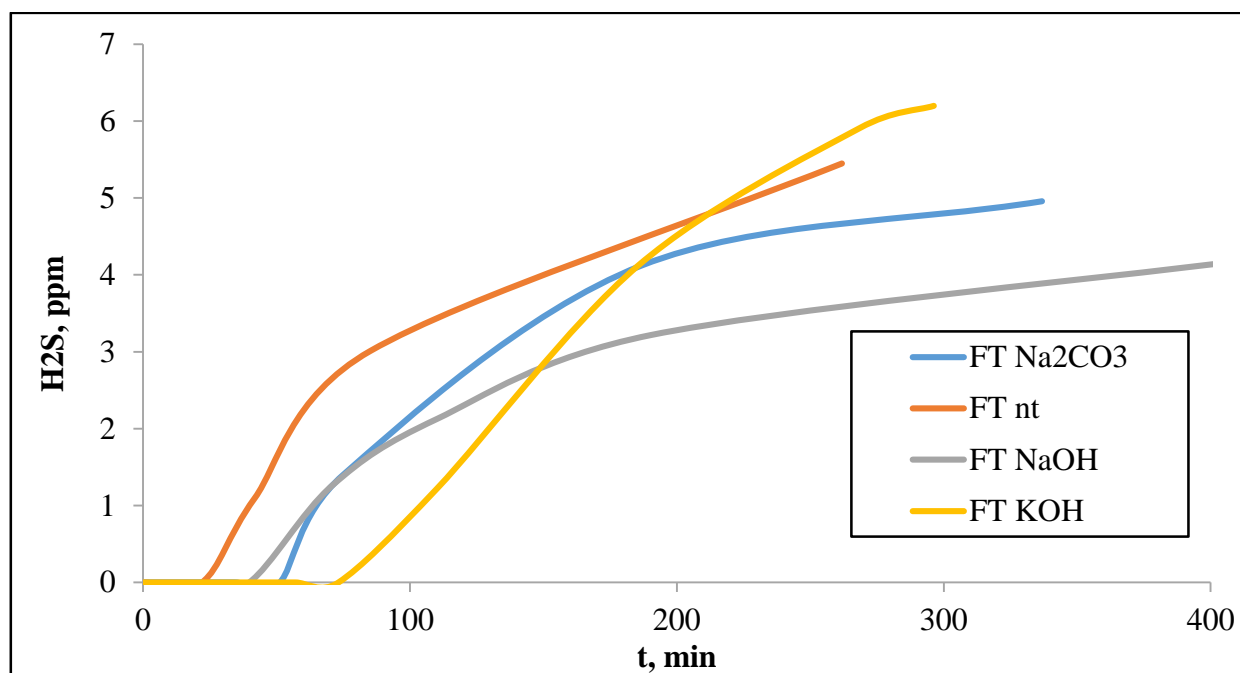


Fig. 3-29 H<sub>2</sub>S Breakthrough curve for Filtrasorb not treated and modified

For the category Filtrasorb, the higher breakthrough times are found for the sample functionalized with KOH. The previously described kinetic mechanism explains the increase of the adsorbing capacity for this sample. The best performance of the modified sample with KOH can probably also due to the higher surface area compared to the other activated carbons. For this type of activated carbons, it is evident that the surface area plays a decisive role on adsorbent capacity (as also happened in the case of HCl).

Figure 3-30 shows the breakthrough curves for the samples Norit RGM3 not treated and treated. Also for Norit samples can be considered the same kinetics reaction used for samples Filtrasorb.

The curve of untreated Norit shows a delay time of about 520 min, after which the H<sub>2</sub>S concentration increases gradually with time. Curves of all modified carbons show high delay time. The breakthrough curves of Norit NaOH and Norit KOH are similar, showing the same breakthrough time of 795 min, followed by a steep increase of H<sub>2</sub>S concentration. The best performance is exhibited by Norit Na<sub>2</sub>CO<sub>3</sub> that gives the longest operating time (840 min), followed by a slow rise of H<sub>2</sub>S concentration.

Considering the very complex surface of activated carbons, the H<sub>2</sub>S adsorption can be related to several types of adsorbing sites: for example, a dipole-dipole interaction can be established between H<sub>2</sub>S and phenolic or chinonic groups [310-313].

The increased performances of modified Norit can be related to an increase of basic groups concentration at the surface of the materials compared to raw sample. This leads to a stronger interaction with the acid H<sub>2</sub>S.

The similar performances of the samples treated with NaOH and KOH appear unexpected because the sample Norit NaOH, containing a higher amount of the basic compound, is expected to adsorb a higher amount of H<sub>2</sub>S. An explanation of this behavior could be that the high content of Na in Norit NaOH causes some occlusion of the micropores, leading to a reduction of surface area (Table 3.6) and thus reducing the amount of H<sub>2</sub>S adsorbed. A similar effect was found in the adsorption of HCl (see par. 3.22.3).

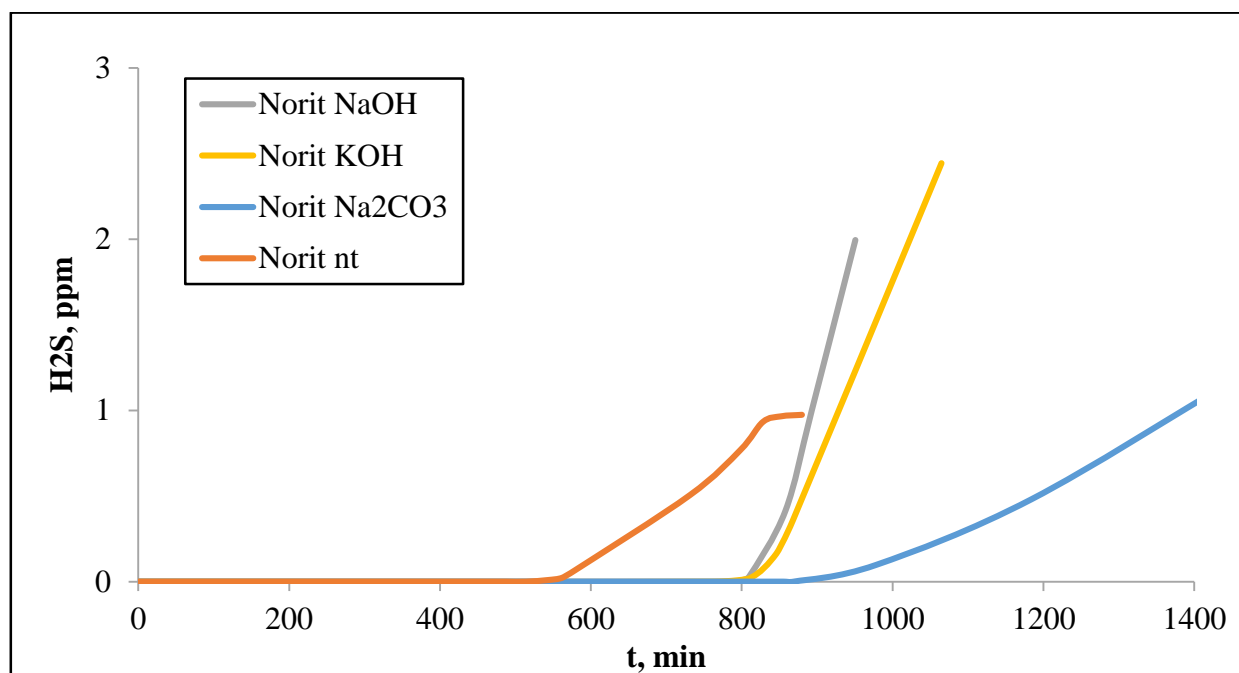


Fig.3-30 H<sub>2</sub>S Breakthrough curve for Norit RGM3 not treated and modified

Figure 3-31 shows the breakthrough curves of the samples Zeolite13X not treated and treated.

In view of the discussion of the H<sub>2</sub>S adsorption data, it is worth noting here that the cations initially present in the zeolite (Na<sup>+</sup>, K<sup>+</sup>, Ca<sup>2+</sup>, Mg<sup>2+</sup>) are replaced in large amount by Cu<sup>2+</sup> or Zn<sup>2+</sup> in the samples prepared by ion exchange, while they are scarcely or not at all replaced in the samples prepared by impregnation. It cannot be excluded that this can affect in some extent H<sub>2</sub>S adsorption. It is probable that Cu and Zn are present as the oxides CuO and ZnO in the impregnated zeolites.

The breakthrough times are longer for all modified zeolites compared to the parent zeolite. The impregnated samples 13X\_Im\_Zn and 13X\_Im\_Cu show similar breakthrough times (63 and 70 min) and also similar curves with the presence of inflection points. The breakthrough times (when H<sub>2</sub>S concentration starts to increase) of the exchanged samples are longer (85 and 200 min). It is worth noting the peculiar behavior of the sample 13X\_Ex\_Cu: this material shows a much longer breakthrough time and a very slow increase of H<sub>2</sub>S concentration after the breakthrough.

Several effects can be supposed. It can be assumed that H<sub>2</sub>S is chemisorbed on 13X zeolite by an acid-base reaction [310], according to Equation:



where only  $\text{Na}^+$  cation is considered for simplicity, but other cations present in the zeolite, that is  $\text{K}^+$ ,  $\text{Ca}^{2+}$ ,  $\text{Mg}^{2+}$ , can give similar reactions. Moreover, similar acid/base reactions can occur in exchanged zeolites where  $\text{Na}^+$  is substituted by  $\text{Cu}^{2+}$  or  $\text{Zn}^{2+}$ : in this case a stronger interaction is expected considering the high stability of  $\text{CuS}$  and  $\text{ZnS}$  compounds.

As regards the impregnated zeolites,  $\text{H}_2\text{S}$  adsorption is due both to the cations present in the zeolite cavities and to the basic oxides  $\text{CuO}$  or  $\text{ZnO}$ , that can react with  $\text{H}_2\text{S}$  according to Eqs. (3.59) and (3.60) [310]:



It was observed that the substitution of  $\text{Na}^+$  in the parent material with divalent cations such as  $\text{Cu}^{2+}$  or  $\text{Zn}^{2+}$  leaves more free space in the zeolitic cages and increases the polarity of the material, thus favouring the adsorption of a polar molecule. However, this effect, that could be important for adsorption of  $\text{HCl}$ , seems to play a minor role for  $\text{H}_2\text{S}$  adsorption: in fact, Fig. 3-31 shows that the sample 13X\_Ex\_Zn, that has the highest degree of exchange, is not the most effective adsorbent: the adsorption performance of this material is definitely lower compared to 13X\_Ex\_Cu and not very different from that of the impregnated samples. It appears clearly from Fig. 3-31 that the most effective  $\text{H}_2\text{S}$  adsorbent among the studied zeolites is 13X\_Ex\_Cu. This can be related to the known affinity of  $\text{Cu}^{2+}$  for  $\text{S}^{2-}$  ions and suggests that the main factor determining the  $\text{H}_2\text{S}$  adsorption properties of these materials is the specific interaction between  $\text{S}^{2-}$  and the metal cation [310].



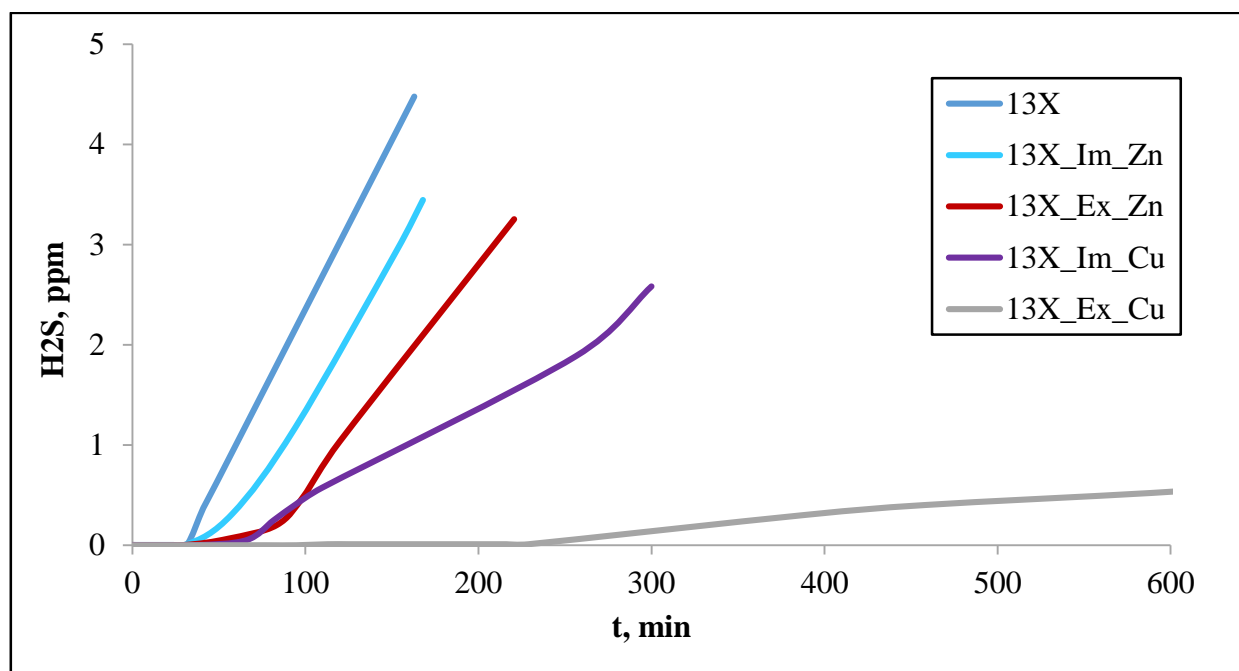


Fig. 3-31 H<sub>2</sub>S Breakthrough curve for Zeolite 13X not treated and modified

Table 3-18 summarize the breakthrough times at 0.5 ppm for 13X zeolites and active carbons not treated and modified. The results show that, treatment with basic solutions, improves the adsorption properties of activated carbons not treated.

In the case of Filtrasorb, all treatments lead to an increase of the performance compared to not treated sample. The best results are obtained for the sample Filtrasorb KOH, which presents a breakthrough time at 0.5 ppm of 101 minutes with a total amount of H<sub>2</sub>S adsorbed approximately 0.2 mmol/g, almost 1.5 higher than the other two treated samples and about 3 times greater compared to not treated Filtrasorb.

Treatments with basic solutions improve the performance of Norit RGM3: the effect is limited with Norit NaOH and Norit KOH, but appears larger with Norit Na<sub>2</sub>CO<sub>3</sub>, that exhibits a much longer delay time and a much larger amount of H<sub>2</sub>S adsorbed (1222 min at 0.5 ppm with 2.46 mmol/g adsorbed), which presents a breakthrough time to 0.5 ppm of about 2 times higher than the untreated Norit.

As regards the other sample considered as a reference material, the RBAA1 (modified by supplier with a KOH solution at 15% wt), it presents a breakthrough time at 0.5 ppm equal to 1070 min with H<sub>2</sub>S adsorbing capacity of 2.05 mmol/g.

<b>Sample</b>	<b>t @ 0.5 ppm (min)</b>	<b>mmol H<sub>2</sub>S ads @ 0.5 ppm (mmol g<sup>-1</sup>)</b>
<b>FT tq</b>	33	0.063
<b>FT NaOH</b>	63	0.12
<b>FT KOH</b>	101	0.20
<b>FT Na<sub>2</sub>CO<sub>3</sub></b>	68.5	0.13
<b>RGM3 tq</b>	725	1.46
<b>RGM3 NaOH</b>	841	1.69
<b>RGM3 KOH</b>	830	1.67
<b>RGM3 Na<sub>2</sub>CO<sub>3</sub></b>	1222	2.46
<b>RBAA1</b>	1070	2.05
<b>13X</b>	47	0.09
<b>13X Ex Cu</b>	580	1.17
<b>13X Ex Zn</b>	111	0.22
<b>13X Im Cu</b>	99	0.20
<b>13X Im Zn</b>	76	0.15

Tab. 3-18 Breakthrough times and adsorbed moles at 0.5 ppm for 13X zeolites and active carbons not treated and modified

For Zeolite 13X the results have shown improved performances of modified 13X zeolites compared to the untreated zeolite: the best results have been obtained with the zeolite ion exchanged with Cu that gives a breakthrough time of 580 min at 0.5 ppm (1.17 mmol H<sub>2</sub>S/g) compared to a breakthrough time of 47 min of the not treated zeolite (0.09 mmol H<sub>2</sub>S/g).

Also for H<sub>2</sub>S adsorption tests, this results confirm the efficiency of the procedure developed in this PhD thesis.

### 3.22.5 Mathematic models of experimental data

Adsorption data can be modeled in order to obtain information of adsorption kinetics.

From the experimental results, which reproduce the initial trend of the breakthrough curves, the complete function can be obtained by curve fitting of the same using some models able to reproduce the adsorption of HCl and H<sub>2</sub>S on activated carbons and zeolites 13X.

In this PhD thesis have been considered two mathematical models: Weibull with 4 parameters and Logistics with 5 parameters.

Among the models that return curves with sigmoid pattern, commonly used, such as Gompertz, Logistics, Hill, Chapman-Richards, Morgan-Mercer-Flodin, Lomolino, the Weibull parameters 4 is the most suitable to approximate the experimental data obtained leading to breakthrough curve of sigmoidal shape.

Some sigmoidal functions are symmetrical respect to the inflection point, while others, including the Weibull are not symmetrical, and effectively approximate the type of breakthrough curves obtained in this thesis (not symmetrical with respect to the inflection point).

Adding the number of parameters in these models, they increase the possibility of regress the shape of the curve, the inflection point, the intersection of the axes and the asymptotes. In particular, the Weibull function, introduced by the physical Swedish Waloddi Weibull is the most versatile because it returns a good approximation since version with only 2 parameters and is used in the modeling of large classes of data in various fields, including the engineering and medical research [315-318].

The Weibull model equation with 4 parameters is the following:

$$y = a * [1 - e^{-(\frac{x-x_0+b*\ln 2^{\frac{1}{c}}}{b})^c}] \quad (3.61)$$

where

$y = c/c_0$  is the ratio between the concentration of compounds ( $H_2S$  or  $HCl$ ) in the effluent stream and the initial concentration;

$x$  = time;

$a$  = upper asymptote;

$b$  = scale parameter;

$c$  = shape parameter: slope;

$x_0$  = inflection point.

The second equation used for curve fitting is the Logistics with 5 parameters (5PL).

The use of this model allows to process experimental data affected by asymmetry.

The commonly used symmetrical pattern, a 4-Parameter Logistic (4PL,  $g = 1$ ) are not able to fitting asymmetric curves and so involves a certain error percentage. For this reason, the 5PL, is able to return a higher accuracy [319].

The equation of the logistics to 5 parameters is the following:

$$y = d + \frac{(a-d)}{(1+(\frac{x}{c})^b)^g} \quad (3.62)$$

where

$y = c/c_0$  is the ratio between the concentration of compounds ( $H_2S$  or  $HCl$ ) in the effluent stream and the initial concentration;

$x$  = time;

$a$  = upper asymptote;

$b$  = hill slope;

$c$  = inflection point;

$d$  = lower asymptote;

$g$  = asymmetry factor.

Table 3-19 shows the effect of the parameters  $a$ ,  $b$  and  $d$  on the slope of the logistic function:

Case	$a, d$	$b$	Slope
1	$a > d$	$> 0$	negative
2	$a > d$	$< 0$	positive
3	$a < d$	$> 0$	positive
4	$a < d$	$< 0$	negative

Tab. 3-19 Correlation between 5PL parameters

The cases 1 and 4 of Table 3-19 are able to model data with decreasing trend, the cases 2 and 3 are suitable for data with increasing trend.

It is possible to summarize the effect of the parameters  $a$ ,  $b$ ,  $c$ ,  $d$  and  $g$  on 5PL curve in the following way:

$a$  = Check the upper asymptote position. With  $b$  and  $d$  controls the slope of the curve. The curve approaches the asymptote  $a$  at small concentrations for  $b > 0$  and at large concentrations for  $b < 0$ ;

$b$  = Check the speed of the transition between the asymptotes of the curve. Its mark, with  $a$  and  $d$  orders, controls the slope of the curve. Alone controls the speed to asymptote  $a$  and with  $g$  controls the asymptote approaching  $d$ ;

$c$  = Control position of the transition region;

$d$  = Check the lower asymptote position. With  $b$  and  $a$  controls the slope of the curve. The curve approaching asymptote  $d$  at small concentrations for  $b < 0$  and at large concentrations for  $b > 0$ ;

$g$  = With  $b$  controls the speed of approach to asymptote  $d$ .

Fitting of experimental data using the 5PL could be more not so easy as for 4PL model. However, recent improvements in numerical methods and greater accuracy in data acquisition, have made it easier to use this model in comparison to the 4PL model.

As an example figures 3-32:3-35 show the data obtained for each type of activated carbon (Filtrisorb, Norit RGM3, RBAA1) and zeolite (13X) used in this thesis. The graphs obtained show that both models are able to reproduce the experimental data.

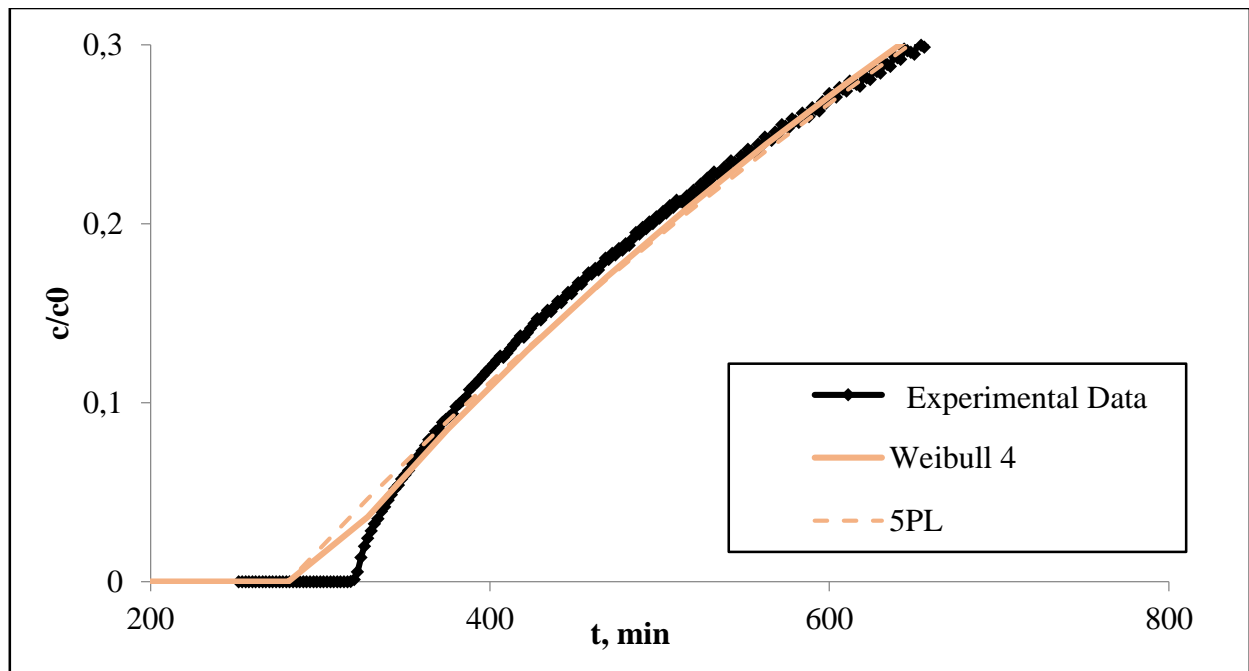


Fig. 3-32 Breakthrough curve for Filtrasorb

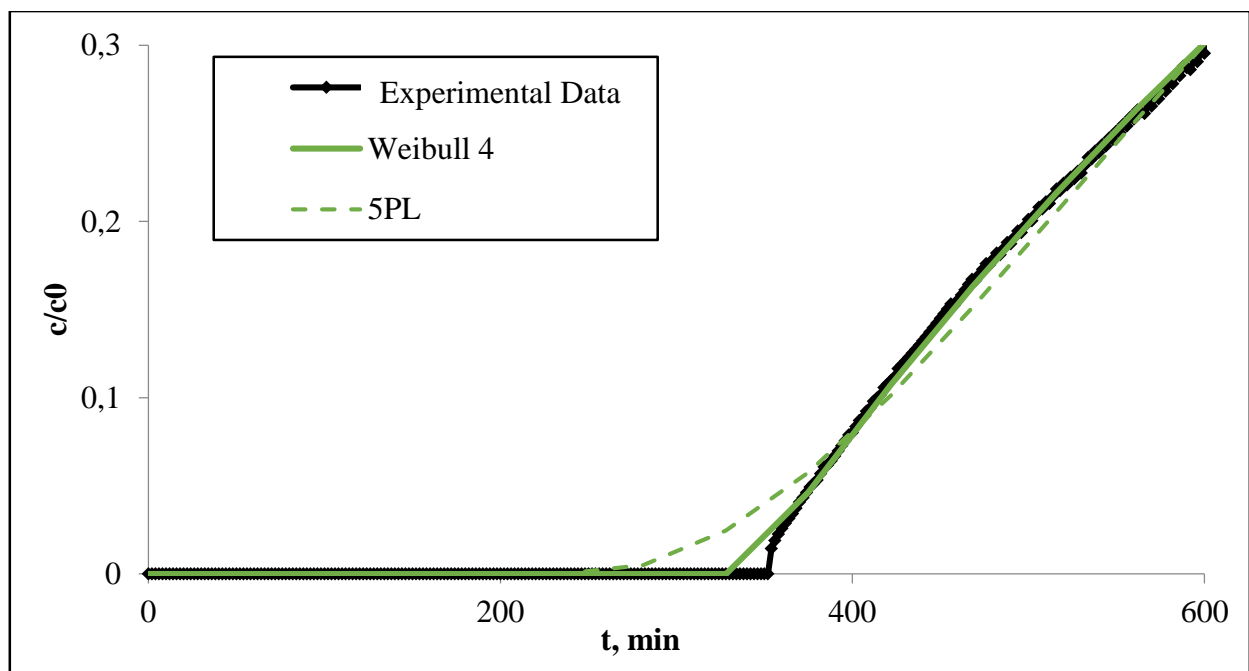


Fig. 3-33 Breakthrough curve for Norit RGM3

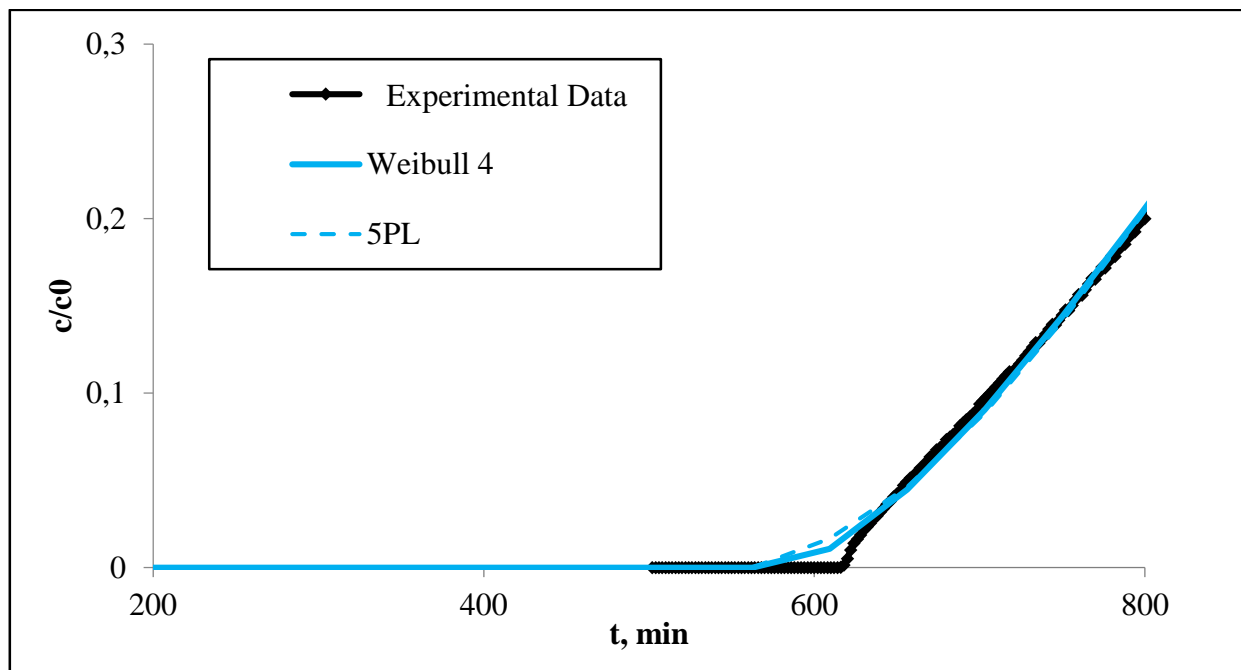


Fig. 3-34 Breakthrough curve for RBAA1

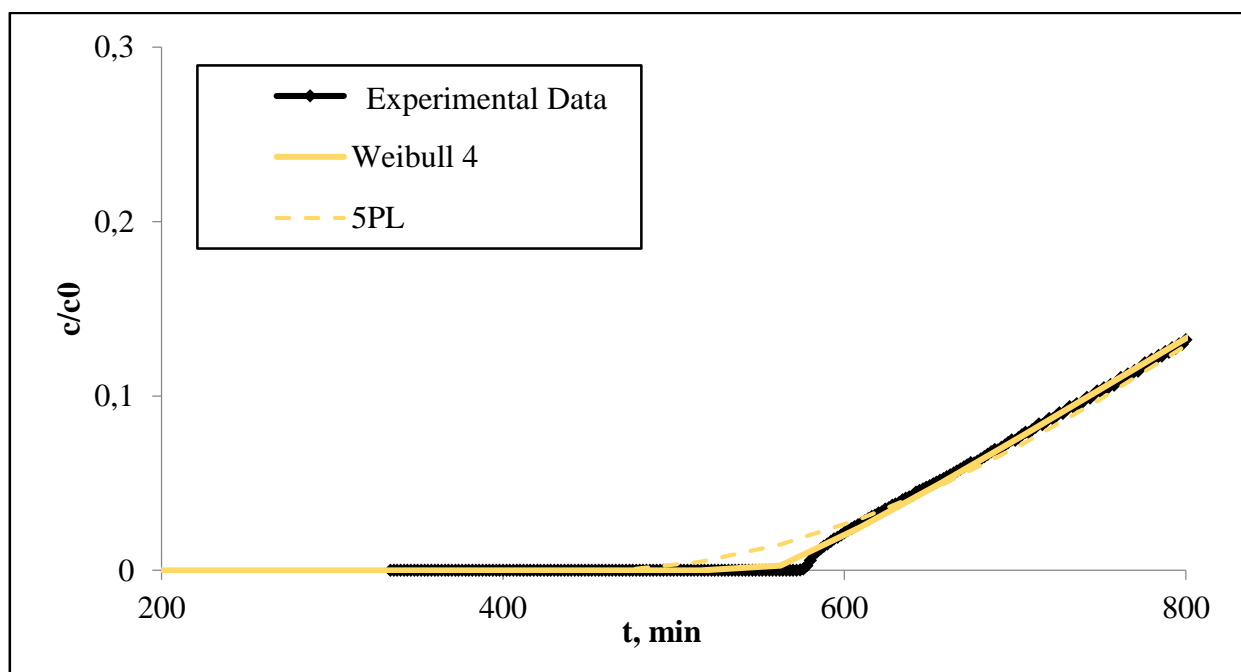


Fig. 3-35 Breakthrough curve for Zeolite 13X

Samples	a	b	c	x <sub>0</sub>	Number of Iterations	R <sup>2</sup>
FT	1	1041	0.9274	1000	4780	0.9953
RGM3	1	735.6	0.9767	848	4515	0.9997
RBAA1	1	574	1.5364	1031.5	4515	0.9989
13X	1	1225	1.2488	1457	4893	0.9997

Tab. 3-20 Regression results for the model Weibull with 4 parameters

<b>Samples</b>	<b>a</b>	<b>b</b>	<b>c</b>	<b>d</b>	<b>g</b>	<b>Number of Iterations</b>	<b>R<sup>2</sup></b>
<b>FT</b>	1	-14.22	2093.9	-0.5885	0.0348	1722	0.9849
<b>RGM3</b>	1	-1.81	2.88	-0.0042	18775	1042	0.9842
<b>RBAA1</b>	1	-3.16	51.37	-0.0092	9053	1497	0.9875
<b>13X</b>	1	-1.89	6.37	-0.0049	18935	1420	0.9839

Tab. 3-21 Regression results for the model 5-Parameter Logistic (5PL)

In addition to the value of the parameters, Tables 3-20 and 3-21 also give the value of the coefficient of determination  $R^2$ . This last parameter is an index of the accuracy of the numerical model used: if the  $R^2$  is close to 1 means that the regression predicts the dependent variable and the experimental data, if it is close to 0 means that the results are not reliable.

In the case of Weibull with 4 parameters have been obtained a coefficient of determination never less than 0.9935, while, in the case of Logistics with 5 parameters,  $R^2$  is never less than 0.9839.

From Tables 3-20 and 3-21 it can be seen that the model Logistic 5 parameters require a less number of iterations; however, the Weibull model to 4 parameters returns a value of the highest coefficient of determination and, therefore, greater fairness in the approximation of the experimental data.

## References

1. Evers AA (2003) Go to where the market is! Challenges and opportunities to bring fuel cells to the international market. *Int J Hydrogen Energy* 28:725–733
2. <http://www.fch.europa.eu/access>. Accessed 11 Feb 2017
3. <http://www.verticale.net/un-centro-di-competenza-permanente-per-7463>. Accessed 11 Feb 2017
4. <http://www.now-gmbh.de/en/about-now/funding-programmes/national-innovation-pro-gramme-nip.html>. Accessed 11 Feb 2017
5. <http://www.iphe.net/partners/republicofkorea.html>. Accessed 11 Feb 2017
6. <http://www.iphe.net/partners/japan.html>. Accessed 11 Feb 2017
7. <http://www.iphe.net/partners/china/research.html>. Accessed 11 Feb 2017
8. <http://www.hydrogen.energy.gov/access>. Accessed 11 Feb 2017
9. Levin DB, Chahine R (2010) Challenges for renewable hydrogen production from biomass. *Int J Hydrogen Energy* 35:4962–4969
10. Bensaid S, Specchia S, Federici F, Saracco G, Specchia V (2009) MCFC-based marine APU: comparison between conventional ATR and cracking coupled with SR integrated inside the stack pressurized vessel. *Int J Hydrogen Energy* 34:2026–2042
11. European Environment Agency (2005) Climate change and a European low-carbon energy system. Report 1/2005. EEA (European Environment Agency) and OPOCE (Office for Official Publications of the European Communities)
12. Feige AK (2007) Effect of the growing bioenergy market on the availability of agricultural raw materials and products. *Zuckerindustrie* 132:687–693
13. Petterson A, Wellinger, A Biogas upgrading—developments and innovations. IEA Bioenergy. [www.iea-biogas.net/publicationspublic.htm](http://www.iea-biogas.net/publicationspublic.htm)
14. Ribeiro RP, Sauer TP, Lopes FV, Moreira RF, Grande CA, Rodrigues AE (2008) Adsorption of CO<sub>2</sub>, CH<sub>4</sub>, and N<sub>2</sub> in activated carbon honeycomb monolith. *J Chem Eng* 53:2311–2317
15. Hernandez S, Scarpa F, Fino D, Conti R (2011) Biogas purification for MCFC application. *Int J Hydrogen Energy* 36:8112–8118
16. Fangmark IE, Hammarstrom LG, Stromqvist ME, Ness AL, Norman PR, Osmond NM (2002) Estimation of activated carbon adsorption efficiency for organic vapours I. A strategy for selecting test compounds. *Carbon* 40:2861–2869
17. Andriani D, Wresta A, Atmaja TD, Saepudin A (2014) A review on optimization production and upgrading biogas through CO<sub>2</sub> removal using various techniques. *Appl Biochem Biotechnol* 172:1909–1928
18. Ryckebosch E, Drouillon M, Vervaeren H (2011) Techniques for transformation of biogas to biomethane. *Biomass Bioenergy* 35:1633–1645
19. Wheless E, Pierce J (2004) Siloxanes in landfill and digester gasupdate. Los Angeles County Sanitation Districts and SCS Energy, Whittier (Canada) and Long Beach (California)
20. Tjaden B, Gandiglio M, Lanzini A, Santarelli M, Jarvinen M (2014) Small-scale biogas- SOFC plant: technical analysis and assessment of different fuel reforming options. *Energy Fuels* 28:4216–4232
21. Wolak F (2012) Fuel cell power plants: biofuel case study—Tulare, CA. In: DOE- NREL Workshop, Golden, Colorado, June 11–13. [http://www1.eere.energy.gov/hydrogenandfuelcells/wkshp\\_biogas\\_fuel\\_cells.html](http://www1.eere.energy.gov/hydrogenandfuelcells/wkshp_biogas_fuel_cells.html)
22. Van Herle J, Marechal F, Leuenberger S, Membrez Y, Bucheli O, Favrat D (2004) Process flow model of solid oxide fuel cell system supplied with sewage biogas. *J Power Sources* 131:127–141
23. Trendewicz A, Braun R (2013) Techno-economic analysis of solid oxide fuel cell-based combined heat and power systems for biogas utilization at wastewater treatment facilities. *J Power Sources* 233:380–393
24. Arnold M (2009) Reduction and monitoring of biogas trace compounds. VTT Research Notes 2496, VTT Technical Research Centre of Finland, Espoo, Finland (2009)
25. Pfeifer T, Nousch L, Lieftink D, Modena S (2013) System design and process layout for a SOFC micro-CHP unit with reduced operating temperatures. *Int J Hydrogen Energy* 38:431–439
26. Du W, Parker W (2012) Modeling volatile organic sulphur compounds in mesophilic and thermophilic anaerobic digestion of methionine. *Water Res* 46:539–546



27. Vassilev S, Baxter D, Andersen L, Vassileva C (2010) An overview of the chemical composition of biomass. *Fuel* 89:913–933
28. Sklorz M, Schnelle-Kreis J, Gottlieb A, Kuhner N, Schmid B (2003) Untersuchungen zum Einsatz von Oxidationskatalysatoren an landwirtschaftlichen Biogas-Verbrennungsmotoren. Bayerisches Institut für Angewandte Umweltforschung und –technik, Augsburg, Germany (2003)
29. Papurello D, Soukoulis C, Schuhfried E, Cappellin L, Gasperi F, Silvestri S, Santarelli M, Biasioli F (2012) Monitoring of volatile compound emissions during dry anaerobic digestion of the organic fraction of municipal solid waste by proton transfer reaction time-of-flight mass spectrometry. *Bioresour Technol* 126:254–265
30. Papadias D, Ahmed S, Kumar R (2012) Fuel quality issues with biogas energy—An economic analysis for a stationary fuel cell system. *Energy* 44:257–277
31. Rasmussen JFB, Hagen A, Thyden K (2011) Durability of solid oxide fuel cells using sulphur containing fuels. *J Power Sources* 196:7271–7276
32. Cheng Z, Wang JH, Choi Y, Yang L, Lin MC, Liu M (2011) From Ni–YSZ to sulphur-tolerant anode materials for SOFCs: electrochemical behavior, in situ characterization, modeling, and future perspectives. *Energy Environ Sci* 4:4380–4409
33. Jeihanipour A, Aslanzadeh S, Rajendran K, Balasubramanian G, Taherzadeh MJ (2013) High-rate biogas production from waste textiles using two-stage process. *Renew Energy* 52:128–135
34. Weiland P (2010) Biogas production: current state and perspectives. *Appl Microbiol Biotechnol* 85:849–860
35. Persson M (2003) Utvärdering av uppgraderingstekniker för biogas, 85 pp. Report SGC 142, Svenskt Gastekniskt Center, Malmö, Sweden, Nov 2003
36. Iovane P, Nanna F, Ding Y, Bikson B, Molino A (2014) Experimental test with polymeric membrane for the biogas purification from CO<sub>2</sub> and H<sub>2</sub>S. *Fuel* 135:352–358
37. Schomaker, AHM, Boerboom AAM, Visser A, Pfeifer AE (2000) Anaerobic digestion of agro-industrial wastes: information networks e technical summary on gas treatment. AD-NETT, Nijmegen, Nederland, Report No.: FAIR-CT 96-2083 (DG12-SSMI)31 Aug 2000
38. Bteuten S, Pasel C, Luckas M, Bathen D (2013) Trace level adsorption of toxic sulphur compounds, carbon dioxide, and water from methane. *J. Chemical Engineering* 58:2465–2473
39. Ferreira D, Magalhaes R, Taveira P, Mendes A (2011) Effective adsorption equilibrium isotherms and breakthroughs of water vapor and carbon dioxide on different adsorbents. *Ind Eng Chem Res* 50:10201–10210
40. Li G, Xiao P, Webley PA, Zhang J, Singh R (2009) Competition of CO<sub>2</sub>/H<sub>2</sub>O in adsorption based CO<sub>2</sub> capture. *Energy Procedia* 1:1123–1130
41. Iwai Y, Oka N, Yamanishi T (2009) Influence of framework silica-to-alumina ratio on the water adsorption and desorption characteristics of MHI-CaX/CaY zeolite. *J Phys Chem Solids* 70:881–888
42. Ribeiro AM, Sauer TP, Grande CA, Moreira RFPM, Loureiro JM, Rodrigues AE (2008) Adsorption equilibrium and kinetics of water vapor on different adsorbents. *Ind Eng Chem Res* 47:7019–7026
43. Lee YC, Weng LC, Tseng PC, Wang CC (2015) Effect of pressure on the moisture adsorption of silica gel and zeolite 13X adsorbents. *Heat Mass Transf* 51:441–447
44. Ozensoy E, Szanyi J, Peden CHF (2005) Interaction of water with ordered  $\theta$ -Al<sub>2</sub>O<sub>3</sub> ultrathin films grown on NiAl(100). *J Phys Chem B* 109:3431–343
45. Kittaka S, Yamaguchi K, Takahara S (2012) High physisorption affinity of water molecules to the hydroxylated aluminum oxide (0 0 1) surface. *J Colloid Interface Sci* 368:552–557
46. Wellinger A, Lindberg A (2005) Biogas upgrading and utilisation. IEA Bioenergy Task 24: Energy From Biological Conversion of Organic Waste (2005)
47. Krich K, Augenstein A, Batmale J, Benemann J, Rutledge B, Salour D (2005) Upgrading dairy biogas to biomethane and other fuels. In: Andrews K (ed) Biomethane from dairy waste—a sourcebook for the production and use of renewable natural gas in California. Clear Concepts, California, pp 47–69
48. Jonsson O (2004) Biogas upgrading and use as transport fuel. Swedish Gas Center, Malmö Sweden, 5 pp. Report
49. Bourque H (2006) Use of liquefied biogas in transport sector. In: Conference sur les crédits CO<sub>2</sub> et la valorisation du biogaz, 20 Apr 2006. [www.apcas.qc.ca](http://www.apcas.qc.ca)
50. Enggas. Gilbertsville: Engineered Gas Systems. Worldwide Inc. (2003). November 2007.

<http://www.enggas.com>

51. Gomes VG, Hassan MM (2001) Coal seam methane recovery by vacuum swing adsorption. *Separ Purif Technol* 24:189–196
52. Welink JH, Dumont M, Kwant K (2014) Groen Gas: Gas van aardgaskwaliteit uit biomassa: update van de studie uit, Jan 2007, Senternovem, Nederland 2004, 34 p [Report]
53. Kim TJ, Li B, Hagg MB (2004) Novel fixed-site-carrier polyvinylamine membrane for carbon dioxide capture. *J Polym Sci, Part B Polym Phys* 42:4326–4336
54. Roks MFM, Luning L, Coops O (1997) Feasibility of applying new membrane for processing landfill gas to natural gas quality at low pressure (8 bar) [Haalbaarheid toepassing nieuw membraan voor opwerking stortgas naar aardgaskwaliteit bij lage druk (8 bar)]. Aquilo Gas Separation bv, Nederland, 57 p. Report
55. Guha AK, Majumdar S, Sirkar KK (1992) Gas separation Modes in a hollow fiber contained liquid membrane permeator. *Ind Eng Chem Res* 31:593–604
56. Esteves IAAC, Mota JPB (2002) Simulation of a new hybrid membrane/pressure swing adsorption process for gas separation. *Desalination* 148:275–280
57. Strevett KA, Vieth RF, Grasso D (1995) Chemo-autotrophic biogas purification for methane enrichment: mechanism and kinetics. *Chem Eng J Biochem Eng J* 58:71–79
58. Persson M (2003) Evaluation of upgrading techniques for biogas. School of Environmental Engineering, Lund. <http://www.sgc.se/dokument/Evaluation.pdf>
59. Tynell A (2005) Microbial growth on pall-rings—A problem when upgrading biogas with the technique absorption with water wash. Svenska Biogas for eningen and Swedish Gas Center, Stockholm, Sweden, 53 p. Report No.: 610408
60. Rutledge B (2005) California biogas industry assessment white paper. WestStart-Calstart, Pasadena, USA, 38 p. Report
61. Miltner M, Makaruk A, Harasek M (2008) Application of gas permeation for biogas upgrade—operational experiences of feeding biomethane into the Austrian gas grid. In: 16th European biomass conference and exhibition. Valencia, Spain, pp. 1905–1911
62. Makaruk A, Miltner M, Harasek M (2010) Membrane biogas upgrading processes for the production of natural gas substitute. *Sep Purif Technol* 74:83–92
63. Di Natale F, Erto A, Lancia A, Musmarra D (2009) A descriptive model for metallic ions adsorption from aqueous solutions onto activated carbons. *J Hazard Mater* 169:360–369
64. Schell WJ, Houston CD (1983) Use of membranes for biogas treatment. *Energy Prog* 3:96–100
65. Roehr M, Wimmerstedt R (1990) A comparison of two commercial membranes used for biogas upgrading. *Desalination* 77:331–345
66. Rautenbach R, Welsch K (1993) Treatment of landfill gas by gas permeation—pilot plant results and comparison to alternatives. *Desalination* 90:193–207
67. Favre E, Bounaceur R, Roizard D (2009) Biogas, membranes and carbon dioxide. *J Membr Sci* 328:11–14
68. Sridhar S, Smitha B, Aminabhavi TM (2007) Separation of carbon dioxide from natural gas mixtures through polymeric membranes: a review. Membrane separations division, center of excellence in polymer science, Karnatak University—India. *Sep Purif Rev* 36:113–174
69. Stern SA, Krishnakumar B, Charati SG, Amato WS, Friedman AA, Fuess DJ (1998) Performance of a bench-scale membrane pilot plant for the upgrading of biogas in a wastewater treatment plant. *J Membr Sci* 151:63–74
70. Bhide BD, Stern SA (1993) Membrane processes for the removal of acid gases from natural gas. Process configurations and optimization of operative conditions. *J Membr Sci* 81:209–237
71. Bhide BD, Stern SA (1993) Membrane processes for the removal of acid gases from natural gas. II. Effects of operating conditions, economic parameters, and membrane properties. *J Membr Sci* 81:239–252
72. Hao J, Rice PA, Stern SA (2002) Upgrading low-quality natural gas with H<sub>2</sub>S- and CO<sub>2</sub>-selective polymer membranes: Part I. Process design and economics of membrane stages without recycle streams. *J Membr Sci* 209:177–206
73. Hao J, Rice PA, Stern SA (2008) Upgrading low-quality natural gas with H<sub>2</sub>S- and CO<sub>2</sub>-selective polymer membranes: Part II. Process design, economics, and sensitivity study of membrane stages with recycle streams. *J Membr Sci* 320:108–122
74. Persson M, Jönsson O (2006) Wellinger “Biogas upgrading to vehicle fuel standards and grid injection. IEA

- Bioenergy Task 37—Energy from biogas and landfill gas. Sweden & Switzerland. [www.iea-biogas.net](http://www.iea-biogas.net)
75. Miltner M, Makaruk A, Krischan J, Harasek M (2012) Chemical-oxidative scrubbing for the removal of hydrogen sulphide from raw biogas: potentials and economics. *Water Sci Technol* 66:1354–1360
  76. Baker WR, Lokhandawa K (2008) Natural gas processing with membranes: an overview. Membrane Technology and Research, Inc. 1360 Willow Road, Suite 103, Menlo Park, California 94025. *Inf Eng Chem Res* 47:2109–2121
  77. Bernardo P, Drioli E, Golemme G (2009) Membrane gas separation: a review/state of the art. *Ind Eng Chem Res* 48:4638–4663
  78. Bhide BD, Voskericyan A, Stern SA (1998) Hybrid processes for the removal of acid gases from natural gas. *J Membr Sci* 140:1–7
  79. Hagen M, Polman E, Jensen J, Myken A, Jonsson O, Dahl A (2001) Adding gas from bio- mass to the gas grid. Swedish Gas Center, Malmo Sweden, July 2001, pp 144. Report SCG 118
  80. Arimi MM, Knodel J, Kiprop A, Namango SS, Zhang Y, Geissen SU (2015) Strategies for improvement of biohydrogen production from organic-rich wastewater: a review. *Biomass Bioenergy* 75:101–118
  81. Luo G, Angelidaki I (2012) Integrated biogas upgrading and hydrogen utilization in an anaerobic reactor containing enriched hydrogenotrophic methanogenic culture. *Biotechnol Bioeng* 109:2729–2736
  82. Tsang YF, Wang L, Chua H (2015) Simultaneous hydrogen sulphide and ammonia removal in a biotrickling filter: crossed inhibitory effects among selected pollutants and microbial community change. *Chem Eng J* 281:389–396
  83. Liu C, Zhao D, Yan L, Wang A, Gu Y, Lee DJ (2015) Elemental sulphur formation and nitrogen removal from wastewaters by autotrophic denitrifiers and anammox bacteria. *Biores Technol* 191:332–336
  84. Xu G, Peng J, Feng C, Fang F, Chen S, Xu Y, Wang X (2015) Evaluation of simultaneous autotrophic and heterotrophic denitrification processes and bacterial community structure analysis. *Appl Microbiol Biotechnol* 99:6527–6536
  85. Mora M, Dorado AD, Gamisans X, Gabriel D (2015) Investigating the kinetics of autotrophic denitrification with thiosulfate: modeling the denitrification mechanisms and the effect of the acclimation of SO-NR cultures to nitrite. *Chem Eng J* 262:235–241
  86. Robinson PJ, Luyben WL (2010) Integrated gasification combined cycle dynamic model: H<sub>2</sub>S absorption/stripping, water-gas shift reactors, and CO<sub>2</sub> absorption/stripping. *Ind Eng Chem Res* 49:4766–4781
  87. Huang X, Zhu D (2004) Review of technologies for removal of H<sub>2</sub>S. *Huaxue Gongye Yu Gongcheng Jishu* 25:47–49
  88. Hix R, Marshall LS (1990) Reactive absorption of hydrogen sulphide by a solution of sulphur dioxide in polyglycol ether. Preprints of Papers—Am Chem Soc, Division of Fuel, Chem 35:128–135
  89. Park D, Lee DS, Joung JY, Park JM (2005) Comparison of different bioreactor systems for indirect H<sub>2</sub>S removal using iron-oxidizing bacteria. *Process Biochem* 40:1461–1467
  90. Nasr MRJ, Abedinzadegan M (1995) Performance of a venturi jet scrubber for H<sub>2</sub>S removal by iron-complex solution. *Chem Eng Technol* 18:166–170
  91. Horikawa MS, Rossi F, Gimenes ML, Costa CMM, da Silva MGC (2004) Chemical absorption of H<sub>2</sub>S for biogas purification. *Braz J Chem Eng* 21:415–422
  92. Belmabkhout Y, De Weireld G, Sayari A (2009) Amine-bearing mesoporous silica for CO<sub>2</sub> and H<sub>2</sub>S removal from natural gas and biogas. *Langmuir* 25:13275–13278
  93. Chang M, Tseng T (1996) Gas-phase removal of H<sub>2</sub>S and NH<sub>3</sub> with dielectric barrier discharges. *J Environ Eng* 122:41–46
  94. Duan H, Yan R, Koe LCC, Wang X (2007) Combined effect of adsorption and biodegradation of biological activated carbon on H<sub>2</sub>S biotrickling filtration. *Chemosphere* 66:1684–1691
  95. Ho KL, Chung YC, Lin YH, Tseng CP (2008) Microbial populations analysis and field application of biofilter for the removal of volatile-sulphur compounds from swine wastewater treatment system. *J Hazard Mater* 152:580–588
  96. Lee EY, Lee NY, Cho KS, Ryu HW (2006) Removal of hydrogen sulphide by sulfate-resistant *Acidithiobacillus thiooxidans* AZ11. *J Biosci Bioeng* 101:309–314
  97. González-Sánchez A, Revah S, Deshusses MA (2008) Alkaline biofiltration of H<sub>2</sub>S odors. *Environ Sci Technol* 42:7398–7404

98. Jiang X, Yan R, Tay JH (2009) Simultaneous autotrophic biodegradation of H<sub>2</sub>S and NH<sub>3</sub> in a biotrickling filter. *Chemosphere* 75:1350–1355
99. Montebello AM, Fernández M, Almenglo F, Ramírez M, Cantero D, Baeza M, Gabriel D (2012) Simultaneous methylmercaptan and hydrogen sulphide removal in the desulphurization of biogas in aerobic and anoxic biotrickling filters. *Chem Eng J* 200–202:237–246
100. Fortuny M, Baeza JA, Deshusses MA, Gamisans X, Casas C, Lafuente J, Gabriel D (2008) Biological sweetening of energy gases mimics in biotrickling filters. *Chemosphere* 71:10–17
101. Fernández M, Ramírez M, Perez RM, Rovira R, Gabriel D, Gomez JM, Cantero D (2010) Hydrogen sulphide removal from biogas using biofiltration under anoxic conditions. In: *Proceedings of the 2010 Duke-UAM Conference on Biofiltration*, CD-ROM, Washington, USA (2010)
102. Gabriel D (2003) Retrofitting existing chemical scrubbers to biotrickling filters for H<sub>2</sub>S emission control. *Proc Natl Acad Sci* 100:6308–6312
103. Kim JH, Rene ER, Park HS (2008) Biological oxidation of hydrogen sulphide under steady and transient state conditions in an immobilized cell biofilter. *Bioresour Technol* 99:583–588
104. Goncalves JJ, Govind R (2009) Enhanced biofiltration using cell attachment promoters. *Environ Sci Technol* 43:1049–1054
105. Ryu HW, Yoo SK, Choi JM, Cho KS, Cha DK (2009) Thermophilic biofiltration of H<sub>2</sub>S and isolation of a thermophilic and heterotrophic H<sub>2</sub>S-degrading bacterium, *Bacillus* sp. TSO3. *J Hazard Mater* 168:501–506
106. Ramírez M, Fernández M, Granada C, Le Borgne S, Gómez JM, Cantero D (2011) Biofiltration of reduced sulphur compounds and community analysis of sulphur-oxidizing bacteria. *Bioresour Technol* 102:4047–4053
107. Ho KL, Lin WC, Chung YC, Chen YP, Tseng CP (2013) Elimination of high concentration hydrogen sulphide and biogas purification by chemical-biological process. *Chemosphere* 92:1396–1401
108. Giro MEA, Garcia O Jr, Zaiat M (2006) Immobilized cells of *Acidithiobacillus ferrooxidans* in PVC strands and sulfite removal in a pilot-scale bioreactor. *Chem Eng J* 28:201–207
109. Alemzadeh I, Kahrizi E, Vossoughi M (2009) Bio-oxidation of ferrous ions by *Acidithiobacillus ferrooxidans* in a monolithic bioreactor. *J Chem Technol Biotechnol* 84:504–510
110. Asai S, Konishi Y, Yabu T (1990) Kinetics of absorption of hydrogen sulphide into aqueous ferric sulfate solutions. *AIChE J* 36:1331–1338
111. Ebrahimi S, Kleerebezem R, van Loosdrecht M, Heijnen J (2003) Kinetics of the reactive absorption of hydrogen sulphide into aqueous ferric sulfate solutions. *Chem Eng Sci* 58:417–427
112. Mousavi SM, Yaghmaei S, Vossoughi M, Roostaazad R, Jafari A, Ebrahimi M, Chabok OH, Turunen I (2008) The effects of Fe(II) and Fe(III) concentration and initial pH on microbial leaching of low-grade sphalerite ore in a column reactor. *Bioresour Technol* 99:2840–2845
113. Chung YC, Ho KL, Tseng CP (2003) Hydrogen sulphide gas treatment by a chemical-biological process: chemical absorption and biological oxidation steps. *J Environ Sci Health, Part B* 38:663–679
114. Chung YC, Ho KL, Tseng CP (2006) Treatment of high H<sub>2</sub>S concentrations by chemical absorption and biological oxidation process. *Environ Eng Sci* 23:942–953
115. Mesa M, Andrades J, Macias M, Cantero D (2004) Biological oxidation of ferrous iron: study of bioreactor efficiency. *J Chem Technol Biotechnol* 79:163–170
116. Pinjing H, Liming S, Zhiwen Y, Guojian L (2001) Removal of hydrogen sulphide and methyl mercaptan by a packed tower with immobilized micro-organism beads. *Water Sci Technol* 44:327–333
117. Soreanu G, Béland M, Falletta P, Edmonson K, Seto P (2008) Laboratory pilot scale study for H<sub>2</sub>S removal from biogas in an anoxic biotrickling filter. *Water Sci Technol* 57:201–207
118. Soreanu G, Béland M, Falletta P, Edmonson K, Seto P (2008) Investigation on the use of nitrified wastewater for the steady-state operation of a biotrickling filter for the removal of hydrogen sulphide in biogas. *J Environ Eng Sci* 7:543–552
119. Manconi I, Carucci A, Lens P, Rossetti S (2006) Simultaneous biological removal of sulphide and nitrate by autotrophic denitrification in an activated sludge system. *Water Sci Technol* 53:91–99
120. Bentley R, Chasteen TG (2004) Environmental VOSCs—formation and degradation of dimethyl sulphide, methanethiol and related materials. *Chemosphere* 55:291–317
121. Sipma J, Svitelskaya A, van der Mark B, Hulstoft Pol LW, Lettinga G, Buisman CJN, Janssen AJH (2004)

- Potentials of biological oxidation processes for the treatment of spent sulfidic caustics containing thiols. *Water Res* 38:4331–4340
122. van Leerdam RC, Bonilla-Salinas M, de Bok FAM, Bruning H, Lens PNL, Stams AJM, Janssen AJH (2008) Anaerobic methanethiol degradation and methanogenic community analysis in an alkaline (pH 10) biological process for liquefied petroleum gas desulphurization. *Biotechnol Bioeng* 101:691–701
  123. van Leerdam RC, van den Bosch PLF, Lens PNL, Janssen AJH (2011) Reactions between methanethiol and biologically produced sulphur particles. *Environ Sci Technol* 45:1320–1326
  124. van den Bosch PLF, de Graaff M, Fortuny-Picornell M, van Leerdam RC, Janssen AJH (2009) Inhibition of microbiological sulphide oxidation by methanethiol and dimethyl polysulphides at natron-alkaline conditions. *Appl Microbiol Biotechnol* 83:579–587
  125. Goyal R, Babu V, Patel GK (2014) Biomethane production. In: Babu V, Thapliyal A, Patel, GK (eds) *Biofuels production*, pp 333–356
  126. Krich K, Augenstein D, Batmale J, Benemann J, Rutledge B, Salour D (2005) Biomethane from dairy waste: a sourcebook for the production and use of renewable natural gas in California. California, Western United Dairymen
  127. Rasi S, Lantela J, Rintala J (2011) Trace compounds affecting biogas energy utilisation—A review. *Energy Convers Manage* 52:3369–3375
  128. Papurello D, Schuhfried E, Lanzini A, Romano A, Cappellin L, Mark T, Silvestri S, Biasioli F (2014) Influence of co-vapors on biogas filtration for fuel cells monitored with PTR-MS (Proton Transfer Reaction-Mass Spectrometry). *Fuel Process Technol* 118:133–140
  129. Salminen E, Rintala J, Härkönen J, Kuitunen M, Hogmander H, Oikari A (2001) Anaerobically digested poultry slaughterhouse wastes as fertilizer in agriculture. *Bioresour Technol* 78:81–88
  130. Woli KR, Nagumo T, Kuramochi K, Hatano R (2004) Evaluating river water quality through land use analysis and N budget approaches in livestock farming areas. *Sci Total Environ* 329:61–74
  131. Li XZ, Zhao QL (1999) Inhibition of microbial activity of activated sludge by ammonia in leachate. *Environ Int* 25:961–968
  132. Battistoni P, Fava G, Pavan P, Musacco A, Cecchi F (1997) Phosphate removal in anaerobic liquors by struvite crystallization without addition of chemicals: preliminary results. *Water Res* 31:2925–2929
  133. Bouwer H, Chaney RL (1974) Land treatment of wastewater. *Adv Agron* 26:133–176
  134. Meinhold J, Pedersen H, Arnold E, Issacs S, Henze M (1998) Effect of continuous addition of an organic substrate to the anoxic phase on biological phosphate removal. *Water Sci Technol* 38:97–105
  135. Bonmati A, Flotats X (2003) Air stripping of ammonia from pig slurry: characterisation and feasibility as a pre- or post-treatment to mesophilic anaerobic digestion. *Waste Manage* 23:261–272
  136. Liao PH, Chen A, Lo KV (1995) Removal of nitrogen from swine manure wastewaters by ammonia stripping. *Bioresour Technol* 54:17–20
  137. Cheung KC, Chu LM, Wong MH (1997) Ammonia stripping as a pretreatment for landfill leachate. *Water Air Soil Pollut* 94:209–220
  138. Minocha VK, Prabhakar AVS (1988) Ammonia removal and recovery from urea fertilizer plant waste. *Environ Technol Lett* 9:655–664
  139. Lei X, Sugiura N, Feng C, Maekawa T (2007) Pretreatment of anaerobic digestion effluent with ammonia stripping and biogas purification. *J Hazard Mater* 145:391–397
  140. Esteves IAAC, Lopes MSS, Nunes PMC, Mota JPB (2008) Adsorption of natural gas and biogas components on activated carbon. *Sep Purif Technol* 62:281–296
  141. Hernandez SP, Chiappero M, Russo N, Fino D (2011) A novel ZnO-based adsorbent for biogas purification in H<sub>2</sub> production systems. *Chem Eng J* 176–177:272–279
  142. Chang FT (2010) Apparatus and method for purification of sulphur-containing waste gas and methane recovery from biogas. *Faming Zhuanli Shenqing*. CN 101884870 A 20101117
  143. Sakanishi K, Matsumura A, Saito I, Hanaoka T, Minowa T, Tomoaki (2004) Removal of hydrogen sulphide and carbonyl sulphide for purification of biomass-gasified synthetic gas using active carbons. *Prepr Symp-Am Chem Soc, Div Fuel Chem* 49:580–581
  144. Richter E, Henning KD, Knoblauch K, Juntgen H (1985) Utilization of activated carbon and carbon molecular sieves in biogas purification and methane recovery. *Comm Eur Communities, [Rep.] EUR, (EUR 10024, Energy Biomass)*, pp 621–624
  145. Shi L, Yang K, Zhao Q, Wang H, Cui Q (2015) Characterization and mechanisms of H<sub>2</sub>S and SO<sub>2</sub>

- adsorption by activated carbon. *Energy Fuels*. Ahead of Print
146. Phooratsamee W, Hussaro K, Teekasap S, Hirunlabh J (2014) Increasing adsorption of activated carbon from palm oil shell for adsorb H<sub>2</sub>S from biogas production by impregnation. *Am J Env Sci* 10:431–445
  147. Aslam Z, Shawabkeh RA, Hussein IA, Al-Baghli N, Eic M (2015) Synthesis of activated carbon from oil fly ash for removal of H<sub>2</sub>S from gas stream. *Appl Surf Sci* 327:107–115
  148. Sisani E, Cinti G, Discepoli G, Penchini D, Desideri U, Marmottini F (2014) Adsorptive removal of H<sub>2</sub>S in biogas conditions for high temperature fuel cell systems. *Int J Hydrogen Energy* 39:21753–21766.
  149. Micoli L, Bagnasco G, Turco M (2014) H<sub>2</sub>S removal from biogas for fuelling MCFCs: new adsorbing materials. *Int J Hydrogen Energy* 39:1783–1787
  150. Liang M, Zhang C, Zheng H (2014) The removal of H<sub>2</sub>S derived from livestock farm on activated carbon modified by combinatory method of high-pressure hydrothermal method and impregnation method. *Adsorption* 20:525–531
  151. An H, Zhao D, Zhao C, Xue J, Li X, Xiuling (2011) Study on removal of H<sub>2</sub>S by modified ACF with impregnation of transition metal. *Huanjing Gongcheng Xuebao* 5:1581–1585
  152. Huang CC, Chen CH (2013) Dynamic adsorption model of H<sub>2</sub>S in a fixed bed of copper impregnated activated carbon. *Separation Sci Technol* 48:148–155
  153. Monteleone G, De Francesco M, Galli S, Marchetti M, Naticchioni V (2011) Deep H<sub>2</sub>S removal from biogas for molten carbonate fuel cell (MCFC) systems. *Chem Eng J* 173:407–414
  154. Yan B, Jiang W, Li F, Liu L (2010) Study on adsorbents from sewage sludge to removal of NH<sub>3</sub> and H<sub>2</sub>S. *Harbin Shangye Daxue Xuebao, Ziran Kexueban* 26:662–666
  155. Polster A, Brummack J (2009) Desulphurization in biogas plants. *VDI-Berichte* 2057 (Biogas 2009), pp 185–193
  156. Shah M, Tsapatsis M, Siepmann JI, Ilja J (2015) Monte carlo simulations probing the adsorptive separation of hydrogen sulphide/methane mixtures using all-silica zeolites. *Langmuir*. Ahead of Print
  157. Liu C, Zhang R, Wei S, Wang J, Liu Y, Li M, Liu R, Rutao (2015) Selective removal of H<sub>2</sub>S from biogas using a regenerable hybrid TiO<sub>2</sub>/zeolite composite. *Fuel* 157:183–190
  158. Yazdanbakhsh F, Blasing M, Sawada JA, Rezaei S, Muller M, Baumann S, Kuznicki SM (2014) Copper Exchanged Nanotitanate for High Temperature H<sub>2</sub>S Adsorption. *Ind Eng Chem Res* 53:11734–11739
  159. Izumi J, Wang H (2010) Methane recovery and purification from biogases using vacuum pressure swing adsorption. In: *Pacificchem 2010, International Chemical Congress of Pacific Basin Societies*, Honolulu, HI, United States, AETECH-264, Dec 15–20 2010
  160. Cosoli P, Ferrone M, Priol S, Fermeglia M (2008) Hydrogen sulphide removal from biogas by zeolite adsorption. Part II. MD simulations. *Chem Eng J* 145:93–99
  161. Qiu G, Huang B, Wang X, Li X, Xiangtong (2006) Theoretical study of H<sub>2</sub>S adsorption on HZSM-5 zeolite. *Shiyou Yu Tianranqi Huagong* 35:107–109
  162. Tomadakis MM, Heck HH, Howell M. Hall, Marilyn (2006) Use of molecular sieves to remove H<sub>2</sub>S and CO<sub>2</sub> from landfill gas, producing a high-energy content methane stream. In: *AIChE Spring National Meeting, Conference Proceedings*, Orlando, FL, United States, Apr 23–27 2006, P43008/1-P43008/6
  163. Gong J, Jiao YF, Su QQ, Mi WL (2015) Deep removal of carbonyl sulphide in biogas. *Gaoxiao Huaxue Gongcheng Xuebao* 29:443–451
  164. Liu Y, Guo BB, Zhu YQ (2013) Research progress in desulphurizers. *Dangdai Huagong* 42:827–829, 840
  165. Sun T, Shen Y, Jia J (2014) Gas cleaning and hydrogen sulphide removal for COREX coal gas by sorption enhanced catalytic oxidation over recyclable activated carbon desulphurizer. *Environ Sci Technol* 48:2263–2272
  166. Hyung-Tae K, Seung-Moon K, Ki-Won J, Young-Seek Y, Jin-Hong K (2007) Desulphurisation of odorant-containing gas: removal of t-butylmercaptan on Cu/ZnO/Al<sub>2</sub>O<sub>3</sub>. *Int J Hydrogen Energy* 32:3603–3608
  167. Osorio F, Torres JC (2009) Biogas purification from anaerobic digestion in a wastewater treatment plant for biofuel production. *Renew Energy* 34:2164–2171
  168. Li YY, Perera SP, Crittenden BD (1998) Zeolite monoliths for air separation, part 2: oxygen enrichment, pressure drop and pressurization. *Trans I Chem E* 76:931–941
  169. Gordon Israelson PE (2009) Hydrocarbon condensation heating of natural gas by an activated carbon desulphurizer. *J Fuel Cell Sci Technol* 6:34506–34518

170. Gordon Israelson PE (2004) Results of testing various natural gas desulphurisation adsorbents. *J Mater Eng Perform* 13:282–286
171. Hernandez S, Solarino L, Orsello G, Russo N, Fino D, Saracco G et al (2008) Desulphurization process for fuel cells systems. *Int. J. Hydrogen Energy* 33:3209–3214
172. Gordon Israelson PE (2008) Water vapor effects on fuel cell desulphurizer performance—a decade of field experience. In: *Proceedings of Fuel Cell 200 Sixth Int Fuel Cell Science Eng Tech*; Conference Denver, Colorado, USA
173. Yang RT, Hernandez-Maldonado AJ, Yang FH (2003) Desulphurization of transportation fuels with zeolites under ambient conditions. *Science* 301:79–81
174. Hernandez-Maldonado AJ, Yang RT (2003) Desulphurization of diesel fuels by adsorption via  $\pi$ -complexation with vapor-phase exchanged Cu(I)-Y zeolites. *Ind Eng Chem Res* 42:3103–3110
175. Velu S, Song CS, Engelhard MH, Chin YH (2005) Adsorptive removal of organic sulphur compounds from jet fuel over K-exchanged NiY zeolites prepared by impregnation and ion exchange. *Ind Eng Chem Res* 44:5740–5749
176. Ko CH, Song HI, Park JH, Han SS, Kim JN (2007) Selective removal of sulphur compounds in city-gas by adsorbents. *Korean J Chem Eng* 24:1124–1127
177. Zhang ZY, Shi TB, Jia CZ, Ji WJ, Chen Y, He MY (2008) Adsorptive removal of aromatic organosulphur compounds over the modified Na-Y zeolites. *Appl Catal B* 82:1–10
178. Xue M, Chitrakar R, Sakane K, Hirotsu T, Ooi K, Yoshimura Y, Toba M, Feng Q (2006) Preparation of cerium-loaded Y-zeolites for removal of organic sulphur compounds from hydrodesulphurized gasoline and diesel oil. *J Colloid Interface Sci* 298:535–542
179. Lam KF, Yeung KL, McKay G (2006) An investigation of gold adsorption from a binary mixture with selective mesoporous silica adsorbents. *J Phys Chem B* 110:2187–2194
180. Lam KF, Yeung KL, McKay G (2006) A rational approach in the design of selective mesoporous adsorbents. *Langmuir* 22:9632–9641
181. Lam KF, Fong CM, Yeung KL (2007) Separation of precious metals using selective mesoporous adsorbents. *Gold Bull.* 40:192–198
182. Lam KF, Yeung KL, McKay G (2007) Efficient approach for  $\text{Cd}^{2+}$  and  $\text{Ni}^{2+}$  removal and recovery using mesoporous adsorbent with tunable selectivity. *Environ Sci Technol* 41:3329–3334
183. Parida KM, Dash SK (2010) Adsorption of  $\text{Cu}^{2+}$  on spherical Fe-MCM-41 and its application for oxidation of adamantane. *J Hazard Mater* 179:642–649
184. Arruebo M, Ho WY, Lam KF, Chen XG, Arbiol J, Santamaria J, Yeung KL (2008) Preparation of magnetic nanoparticles encapsulated by an ultrathin silica shell via transformation of magnetic Fe-MCM-41. *Chem Mater* 20:486–493
185. Lam KF, Chen XQ, McKay G, Yeung KL (2008) Anion Effect on  $\text{Cu}^{2+}$  Adsorption on  $\text{NH}_2$ -MCM-41. *Ind Eng Chem Res* 47:9376–9383
186. Lam KF, Fong CM, Yeung KL, McKay G (2008) Selective adsorption of gold from complex mixtures using mesoporous adsorbents. *Chem Eng J* 145:185–195
187. Lam KF, Chen XQ, Fong CM, Yeung KL (2008) Selective mesoporous adsorbents for  $\text{Ag}^+/\text{Cu}^{2+}$  separation. *Chem Commun* 17:2034–2036
188. Chen XQ, Lam KF, Zhang QJ, Pan BC, Arruebo M, Yeung KL (2009) Synthesis of highly selective magnetic mesoporous adsorbent. *J Phys Chem* 113:9804–9813
189. Wang YH, Yang RT, Heinzl JM (2009) Desulphurization of jet fuel JP-5 light fraction by MCM-41 and SBA-15 supported cuprous oxide for fuel cell applications. *Ind Eng Chem Res* 48:142–147
190. Park JG, Ko CH, Yi KB, Park JH, Han SS, Cho SH, Kim JN (2008) Reactive adsorption of sulphur compounds in diesel on nickel supported on mesoporous silica. *Appl Catal B* 81:244–250
191. Wang Y, Yang RT, Heinzl JM (2008) Desulphurization of jet fuel by  $\pi$ -complexation adsorption with metal halides supported on MCM-41 and SBA-15 mesoporous materials. *Chem Eng Sci* 63:356–365
192. Li WL, Liu QF, Xing JM, Gao HS, Xiong XC, Li YG, Li X, Liu HZ (2007) High-efficiency desulphurization by adsorption with mesoporous aluminosilicates. *AIChE J* 53:3263–3268
193. Yang LM, Wang YJ, Huang D, Luo GS, Dai YY (2007) Preparation of high performance adsorbents by functionalizing mesostructured silica spheres for selective adsorption of organosulphur compounds. *Ind Eng*

194. Yin Y, Jiang WJ, Liu XQ, Li YH, Sun LB (2012) Dispersion of copper species in a confined space and their application in thiophene capture. *J Mater Chem* 22:18514–18521
195. Samadi-Maybodi A, Teymouri M, Vahid A, Miranbeigi A (2011) In situ incorporation of nickel nanoparticles into the mesopores of MCM-41 by manipulation of solvent-solute interaction and its activity toward adsorptive desulphurization of gas oil. *J Hazard Mater* 192:1667–1674
196. Li WL, Tang H, Zhang T, Li Q, Xing JM, Liu HZ (2010) Ultra-deep desulphurization adsorbents for hydrotreated diesel with magnetic mesoporous aluminosilicates. *AIChE J* 56:1391–1396
197. Tao YS, Kanoh H, Abrams L, Kaneko K (2006) Mesopore-modified zeolites: preparation, characterization, and applications. *Chem Rev* 106:896–910
198. Xiao FS, Wang LF, Yin CY, Lin KF, Di Y, Li JX, Xu RR, Su DS, Schlogl R, Yokoi T, Tatsumi T (2006) Catalytic properties of hierarchical mesoporous zeolites templated with a mixture of small organic ammonium salts and mesoscale cationic polymers. *Angew Chem Int Ed* 45:3090–3093
199. Wang H, Pinnavaia TJ (2006) MFI zeolite with small and uniform intracrystal mesopores. *Angew Chem Int Ed* 45:7603–7606
200. Choi M, Cho HS, Srivastava R, Venkatesan C, Choi DH, Ryoo R (2006) Amphiphilic organosilane-directed synthesis of crystalline zeolite with tunable mesoporosity. *Nat Mater* 5:718–723
201. Zhang XY, Liu DX, Xu DD, Asahina S, Cychosz KA, Agrawal KV, Wahedi YA, Bhan A, Hashimi SA, Terasaki O, Thommes M, Tsapatsis M (2012) Synthesis of Self-Pillared Zeolite Nanosheets by Repetitive Branching. *Science* 336:1684–1687
202. Tang K, Song LJ, Duan LH, Li XQ, Gui JZ, Sun ZL (2008) Deep desulphurization by selective adsorption on a heteroatoms zeolite prepared by secondary synthesis. *Fuel Process Technol* 89:1–6
203. Jiang M, Ng FTT (2006) Adsorption of benzothiophene on Y zeolites investigated by infra-red spectroscopy and flow calorimetry. *Catal Today* 116:530–536
204. Jayaraman A, Yang FH, Yang RT (2006) Effects of nitrogen compounds and polyaromatic hydrocarbons on desulphurization of liquid fuels by adsorption via  $\pi$ -complexation with Cu(I)Y Zeolite. *Energy Fuels* 20:909–914
205. Hernandez-Maldonado AJ, Yang RT, Cannella W (2004) Desulphurization of commercial jet fuels by adsorption via  $\pi$ -complexation with vapor phase ion exchanged Cu(I)-Y zeolites. *Ind Eng Chem Res* 43:6142–6149
206. Hernandez-Maldonado AJ, Yang RT (2004) New sorbents for desulphurization of diesel fuels via  $\pi$ -complexation. *AIChE J* 50:791–801
207. Hernandez-Maldonado AJ, Yang RT (2004) Desulphurization of diesel fuels via  $\pi$ -complexation with nickel(II)-exchanged X- and Y-zeolites. *Ind Eng Chem Res* 43:1081–1089
208. Lee J, Beum HT, Ko CH, Park SY, Park JH, Kim JN, Chun BH, Kim SH (2011) Adsorptive removal of dimethyl disulphide in olefin rich C4 with ion-exchanged zeolites. *Ind Eng Chem Res* 50:6382–6390
209. Jung GS, Park DH, Lee DH, Lee HC, Hong SB, Woo HC (2010) Adsorptive removal of tert-butylmercaptan and tetrahydrothiophene using microporous molecular sieve ETS-10. *Appl Catal* 100:264–270
210. Yeung KL, Han W (2014) Zeolites and mesoporous materials in fuel cell applications. *Catal Today* 236:182–205
211. Cigolotti V, McPhail S, Moreno A, Yoon SP, Han JH, Nam SW, Lim T (2011) MCFC fed with biogas: experimental investigation of sulphur poisoning using impedance spectroscopy. *Int J Hydrogen Energy* 36:10311–10318
212. Hoffmann J (2005) Applications of molten carbonate fuel cells with biofuels. In: Lens P, Westermann P, Haberbauer M, Moreno A (eds) *Cells biofuels for fuel*. IWA Publishing, pp. 478–94
213. Vogel WM, Smith SW (1982) The effect of sulphur on the anodic H<sub>2</sub> (Ni) electrode in fused Li<sub>2</sub>CO<sub>3</sub>-K<sub>2</sub>CO<sub>3</sub> at 650 °C. *J Electrochem Soc* 129(7):1441–1445
214. Cigolotti V, McPhail S, Moreno A (2009) Non-conventional fuels for high-temperature fuel cells: status and issue. *ASME J Fuel Cell Sci Tech* 6(2)
215. Ciccoli R, Cigolotti V, Lo Presti R, Massi E, McPhail S, Monteleone G et al (2010) Molten carbonate fuel cells fed with biogas: combating H<sub>2</sub>S. *Waste Manag* 30(6):1018–1024
216. Sammells AF, Nicholson SB, Ang PGP (1980) Development of sulphur-tolerant components for the molten carbonate fuel cell. *J Electrochem Soc* 127(2):350–357



- 217.Devianto H, Yoon SP, Nam SW, Han J, Lim T-H (2006) The effect of ceria coating on the H<sub>2</sub>S tolerance of a molten carbonate fuel cell. *J Power Sources* 159:1147–1152
- 218.Kawase M, Mugikura Y, Watanabe T (2000) The effects of H<sub>2</sub>S on electrolyte distribution and cell performance in the molten carbonate fuel cell. *J Elect Soc* 147(4):1240–1244
- 219.Uchida, Ohuchi S, Nishina T (1994) Kinetic studies of the effects of H<sub>2</sub>S impurity on hydrogen oxidation in molten (Li + K)CO<sub>3</sub>. *J Elect Chem* 369:161–168
- 220.Jablonski G, Hamm JR, Alvin MA, Wenglarz RA, Patel B (1982) Evaluation of Gasification and Gas Cleanup Process for Use in Molten Carbonate Fuel Cell Power Plants. Department of Energy, Morgantown Energy Technology Center, Report DOE/MC/16220-1306 (DE83003821)
- 221.Zaza F, Paoletti C, Lo Presti R, Simonetti E, Pasquali M (2008) Effects of hydrogen sulphide impurities on MCFC performance. In: Fundamentals and developments of fuel cells conference—FDFC2008, Nancy, France, 10–12 Dec 2008
- 222.Kawase M, Mugikura Y, Izaki Y, Watanabe T (1999) Effects of H<sub>2</sub>S on the performance of MCFC. II. Behavior of sulphur in the cell. *Electrochemistry* 4:67
- 223.Weaver D, Winnik J (1989) Sulphuration of molten carbonate fuel cell anode. *J Electrochem Soc* 136(6):1679–1686
- 224.Townley D, Winnick J, Huang HS (1980) Mixed potential analysis of sulphuration of molten carbonate fuel cells. *J Electrochem Soc* 125(5):1104–1106
- 225.Marianowski LG, Anderson GL, Camara EH (1991) Use of sulphur containing fuel in molten carbonate fuel cells. United States Patent, No 5,071,718
- 226.Dong J, Cheng Z, Zha S, Liu M (2006) Identification of nickel sulphides on Ni-YSZ cermet exposed to H<sub>2</sub> fuel containing H<sub>2</sub>S using Raman spectroscopy. *J Power Sources* 156:461–465
- 227.Gong M, Liu X, Tremblay J, Johnson C (2007) Sulphur-tolerant anode materials for solid oxide fuel cell application. *J Power Sources* 168:289–298
- 228.Zaza F, Paoletti C, LoPresti R, Simonetti E, Pasquali M (2010) Studies on sulphur poisoning and development of advanced anodic materials for waste-to-energy fuel cells applications. *J Power Sources* 195:4043–4050
- 229.Watanabe T, Izaki Y, Mugikura Y, Morita H, Yoshikawa M, Kawase M et al (2006) Applicability of molten carbonate fuel cells to various fuels. *J Power Sources* 160:868–871
- 230.Hernandez S, Scarpa F, Fino D, Conti R (2011) Biogas purification for MCFC application. *Int J Hydrogen Energy* 36:8112–8118
- 231.Devianto H, Simonetti E, McPhail SJ, Zaza F, Cigolotti V, Paoletti C, Moreno A, La Barbera A, Luisetto I (2012) Electrochemical impedance study of the poisoning behaviour of Ni-based anodes at low concentrations of H<sub>2</sub>S in an MCFC. *Int J Hydrogen Energy* 37:19312–19318
- 232.Cheng Z, Zha S, Liu M (2006) Stability of materials as candidates for sulphur-resistant anodes of solid oxide fuel cells. *J Electrochem Soc* 153(7):A1302–A1309
- 233.Rexed, Lagergren C, Lindbergh G (2014) Effect of sulphur contaminants on MCFC performance. *Int J Hydrogen Energy* 39:12242–12250
- 234.Jurgensen L, Ehimen EA, Born J, Holm-Nielsen JB (2015) Dynamic biogas upgrading based on the Sabatier process: Thermodynamic and dynamic process simulation. *Biores Technol* 178:323–329
- 235.Hagen M, Polman E, Jensen J, Myken A, Jonsson O, Dahl A (2001) Adding gas from bio-mass to the gas grid. Swedish Gas Center, Malmö, Sweden, July 2001, Report SCG 118, p 144
- 236.Wellinger A, Lindberg A (2001) Biogas upgrading and utilisation. IEA Bioenergy Task 24: Energy from biological conversion of organic waste 24, pp 1–20
- 237.Ryckebosch E, Drouillon M, Vervaeren H (2011) Techniques for transformation of biogas to biomethane. *Biomass Bioenergy* 35:1633–1645
- 238.Papurello D, Lanzini A, Leone P, Santarelli M, Silvestri S (2014) Biogas from the organic fraction of municipal solid waste: dealing with contaminants for a solid oxide fuel cell energy generator. *Waste Manag* 34:2047–2056
- 239.Rasmussen JFB, Hagen A, Thyden K (2011) Durability of solid oxide fuel cells using sulphur containing fuels. *J Power Sources* 196:7271–7276
- 240.Lanzini A, Leone P (2010) Experimental investigation of direct internal reforming of biogas in solid oxide fuel cells. *Int J Hydrogen Energy* 35:2463–2476

241. Shiratori Y, Ijichi T, Oshima T, Sasaki K (2010) Internal reforming SOFC running on biogas. *Int J Hydrogen Energy* 35:7905–7912
242. Sasaki K, Haga K, Yoshizumi T, Minematsu D, Yuki E, Liu R, Uryu C, Oshima T, Ogura T, Shiratori Y, Ito K, Koyama M, Yokomoto K (2011) Chemical durability of solid oxide fuel cells: influence of impurities on long-term performance. *J Power Sources* 196:9130–9140
243. Mermelstein J, Millan M, Brandon NP (2011) The interaction of biomass gasification syngas components with tar in a solid oxide fuel cell and operational conditions to mitigate carbon deposition on nickel-gadolinium doped ceria anodes. *J Power Sources* 196:5027–5034
244. Zheng K, Swierczek K, Polfus JM, Sunding MF, Pishahang M, Norby T, Truls (2015) Carbon Deposition and Sulphur Poisoning in  $\text{SrFe}_{0.75}\text{Mo}_{0.25}\text{O}_{3-\delta}$  and  $\text{SrFe}_{0.5}\text{Mn}_{0.25}\text{Mo}_{0.25}\text{O}_{3-\delta}$  Electrode Materials for Symmetrical SOFCs. *J Electrochem Soc* 162:F1078–F1087
245. Singh D, Hernandez-Pacheco E, Hutton PN, Patel N, Mann MD (2005) Carbon deposition in an SOFC fueled by tar-laden biomass gas: a thermodynamic analysis. *J Power Sources* 142:194–199
246. Gunji A, Wen C, Otomo J, Kobayashi T, Ukai K, Mizutani Y, Takahashi H (2004) Carbon deposition behaviour on Ni-ScSZ anodes for internal reforming solid oxide fuel cells. *J Power Sources* 131:285–288
247. Cheng Z, Wang JH, Choi Y, Yang L, Lin MC, Liu M (2011) From Ni-YSZ to sulphur-tolerant anode materials for SOFCs: electrochemical behavior, in situ characterization, modeling, and future perspectives. *Energy Environ Sci* 4:4380–4409
248. Rostrup-Nielsen JR, Hansen JB, Helveg S, Christiansen N, Jannasch AK (2006) Sites for catalysis and electrochemistry in solid oxide fuel cell (SOFC) anode. *Appl Phys A Mater Sci Process* 85:427–430
249. Bao J, Krishnan GN, Jayaweera P, Perez-Mariano J, Sanjurjo A (2009) Effect of various coal contaminants on the performance of solid oxide fuel cells: part I. Accelerated testing. *J Power Sources* 193:607–616
250. Ruokomäki J (2009) Biogas criteria for SOFC. Product Centre Ecotech. Wärtsilä. <http://www.vtt.fi/inf/pdf/tiedotteet/2009/T2496.pdf>. Accessed 11 Feb 2017
251. Haga K, Adachi S, Shiratori Y, Itoh K, Sasaki K (2008) Poisoning of SOFC anodes by various fuel impurities. *Solid State Ionics* 179:1427–1431
252. Sasaki K, Adachi S, Haga K, Uchikawa M, Yamamoto J, Iyoshi A, Chou J, Shiratori Y, Ito K (2007) Fuel impurity tolerance of solid oxide fuel cells. *ECS Trans* 7:1675–1683
253. Arnold M (2009) Reduction and monitoring of biogas trace compounds. VTT Research Notes 2496; VTT Technical Research Centre of Finland: Espoo, Finland
254. Blesznowski M, Jewulski J, Zieleniak A (2013) Determination of  $\text{H}_2\text{S}$  and  $\text{HCl}$  concentration limits in the fuel for anode supported SOFC operation. *Cent Eur J Chem* 11:960–967
255. Tremblay JP, Gemmen RS, Bayless DJ (2007) The effect of coal syngas containing  $\text{HCl}$  on the performance of solid oxide fuel cells: investigations into the effect of operational temperature and  $\text{HCl}$  concentration. *J Power Sources* 169:347–354
256. Cayana FN, Zhia M, Pakalapatia SR, Celika I, Wua N, Gemmenb R (2008) Effects of coal syngas impurities on anodes of solid oxide fuel cells. *J Power Sources* 185:595–602
257. Tjaden B, Gandiglio M, Lanzini A, Santarelli M, Jarvinen M (2014) Small-scale biogas- SOFC plant: technical analysis and assessment of different fuel reforming options. *Energy Fuels* 28:4216–4232
258. Papurello D, Schuhfried E, Lanzini A, Romano A, Cappellin L, Mark T, Silvestri S, Biasioli F (2014) Influence of co-vapors on biogas filtration for fuel cells monitored with PTR-MS (Proton Transfer Reaction-Mass Spectrometry). *Fuel Process Technol* 118:133–140
259. Larminie J, Dicks A (2003) Fuel cell systems explained, 2nd edn. John Wiley & Sons Ltd., England
260. Matsuzaki Y, Yasuda I (2000) The poisoning effect of sulphur-containing impurity gas on a SOFC anode: Part I. Dependence on temperature, time, and impurity concentration. *Solid State Ion.* 132:261–269
261. Riegraf M, Schiller G, Costa R, Friedrich KA, Latz A, Yurkiv V (2015) Elementary kinetic numerical simulation of Ni/YSZ SOFC anode performance considering sulphur poisoning. *J Electrochem Soc* 162:F65–F75
262. Aguilar L, Zha S, Li S, Winnick J, Liu M (2004) A solid oxide fuel cell operating on hydrogen sulphide ( $\text{H}_2\text{S}$ ) and sulphur-containing fuels. *J Power Sources* 135:17–24
263. Tremblay JP, Marquez AI, Ohn TR, Bayless DJ (2006) Effects of coal syngas and  $\text{H}_2\text{S}$  on the performance of solid oxide fuel cells: single-cell tests. *J Power Sources* 158:263–273
264. Sasaki K, Teraoka Y (2003) equilibria in fuel cell gases. *J Electrochem Soc* 150(11):A885–A888
265. Jess A (1996) Catalytic upgrading of tarry fuel gases: A kinetic study with model components. *Chem Eng*

- 266.Sasaki K (2008) Thermochemical stability of sulphur compounds in fuel cell gases related to fuel impurity poisoning. *J Fuel Cell Sci Technol* 5, 031212-1/031212-8
- 267.Lima da Silva A, Heck NC (2015) Thermodynamics of sulphur poisoning in solid oxide fuel cells revisited: the effect of H<sub>2</sub>S concentration, temperature, current density and fuel utilization. *J Power Sources* 296:92–101
- 268.Sapountzi FM, Tsampas MN, Zhao C, Boreave A, Retailleau L, Montinaro D, Vernoux P (2015) Triode operation for enhancing the performance of H<sub>2</sub>S-poisoned SOFCs operated under CH<sub>4</sub>-H<sub>2</sub>O mixtures. *Solid State Ionics* 277:65–71
- 269.Hagen A, Johnson GB, Hjalmarsson P (2014) Electrochemical evaluation of sulphur poisoning in a methane-fuelled solid oxide fuel cell: Effect of current density and sulphur concentration. *J Power Sources* 272:776–785
- 270.Ma J, Jiang C, Connor PA, Cassidy M, Irvine JTS (2015) Highly efficient, coking-resistant SOFCs for energy conversion using biogas fuels. *J Mater Chem A: Mater Energy Sustain* 3:19068–19076
- 271.Escudero MJ, Gomez de Parada I, Fuerte A (2015) Performance evaluation of WNi-CeO<sub>2</sub> as anode in a solid oxide fuel cell fed by simulated biogas mixtures. *Int J Hydrogen Energy* 40:11303–11314
- 272.Sasaki K, Susuki K, Iyoshi A, Uchimura M, Imamura N, Kusaba H, Teraoka Y, Fuchino H, Tsujimoto K, Uchida Y, Jingo N (2006) H<sub>2</sub>S poisoning of solid oxide fuel cells. *J Electrochem Soc* 153:A2023–A2029
- 273.Brown AS, van der Veen AMH, Arrhenius K, Murugan A, Culleton LP, Ziel PR, Li J (2015) Sampling of gaseous sulphur-containing compounds at low concentrations with a review of best-practice methods for biogas and natural gas applications. *Trends Anal Chem* 64:42–52
- 274.Montebello AM, Fernández M, Almenglo F, Ramírez M, Cantero D, Baeza M, Gabriel D (2012) Simultaneous methylmercaptan and hydrogen sulphide removal in the desulphurization of biogas in aerobic and anoxic biotrickling filters. *Chem Eng J* 200–202:237–246
- 275.Anderson FAT, Karlsson A, Svensson BH, Ejlerstsson J (2004) Occurrence and abatement of volatile sulphur compounds during biogas production. *J Air Waste Manag Assoc* 54:855–861
- 276.van den Bosch PLF, de Graaff M, Fortuny-Picornell M, van Leerdam RC, Janssen AJH (2009) Inhibition of microbiological sulphide oxidation by methanethiol and dimethyl poly- sulphides at natron-alkaline conditions. *Appl Microbiol Biotechnol* 83:579–587
- 277.Parker T, Dottridge J, Kelly S (2002) Investigation of the composition and emissions of trace components in landfill gas, R&D Technical Report P1-438/TR Environment Agency, Bristol, UK
- 278.Deublein D, Steinhäuser A (2008) Biogas from waste and renewable resources. Wiley-VCH Verlag GmbH & Co. KGaA, Weinheim
- 279.Directive 2009/28/EC on the promotion of the use of energy from renewable sources (2009). Off J Eur Union L140:16–62
- 280.Directive 2003/55/EC concerning the common rules for the internal market in natural gas (2003). Off J Eur Union L176:57–78
- 281.COM (2010) 639 Energy 2020: a strategy for competitive sustainable and secure energy, European Commission, Bruxelles
- 282.Biomass barometer ObservER (2012). <http://www.eurobserv-er.org/pdf/baro212.pdf>. Accessed 11 Feb 2017
- 283.European Commission Mandate M/475, Mandate to CEN for standard for biomethane for use in transport and injection in natural gas pipeline (2010)
- 284.Deublein D, Steinhäuser A (2011) Biogas from waste and renewable resources, 2nd edn. Wiley-VCH Verlag, Weinheim (2011)
- 285.Injection of gases from non-conventional sources into gas networks, Marcogaz report D497 (2006)
- 286.Gas quality harmonisation: cost benefit analysis, GL Noble Denton and Poyry Management Consulting (2012)
- 287.Haga K, Adachi S, Shiratori Y, Ito K, Sasaki K (2008) Poisoning of SOFC anodes by various fuel impurities. In: *Solid State Ionics 16: Proceedings of the 16th International Conference on Solid State Ionics (SSI-16)*, Part II, vol 179, pp 1427–1431. Shanghai, China, July 1–6 2008
- 288.Li Y, Zhang Y, Zhu X, Wang Z, Lü Z, Huang X, Zhou Y, Zhu L, Jiang W (2015) Performance and sulphur poisoning of Ni/CeO<sub>2</sub> impregnated La<sub>0.75</sub>Sr<sub>0.25</sub>Cr<sub>0.5</sub>Mn<sub>0.5</sub>O<sub>3-δ</sub> anode in solid oxide fuel cells. *J Power Sources* 285:354–359
- 289.Cheng Z, Liu M (2007) Characterization of sulphur poisoning of Ni-YSZ anodes for solid oxide fuel cells using in situ Raman microspectroscopy. *Solid State Ionics* 178:925–935
- 290.Thi HHM, Saubat B, Sergeant N, Pagnier T (2015) In situ Raman and optical characterization of H<sub>2</sub>S reaction

- with Ni-based anodes for SOFCs. *Solid State Ionics* 272:84–90
291. Lohsoontorn P, Brett DJL, Brandon NP (2008) Thermodynamic predictions of the impact of fuel composition on the propensity of sulphur to interact with Ni and ceria-based anodes for solid oxide fuel cells. *J Power Sources* 175:60–67
  292. Wang J-H, Liu M (2007) Computational study of sulphur-nickel interactions: A new S-Ni phase diagram. *Electrochem Commun* 9:2212–2217
  293. Zha S, Cheng Z, Liu M (2007) Sulphur poisoning and regeneration of Ni-based anodes in solid oxide fuel cells. *J Electrochem Soc* 154:B201–B206
  294. Lohsoontorn P, Brett DJL, Brandon NP (2008) The effect of fuel composition and temperature on the interaction of H<sub>2</sub>S with nickel-ceria anodes for solid oxide fuel cells. *J Power Sources* 183:232–239
  295. Nurk G, Huthwelker T, Braun A, Ludwig C, Lust E, Struis RPWJ (2013) Redox dynamics of sulphur with Ni/GDC anode during SOFC operation at mid- and low-range temperatures: an operando S K-edge XANES study. *J Power Sources* 240:448–457
  296. Harris WM, Lombardo JJ, Nelson GJ, Lai B, Wang S, Vila-Comamala J, Liu M, Liu M, Chiu WKS (2014) Three-dimensional microstructural imaging of sulphur poisoning-induced degradation in a Ni-YSZ anode of solid oxide fuel cells. *Sci Rep* 4:5246
  297. Lussier A, Sofie S, Dvorak J, Idzerda YU (2008) Mechanism for SOFC anode degradation from hydrogen sulphide exposure. *Int J Hydrog Energy* 33:3945–3951
  298. Dong J, Cheng Z, Zha S, Liu M (2006) Identification of nickel sulphides on Ni-YSZ cermet exposed to H<sub>2</sub> fuel containing H<sub>2</sub>S using Raman spectroscopy. *J Power Sources* 156:461–465
  299. Monder DS, Karan K (2010) Ab initio adsorption thermodynamics of H<sub>2</sub>S and H<sub>2</sub> on Ni(111). The importance of thermal corrections and multiple reaction equilibria. *J Phys Chem C* 114:22597–22602
  300. Bartholomew CH, Agrawal PK, Katzer JR (1982) Sulphur poisoning of metals. *Adv Catal* 31:135–242
  301. Kurokawa H, Sholkapper TZ, Jacobson CP, Jonghe LCD, Visco SJ (2007) Ceria nanocoating for sulphur tolerant Ni-based anodes of solid oxide fuel cells. *Electrochem Solid-State Lett* 10:B135–B138
  302. Siriwardane RV, Poston JA Jr, Fisher EP (2005) Interaction of hydrogen sulphide with Zr<sub>0.92</sub>Y<sub>0.08</sub>O<sub>2-δ</sub>/40 % Ni cermet. *Appl Surf Sci* 243:40–54
  303. Schubert SK, Kusnezoff M, Michaelis A, Bredikhin SI (2012) Comparison of the performances of single cell solid oxide fuel cell stacks with Ni/8YSZ and Ni/10CGO anodes with H<sub>2</sub>S containing fuel. *J Power Sources* 217:364–372
  304. Singhal SC, Ruka RJ, Bauerle JE, Sprengler CJ (1986) US Department of Energy Report No. DOE/MC/22046-237 I, Washington D.C
  305. Zhang L, Jiang SP, He HQ, Chen X, Ma J, Song XC (2010) A comparative study of H<sub>2</sub>S poisoning on electrode behavior of Ni/YSZ and Ni/GDC anodes of solid oxide fuel cells. *Int J Hydrog Energy* 35:12359–12368
  306. Choi YM, Compson C, Lin MC, Liu ML (2006) A mechanistic study of H<sub>2</sub>S decomposition on Ni- and Cu-based anode surfaces in a solid oxide fuel cell. *Chem Phys Lett* 421:179–183
  307. McCarty JG, Wise H (1980) Thermodynamics of sulphur chemisorption on metals. I. Alumina-supported nickel. *J Chem Phys* 72:6332–6337
  308. Oliphant JL, Fowler RW, Pannell RB, Bartholomew CH (1978) Chemisorption of hydrogen sulphide on nickel and ruthenium catalysts: I. Desorption isotherms. *J Catal* 51:229–242
  309. Vahc ZY, Jung CY, Yi SC (2014) Performance degradation of solid oxide fuel cells due to sulphur poisoning of the electrochemical reaction and internal reforming reaction. *Int J Hydrogen Energy* 39:17275–17283
  310. Turco M, Ausiello A, Micoli L (2016) *Treatment of Biogas for Feeding High Temperature Fuel Cells*, Springer International Publishing Switzerland, Green Energy and Technology, DOI 10.1007/978-3-319-03215-3\_1
  311. Rouquerol F, Rouquerol J, Sing K, *Adsorption by Powders & Porous Solids, Principles, Methodology and Applications*. Ed by Academic Press.
  312. Dabrowski A, *Adsorption-from theory to practice*, *Advances in Colloid and Interface Science*, 93 (2001) 135–224.
  313. Cigolotti V, McPhail S, Moreno A. Nonconventional fuels for high-temperature fuel cells: status and issues. *J Fuel Cell Sci Technol* 2009;6:0213111-8.
  314. Andrey Bagreev, Teresa J. Bandoz, “A Role of Sodium Hydroxide in the Process of Hydrogen Sulphide Adsorption/Oxidation on Caustic-Impregnated Activated Carbons”, *Ind. Eng. Chem. Res.* (2002), 41. pp. 672–

679.

315. "MAXIMUM-LIKELIHOOD ESTIMATION OF THE 4-PARAMETER GENERALIZED WEIBULL DISTRIBUTION", Manmohan S. Arora.
316. "On the Three-Parameter Weibull Distribution Shape Parameter Estimation", Mahdi Teimouri and Arjun K. Gupta; Amirkabir University of Technology, Gonbad Kavous University and Bowling Green State University.
317. "Curvas en s tecnologia medica – Citometria de flujo", José Wilton Vieira Ricardo; Andrés Felipe Avalos.
318. "Shapes and functions of species–area curves: a review of possible models", Even Tjørve Lillehammer College, 2626 Lillehammer, Norway
319. "The five parameter logistic: A characterization and comparison with the four parameter logistic", Paul G. Gottschalk, John R. Dunn, 2005.

## Chapter 4: Integrated System Anaerobic Digester/Fuel Cell

### 4.1 Introduction

Fuel Cells can be integrated to biogas producing plants. The first applications of fuel cells (FCs) of industrial size fed with biogas from anaerobic digesters downstream of the water treatment plants date back to the ninety years [1]. The US EPA (Environment Protection Agency), along with ONSI, has made a series of tests on different plants equipped with Phosphoric acid fuel cells (PAFC) with a power of 200 kWe (ONSI PC unit 25).

Figure 4-1 shows one unit ONSI PC25 installed at the Columbia Boulevard Wastewater Treatment Plant in Portland (Oregon) [2].



Fig. 4-1 PAFC system ONSI (200 kWe) fueled with biogas produced from anaerobic digester  
Columbia Boulevard Wastewater Treatment Plant in Portland (Oregon)

The typical composition of the biogas produced in these digesters is the following:  $\text{CH}_4$  (57-66% vol),  $\text{CO}_2$  (33-39% vol),  $\text{N}_2$  (1-10% vol) and  $\text{O}_2$  (<0.5% vol). The gas is typically saturated with water vapor at 35 °C. The concentration of sulphur, mainly hydrogen sulphide, is in a range 6-200 ppmv, while the chlorinated compounds concentration is less than 4 ppmv. The calorific value of the biogas produced by the digester is 5,34-6,23 kcal / L (dry basis) [3].

Concentrations of sulphur compounds present in the biogas up to 200 ppmv are clearly incompatible with FCs plant. Thus clean-up system is needed to obtain purity levels required by FCs.

The biogas treatment system tested in this test campaign of PAFC cell is based on the hydrogen sulphide absorption on non-regenerative beds [4]. This pre-treatment of the biogas system has given satisfactory results with an efficiency of abatement of 98% approximately and the concentrations of

hydrogen sulphide in output is lower the limit of detection of 10 ppbv. The residue of sulphur, present in the form of organic compounds (about 0.5 ppmv), is eliminated by desulphurizer present in the power system PAFC PC25. The residual levels were compatible with the expected life of the catalyst (5 years and 40,000 hours of operation). The PAFC plant Yonkers [2] has worked mostly at a power of 150 kWe, with peaks at 200 kWe.

“Fuel Cell Energy” and the German partners of MTU Onsite Energy, leading companies in the production of molten carbonate FCs technology (MCFC), installed in Europe, U.S.A., Japan and Korea many sized plants between 200 kWe and 1 MWe fueled with gas from anaerobic digesters of industrial waste and wastewater treatment plants. Also Ansaldo Fuel Cells has been studied application of FCs fueled with biogas. In view of this type of application, in the context of national and international projects involving ENEA, ERSE (Energy Services Regulatory Authority) have been studied the effects of sulphur compounds on MCFC and the fuel pre-treatment systems.

The MCFCs and SOFCs has been considered, in recent years, the most promising for applications with biogas, (especially for plants exceeding a few hundred kWe) since they are able to tolerate several compounds present in the biogas which are harmful to the low temperature FCs (PEMFC and PAFC). Furthermore, the MCFC has the advantage of using CO<sub>2</sub> as a reactant to the cathode, a prerogative that allows to gain a few percentage points of efficiency compared to the other FCs [5]. For the last decade the attention of the scientific community has focused on reducing greenhouse gas emissions with initiatives and regulations to promote the reduction of greenhouse gas emissions (see chapter 1). In this context fits perfectly the integrated plant Biomass / Digester / FC.

Fuel Cell Energy (Germany company) has been installed more than 50 worldwide plants in power range 100 kWe-2 MWe. About 30% of this plants are powered by gas produced from renewable sources, including the product gas from anaerobic digesters in systems for Water Treatment. [5].

The Tulare plant (California) consists of three DFC300<sup>TM</sup> Unit, for a total of 900 kWe. The thermal energy produced by the FCs system is used to preheat the sludge in the digester.

The Oxnard facility (California) consists in two units for a total of 600 kWe. It has been developed at the Gills Onions, the largest US company in the field of onion processing. Gills Onions disposing of about 30000 tons per year of processing waste and the composting, besides being expensive, generates significant emissions of CH<sub>4</sub> in the atmosphere, much more GHG than CO<sub>2</sub>. The organic compounds are sent to a digester and the biogas is used to power the fuel cells after appropriate treatments.

In cooperation with the Korean company POSCO, Fuel Cell Energy has installed and has planned to install several plants also in South Korea, some of which fed with biogas.

In Europe, the first installation of a system of MCFC fueled by biogas was produced by RWE Fuel Cells GmbH in Germany (Ahlen) [6]. The MCFC unit is an “Hot Module 250 kWe” supplied by MTU Onsite Energy. The biogas is produced from an anaerobic digester installed in a wastewater treatment plant. The plant is able to produce between 1500-2000 m<sup>3</sup> of gas per day with an average methane content of 60 % vol. The Hot Module is a compact unit designed to run with natural gas grid and its use with biogas unit requires some additional external modules. The concentration of carbon dioxide in the biogas produced by the digester in Ahlen is 38 % vol and the low calorific value of the biogas due to methane dilution, requires an increase of about 50% of the fuel gas flow rate at full power. To this purpose, on the system of Ahlen, a compressor is needed to maintaining the pressure required at the entrance of Hot Module. Some technical solutions have also been required to protect the fuel cell from the non-negligible concentrations of oxygen present in the biogas. An analysis system of continuous gas, at the entrance of the Hot Module, allows to control both the oxygen content than the hydrogen sulphide remaining in the clean biogas.

At European level, the “EFFECTIVE” project, concluded in 2004, and partially funded by the European Commission, has provided interesting results on the integration of MCFs with biogas production from renewable sources (biomass) [7]. The project consortium was led by Profactor, an Austrian company active in the field of nanotechnologies and innovative solutions for the exploitation of renewable energy sources (biomass, biogas treatment). The project leads to the creation of two separate biogas treatment systems integrated in two test stations for laboratory MCFC stack (300 We), which were located in different Europeans biogas plants and tested for 2000-5000 hours.

As previously discussed the use of biogas in fuel cells requires the almost complete removal of hydrogen sulphide. In EFFECTIVE project have been developed two distinct systems able to obtain concentration of hydrogen sulphide in the biogas lower than 10 ppmv: a chemical system, realized by Seaborne, and a biological system developed by Profactor. A second subsequent stage of purification with activated carbon then allowed in both cases to obtain sufficiently pure gases to feed the MCFC stack (MTU / FCE with internal reforming technology). During the project, between 2002 and 2004 has been tested biogas obtained from landfill, water treatment, agricultural waste and co-fermentation, respectively, in Spain, Germany, Austria and Slovakia, for a total of 15000 operating hours [7].

Table 4-1 shows the installations to FC fueled by biogas with the respective power range.



<b>Location and FCs type</b>	<b>Power [kWe]</b>
Portland (USA)/PAFC	200
Yonkers (USA)/PAFC	150
Tulare (USA)/MCFC	900
Oxnord (USA)/MCFC	600
San Diego (USA)/MCFC	1000
Fontana (USA)/MCFC	2000
Ahlen (Germany)/MCFC	250
Consortium FCs South Korea/MCFC	100-900
Consortium FCs Japan/MCFC	100-900

Tab. 4-1 Location, type and power of the FCs plants fueled by biogas

## 4.2 Content of Chapter

In this chapter will be designed an integrated plant anaerobic digester/fuel cells. Part of the research during the PhD has been carried out at the Paul Scherrer Institut (PSI) (Villigen, Switzerland). During this period was developed the project "Manure to Electricity" in the field "Biosweet (Biomass for Swiss Energy Future). This project was done in collaboration with other Swiss universities (Ecole Polytechnique Federale de Lausanne, Zurich University of Applied Sciences) and research centers (WSL, Federal Institute for Forest, Snow and Landscape Research). This plan provides for the development of small systems (up to 100 kWe) based on fuel cells, in particular the SOFCs fed by renewable sources. The coordinator of the project is Dr. Serge Biollaz (Head of Thermochemical Group at PSI).

Solid oxide fuel cells have been preferred because more flexible and adaptable than the MCFCs and therefore more suitable for low power plant. Moreover, many companies are beginning to develop industrially Small systems for sale on a large scale.

The biomass choice is the manure since Switzerland has a large availability of such biomass, mainly concentrated in small farms. This project is also interesting for Italy due to the large availability of manure derived by agro livestock activities. As seen in Chapter 2, there are more than 6 million of cattle on our territory (about 350000 in Campania region) [8].

The feasibility study of an integrated plant anaerobic digester/SOFCs for electricity production (power range 2-100 kWe) is carried out with focus on CH<sub>4</sub> production taking into account the productivity of the different farms insisting in the different area of the country, clean up system,

choice of SOFCs and flow-sheet of the global plant. The use of biohydrogen produced by ADH, ADHexp, litter, OFMSW, that are studied in this PhD thesis has been considered.

#### **4.3 Manure to Electricity using Fuel Cells**

Switzerland has a considerable but under-utilized bioenergy potential in the form of manure. This manure originates primarily from cattle. It is distributed across many small farms. In 2015 the average animal density was 24 animals (GVE) per farm. The small size and decentralized nature of these manure sources result in challenging questions: how do we make best use of Swiss manure for energy use at a scale of 2-100 kWe; what limiting conditions prevent the use of this energy source; by which means farmers can be encouraged to implement energetic use of manure; what technology chains are most promising. These questions are addressed by a SCCER BIOSWEET team consisting of several independent research groups and external partners.

At this early stage of the study, the scope of the Manure-to-Electricity project is focused on developing concepts for value chains that make such technologies attractive for Swiss agriculture. The development of such technology involves several technical features and an adequate “technology supply chain” to the market.

The Manure-to-Electricity team in SCCER BIOSWEET was assembled from research groups with an expertise in each of the key areas needed to develop this value chain. A detailed assessment of Swiss manure resources is provided by Vanessa Burg from the WSL.

On a technical level, several process steps are necessary to generate electricity from manure. Manure can be easily converted to biogas by anaerobic digestion processes, which is the research area of Prof. Urs Baier’s group at ZHAW. At the current state of the project the operating conditions of a small size digester have been selected and several companies have been identified in the international market, which can supply such small scale digesters.

The quality of biogas is a key point since several harmful compounds, even in trace amounts, can irreversibly damage the electricity generation unit (fuel cell, internal combustion engine). With support from the group of Dr. Serge Biollaz at PSI, a clean-up system was evaluated and several adsorbing materials have been identified to remove such compounds up to the concentration limits defined by fuel cells. The final step is to convert this biogas to electricity. The use of solid oxide fuel cell (SOFC) technology for the production of electricity (2-5 kWe) from agro-biogas was assessed by a research group at EPFL, led by Dr. Jan Van herle. Several fuel cell companies were identified in the European market as potential suppliers.

An ongoing difficulty concerns the economics and cost structure of such a system. This is an issue which can only be resolved by close collaboration between technology experts, Swiss farmers, and

research groups. A review of the cost structure and possible revenues is the focus of the next stage of analysis.

The SCCER BIOSWEET-team is perfectly positioned to initiate this dialog. In the end, the project “Manure to Electricity” should lead to better “waste to energy” processes that allow to reduce the use of fossil fuels and greenhouse gas emissions by the use of renewable sources that exist already today in Switzerland. In the short term this joint effort should lead to a smart pilot and demonstration project, which validates the outcome of the ongoing study. Ultimately, electricity generation from biowaste in this way could raise its contribution to the Swiss electricity supply from currently 0.5% to 5%, additionally recovering some useful heat [9].

#### **4.3.1 Concept Development and Feasibility Study**

Technical scope of the ongoing project is developing a value chain “energy & money”. For a successful implementation of such technology, a “technology supply chain” is needed [9].

Main tasks to be treated deal with power scale, costs, technological readiness, and dynamic response. For example, it is relevant to define the type of manure resource size/type characterizing the chemical/physical properties (humidity, C/H/N ratio, the organic fraction); the anaerobic digester techno-economic feasibility at small scale; the gas cleaning materials; the SOFC stack; the storage or transportation issue for manure/digestate/biogas.

The power range of 2-5 kWe (and in future up to 100 kWe) has been defined taking into account that in Switzerland there are many small farms that have a gross average potential of 1-10 kWe. The aim of the project is the development of 1000-5000 units in the next years for the production of renewable energy for local use.

It is important to know the regulations for the development of a plant and the possible incentives to make attractive the project for the users.

This involves at least two scenarios for the realization of the project: the first (Fig. 4-2) is to use the biomass available in the farm to produce energy, the second option (Fig. 4-3) is to concentrate the biomass from two or more farms and produce electricity in a plant which is located near the farms.

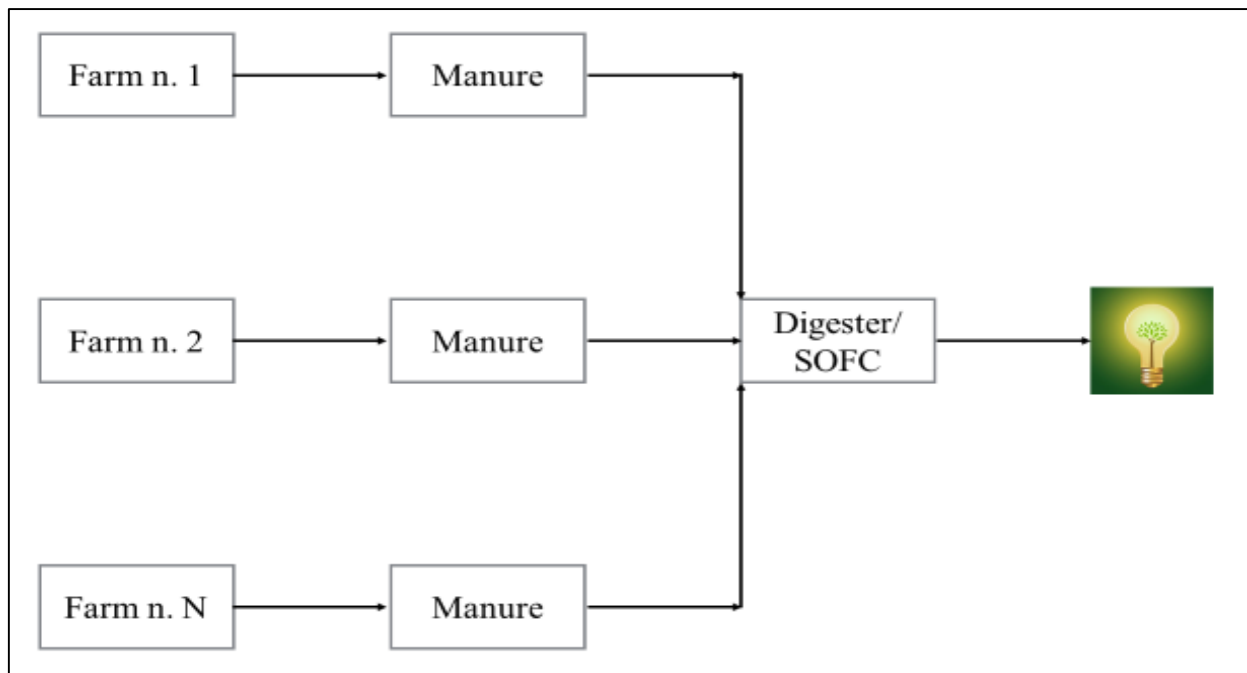


Fig. 4-2 Scenario n. 1: Centralized energy use

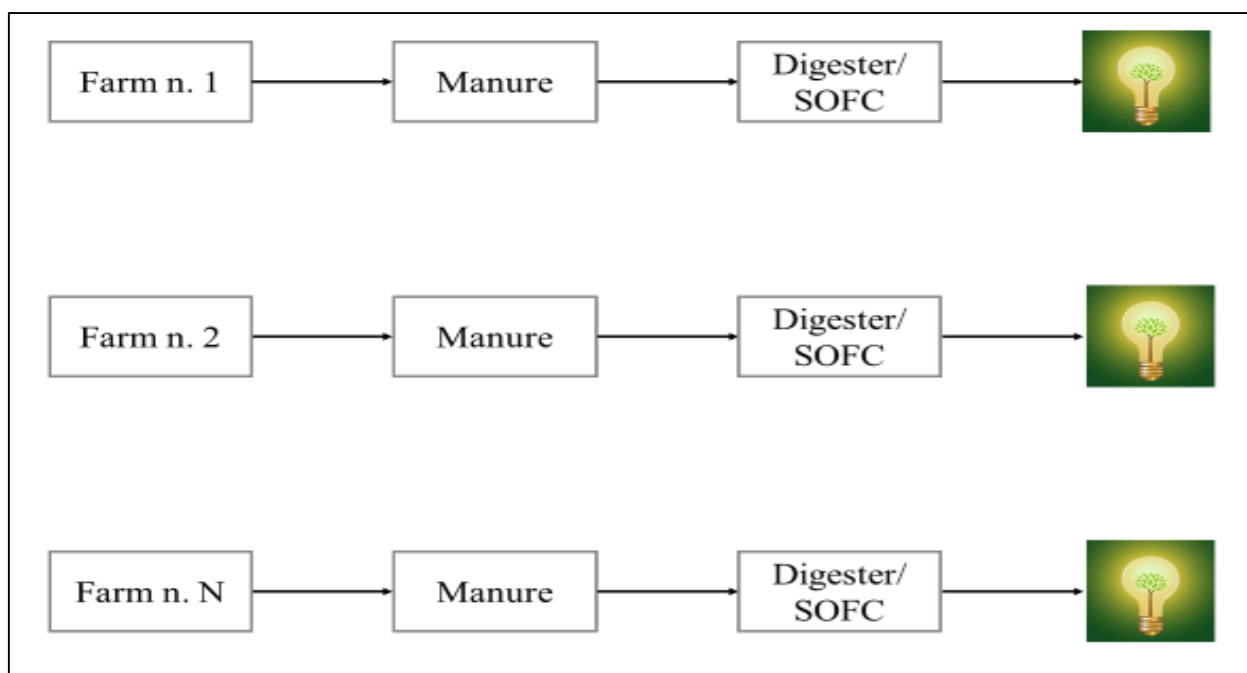


Fig. 4-3 Scenario n. 2: local energy use

### *Feasibility Study*

The feasibility study has been performed considering the different aspects related to the integrated plant taking into account the socio economic context to which it is addressed. Thus this study considered the following steps: resources assessments; AD process; biogas clean-up; SOFCs stack and commercial availability, economic analysis.

At First it is important to evaluate the project, wondering if it makes sense or not by studying and analyzing the different components needed to realize the plant. General approach is needed to evaluate the theoretical and sustainable potential of biomass for biogas production (animal number, farms, stabling system). In Switzerland are available 2000000 tons of dry matter from cattle, with 36 PJ of primary energy content [9].

After the resource assessment, is possible to analyze the single farms in details. Most single farms show a gross biogas potential of 10-20 kWe (this data is crucial to choice the power of integrated plant). There are almost no decentralized off-grid solutions, so it is necessary develop a technology for local use of the electricity produced.

The primary goal of the project is to define operational limits for AD process, gas cleaning and SOFC stack. To this purpose is necessary the evaluation of critical biogas parameters for biogas cleaning, SOFC and identify operational AD parameters to positively influence them.

On the other hands the identification limits of load and flow variation and on/off operation for biogas cleaning and SOFC operation are also be considered.

The biogas clean-up deserves thorough investigation because no dominant “off-the-shelf” design exists for biogas cleaning for sensitive end use like a SOFC operated on biogas from manure. This is due to possible variability of contaminant amounts, novelty of the integration with fuel cells and difficulty of laboratory testing with representative gas mixture. The primary goal is to determine cost-effective gas cleaning sequence for manure digestion to the electricity conversion unit at small scale.

Finally, the integration of digester plant with SOFCs stack must be investigated defining how to start-up of a SOFC system with small scale agro-biogas production and operate it with low (thermal) cycling needed. Moreover, it is important to assess how to make the whole small-scale conversion chain cheap and simple in order to compete with ICE, and define the appropriate power size(s)., The study also involves the determination of the heat needs and how they can be optimally covered, the threshold level of contaminants present in biogas stream. The expected building up of the plant requires a market investigation aimed to identify a possible supplier for SOFCs stack.

#### **4.3.2 Plant Design and Development**

Now, it is important define the main devices and parameters of the global plant. In table 1 has been reported the calorific value of manure, methane and hydrogen which will be useful for the characterization of the plant.

Compound	Calorific Value				
	<b>kJ/m<sup>3</sup></b>	<b>kWh/m<sup>3</sup></b>	<b>kcal/m<sup>3</sup></b>	<b>kJ/kg</b>	<b>kcal/kg</b>
Manure*	24000	6,67	5732	24,30	8,19
Methane	31650	8,79	7564	50000	11940
Hydrogen	10760	2,99	2572	120000	28680

Table 4-2: Calorific value of Manure, CH<sub>4</sub> and H<sub>2</sub>

\*For the calorific value of manure an average value was considered.

Typical production availability for the anaerobic digestion process using manure from cattle is the following:

The amount of manure produced per day is 61.5 kg per head. The manure is composed from different fraction, only 20% is available for the anaerobic digestion process (12.3 kg, total solid), consequently the amount of volatile solid (80%) is 9.7 kg per head.

The production of biogas expected from manure correspond to: 0.2-0.4 m<sup>3</sup> biogas/kg v.s. [10].

Figure 4-4 shows the global flow-sheet of the plant with the devices and necessary auxiliary equipment. For the scenario n.1 the method for the accumulation of biomass before the digester will be studied to reduce environmental impact due to the transportation of biomass. For this reasons, the scenario n.1 is interesting for farms not very far (within 30 km from the plant). For the scenario n. 2, differently from scenario n.1, the distribution of energy to different farms (for local use) must be designed.

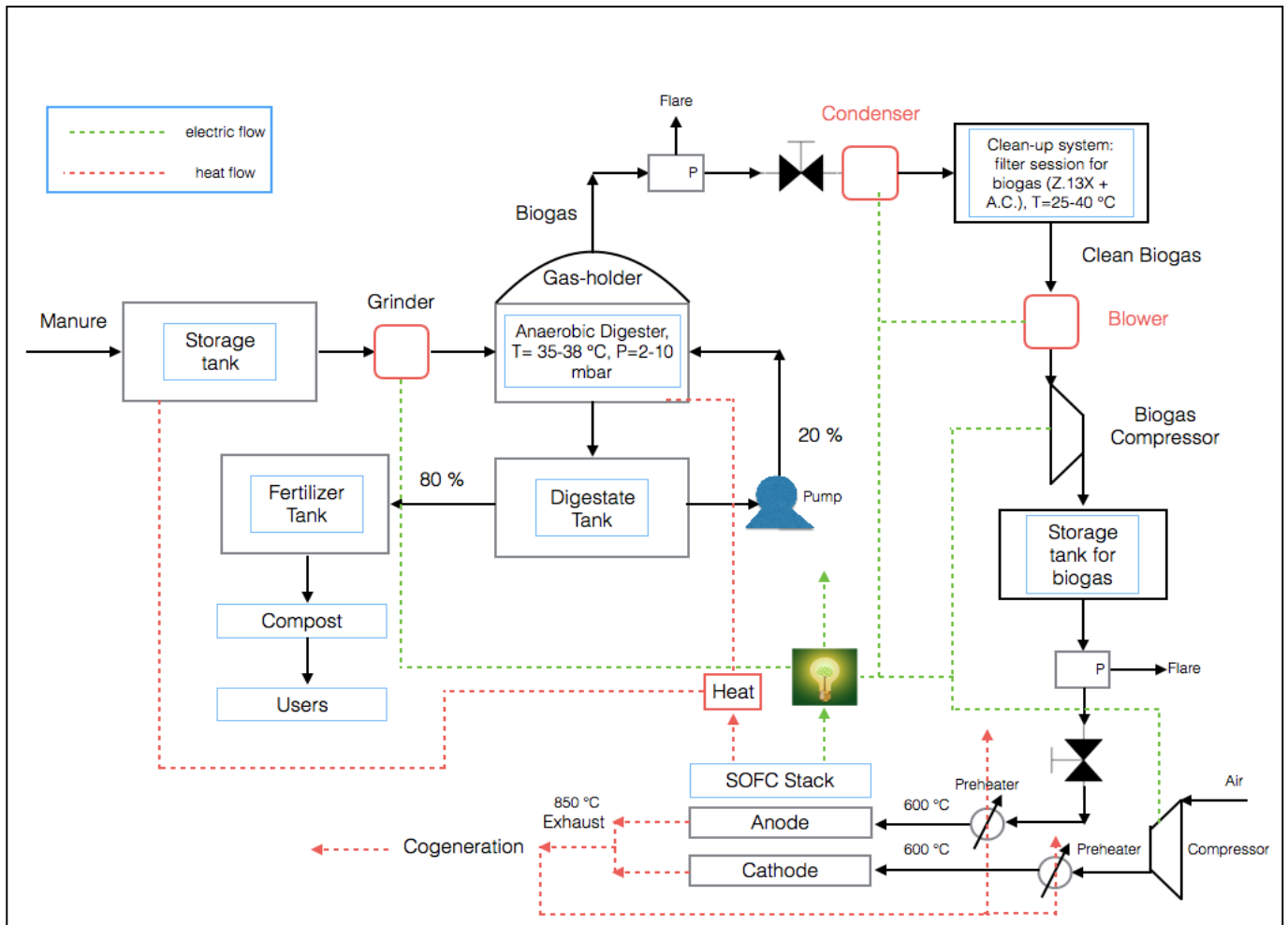


Figure 4-4: Flow-sheet of global integrate plant Anaerobic Digester/SOFC

The integrated plant anaerobic digester/FCs consists of different section:

- 1) Biomass storage and pre-treatment
- 2) Anaerobic Digester and digestate tank
- 3) Upgrade and clean-up systems
- 4) Storage tank for biogas and SOFC

### Section 1

The first step is the sizing of the storage tank for the manure. Storage tank allows the accumulation of biomass to granting the reserve necessary for the plant. Typically, it is preferred to obtain a biomass reserve necessary for 1-6 months of operation of the plant. The storage tank is sized taking into account the power required (2-100 kWe) and corresponding to different biomethane flows and consequently the amount of biomass needed. Biomethane flows are calculated by Eq. (4.1)

$$\eta = \frac{P_{el}}{Q \cdot H_i} \quad (4.1)$$

where:  $\eta$  is the efficiency of SOFC, equal to 0.6,  $Q$  is the amount of biomethane needed to obtain the power required ( $P_{el}$ ) and  $H_i$  is the calorific value of methane (31650 kJ/m<sup>3</sup>).

Table 4-3 summarizes the biomethane flows calculated:

Power [kWe]	CH <sub>4</sub> Flow Rate	
	[m <sup>3</sup> /h]	[m <sup>3</sup> /d]
2	0.39	9.36
10	1.896	45.504
75	14.218	341.232
100	18.957	454.968

Table 4-3: Methane needed for a power required

It is important to make some considerations about the biogas obtained from manure.

The typical composition of biogas from manure is CH<sub>4</sub> 50% vol, CO<sub>2</sub> 45% vol, other compounds 5% vol. The other compounds can be divided in: H<sub>2</sub>O up to 50000 ppm, H<sub>2</sub>S up to 3000 ppm, siloxanes up to 0.6 ppm, halogens up to 0.2 ppm and other traces.

From the biomethane flow rate the amount of manure should be calculated. As previously mentioned, the manure is typically composed of 20% wt (total solid) of organic matter able for the anaerobic digestion process and the remaining 80% is not able for the biogas production and the yields to biogas is 0.2-0.4 m<sup>3</sup>/kg v.s.

For the calculation it has been considered a concentration of methane in biogas of 50% and a productivity of 0.4 m<sup>3</sup>/kg v.s. From this data the volume of manure can be evaluated with an average density of manure is 700 kg /m<sup>3</sup>. In Table 4-4: the amount of biomass per day, the corresponding number of animals and the volume of storage tank (V S.T.) needed to obtain the power required are summarized.



<b>P</b> [kWe]	<b>Manure</b> [kg/d]	<b>V<sub>manure</sub></b> [m <sup>3</sup> /d]	<b>Head</b> <b>Number</b>	<b>V<sub>s.t.</sub></b> <b>[m<sup>3</sup>]</b>		
				<b>30 d</b>	<b>90 d</b>	<b>180 d</b>
2	260	0.38	5	12	34	67
10	1296	1.86	26	56	167	334
75	9719	14	194	417	1250	2499
100	12958	19	260	556	1666	3332

Tab. 4-4: Amount of biomass, number of head and the volume of storage tank (S.T.)

The design of storage tank must be considering different points. The first one is that depending on the type and the size of manure (diluted, not diluted, or in a slurry). It can be expected before the inlet to the digester a pump (for the liquid manure) or a grinder to homogenize the biomass inside the digester. For the optimization of anaerobic digestion process, it is important that the final size of biomass particles is about 10-15 mm. Other important parameter is the temperature. To reduce the lag phase in the digester, some plants use a pre-heating system to bring the inlet temperature of biomass near to the operating temperature of digester [11].

## Section 2

The digester considered is CSTR type. It consists of a stirred tank for the biomass digestion process and of a gas holder that has the function of collecting the biogas up to a fixed pressure (about 2-3 bar). For the calculation the volume of digester is calculated by the following equation:

$$V_{\text{dig}} = (Q_{\text{biomass}} + Q_{\text{digestate recycled}}) * \text{HRT} * \text{SF} \quad (4.2)$$

where:  $Q_{\text{biomass}}$  is the amount per day of biomass [m<sup>3</sup>/d],  $Q_{\text{digestate}}$  is the amount of digestate per day [m<sup>3</sup>/d], HRT (hydraulic retention time) [d], SF: safety factor.

For the calculation of digester volume HRT is in a range 15-30 days; while for the SF a value of 1.10-1.15. The volume of digester is calculated taking into account that the digestate recycled in the digester is about 20% of total. The volume of digester is calculated from the manure density (700 kg /m<sup>3</sup>) and are reported in Table 4-5.

<b>P</b> <b>[kWe]</b>	<b>V<sub>digester</sub></b> <b>[m<sup>3</sup>]</b>
2	15
10	74
75	550
100	740

Tab. 4-5: Volumes of digester need for a power of 2,10, 75, 100 kWe

The volume of digestate tank can be calculated considering the volume of biomass that is residual from the process of digestion leading to biogas. This can be calculated by Eq. (4.3).

$$V_{\text{digestate}} = (Q_{\text{biomass in}} - Q_{\text{biogas}}) * D \quad (4.3)$$

where  $Q_{\text{biomass in}}$  is the amount per day of biomass [m<sup>3</sup>/d],  $Q_{\text{biogas}}$  is the volume of biomass needed to produce biogas [m<sup>3</sup>/d] and D is the storing time of digestate [d].

Table 4-6 summarizes the volume of digestate tank for the different power considered.

<b>P</b> <b>[kWe]</b>	<b>V s.t.</b> <b>[m<sup>3</sup>]</b>		
	<b>30 d</b>	<b>90 d</b>	<b>180 d</b>
2	10.4	32.6	66
10	52	162	330
75	388	1222	2471
100	520	1620	3300

Tab. 4-6 Volume of the tank for digestate storage

### Section 3

Before moving to the sizing of the absorbent bed it is important to establish the composition of the biogas output from the digester. The composition of biogas from manure, considering that the amount of methane and of the other compound may change depending of the type of manure is the following (Tab. 4-7):

Compound	Concentration
CH <sub>4</sub>	50-55 %
CO <sub>2</sub>	40-50 %
NH <sub>3</sub>	up to 500 ppm
H <sub>2</sub> S	up to 3000 ppm
Siloxanes	up to 0.6 ppm
Halogens	up to 0.2 ppm
H <sub>2</sub> O	up to 5 %

Tab. 4-7 Biogas composition after the anaerobic digestion phase

The upgrading is a step necessary to increase the calorific value of biogas stream by removal compounds such as CO<sub>2</sub> and H<sub>2</sub>O that are present in concentration reported in table 4-7. Upgrading is typically carried out by condensing water in a temperature range of 10-25 °C. Considering that the H<sub>2</sub>O partial pressure at 10 °C is 9.5 mmHg and at 25 °C is 24 mmHg it is possible considerer that the concentration of water after the condenser is lower than 2% vol. It must be remarked that during the concentration some H<sub>2</sub>S can be adsorbed in liquid H<sub>2</sub>O leading to a reduction of the content in gas phase.

The composition of biogas out coming from the condenser are reported in table 4-8

Compound	Concentration
CH <sub>4</sub>	50-55%
CO <sub>2</sub>	45-50%
NH <sub>3</sub>	traces
H <sub>2</sub> S	100-300 ppm
Siloxanes	0.6 ppm
Halogens	0.2 ppm
H <sub>2</sub> O	< 2%

Tab. 4-8 Biogas composition before the clean-up step

Clean-up is required for purification of biogas stream from harmful compounds (mainly H<sub>2</sub>S and HCl) that can poison SOFCs stack. Clean up is generally carried out by adsorption on microporous materials (see chapter 3) in fixed bed devices.

Particular attention needs to be done to sulphur compounds. Production of sulphur compounds by anaerobic bacteria involves sulfate reduction and metabolism of sulphur-containing amino acids.

Sulfate reduction proceeds via assimilatory or dissimilatory pathways. In the assimilatory process, bacteria produce enough reduced sulphur for cell biosynthesis of cysteine and methionine by transporting sulfate into the cell and activation to adenosine-5'-phosphosulfate [10]. This is in contrast to the dissimilatory process in which sulfate is used as terminal electron acceptor and copious amounts of malodorous, toxic sulphide are produced as follows:



Sulfate can be supplied by dietary means or by depolymerization and desulfation of endogenously produced, sulfated glycoproteins such as mucins. Also,  $\text{H}_2$  availability in the medium may influence competition between sulfate reducers and methanogens with non-limiting concentrations of  $\text{H}_2$  allowing both processes to occur concomitantly. In the gut, the major hydrogenotrophic sulfate reducer is the genus *Desulfovibrio*, which is numerically dominant in feces. Assimilatory sulfate reducing bacteria are probably ubiquitous but include the genera *Veillonella*, *Megasphaera*, and the enterobacteria [10].

Metabolism of S-containing amino acids also gives rise to sulphide and mercaptans as follows:



So the origin of the manure is not absolutely neglected because it can lead to important differences in the biogas produced. For example, biogas obtained from cattle or pigs manure will have a concentration of  $\text{H}_2\text{S}$  very different from that from poultry manure. This is because the food of chickens is based on proteins (for increase the growth) and then the manure will have a higher concentration of protein and thus biogas with a higher concentration of  $\text{H}_2\text{S}$ .

$\text{H}_2\text{S}$  can be partially removed in the some instant in upgrading step or during digestion by adding a small amount of oxygen (2-6%) or iron salts [10].

The addition of oxygen in the digester allows the life of some aerobic microorganisms capable of oxidizing the sulphides to elemental sulphur, but unfortunately this step alone does not allow to sufficiently reduce the level of sulphides in the biogas. The addition of iron salts in the digester leads to the precipitation of the sulphides in the digester itself, but it is a less efficient process. Furthermore, this process does not allow to recover the iron at the end of the process. So, for the first step of  $\text{H}_2\text{S}$  removal during the digester it can be profitable the addition of oxygen to reduce the  $\text{H}_2\text{S}$  concentration to 100-300 ppm.

It is important to estimate the amount of activated carbons (AC) and Zeolites 13 X (13X) needed to reduce the concentration of H<sub>2</sub>S and other harmful compounds up to the tolerance limit of SOFC.

The adsorbent capacity of modified AC and 13X are respectively 0.14 g H<sub>2</sub>S/g AC and 0.08 g H<sub>2</sub>S/g 13 X and the siloxanes can be completely removed in the same adsorbent bed (see Chapter 3).

The quantity of AC and 13X depends from the electricity power that to be obtained. Table 4-9 summarize the amount of AC and 13X necessary to obtain a complete removal of harmful compounds. It was considered a concentration of H<sub>2</sub>S in the biogas equal to 300 ppm after reduction using 2-6% vol of O<sub>2</sub> in digester [10]:

<b>Power [kWe]</b>	<b>Material Amount [kg/y]</b>	
	<b>13X</b>	<b>AC</b>
2	38	22
10	190	108
75	1418	810
100	1890	1080

Tab. 4-9 Amount of 13X and AC necessary for biogas clean-up

After the clean-up system, there are two options: directly feed the biogas to the stack of SOFC, or to have a storage tank for biogas.

To get a constant feed of biogas to the stack of SOFC, it is preferable, before the SOFC stack, a storage tank.

#### 4.3.2 Economic Analysis

After the technical analysis, it is possible to evaluate the economic aspect of the project considering the ancillary, the investment costs. The total investment costs including thus the ancillary devices consider the realization of the plant, the maintenance costs and any extra costs.

#### 4.3.2.1 Investment costs

##### *AD Plant*

The plant costs include the costs necessary for the realization of the digester, the storage tanks for manure and digestate, the ancillary devices, the cost for the clean-up system and the cost necessary to the implementation of SOFC stack. Firstly, the costs of units necessary for AD process are calculated. This evaluation is performed for Switzerland but lower investment costs are expected for UE market.

It can be assumed that the costs for a digestion plant, that include all ancillary devices (pumps, heating digester, grinder, storage tank for manure and digestate), is about 10000 CHF/kWeI to which are added installation costs that are approximately 500 CHF/m<sup>3</sup> V<sub>digester</sub>.

For the total costs of AD steps have been used the following equation:

$$C_{AD} = (10000 \text{ [CHF/kWe]} * P_{el} \text{ [kWe]}) + (V_{\text{digester}} \text{ [m}^3\text{]} * 500 \text{ [CHF/m}^3\text{]}) \quad (4.7)$$

This cost must be increased by 10% for incidental charges. Table 4-10 summarize the costs for different plant size.

<b>P</b> <b>[kWe]</b>	<b>AD plant costs</b>	
	<b>[CHF]</b>	<b>[€]</b>
2	27500	25785
10	137000	128460
75	1025000	961100
100	1370000	1284593

Tab. 4-10 Total costs for AD process

##### *Clean-up step*

The biogas clean-up is carried out in an absorbent bed of zeolites and/or activated carbons. The amount of 13X and AC needed have been calculated previously (see Table 4-9).

For the 13X the range costs are about 1-3 CHF/kg while for the AC is about 12-15 CHF/kg. Therefore the average value of 2 CHF/kg for 13X and 13 CHF/kg for AC was considered for the economic analysis. About 25% of the costs must be added for the accessory devices.

P [kWe]	Adsorbents Mass [kg/y]		Costs [CHF/y]		Costs [€/y]	
	13X	AC	13X	AC	13X	AC
2	38	22	95	358	89	335
10	190	108	475	1755	445	1646
75	1418	810	3545	13163	3325	12347
100	1890	1080	4725	17550	4432	16462

Tab. 4-11 Average costs for clean-up

### SOFC stack

The global cost of SOFC stack apparatus is not proportional with the power and it's not possible a precise estimation of the costs since this largely vary depends on the supplier. For example, the BluGen stack (1.5-2 kWe) collected by SolidPower has a price of about 20000 CHF, with an average cost of 10000 CHF/kW.

Practically the range of costs for the SOFC is very large, several and market prices vary in the range costs from 3000-7000 [CHF/kW] [12]. It was decided to consider the higher price (7000 CHF/kW) for a conservative estimate of the costs. Table 4-12 summarize the total costs for the SOFC stack.

P [kWe]	SOFC Cost	
	[CHF]	[€]
2	20000*	18756
10	70000	65646
75	525000	492343
100	700000	656457

Tab. 4-12 Average costs for SOFC stack

\*(BluGen)

Investment costs are reported in the following Table 4-13: the global plant is the sum of 4 amount, the anaerobic digester part, the clean-up, the SOFC and other costs that include the operating costs of the various devices (pump, compressor, condenser etc.) and can be considered about the 10% of the global costs.

<b>P</b> <b>[kWe]</b>	<b>Costs</b> <b>[CHF]</b>					<b>Costs</b> <b>[€]</b>
	<b>AD Plant</b>	<b>Clean up per year</b>	<b>SOFC</b>	<b>Other costs</b>	<b>Total</b>	<b>Total</b>
2	27500	360	20000	4786	52646	49383
10	137000	1760	70000	20876	229636	215405
75	1025000	13170	525000	156317	1719487	1612928
100	1370000	17600	700000	208760	2296360	2154052

Tab. 4-13 Initial investments costs

#### 4.3.3 Future Scenarios








It is important to consider that in the next years the costs of devices are expected to decrease due to advancement of scientific and technological research and the opening of new markets. Just think about the many research projects that are being developed on these issues: in particular, the EU project, “Horizon 2020” with the specific topic “Fuel Cells and Hydrogen Joint Undertaking”, in US, the energy department continues to allocate considerable funds for the development of FCs and hydrogen technologies. Moreover, there are other two emerging excellences in Asia, South Korea and Japan which provide different investments to develop FCs for the production of domestic energy and for road transport with the construction of about 1000 hydrogen distributors (see Chapter 1 and 2).

On this basis the economic analysis is taken into account an accurate market survey and numerous companies have been contacted to comprehend how the cost of all devices will evolve in the future. Such survey points to a costs reduction in the medium/short period.

The following companies that can supplier anaerobic digesters have been selected: Bioelectric, Qube, Aspireco, EnertecBiogas, Hera Group, AB Cogeneration World, Agrikomp, BTS Italia, BTA International. All industries expect a cost of 350-700 €/m<sup>3</sup> at 2018.

In table 4-14 are indicated the possible suppliers for SOFCs stack. It is possible noted that for a small scale application the predict cost (2018-2020) is lower than 5000 €/kWe that should be considered as competitive price [12].



Companies	SOFC stack			
	Up to 50 kW <sub>e</sub>		Up to 250 kW <sub>e</sub>	
	2016	2018/2020	2016	2018/2020
	5000 €/kW <sub>e</sub> (AVL) to 19000 €/kW <sub>e</sub> (Sunfire)	< 5000 €/kW <sub>e</sub>	1500 €/kW <sub>e</sub>	< 500€/kW <sub>e</sub>
				
				
				
				
				
				

Tab. 4-14 Market survey and prediction costs of SOFC stacks

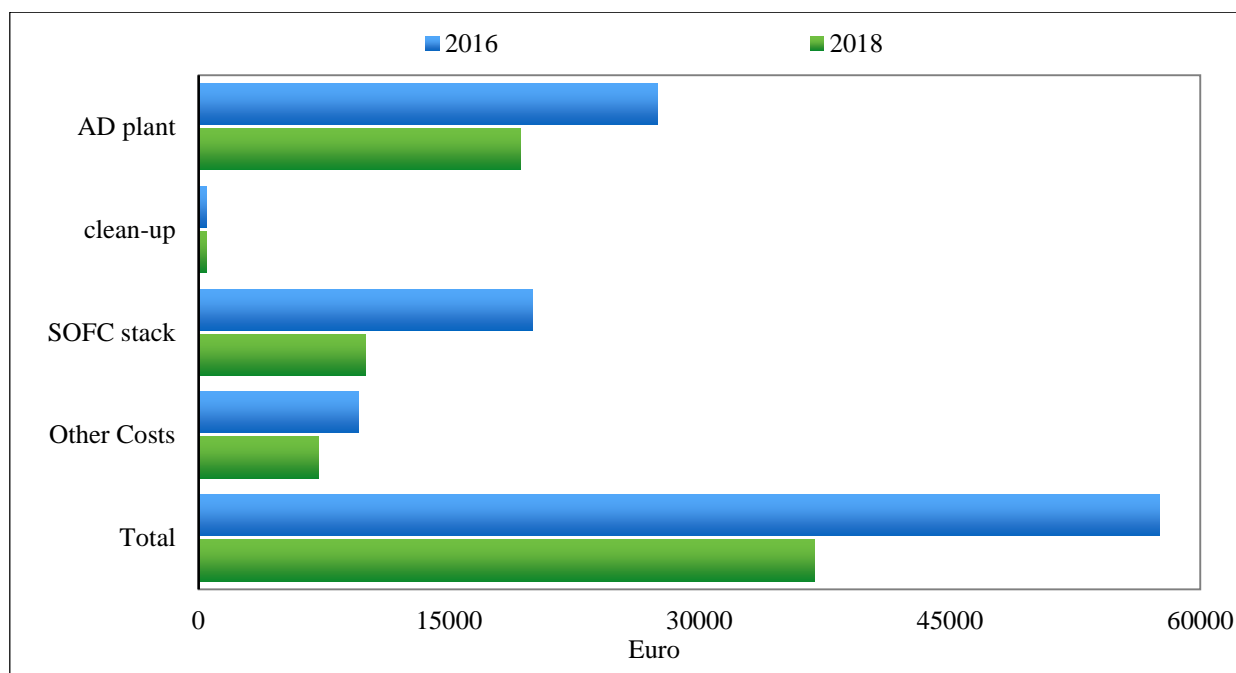


Fig. 4-5 Costs estimate for integrated system Anaerobic Digester / SOFCs in 2018

<b>Device</b>	<b>Prediction Costs Reduction (@ 2018)* (%)</b>
AD Plant	- 30
Clean-up System	/
SOFCs Stack	-50
Other Costs	-15
Total	-36

Tab. 4-15 Investments costs reduction @ 2018

\*referred to 2016 (see Tab. 4-13)

Figure 4-5 and Table 4-15 provide a cost estimate for 2018. It is important to note the strong total cost reduction (36%) and that this is only a conservative estimate because, with the large-scale development of FCs technology, these costs may be subject to a further decrease resulting in the growth of the competitiveness for this facility [12]

#### 4.4 Evaluation of Biomass for Fueling Biohydrogen

As mentioned in chapter 1, the SOFCs have the remarkable advantage of being fueled with both biomethane and biohydrogen.

The feeding with biohydrogen is interesting because it does not use the pre-reformer in the stack of SOFCs (see Chapter 1). A power size of 10 kWe has been considered because it represents the optimal size of such integrated plant in dependence on the biomass availability for local use of energy in the context of economic and productive reality in Italy and in particular in Southern Italy.

The volume of H<sub>2</sub> corresponding to 10 kWe is calculated by equation (4.1) considering the calorific value of H<sub>2</sub> (10760 kJ/m<sup>3</sup>) and corresponds to 5580 L. The amounts of different biomass needed to obtain the required biohydrogen flows have been calculated from data of Chapter 2 (Tab 4-16).

It is possible noted that the lower amount of biomass is for ADH (587 kg) while the higher amount is with manure (1641 kg).

For all the biomass this results are very interesting taking into account the wide availability on our territory and in the world of biomass used in this thesis.

<b>Sample</b>	<b>mL H<sub>2</sub>/g Biomass</b>	<b>kg biomass</b>
<b>ADH</b>	9,50	587
<b>ADHexp</b>	8,04	689
<b>Manure</b>	3,40	1641
<b>Litter</b>	3,81	1468
<b>OFMSW</b>	8,82	634

Tab. 4-16 Amount of biomass needed for AD/SOFC integrated plant of 10 kWe

## References

1. Spiegel R J, Thorneloe S A, Trocciola J C, Preston J L (1999) Fuel cell operation on anaerobic digester gas: conceptual design and assessment, *Waste Management* 19, 389-399
2. Scagliotti M, Valli C, (2010), Utilizzo del biogas per alimentazione di fuel cells: stato dell'arte e sperimentazioni con MCFC, Rapporto ERSE
3. Spiegel R J, Preston J L (2000) Test results for fuel cell operation on anaerobic digester gas, *Journal of Power Sources*, 86, 283-288
4. Spiegel R J, Trocciola J C, Healy H C and Lesieur R R (1999) Removal of hydrogen sulphide from anaerobic digester gas, US Patent Number 5,916,438.
5. Trogisch S, "Potential applications and synergies of biogas fuel cells as an efficient alternative energy conversion technology", in IEA Conference: Hydrogen and fuel cell based Energy systems, Vienna, Austria, 31/3-1/4/2004.
6. Krumbeck M, Klinge T and Döding B (2006) First European fuel cell installation with anaerobic digester gas in a molten carbonate fuel cell, *Journal of Power Sources*, 157, 902-905.
7. Trogisch S, Hoffmann J and Daza Bertrand L (2005) Operation of molten carbonate fuel cells with different biogas sources: A challenging approach for field trials, *Journal of Power Sources*, 145, 632-638.
8. <http://www.agricoltura.regione.campania.it/statistica/xls/14P.xls> Accessed 13 Feb 2017
9. <http://www.sccer-biosweet.ch/manure-to-electricity-at-small-scale-a-new-approach/> Accessed 13 Feb 2017
10. Turco M, Ausiello A, Micoli L (2016) *Treatment of Biogas for Feeding High Temperature Fuel Cells*, Springer International Publishing Switzerland, Green Energy and Technology, DOI 10.1007/978-3-319-03215-3\_1
11. Deublein D, Steinhauser A (2008) *Biogas from Waste and Renewable Resources*, Ed. By Wiley-VCH
12. 12<sup>th</sup> European SOFC & SOE Forum 2016, 5-8 July 2016, Lucerne, Switzerland.

## Conclusions

This PhD thesis concerns the study of an integrate system Anaerobic Digester/SOFC stack using biogas produced by anaerobic digestion (AD) of waste biomass.

The main topics treated are: the study of AD process, aimed to evaluate the potential of different waste biomass for energy recovery; the clean-up of biogas streams for removal of harmful compounds that can irreversibly damage SOFCs stack; the feasibility study of the integrated plant and economic analysis.

### *AD process*

This study has the main purpose to obtain CH<sub>4</sub> and/or H<sub>2</sub> rich biogas streams. Biomethane production is an established process, even although with room for improvement, but the production of biohydrogen by AD represents still a challenge and the present study has some novel features. The AD process studied is the Dark Fermentation (DF), the digestion in absence of sunlight, under mesophilic conditions (T=38°C). Different biomasses are studied: Arundo donax, litter for mice, manure from cattle and the organic fraction of municipal solid waste. An innovative experimental procedure for biomass digestion has been developed to promote H<sub>2</sub> production. This is based on successive adaptations of microbial consortia and on the use of an appropriate medium of salts and nutrients enabling to enhance the growth of bacteria hydrogen producers to the detriment of methanogenic ones. The results obtained are very interesting because high biogas volumes with H<sub>2</sub> concentrations, up to 70%, have been stably obtained. Experimental data indicate that after the third adaption the microbial consortium is composed essentially of H<sub>2</sub> producer bacteria and H<sub>2</sub> yields are constant for long reaction times. Such procedure, that has been successfully employed in laboratory scale, could be also of interest for industrial applications because the successive adaptations occur at the same temperature of AD and do not require additional equipment nor additional energy supply.

All biomass studied have given high biogas production rate and H<sub>2</sub> yields, but in different extent; best performances are obtained with Arundo donax and organic fraction of municipals solid wastes, due to the higher availability of reducing sugars in comparison to other substrates.

### *Clean-up*

This part concerns the study of H<sub>2</sub>S and HCl removal by adsorption on microporous materials to obtain very pushed purity levels (concentrations lower than 1 ppm).

A thorough literature review is effected in which the state of art of purification processes of biogas for feeding high temperature FCs is reported. The effects of harmful compounds on the MCFCs and SOFCs components are described and the more recent works on adsorption materials enabling to achieve purity levels compatible with the feeding of FCs are widely discussed.

The adsorbing materials studied were activated carbons and 13X-zeolites. These materials were studied as such or properly modified by treatment with basic solutions of KOH, NaOH and Na<sub>2</sub>CO<sub>3</sub> in order to improve the adsorption capacity towards H<sub>2</sub>S and HCl.

H<sub>2</sub>S and HCl adsorption tests were carried out in innovative laboratory plants that permit the continuous monitoring of the H<sub>2</sub>S and HCl concentrations with high accuracy of analysis. Breakthrough curves of the different materials have been obtained, from which the saturation times and adsorption capacity was calculated. These data allowed to compare the performance of the different materials and to identify the optimal ones. The results obtained have shown the effectiveness of the materials studied in obtaining high purity levels. The functionalization with basic solutions is effective in improving the adsorption properties of activated carbons and 13 X-zeolites: breakthrough times increase up to 5 for activated carbons (Norit RGM3 impregnated with - Na<sub>2</sub>CO<sub>3</sub>) and up to 12 times for zeolites (13X zeolite exchanged with Cu). Two kinetic models were studied for the regression of adsorption data: 4 parameters Weibull and 5 parameters Logistic models equations. Both models well fit the experimental data giving determination coefficient (R<sup>2</sup>) close to 1 for all materials. Logistic model however, although the slightly lower R<sup>2</sup> values, was preferred because of the lower computing times

#### *Integrated Plant Anaerobic Digester/SOFCs*

The last part concerns the study of the integrated plant anaerobic digester/Fuel Cell fed by biogas. The biomass considered is manure from cattle. This study has been placed in the project "Manure to electricity" that is in the frame of BIOSWEET (Biomass for Swiss Energy Future, supported by government of Swiss). This project has been developed at Paul Scherrer Institute (Villigen) where part of research activity has spent.

The integrated plant consists of different sections: biomass storage and pre-treatment; anaerobic digester and digestate tank; upgrade and clean-up systems; storage tank for biogas; SOFCs stack. SOFC was preferred with respect to MCFC because of the higher flexibility.

The feasibility study takes into account the several solutions to be found for the realization of the plant: resources assessment; optimization of AD process; designing of biogas clean-up device; SOFCs stack and commercial availability; economic analysis and prediction of future scenarios.

The first approach was to evaluate the theoretical and sustainable potential of biomass for biogas production (animal number, farms, stabling system). This addressed the choice of the biomass, the power range and the plant flow sheet.

After, the socio-economic context was examined to ascertain the usefulness of this technology for local use of the electricity. Most single farms operate in areas where there are almost no decentralized off-grid solutions, by contrast have a gross biogas potential (10-20 kWe). The power

range of 2-5 kWe (and in future perspective up to 100 kWe) has been defined. Two different scenarios have been considered: centralized power generation, collecting the manure from different farms, or local power generation, using the manure produced by the farm itself. They were compared taking into account different productivity contexts.

The operational limits for AD process, gas cleaning and SOFC stack were defined evaluating the critical biogas parameters that influence the cleaning step and SOFC stack performance.

The different devices, biomass storage tank, digester, digestate tank, clean-up system, SOFC stack were designed for different power sizes (in the range 2-100kWe).

The plant costs were calculated considering the costs of the different devices: digester, storage tanks for manure and digestate, ancillary devices, clean-up system, implementation of SOFC stack. The whole cost appears nowadays not competitive with traditional ICE. However, a significative cost reduction (36%) can be forecasted considering the commercial trend and the deeper market penetration of FCs technology in medium-short period.

The development of a technology based on the integration of SOFC with biogas production process deserves indubitable interest for practical applications: it allows the energy upgrading of waste biomass with consequent reducing in disposal costs and at the same time ensures higher efficiency and lower environmental impact in comparison to conventional thermal engines. Further steps are needed to complete the engineering of the system but as shown in this PhD thesis the time is ready for large-scale development of FCs technology.